X-Ray Scattering
Contractors Meeting

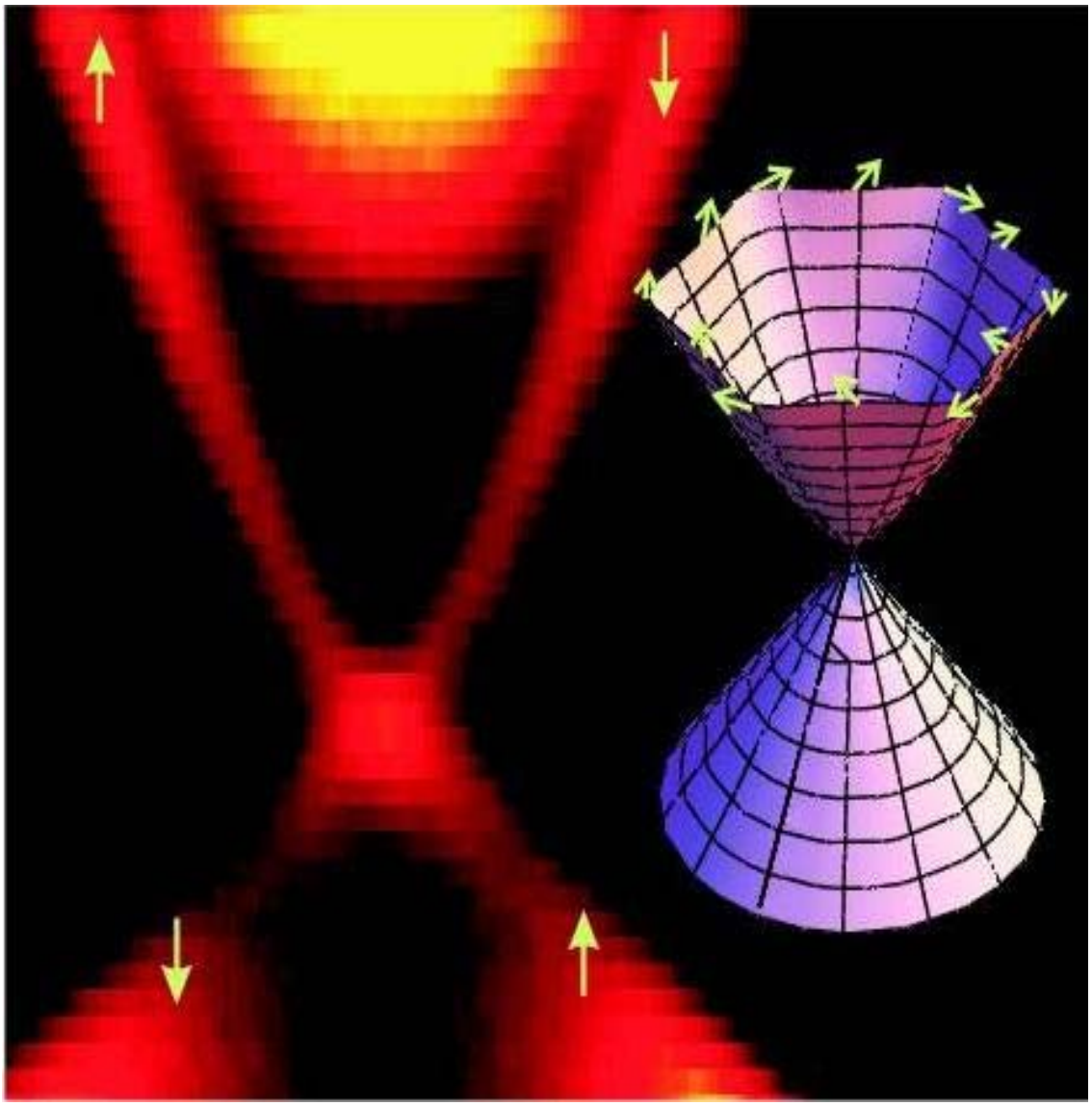

Airlie Conference Center
Warrenton, Virginia
November 14 – 17, 2010

On the Cover

The energy vs. momentum ARPES map of the states on the surface of a 3D topological insulator, indicative of a spin textured Dirac cone (inset). The spin circulation pattern is responsible for most of the novel properties of a topological insulator. [Provided by Zahid Hasan and detailed in Hsieh et al., *Nature* 2009.]

This document was produced under contract number DE-AC05-06OR23100 between the U.S. Department of Energy and Oak Ridge Associated Universities.

The research grants and contracts described in this document are supported by the U.S. DOE Office of Science, Office of Basic Energy Sciences, Materials Sciences and Engineering Division.

Foreword

This abstract book summarizes the scientific content of the 2010 X-ray Scattering Contractors Meeting sponsored by the Division of Materials Sciences and Engineering (DMSE) of the Office of Basic Energy Sciences (BES) of the U.S. Department of Energy. This meeting held on November 15–16, 2010 at the Airlie Conference Center, Warrenton, VA, is the second in the series covering the projects funded by the X-ray Scattering Program. The first meeting held October 16–19, 2007, included the Neutron Scattering program. BES DMSE has a long tradition of supporting a comprehensive scattering program in recognition of the high impact these tools have in discovery and use-inspired research. The size of the BES Scattering program has grown to the point where Neutron Scattering now has a separate program manager and contractors meeting parallel to X-ray Scattering.

The DMSE X-ray Scattering Program supports basic research using x-ray scattering, spectroscopy, and imaging for materials research, primarily at major BES-supported user facilities. X-ray scattering serves as one of the primary tools for characterizing the atomic, electronic and magnetic structures and excitations of materials. Information on structure and dynamics becomes the basis for identifying new materials and describing mechanisms underlying their unique behavior. Other key aspects of this activity are the development and improvement of next-generation instrumentation involving innovative focusing optics, detectors, sample environments, and data analysis tools; including the development of ultra-fast techniques involving pulsed radiation sources.

The purpose of the contractors meeting is to bring together researchers funded by BES in the x-ray scattering research area, to facilitate the exchange of new results and research highlights, to foster new ideas and collaborations among the participants, and to identify the needs of the research community. The meeting will also help DMSE to assess the state of the program and chart future directions.

We thank all the meeting participants for their active contributions in sharing their ideas and research accomplishments. Sincere thanks are also due to the speakers from other BES programs involved with x-ray scattering in multi-disciplinary research. The advice and help of the meeting chairs, John Hill and Roy Clarke, in planning for the meeting are deeply appreciated. We also thank Teresa Crockett of DMSE and Lee-Ann Talley at the Oak Ridge Institute for Science and Education for their outstanding work in all aspects of the meeting organization.

Lane Wilson and Helen Kerch
Division of Materials Sciences and Engineering
Office of Basic Energy Sciences
Office of Science
U.S. Department of Energy

DOE BES DMSE X-ray Scattering Contractors Meeting
Airlie Conference Center, Warrenton VA
November 15 & 16, 2010

Monday

8:00 **BES Welcome**
Linda Horton, BES
Lane Wilson, BES

Panel 1: **Science motivating facility upgrades; Innovation in instrumentation**
8:20 - 8:40 Introductory talk by Panel Chair: Harald Reichert, ESRF
8:40 - 9:30 Latest results highlight by Panelists (7 mins each)
Brian Stephenson, ANL
Jo Stohr, SLAC
Chi-Chang Kao, SLAC
John Hill, BNL
Steve Kevan, U. Oregon
Aaron Bostwick, LBNL
Gene Ice, ORNL
9:30 - 10:15 Small group discussions at each panelist poster
10:15 - 10:30 Panel Discussion

10:30 - 10:45 Changeover break

Panel 2: **Catalysis, deposition, magnetism & multiferroics**
10:45 - 11:05 Introductory talk by Panel Chair: Hoydoo You, ANL
11:05 - 11:55 Latest results highlight by Panelists (7 mins each)
Anders Nilsson, SLAC
Dillon Fong, ANL
Jeff Eastman, ANL
Karl Ludwig, Boston U.
Randy Headrick, U. Vermont
Paul Evans, U. Wisconsin
Alan Goldman, AmesNL
11:55 - 12:40 Small group discussions at each panelist poster
12:40 - 12:55 Panel Discussion

12:55 - 2:00 Lunch break

Panel 3: **Nanoparticles, interfaces, and surfaces**
2:00 - 2:20 Introductory talk by Panel Chair: Simon Billinge, BNL
2:20 - 3:10 Latest results highlight by Panelists (7 mins each)
Tom Russell, U. Massachusetts
Tabbetha Dobbins, Louisiana Tech
Roy Clarke, U. Michigan

Paul Lyman, U. Wisconsin-Milw
Chuck Fadley, LBNL
Barry Wells, U. Connecticut
Mike Bedzyk, Northwestern U.

3:10 - 3:55 Small group discussions at each panelist poster
3:55 - 4:10 Panel Discussion

4:10 - 6:30 Afternoon break for interactive discussion and free time

6:30 - 7:30 Dinner

Panel 4: **Ultra-fast x-rays**
7:30 - 7:50 Introductory talk by Panel Chair: David Reis, SLAC
7:50 - 8:40 Latest results highlight by Panelists (7 mins each)
Phil Bucksbaum, SLAC
Margaret Murnane, U. Colorado
Robert Schoenlein, LBNL
Paul Fuoss, ANL
Aaron Lindenberg, SLAC
Robert Kaindl, LBNL
Hermann Durr, SLAC
8:40 - 9:25 Small group discussions at each panelist poster
9:25 - 9:40 Panel Discussion

9:40 End of day wrap up
****

Tuesday

8:00 **BES Program Business**
Lane Wilson, BES

Panel 5: **ARPES and electron correlations**
8:20 - 8:40 Introductory talk by Panel Chair: Zahid Hasan, Princeton U.
8:40 - 9:30 Latest results highlight by Panelists (7 mins each)
Yulin Chen, SLAC
J.C. Campuzano, ANL
Z.X. Shen, SLAC
Tai Chiang, U. Illinois
Dan Dessau, U. Colorado
Tomasz Durakiewicz, LANL
Adam Kaminski, AmesNL
9:30 - 10:15 Small group discussions at each panelist poster
10:15 - 10:30 Panel Discussion

10:30 - 10:45 Changeover break

Panel 6: **High pressure and extreme environments**
10:45 - 11:05 Introductory talk by Panel Chair: Victor Struzhkin, Carnegie Inst. Wash.
11:05 - 11:55 Latest results highlight by Panelists (7 mins each)
Wendy Mao, SLAC
George Srajer, ANL
Jiuhua Chen, Florida Int. U.
David Mao, Carnegie Inst. Wash.
Andrew Cornelius, UNLV
Todd Hufnagel, Johns Hopkins U.
Eliot Specht, ORNL
11:55 - 12:40 Small group discussions at each panelist poster
12:40 - 12:55 Panel Discussion

12:55 - 2:00 Lunch break

Panel 7: **Structural ordering: soft matter, hard metals**
2:00 - 2:20 Introductory talk by Panel Chair: John Parise, BNL
2:20 - 3:10 Latest results highlight by Panelists (7 mins each)
Simon Mochrie, Yale U.
Jeff Kortright, LBNL
Mike Toney, SLAC
Ben Ocko, BNL
Rosa Barabash, ORNL
Bob Suter, Carnegie Mellon U.
John Budai, ORNL
3:10 - 3:55 Small group discussions at each panelist poster
3:55 - 4:10 Panel Discussion

4:10 - 6:30 Afternoon break for interactive discussion and free time

6:30 - 7:30 Dinner

Panel 8: **RIXS, RSXS, and CXI**
7:30 - 7:50 Introductory talk by Panel Chair: Peter Abbamonte, U. Illinois
7:50 - 8:32 Latest results highlight by Panelists (7 mins each)
Tom Devereaux, SLAC
Stuart Wilkins, BNL
Clem Burns, Western Michigan U.
Oleg Shpyrko, UCSD
Chris Jacobsen, ANL
Andreas Scherz, SLAC
8:32 - 9:25 Small group discussions at each panelist poster
9:25 - 9:40 Panel Discussion

9:40 End of meeting wrap up

Table of Contents

Table of Contents

Abstracts

Elementary electronic excitations in strongly correlated systems under quantum confinement

Peter Abbamonte
abbamonte@mrl.uiuc.edu
Department of Physics and Frederick Seitz Materials Research Laboratory
University of Illinois, Urbana, IL, 61801

Award Nos.: DE-FG02-07ER46459, DE-FG02-06ER46285

Research Scope

The purpose of these two activities is to study elementary excitations in interacting electron systems under conditions of quantum confinement.

The first activity (DE-FG02-07ER46459) is focused on using inelastic x-ray scattering, coupled with advanced phase retrieval algorithms, to image the motion of electrons in condensed matter with attosecond time resolution. This project is currently being applied to electrons in materials with reduced dimensionality, most recently graphene (see below).

The second activity (DE-FG02-06ER46285) is focused on the interplay between engineered nanoscale order, created artificially by nanofabrication techniques, and the various innate electronic instabilities known to take place in these systems, such as stripe phases, charge or spin density waves, orbital order, or intrinsic electronic inhomogeneity due to proximity to a quantum critical point. The long-term goal is to understand how these two types of nanoscale order cooperate to create new phenomena, with hopes of contributing eventually to a revolution in strongly correlated electronic devices. This project is based on the technique of resonant soft x-ray scattering (RSXS), which is one of the only techniques in existence that can selectively probe nanoscale valence, spin, orbital and lattice degrees of system, with bulk sensitivity.

Recent Progress under DE-FG02-07ER46459 (selected)

Measurement of the effective fine structure constant for freestanding graphene. Electrons in graphene behave like Dirac fermions, permitting phenomena from high energy physics to be studied in a solid state setting. A key question is whether or not these Fermions are critically influenced by Coulomb correlations. We performed inelastic x-ray scattering experiments on crystals of graphite, and applied reconstruction algorithms to image the dynamical screening of charge in a freestanding, graphene sheet (Fig. 1). We found that the polarizability of the Dirac fermions is amplified by excitonic effects, improving screening of interactions between low energy quasiparticles. The strength of interactions in graphene is characterized by a scale-dependent, effective fine structure constant, $\alpha_g(k,\omega) = e^2 / \hbar v_F \varepsilon(k,\omega)$, whose value we show approaches $\alpha_g = 0.14 \pm 0.092 \sim 1/7$ at low energy and large distances. This value is substantially smaller than the nominal

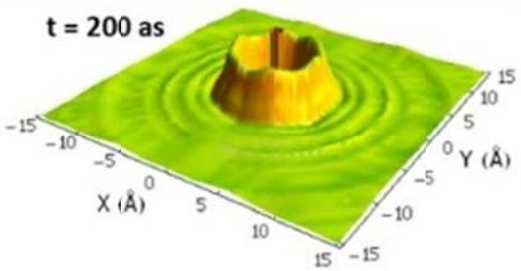

Figure 1 Image of the electron density in a graphene sheet, 200 attoseconds after being "struck" by a point perturbation. From images of this type it is possible to deduce the fine structure constant, which is a dimensionless measure of the strength of electron-electron interactions in graphene.

$\alpha_g = 2.2$, suggesting that, on the whole, graphene is more weakly interacting than previously believed. This study will appear soon in *Science* [1].

Attosecond imaging of the valence exciton in LiF. The absorption of light by materials proceeds through the formation of excitons, which are states in which an excited electron is bound to the valence hole it vacated. Understanding the structure and dynamics of excitons is important, for example, for developing technologies for light-emitting diodes or solar energy conversion. However, there has never been an experimental means to study the time-dependent structure of excitons directly. In this project we used causality-inverted inelastic x-ray scattering (IXS) to image the charge-transfer exciton in the prototype insulator LiF, with resolutionsΔt=20.67 as (2.067×10-^{17} s) in time and Δx=0.533 Å (5.33×10^{-11} m) in space. Our results showed that the exciton has a modulated internal structure and is coherently delocalized over two unit cells of the LiF crystal (~8 Å). This structure changes only modestly during the course of its life, which establishes it unambiguously as a Frenkel exciton and thus amenable to a simplified theoretical description. Our results resolved an old controversy about excitons in the alkali halides and demonstrate the utility of IXS for imaging attosecond electron dynamics in condensed matter. This study was published in *PNAS* [12].

Recent Progress under DE-FG02-06ER46285 (selected)

Interface charge transfer and superconductivity in $La_{2-x}Sr_xCuO_4$ heterostructures. We used resonant soft x-ray scattering (RSXS) to quantify the hole distribution in a superlattice of insulating La_2CuO_4 (LCO) and overdoped $La_{2-x}Sr_xCuO_4$ (LSCO). Despite its nonsuperconducting constituents, this structure is superconducting with T_c = 38 K. We found that the conducting holes redistribute electronically from LSCO to the LCO layers. The LCO layers were found to be optimally doped, suggesting they are the main drivers of superconductivity, in support of past measurements of interface superconductivity in this system. This study was published in *Phys. Rev. Lett*. [10].

Magnetism and structural variations in $La_{1-x}Sr_xMnO_3$ quantum wire arrays. One of the central ongoing projects of this grant is to study the electronic structure transition metal oxide quantum wires, in particular whether they exhibit stripe correlations. Our first study, on $La_{1-x}Sr_xMnO_3$ quantum wires (see Fig. 2) revealed diffuse, but temperature-reversible, magnetic x-ray scattering from the ferromagnetic domains in the wires. These results, which were confirmed by magnetic force microscopy measurements, suggest that fluctuations are enhanced in our wires because of quantum confinement effects. The manuscript in preparation.

Electronic structure of conducting domain walls in $BiFeO_3$ films. $BiFeO_3$ (BFO) is an insulating ferrimagnet (0T_N=650K) which is also ferroelectric because of a rhombohedral. When grown epitaxially

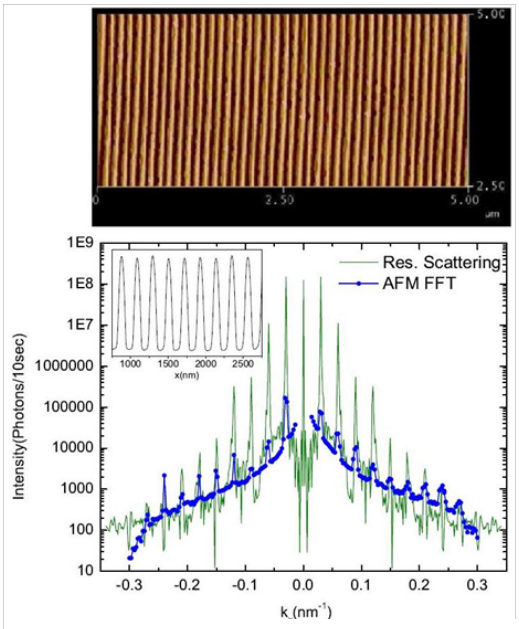

Figure 2 (top) AFM image of an array of $La_{1-x}Sr_xMnO_3$ quantum wires. (bottom) Comparison of RSXS experiments to the Fourier transform of the AFM. This study showed that the diffuse elastic RSXS signal arises from random height variations among the wires.

on $SrTiO_3$, BFO forms domain walls that, under appropriate condition, will order into a quasiperiodic structure. It was recently shown, further, that the domain walls are conducting, though the mechanism behind metallic behavior is not known. We have studied these structures with RSXS, and have successfully observed the domain walls in the form on off-specular sidebands, which are visible only at the Fe *L* edge. Their energy dependence suggests that metallic behavior arises from a *raising* of the crystal symmetry (i.e. a suppression of the rhombohedral distortion) near the domain wall, suggesting a structural mechanism behind metallic conduction.

Future Plans

Concerning ultrafast activities, in the near future we will expand these studies to higher resolution to quantify better the excitonic effects observed in graphene in our previous experiments. We will also expand these measurements to intercalated graphite, to learn about the properties of doped graphene.

Concerning soft x-ray activities, our main objective is to extend our quantum wire studies to materials that exhibit charge order. The material we will begin with is $La_{1-x}Ca_xMnO_3$, which has robust charge order for x>0.5. In the longer term, our goal is to study $La_{2-x}Ba_xCuO_4$ (LBCO), which was the original proposal. The overarching goal is to see if stripes are more stable in a finite structure due to the stabilizing effect of the boundaries.

We are also engaged in an exploratory experiment to study collective excitations in stripe materials with time-resolved RSXS at the LCLS, in collaboration with Wei Sheng Lee and Z. X. Shen of Stanford, and Yi-De Chuang and Zahid Hussein at LBNL. As part of this project we intend to explore, in collaboration with Shaul Mukamel of U.C. Irvine, the possibility of measuring four-point correlation functions with nonlinear x-ray optical techniques, which might reveal new phenomena such as an electron nematic state.

DOE-sponsored publications, 2008-pres.

1. J. P. Reed, B. Uchoa, Y. I. Joe, Y. Gan, D. Casa, E. Fradkin, P. Abbamonte, The effective fine structure constant of graphene, to appear in *Science*
2. A. Rusydi, W. Ku, B. Schulz, R. Rauer, I. Mahns, D. Qi, X. Gao, A. T. S. Wee, P. Abbamonte, H. Eisaki, Y. Fujimaki, S. Uchida, M. Rubhausen, Experimental observation of the crystallization of a paired holon state, Phys. Rev. Lett. **105**, 026402 (2010)
3. M. Kim, X. M. Chen, E. Fradkin, P. Abbamonte, S. L. Cooper, Mapping the magneto-structural quantum phases of Mn_3O_4, Phys. Rev. Lett. **105**, 026402 (2010)
4. P. Abbamonte, G. C. L. Wong, D. Cahill, J. P. Reed, R. H. Coridan, N. W. Schmidt, G. H. Lai, Y. I. Joe, D. Casa, Ultrafast Imaging and the Phase Problem for Inelastic X-Ray Scattering, Advanced Materials **22**, 1141 (2010)
5. M. Kim, H. Barath, X. Chen, Y. I. Joe, E. Fradkin, P. Abbamonte, S. L. Cooper, Magnetic-field– and pressure-induced quantum phases in complex materials, Advanced Materials **22**, 1148 (2010)
6. A. B. Shah, Q. M. Ramasse, X. F. Zhai, J. G. Wen, S. J. May, I. Petrov, A. Bhattacharya, P. Abbamonte, J. N. Eckstein, J. M. Zuo, Probing Interfacial Electronic Structures in Atomic Layer LaMnO3 and SrTiO3 Superlattices, Advanced Materials **22**, 1156 (2010)
7. T. Kroetz, M. Roberto, I. L. Caldas, R. L. Viana, P. J. Morrison, P. Abbamonte, Integrable maps with non-trivial topology: application to divertor configurations, Nuclear Fusion **50**, 034003 (2010)
8. R. H. Coridan, N. W. Schmidt, G. H. Lai, R. Godawat, M. Krisch, S. Garde, P. Abbamonte, G. C. L. Wong, Hydration dynamics at femtosecond timescales and Angstrom lengthscales from inelastic x-ray scattering, Phys. Rev. Lett. **103**, 237402 (2009)

9. P. Abbamonte, J. P. Reed, Y. I. Joe, Yu Gan, D. Casa, Implicit spatial averaging in inversion of inelastic x-ray scattering data, Phys. Rev. B **80**, 054302 (2009)
10. S. Smadici, J. C. T. Lee, S. Wang, P. Abbamonte, A. Gozar, G. Logvenov, C. D. Cavellin, I. Bozovic, Superconducting transition at 38 K in insulating-overdoped La_2CuO_4-$La_{1.64}Sr_{0.36}CuO_4$ superlattices: Evidence for interface electronic redistribution from resonant soft x-ray scattering, Phys. Rev. Lett. **102**, 107004 (2009)
11. H. Barath, M. Kim, S. L. Cooper, P. Abbamonte, E. Fradkin, I. Mahns, M. Rubhausen, N. Aliouane, D. N. Argyriou, Domain fluctuations near the field-induced incommensurate-commensurate phase transition of $TbMnO_3$, Phys. Rev. B **78**, 134407 (2008)
12. Peter Abbamonte, Tim Graber, James P. Reed, Serban Smadici, Chen-Lin Yeh, Abhay Shukla, Jean-Pascal Rueff, and Wei Ku, Dynamical reconstruction of the exciton in LiF with inelastic x-ray scattering, Proc. Natl. Acad. Sci. **105**, 12159 (2008)
13. A. Rusydi, I. Mahns, S. Muller, M. Rübhausen, S. Park, Y. J. Choi, C. L. Zhang, S. W. Cheong, S. Smadici, P. Abbamonte, M. v. Zimmermann, G. A. Sawatzky, Multiferroicity in the spin-1/2 quantum matter of $LiCu_2O_2$, Appl. Phys. Lett. **92**, 262506 (2008)
14. M. Kim, H. Barath, S.L. Cooper, P. Abbamonte, E. Fradkin, M. Rubhausen, C.L. Zhang, S-W. Cheong, Raman scattering studies of temperature- and field-Induced melting of charge order in $(La,Pr,Ca)MnO_3$, Phys. Rev. B **77**, 134411 (2008)
15. H. Barath, M. Kim, J.F. Karpus, S.L. Cooper, P. Abbamonte, E. Fradkin, E. Morosan, R.J. Cava, Quantum and Classical Mode Softening Near the Charge-Density-Wave-Superconductor Transition of Cu_xTiSe_2, Phys. Rev. Lett. **100**, 106402 (2008)
16. A. Rusydi, P. Abbamonte, H. Eisaki, Y. Fujimaki, S. Smadici, N. Motoyama, S. Uchida, Y.-J. Kim, M. Rubhausen, G. A. Sawatzky, Strain amplification of the $4k_F$ chain instability in $Sr_{14}Cu_{24}O_{41}$, Phys. Rev. Lett. **100**, 036403 (2008)

Indentation-induced Localized Deformation and Elastic Strain Partitioning in Composites at Submicron Length Scale

R. I. Barabash and G. E. Ice
Oak Ridge National Laboratory, Oak Ridge TN 37831-6118, barabashr@ornl.gov, IceGE@ornl.gov

Research Scope

The goal of this research is to understand small-scale deformation and strain partitioning in composite materials and is an integrated part of our overall research goal of understanding the role of local structure and defects on materials behavior (See for example abstracts by Larson et al., Budai et al., Ice et al., Pang et al. and Tischler et al.). Our primary tool is 3D submicron-resolved polychromatic and scanning energy X-ray diffraction microscopy. Measurements are made on unique composite materials composed of Mo fibers in a NiAl or Ni matrix. These composites are made by collaborators Bei and George in the ORNL Alloy Design Group. Measurements are compared with electron microscopy and finite element modeling at ORNL. What makes these experiments compelling, is the nondestructive 3D measurements and the unusual composite fabrication method that allows for the creation of nearly defect-free fibers. These fabrication methods have for example been used to create nearly defect-free nanopillars that have clarified the role of defect density and size in nanopillar behavior. Because we can now study materials with controlled defect densities and fiber size/density, we have an ideal model system for understanding the role of length scales on composite behavior. In this abstract we describe recent measurements on nanoindented composites.

The deformation behavior of composite materials depends on local-mechanisms taking place in the fibers, the matrix, and the matrix/fiber interface. With nanoindented samples, all aspects of plastic deformation are confined within a volume that can be *both probed by 3D x-ray microscopy and simulated computationally*. Therefore, measurements/calculations within the confined volume provide for a direct quantitative connection between 3D x-ray microscopy measurements and computer simulations and modeling. Of course, the strong deformation gradients inherent in indentations present difficult experimental and theoretical challenges, but also provide stringent tests of strain gradient effects and issues with respect to fundamental length scales in materials. In nano- and micro-composites, a weak fiber phase can increase the fracture toughness of a weak matrix phase by orders-of-magnitude. Clearly such a dramatic behavior can only be predicted with a fundamental understanding of interface deformation behavior. State-of-the-art characterization methods have been based on ex situ microscopy studies or destructive evaluations. However, with the development of depth-resolved 3D X-ray microprobe it is now possible to nondestructively probe the local strain gradients and interfacial interactions near buried interfaces with the needed submicron resolution**.**

Recent Progress

We found during measurements on nanopillars, that microdiffration methods can be used to determine the elastic strain state of pillars, fibers and their matrix, as well as their defect density and the strength of the fiber matrix interface. Using depth-resolved X-ray microdiffraction we have found that the deformation behavior of NiAl-Mo composites is distinct from the behavior of single-phases materials and dependent on the strain partitioning between the two phases of the composite. For example, a dramatic change is observed in the Mo fiber orientation distribution after indentation. In addition, the superposition of mechanically-applied external stresses with the original thermal-mismatch-induced stresses causes an unusual depth-dependent residual strain distribution both in the NiAl matrix and in the Mo fibers; in the NiAl matrix we find a tensile-compressive-tensile residual strain distribution with depth through the most deformed regions of the sample. Our ultimate goal is to use these observations to study size-dependent changes in behavior.

A typical Laue pattern (Inset in Fig. 1a) with enlarged patterns near the (00*h*) type reflection at two different locations near the indent are shown in Figs. 1a and b. An SEM image of the indented region is shown in Fig. 1c. Polychromatic X-ray Microbeam (PXM) was used to map regions of maximal deformation and to identify locations for depth-resolved measurements.

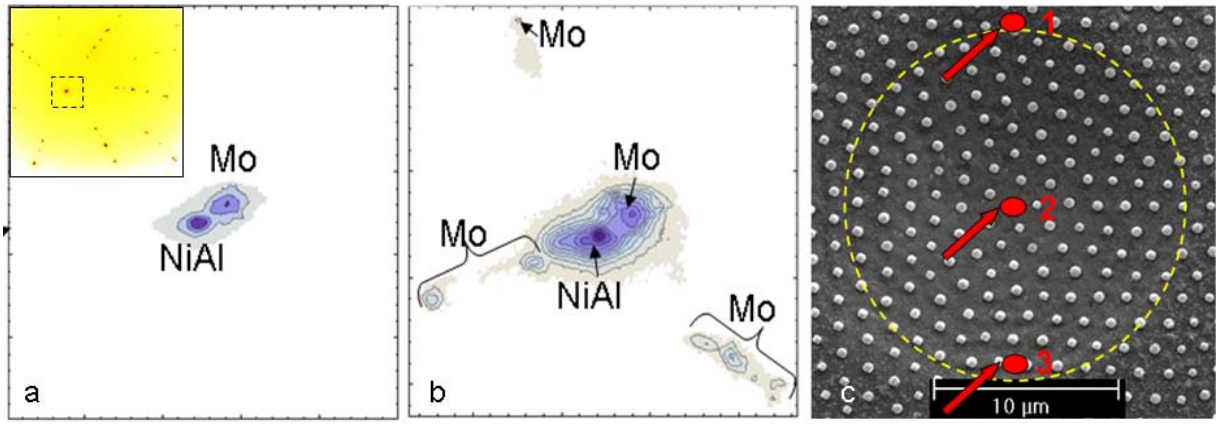

Fig.1. Enlarged region around (00h) Laue spot for location 1 far from the indented area (a) and location 2 in the center of the indented area (b). Inset in (a) shows a typical Laue pattern from as-grown NiAl/Mo alloy. The general view of the indented area and probed locations (c).

The Laue pattern in Fig.1a is from outside the indented area and both the NiAl and Mo (00*h*) Laue spots are sharp. Although the beam intercepts several (typically up to 10 Mo fibers), they all diffract intensity into nearly the same direction, indicating very high alignment of the fibers along the <001> NiAl and Mo growth direction. In the indented zone the character of the Laue spots indicates the presence of lattice rotations. The most dramatic changes in the indented area are observed for the Mo fibers; instead of one Laue spot arising from different probed fibers, multiple Mo Laue spots are observed when the X-ray beam probes a volume within the indent (Fig. 1b). The depth-resolved measurements of the dilatational strain along the fiber were probed at positions 1-3 in Fig. 1 c. To determine the fiber axis strain, the (006) *d*-spacing was measured for both the NiAl matrix and Mo fibers.

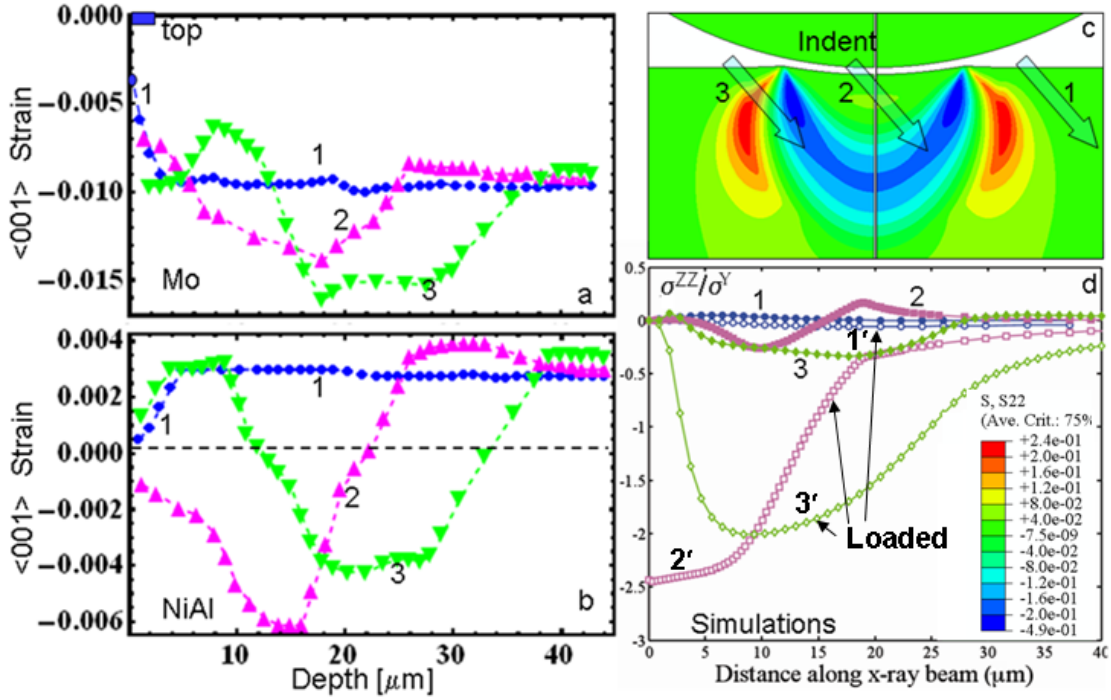

Fig.2 Distribution of <001> lattice strain along the beam directions experimentally determined in (a) Mo fibers and (b) NiAl matrix at three different locations: (1) outside indent - filled circles; (2) entering the sample at the center of indent – triangles; (3) entering the sample at the left edge of the indent – inverse triangles. (c) A sketch of the model used in the simulations for three different entrance locations with simulated strain contours, and (d) simulated depth-dependent strains for the three locations – unloaded (1, 2, 3) and loaded (1′, 2′, 3′).

The elastic lattice strain in both the Mo fibers and the NiAl matrix changes character with location (Fig. 2). Far from the indented area (Location 1) the indentation-induced stress fields are negligible and the strain distribution can be explained by the mismatch in the coefficients of thermal expansion (CTE) between Mo and NiAl. Near the surface these thermal strains relax and result in a large near-surface strain gradient (circles in Figs. 2a, b). This near-surface relaxation is similar to a pull-out test and is used to determine the interface strength. Completely stress free Mo lattice parameters are measured at the tops of exposed Mo pillars when the matrix is etched away.

The experimental strain distribution in Figs. 2 a and b can be qualitatively understood by combining thermal and indentation micromechanical stress analyses. Finite element modeling of the spherical indentation shows, that material at a depth about half of the contact radius yields first and the plastic zone size increases as the applied load increases (Fig. 2 c). The resulting elastic stress field has an arc-like shape centered near the contact center. During unloading, the plastically deformed material tends to preserve its shape in the simulations, while the surrounding elastic material tends to spring back and thus transmit compressive stress to the plastic zone. A more detailed picture of the residual stress distribution can be gained through the simulated strain profiles in Fig. 2d, which shows compressive residual stress at the center and tensile stress near the contact edge.

Despite the qualitative agreement between experiment and model, the predicted change is about 1/3 of the observed strain change. This discrepancy is believed to be due to the complicated interaction of thermal and indentation stress fields, which is not correctly incorporated in the current finite element simulations. The tensile thermal residual stress in NiAl is one order of magnitude smaller than the compressive thermal residual stress in Mo. Thus, during indentation, Mo fibers tend to yield first, and the contact load is supported by a larger plastic zone than predicted in a homogeneous solid.

Future Plans

The matrix/fiber interface plays a crucial role in the mechanical properties of composite materials. However, the strength of the interface and the response of small fibers to an external load are in general largely unknown. Exploring these plastic/elastic phenomena and interfacial effects in composite materials under various external stress loading will be the focus of our future research. Specifically, we plan to non-destructively study 3D spatially-resolved depth-dependent strain and dislocation gradients in the matrix and fibers of several eutectic composites with different fiber shapes, sizes, elastic moduli misfits, and thermal expansion coefficients under both nanoindentation and uniform external stress load. These studies will provide new information about how deformation is accommodated in two-phase composite materials as a function of fiber size, elastic properties, morphology and volume fraction of the second phase. Experimental 3D results for strain gradients in composites under external fields also call for more detailed finite element simulations taking into account real microstructure parameters and interactions at the matrix/fiber interface.

Publications (FY08-FY10)

1. R. I. Barabash, H. Bei, Y. F. Gao, G. E. Ice, “Indentation-induced Localized Deformation and Elastic Strain Partitioning in Composites at Submicron Length Scale”, *Acta Materialia,* 2010 accepted (in print).
2. R.I. Barabash, E. Huang, J. Wall, J. Wilkerson, Y. Ren, W. Liu, S. Vogel, G.E. Ice, L. Pike, and P. Liaw, “Texture Crossover: Trace from Multiple Grains to a Subgrain” *Mat Sci Eng A* accepted 2010 (in print).
3. R. Barabash, Y. Gao, G. Ice, O.M. Barabash, J. Chung *et al*., “Mapping Strain Gradients in the FIB-Structured InGaN/GaN Multilayered Films with 3D X-ray Microbeam”, *Mat Sci Eng A* accepted 2010 (in print)
4. O. M. Barabash, M. Santella, R.I. Barabash, G. E. Ice, J. Tischler, “Depth-Dependent Dislocation Densities and Elastic Strains in an Indented Ni-based Superalloy from 3D X-ray Microdiffraction and EBSD”, *JOM* accepted (2010).
5. Ch. Del Genio, K. Bassler, A. Korzenevskii, R. Barabash, J. Trenkler, G.F. Reiter, S.C. Moss, “Depth-dependent ordering, two-length-scale phenomena, and crossover behavior in a crystal featuring a skin layer with defects”, *Phys Rev B* 81, 144111-1 -144111-10, (2010)

6. L. Wang, R. Barabash, Y. Yang, T. Bieler, M. Crimp, P. Eisenlohr, W. Liu, G. Ice, "Experimental characterization and crystal plasticity modeling of heterogeneous deformation in polycrystalline α-Ti", *Met Mat Trans A* accepted 2010 (in print)
7. E. Huang, R.I. Barabash, G. E. Ice *et al*., "Fatigue-induced Reversible/Irreversible Structural-transformations In a Ni-based Superalloy", *International Journal of Plasticity*, 26, 1124-1137 (2010)
8. R. I. Barabash, H. Bei, Y. F. Gao, G. E. Ice, and E. P. George, "3D X-ray Microprobe Investigation of Local Dislocation Densities and Elastic Strain Gradients in a NiAl-Mo Composite and Exposed Mo Micropillars as a Function of Pre-strain", *JMR* 25, 2, 199- 206, (2010)
9. E. Huang, R.I. Barabash, G.E. Ice, *et al.*, "Cyclic-loading-induced Accumulation of Geometrically Necessary Dislocations near Grain Boundaries in a Ni-Based Superalloy", *JOM*, 61, 12, 51-56, (2009).
10. R.I. Barabash, G.E. Ice, M. Kumar, J. Ilavsky, J. Belak, "Polychromatic microdiffraction analysis of defects self-organization in shock deformed single crystals", *International Journal of Plasticity*, (2009), 25, 2081-2093.
11. O.M. Barabash, R.I. Barabash, G.E. Ice, Z. Feng, D. Gandy, "X-ray Microdiffraction and EBSD Study of FSP Induced Structural/Phase Transitions in a Ni-based Superalloy", *Mat. Sci. Eng. A* 524/1-2, 10-19, (2009).
12. R. Barabash, G. Ice, "Probing strains and dislocation gradients with diffraction", *Mat. Sci. Eng. A* 524, 1-2, (2009).
13. T. Ohashi, R.I. Barabash, J. Pang, G.E. Ice, O.M. Barabash, "X-ray Microdiffraction and Strain Gradient Crystal Plasticity Studies of Geometrically Necessary Dislocations Near a Ni Bicrystal Grain Boundary", *International Journal of Plasticity*, (2009), 25, 920-941
14. R.I. Barabash, G.E. Ice, W. Liu, O.M. Barabash, "Polychromatic Microdiffraction Characterization of Defect Gradients In Severely- Deformed Materials", *Micron*, (2009) 40, 28 - 36.
15. H. Bei, R.I. Barabash, G.E. Ice, W. Liu, J. Tischler, and E.P. George, "Spatially resolved strain measurements in Mo-alloy micropillars by differential aperture x-ray microscopy" *Appl. Phys. Let*., 93, 071904 (2008)
16. E. Huang, R. Barabash, N. Jia, Y. Wang, G.E. Ice, B. Clausen, J. Horton, and P. Liaw, "Slip-System-Related Dislocation Study from *In-Situ* Neutron Measurements", *Met. Mat. Trans. A*, (2008) 39A, 3079 -3088.
17. S. Lee, R. Barabash, J. Chung, P. Liaw, H. Choo, Y. Sun, C. Fan, L. Li, D. Brown and G. Ice, "Neutron and X-ray Microbeam Diffraction Studies around a Fatigue-Crack Tip after Overload", *Met Mat Trans A*, (2008) 39A, 3164- 3169.
18. R. Barabash, Y. Gao, Y. Sun, S. Lee, H. Choo, P. Liaw, D. Brown, G. Ice, "Neutron and X-ray diffraction studies and cohesive interface model of the fatigue crack deformation behavior" *Phil Mag Let* (2008) 88, 553-565
19. R.I. Barabash, G.E. Ice, B.A. Haskell, S. Nakamura, J. Speck, W. Liu, "White X-ray Microdiffraction Analysis of Defects, Strain and Tilts in a Free Standing GaN Film", *Phys Stat Sol* (2008) 245, 5, 899-902.
20. E. Huang, R.I. Barabash, Y. Wang, B. Clausen, L. Li, P. Liaw, G.E. Ice, Y. Ren, H. Choo, L. Pike, D. Klarstrom, "Plastic Behavior of a Nickel-Based Alloy under Monotonic-Tension and Low-Cycle-Fatigue Loading", *International Journal of Plasticity* vol. 24/08, 1440-1456 (2008).
21. D. Nicholson, R. Barabash, Y. Puzyrev, C. Gao, D. Keffer and G. Ice, "The role of chemical and displacement pair correlation in the determination of higher order correlation", in: "*Diffuse scattering and the fundamental properties of materials"*, Eds. R.I. Barabash, G.E. Ice, P.E.A. Turchi, Momentum Press, LLC NY, 303-316, (2009).
22. G. Ice, J. Pang, R. Barabash, "Polychromatic microdiffraction studies of inhomogeneous deformation", in "*Perspectives in Materials Characterization*" Uni Press, Ed. B. Raj, Priv Lim, Hyderabad, India, 55-76, (2009).
23. R.I. Barabash, J. Tischler, G. E. Ice, O.M. Barabash. "Small Scale Mechanical Behavior and Interface strength in Ni-Mo Composites from 3D X-Ray Microdiffraction", in: 31st Risø International Symposium on Materials Science: Challenges in Materials Science and possibilities in 3D and 4D techniques, Denmark, 1-9, (2010).
24. G.E. Ice, R.I. Barabash, A. Khounsary, "Nested mirrors for X-rays and Neutrons", In: "Advances in X_Ray/EUV Optics and Components IV",v. 7448, Eds. A. Khounsary, C. Morawe; S. Goto; proceedings of the SPIE conference, V.7448, . 74480B-1 - 74480B-8 (2009).
25. J. Chao, A. Mark, M.L. Fuller, R.I. Barabash, N.S. McIntyre, R.A. Holt, R.J. Klassen, W. Liu, "X-ray Laue micro diffraction and neutron diffraction analysis of residual elastic strains and plastic deformation in a 1% uniaxial tensile tested nickel alloy 600 sample", Mater. Res. Soc. Sym. Proc. **1137**, Warrendale, PA, EE10-28 (2009).

X-ray atomic-scale studies of interfaces

PI: Michael Bedzyk
Materials Science and Engineering, Northwestern University, Evanston, IL 60208
bedzyk@northwestern.edu

Research Scope:
Work is aimed at understanding the atomic-scale structural and chemical properties of interfaces together with the development of novel in situ X-ray probes.

DOE/BES funded research includes:

- Center for Electrical Energy Storage (EFRC) DE-AC02-06CH11357
  - Bedzyk: In situ X-ray studies of Li-ion battery related solid-electrolyte interfaces
  - Primary NU Collaborators: M. Hersam
  - Primary ANL Collaborators: M. Thackeray, P. Fenter, L. Curtiss. P. Zapol

- Electrostatic Driven Self-Assembly Design of Functional Nanostructures, -ER46539
  - Bedzyk: In situ SAXS – WAXS studies of crystallization of buckled membranes in mixed-valence ionic amphiphile vesicles
  - Primary NU Collaborator: M. Olvera

- Funding of NU graduate students and partial summer salary through subcontracts with Argonne National Laboratory
  - Primary ANL collaborators: P. Fenter, J. Freeland, O. Auciello, G. Stephenson

- Institute for Catalysis in Energy Processes DE-FG02-03ER15457
  - Bedzyk: Catalyst characterization: In-situ structure/species determination
  - Primary NU Collaborators: P. Stair, M. Hersam, D. Ellis, K. Poeppelmeier
  - Primary ANL Collaborators: J. Elam, L. Curtiss. P. Zapol

Recent Progress:

X-ray Atomic-scale studies of oxide supported monolayer catalysts
Metal oxides anchored to oxide supports often exhibit greater catalytic activity as monolayers than as thicker films. Understanding this phenomenon requires a chemically sensitive, atomic-scale view of the interfacial processes. We use *in situ* X-ray standing wave (XSW) 3D atomic imaging combined with *ex situ* X-ray photoelectron spectroscopy (XPS) and X-ray absorption fine structure measurements to follow the redox-induced surface site exchange of cations on a single crystal oxide support as well as the concurrent changes in the oxidation states of the supported cations. This is then compared to density functional theory predictions from our collaborators D. Ellis (NU), L. Curtiss (ANL) and P. Zapol (ANL). As an example, we follow the reversible changes during the redox cycle of a $^1/_3$ ML WO_X / α-Fe_2O_3 (0001) interface grown by atomic layer deposition by our ANL collaborator J. Elam. The XSW measured W atomic maps (as illustrated below) and XP spectra show dramatic changes for the as-deposited, oxidized and reduced interfaces, which are explained by models that account for W incorporation at Fe sites with various coordination schemes.[1] The 3D W atomic map for each condition is measured by the summation of the XSW measured *hkl* Fourier components for the XRF selected W distribution.[2] This strategy was then also applied to redox-induced structural and chemical changes for the sub-ML and 2 ML VO_X / α-TiO_2 (110) interfaces. We have also produced 3D atomic maps for the cube-on-cube epitaxy of Pt nanocrystals grown by molecular beam epitaxy on $SrTiO_3$(001). For this our NU collaborator, M. Hersam, provides surface morphology changes via scanning probe microscopy.

[1] Z. Feng, C.-Y. Kim, J.W. Elam, Q. Ma, Z. Zhang, M.J. Bedzyk, *J. Am. Chem. Soc.* **131**, 18200 (2009).
[2] L. Cheng, P. Fenter, M. J. Bedzyk, N. C. Sturchio, Phys. Rev. Lett. 90, 255503 (2003).

1/3 ML WO_X/ α-Fe_2O_3 (0001) interface: *(11$\underline{2}$0) 2D cuts through the XSW measured 3D tungsten atomic density maps for the as-deposited (AD), oxidized (Ox) and reduced (Re) WO_X/a-Fe_2O_3 (0001) interface and projections of the α-Fe_2O_3 ball-and-stick model. The small white balls represent Fe cations and the larger brown balls are O-anions. The map for the Ox surface is recovered after a second oxidization.*

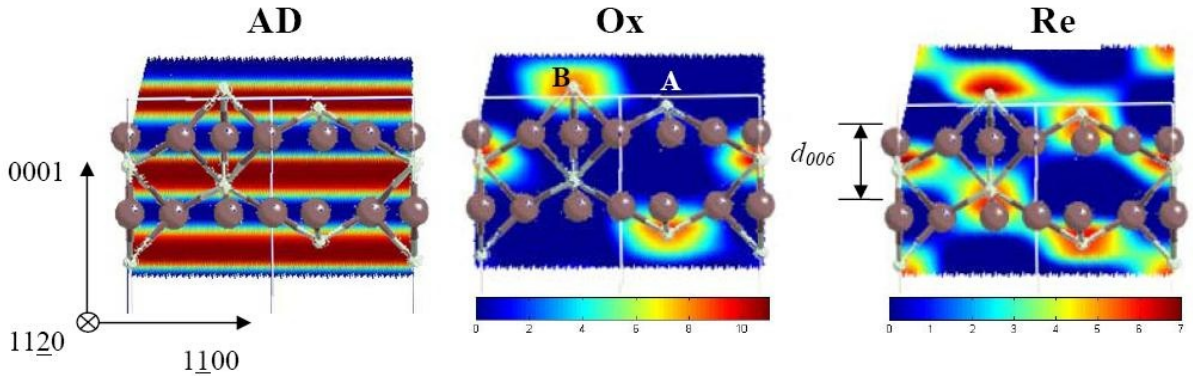

Future Plans:

- We presently use x-ray standing waves (XSW) with x-ray fluorescence (XRF) to produce element-specific 3D atomic maps of the XRF species within the interfacial structure and then we separately determine the chemical state of the interfacial species by X-ray photoelectron spectroscopy (XPS). One of our plans is to directly combine XPS with XSW to produce chemical-state-specific 3D atomic maps. This is important for cases in which we find an interfacial atom with multiple oxidation states and occupying multiple lattice sites on the supporting substrate surface.

References to publications of DOE sponsored research that have appeared in 2008-2010 or that have been accepted for publication.

1. (Cover) "Nanoscale Piezoresponse Studies of Ferroelectric Domains in Epitaxial BiFeO3 Nanostructures", S. Hong, J. A. Klug, M. Park, A. Imre, M. J. Bedzyk, K. No, A. Petford-Long and O. Auciello, J. Appl. Phys. 105, 061619-060624 (2009).
2. "Hydration and Reduction of Molecular Beam Epitaxy Grown VO_x/a-Fe_2O_3 (0001): Ambient Pressure Study", C.-Y. Kim, J. A. Klug, P. C. Stair, and M. J. Bedzyk, J. Phys. Chem. C 113, 1406-1410 (2009).
3. "Nanoscale Structure and Morphology of Atomic Layer Deposition Platinum on SrTiO3 (001)", S. T. Christensen, J. W. Elam, B. Lee, Z. Feng, M. J. Bedzyk and M. C. Hersam, Chem. Mater. 21 516-521 (2009).
4. (Cover)"Controlled Growth of Platinum Nanoparticles on Strontium Titanate Nanocubes By Atomic Layer Deposition", S.T. Christensen, J.W. Elam, F.A. Rabuffetti, Q. Ma, S.J. Weigand, B. Lee, S. Seifert, P.C. Stair, K.R. Poeppelmeier, M.C. Hersam, M.J. Bedzyk, *Small* 5, 750-757 (2009).
5. "A Ferroelectric Oxide Made Directly on Silicon", M.P. Warusawithana, C. Cen, C.R. Sleasman, J.C. Woicik, Y. Li, L.F. Kourkoutis, J.A. Klug, H. Li, P. Ryan, L.-P. Wang,

M. Bedzyk, D.A. Muller, L.-Q. Chen, J. Levy, D.G. Schlom, *Science* 324, 367-370 (2009).

6. "Spin-Charge-Lattice Coupling Through Resonant Multimagnon Excitations in Multiferroic $BiFeO_3$", M.O. Ramirez, A. Kumar, S.A. Denev, Y.H. Chu, J. Seidel, L.W. Martin, S.-Y. Yang, R.C. Rai, X.S. Xue, J.F. Ihlefeld, N.J. Podraza, E. Saiz, S. Lee, J. Klug, S.W. Cheong, M.J. Bedzyk, O. Auciello, D.G. Schlom, J. Orenstein, R. Ramesh, J.L. Musfeldt, A.P. Litvinchuk, V. Gopalan, *Appl. Phys. Lett.* 94, 161905-1 to -3 (2009).
7. "Magnon Sidebands and Spin-Charge Coupling in Bismuth Ferrite Probed By Nonlinear Optical Spectroscopy", M. O. Ramirez, A. Kumar, S. A. Denev, N. J. Podraza, X. S. Xu, R. C. Rai, Y. H. Chu, J. Seidel, L. W. Martin, S.-Y. Yang, E. Saiz, J. F. Ihlefeld, S. Lee, J. Klug, S. W. Cheong, M. J. Bedzyk, O. Auciello, D. G. Schlom, R. Ramesh, J. Orenstein, J. L. Musfeldt, . V. Gopalan, *Phys. Rev. B* 79, 224106-1 to -9 (2009).
8. "Hierarchical nanoparticle morphology for platinum supported on $SrTiO_3$ (0 0 1): A combined microscopy and X-ray scattering study", S.T. Christensen, B. Lee, Z. Feng, M. C. Hersam, M. J. Bedzyk, *Appl. Surf. Sci.* 256, 423-427 (2009).
9. "Direct Atomic-Scale Observation of Redox-Induced Cation Dynamics in an Oxide-Supported Monolayer Catalyst: WO_X/a-Fe_2O_3(0001)", Z. Feng, C.-Y. Kim, J. W. Elam, Q. Ma, Z. Zhang, M. J. Bedzyk, *J. Am. Chem. Soc.* 131, 18200-18201 (2009).
10. "A Direct-Method for Imaging Elemental Distribution Profiles with Long-Period X-ray Standing Waves", V. Kohli, M. J. Bedzyk, P. Fenter, *Phys. Rev. B* 81, 054112-1 to -14 (2010).
11. (Cover) "Effects of cantilever buckling on vector piezoresponse force microscopy imaging of ferroelectric domains in BiFeO3 nanostructures", R. Nath, S. Hong, J. A. Klug, A. Imre, M. J. Bedzyk, R. S. Katiyar, and O. Auciello, *Appl. Phys. Lett.* 96, 163101-1-3 *(*2010).
12. "Three-dimensional ferroelectric domain imaging of epitaxial $BiFeO_3$ thin films using angle-resolved piezoresponse force microscopy", M. Park, S. Hong, J. A. Klug, M. J. Bedzyk, O. Auciello, K. No, A. and Petford-Long, *Appl. Phys. Lett.* 97, 112907-1-3 (2010).

The following publications were primarily NSF sponsored, but acknowledged DOE funded facilities (Advanced Photon Source)

13. "Nanoscale Structure of Self-Assembling Hybrid Materials of Inorganic and Electronically Active Organic Phases", M. Sofos, D.A. Stone D.K. Goswami, J.S. Okasinski, H. Jin, M.J. Bedzyk, S.I. Stupp, J. Phys. Chem. C 112, 2881-2887, (2008).
14. "Probing Surface-Adlayer Conjugation on Organic-Modified Si(111) Surfaces With Microscopy, Scattering, Spectroscopy, and Density Functional Theory", J. A. Kellar, J.-C. Lin, J.-H. Kim, N. L. Yoder, K. H. Bevan, G. Y. Stokes, F. M. Geiger, S. T. Nguyen, M. J. Bedzyk and M. C. Hersam, J. Phys. Chem C 113, 2919-227 (2009).
15. "Atomic-Scale X-Ray Structural Analysis of Self-Assembled Monolayers on Silicon", J.-C. Lin, J.A. Kellar, J.-H. Kim, N.L. Yoder, K.H. Bevan, S.T. Nguyen, M.C. Hersam, M.J. Bedzyk, *Eur. Phys. J. Special Topics* 167, 33-39 (2009).
16. "X-ray absorption spectroscopy study of the local structures of crystalline Zn–In–Sn oxide thin films", D. E. Proffit, D. B. Buchholz, R. P. H. Chang, M. J. Bedzyk, T. O. Mason, and Q. Ma, *J. Appl. Phys.* 106, 113524 (2009).
17. "Building Conjugated Organic Structures on Si(111) Surfaces via Microwave-Assisted Sonogashira Coupling" J.-C. Lin, J.-H. Kim, J. A. Kellar, M. C. Hersam, S. T. Nguyen, and M. J. Bedzyk, *Langmuir Letter* 26, 3771-3773 (2010).

MAESTRO, a new facility for ARPES at the ALS

Aaron Bostwick (abostwick@lbl.gov) and Eli Rotenberg (erotenberg@lbl.gov)
Advanced Light Source, Berkeley Ca

MAESTRO, the Microscopic and Electronic Structure Observatory — is a new facility dedicated to imaging the electronic structures of *in situ* and *ex situ* prepared samples in both real and momentum space. It is a rebuild of the present sector 7 photoemission branchline (currently called the Electronic Structure Factory, or ESF) into the new MAESTRO facility with two photoemission branchlines and a dedicated insertion device. This project includes:

- the next-generation *nanoARPES* chamber for nanometer-scale photoemission.
- new beamline optics for sector 7, optimized for delivery of photons with sufficient flux and energy resolution to achieve down to 50 nm spot size.
- a sample transfer system to existing preparation/characterization chambers.

MAESTRO also integrates existing growth and characterization tools from the existing ESF facility:

- the existing μARPES endstation, which will probe down to ~10 μm sample size.
- the existing crystal growth chambers (MBE and laser-based).
- a new PEEM, already funded, to be built in FY11.

The completed MAESTRO facility is shown schematically in Fig. 1, while the overall sector layout, including new beamline and optics, is in Fig. 2. Each endstation has a branchline that shares a monochrometer and a half-length, 80mm period elliptically polarized undulator.

The beamline and endstation portion of MAESTRO was funded though the DOE SISGR / Midscale Instrumentation program in 2009. Additional funding for the front end and insertion

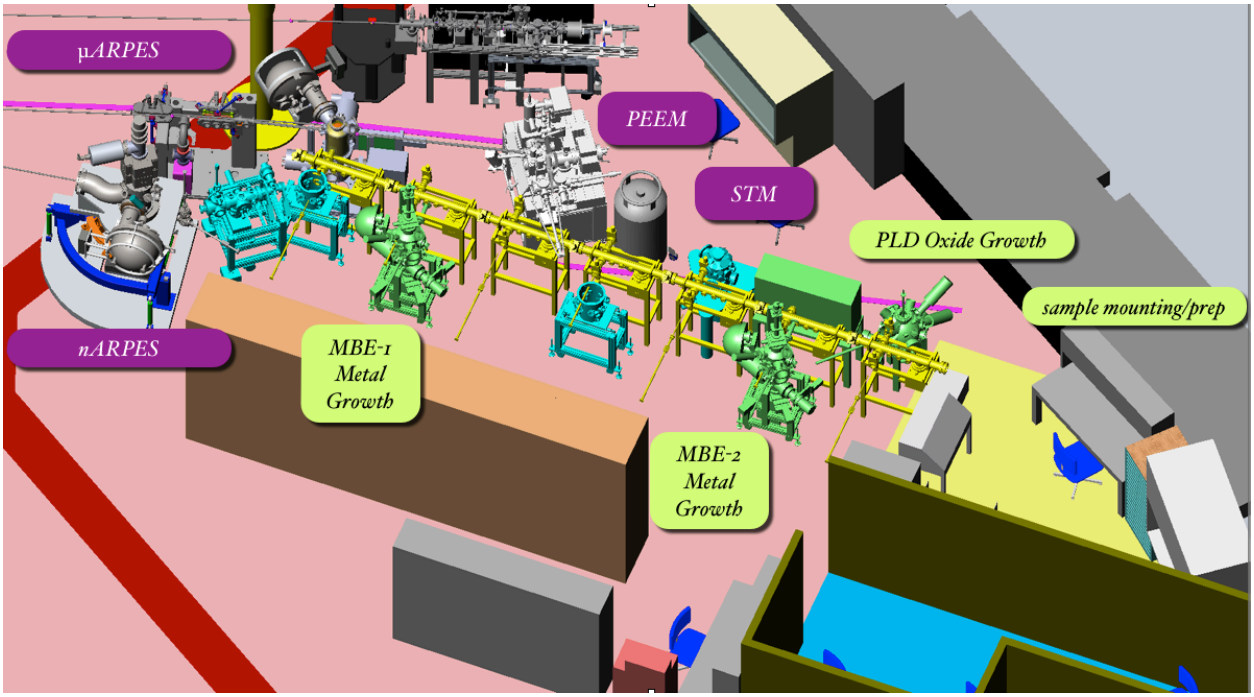

Figure 1. Conceptual CAD model of the new MAESTRO facility showing the variety of sample characterization and preparation capabilities.

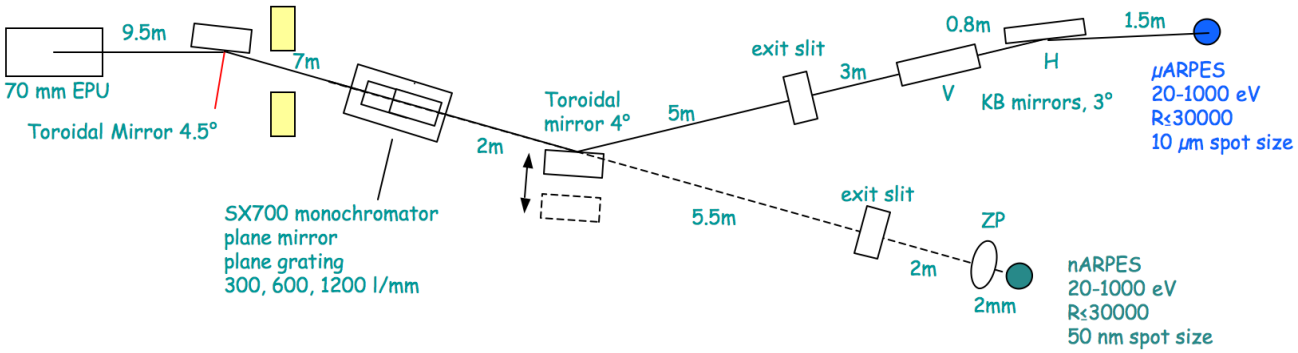

Figure 2. Optical layout of the MAESTRO beamline and branchline.

device was provided by DOE facilities. The beamline and end stations are currently under development with a estimated completion date in late 2012.

*nano*ARPES

Adaptation of ARPES to nanometer-scale spatial resolution will let us determine the electronic properties of new materials whose confined geometries are an intrinsic part of their behavior, or that exist only in nanoscale forms. As a general user facility, nanoARPES enables use-inspired discovery in materials-driven research (catalysis, hydrogen storage, solid state lighting and superconductivity). For example, segregation of nominally homogeneous correlated oxides and doped Mott-Hubbard insulators into electronically distinct domains appears to be a common phenomenon over a wide variety of length scales (many accessible to nanoARPES, see Fig. 3[1,2,3]) but its origin, whether intrinsic or extrinsic, is still obscure. NanoARPES will be able to correlate the electronic structure of individual domains with

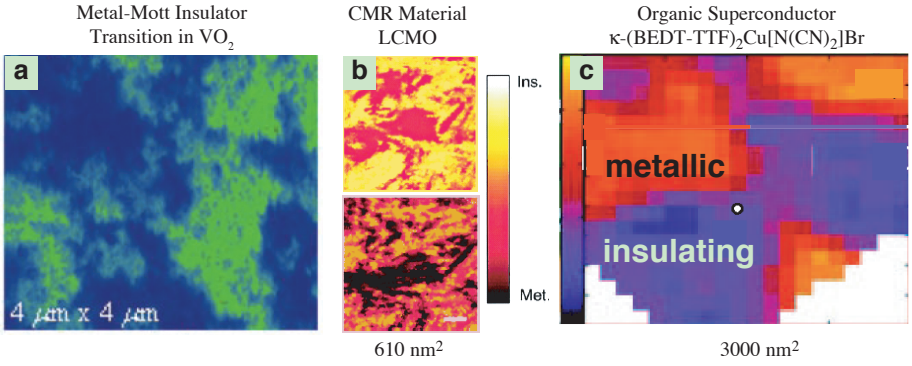

Figure 3. Spatial fluctuations in doped Mott-Hubbard insulators. (a) Metallic "puddles" in the metal-insulator phase transition in VO_2; (b) segregation of insulating and metallic phases in CMR manganite sample; (c) segregation of metallic and insulating phases in an organic superconductor [2-4].

simultaneous chemical, magnetic, and structural sensitivity to address this issue. As a second example, optimization of thermoelectrics requires control of both phonon and electron degrees of freedom, which

[1]Qazilbash, M.M., et al., Mott Transition in VO2 Revealed by Infrared Spectroscopy and Nano-Imaging. Science, 2007. 318 (5857): p. 1750-1753.

[2]Fath, M., et al., Spatially Inhomogeneous Metal-Insulator Transition in Doped Manganites. Science, 1999. 285: p. 1540-2.

[3]Sasaki, T., et al., Real Space Imaging of the Metal-Insulator Phase Separation in the Band Width Controlled Organic Mott System k-(BEDT-TTF)2Cu[N(CN)2]Br. J. Phys. Soc. Jpn., 2005. 74: p. 2351-2360.

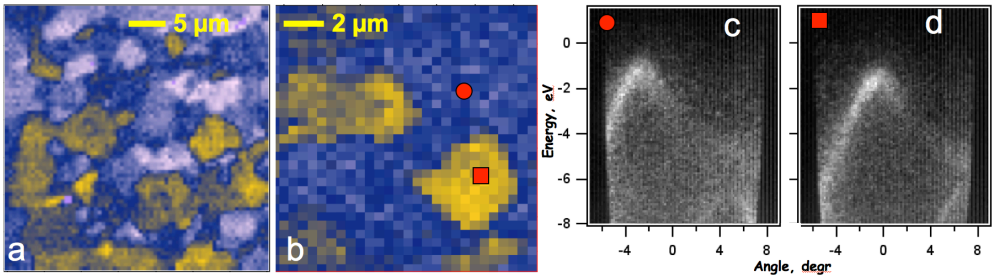

Figure 4. (a-b) nARPES images of polycrystalline (HOPG) graphite, composed of individual microscopic crystalline grains of graphite. **(c-d)** bands acquired from individual crystalline grains.

can be achieved in materials whose dimensions are comparable to phonon wavelengths.[4] Measuring the electron-phonon coupling in such systems will be possible for the first time, providing valuable information for energy utilization.

Furthermore, while the *control* of properties such as quasiparticle coherence[5], electron-phonon coupling[6], and magnetism[7] by crude macroscopic chemical doping could be studied by ARPES, with nanoARPES these properties can be studied in nanoscale gated device geometries with true electronic control of many-body interactions. For example, we plan to measure electronic properties of laterally confined, gated devices made from graphene and related materials. This program will explore the fundamental physics of such devices, which are proposed to extend Moore's law as a low-power, smaller-device replacement for silicon, and for quantum computing at room temperature.[8]

How does nanoARPES compare to other tools for spatially-resolved electronic measurements? It can provide both momentum-resolved electronic structure as well as chemical composition and structural information (obtained through core-level photoemission and photoelectron diffraction), which are missing from STM and other atomic-scale scanning probes. It can measure bandstructures with ~20 times smaller length scale and ~20 times better energy resolution than newly developed full-field angular-imaging PEEM-type detectors[9]. Therefore nARPES can spatially resolve many-body interactions and other details that cannot be measured by other techniques.

We demonstrated the feasibility of the nanoARPES technique by building a testbed endstation employing a novel scanning angular-imaging electron lens, and the results are presented in Fig. 4. By this demonstration, we have established a unique capability for small-spot ARPES, although the present capabilities scarcely fulfill the potential of the technique. The endstation is currently limited to moderate spot size (~300 nm) determined by the xray Fresnel zone plates (which are not state of the art), and its sensitivity to vibrations; it also lacks variable temperature control. These limitations will be fixed in the new nanoAPRES system currently under construction.

---

[4]DOE, Basic Research Needs for Solar Energy Utilization (2005); Hicks, L.D. and M.S. Dresselhaus, Effect of quantum-well structures on the thermoelectric figure of merit. Phys. Rev. B, 1993. 47(19): p. 12727.

[5] Hossain, M.A., et al., In situ doping control of the surface of high-temperature superconductors. Nat Phys, 2008. 4(7): p. 527.

[6]Rotenberg, E., J. Schaefer, and S.D. Kevan, Coupling between Adsorbate Vibrations and an Electronic Surface State. Phys. Rev. Lett., 2000. 84: p. 2925-8..

[7] Krupin, O., E. Rotenberg, and S.D. Kevan, Controlling the Magnetic Ground State in Cr1-xVx Films. Phys. Rev. Lett., 2007. 99 (14): p. 147208-4.

[8]Geim, A.K. and K.S. Novoselov, The rise of graphene. Nat Mater, 2007. 6(3): p. 183-191; Ohta, T., et al., Controlling the Electronic Structure of Bilayer Graphene. Science, 2006. 313: p. 951-954.

[9] Fink, R., et al., SMART: a planned ultrahigh-resolution spectromicroscope for BESSY II. Journal of Electron Spectroscopy and Related Phenomena, 1997. 84(1-3): p. 231-250.

The PULSE Institute for Ultrafast Energy Science at SLAC

P.H. Bucksbaum (Director), M. Bogan, H. Dürr, K. Gaffney, M. Gühr, A. Lindenberg, T. Martinez, D. Reis (Deputy Director), J. Stohr, SLAC National Accelerator Laboratory, phb@slac.stanford.edu

PULSE Vision Statement, 2010: The ultrafast laser science initiative underway now at the SLAC National Accelerator Laboratory, has as its centerpiece the Linac Coherent Light Source. LCLS, has been conducting user operations now for nearly a year. It routinely exceeds its original design goals, and reaches new milestones regularly in both tuning capability and instrumentation. Its x-rays are a billion times more brilliant than any other laboratory source. This new class of x-ray sources is revolutionizing many areas of science by making it possible for the first time to see atomic scale structures and simultaneously track atomic motions of the underlying nanoscale processes of energy conversion and transport.

The PULSE mission is to advance the frontiers of ultrafast science at SLAC with particular emphasis on discovery and Grand Challenge energy-related research enabled by LCLS. The PULSE Institute initiates and leads multidisciplinary collaborative research programs in studies of atoms, molecules, nanometer-scale systems, and condensed matter systems, where motion and energy transfer occurs on picosecond, femtosecond, and attosecond time scales. Ultrafast energy research at PULSE combines the disciplines of atomic and molecular physics, ultrafast chemistry and biochemistry, ultrafast condensed matter and materials science, ultrafast x-ray science, nanoscale x-ray imaging science, and the enabling science for next-generation ultrafast light and electron sources. Our metrics of success are the level of the ultrafast science challenges we address, and our progress toward and impact on their solution.

SLAC Photon Science Directorate Reorganization: PULSE has completed a transition mandated by SLAC's reorganization of the Photon Science Directorate. The Institute is no longer a research division at SLAC, but it still has the status as a Stanford University Independent Laboratory, organized under the office of the Stanford Associate Provost and Dean of Research. The DOE component of PULSE research is now organized by SLAC through two of its newly chartered research divisions. Approximately 40% of the PULSE DOE research portfolio is now managed by the newly-created SLAC Materials Science Division, while the remaining 60% is managed by a new SLAC Chemical Science Division. This annual summary concerns the Materials Science component. We anticipate that this organizational change will allow PULSE to pursue broader collaborative activities in ultrafast science.

The PULSE Institute Laboratory Building at SLAC: PULSE now occupies a newly renovated 18,000 sf laboratory and office building, formerly known as the SLAC Central Lab. This is SLAC's first venue for laboratory-scale research, and is a model for future program expansion at SLAC. The renovated space provides 18000sf of laboratory and office areas, to enable us to develop close collaborations in important ultrafast areas such as time-resolved photoemission, time-resolved x-ray scattering, support for ultrafast biological imaging, and multidimensional spectroscopy.

PULSE also takes advantage of our proximity to SSRL and to LCLS to build strong SLAC core facilities in laser science and accelerator science. PULSE research utilizes the capabilities of LCLS, but also goes beyond this. For example, PULSE has a vigorous program on high harmonics generation and associated measurement techniques for atoms and molecules on the sub-femtosecond timescale. PULSE research extends to the research floor of the SPEAR3 synchrotron at SLAC, where ultrafast lasers can create transient conditions that are probed by synchrotron radiation. Finally, PULSE develops frontier research that makes use of technologies such as ultrafast imaging of biological and nanoscale materials, and ultrafast x-ray studies of matter in extreme environments. Our aim is to establish the leadership of SLAC research in these areas to solve fundamental challenges in basic energy science.

Education and Outreach: The major educational, physical research, engineering research, and medical research activities at Stanford provide strong support for all of our activities in PULSE. In addition, PULSE has run a successful international ultrafast X-ray Summer School. **The Ultrafast X-ray Summer School** is a five day residential program hosted annually by PULSE. The goal is to disseminate information and train students and post-docs on new opportunities in ultrafast science, particularly using X-ray Free Electron Lasers. Lectures are presented by expert scientists in this exciting new field. The attendees are expected to

participate in the discussions and to prepare a mock beamtime proposal poster with input from the instrument scientists for the Linac Coherent Light Source. This year's Ultrafast X-ray Summer School was co-directed by Aaron Lindenberg and Ken Schafer. Next year we will begin an arrangement with CFEL at DESY to alternate responsibility for the summer school. The school will be directed by CFEL scientist Robin Santra, with PULSE scientist Hermann Duerr as co-chair.

PULSE maintains a **visitors program** to enable researchers from around the world to work in our center. These visitors are extremely valuable to the PULSE primary research program. Visitors are given an office, access to PULSE laboratories and institute services, and some expense reimbursement, according to SLAC rules. PULSE extends to them the Stanford designation of Visiting Scientist or Visiting Professor (in line with their rank at their home institution), which entitles them to access to the Stanford Housing Office and the use of the Stanford Library. The budget for this program is relatively modest, particularly when one considers that a senior investigator with major talents and established abilities can be associated as a sabbatical visitor for a year, for less than the cost of a Postdoc. In 2009-2010 the sabbatical visitors were Steve Durbin (Purdue), Ken Schaffer and Mette Gaarde (LSU) and Jon Marangos (Imperial).

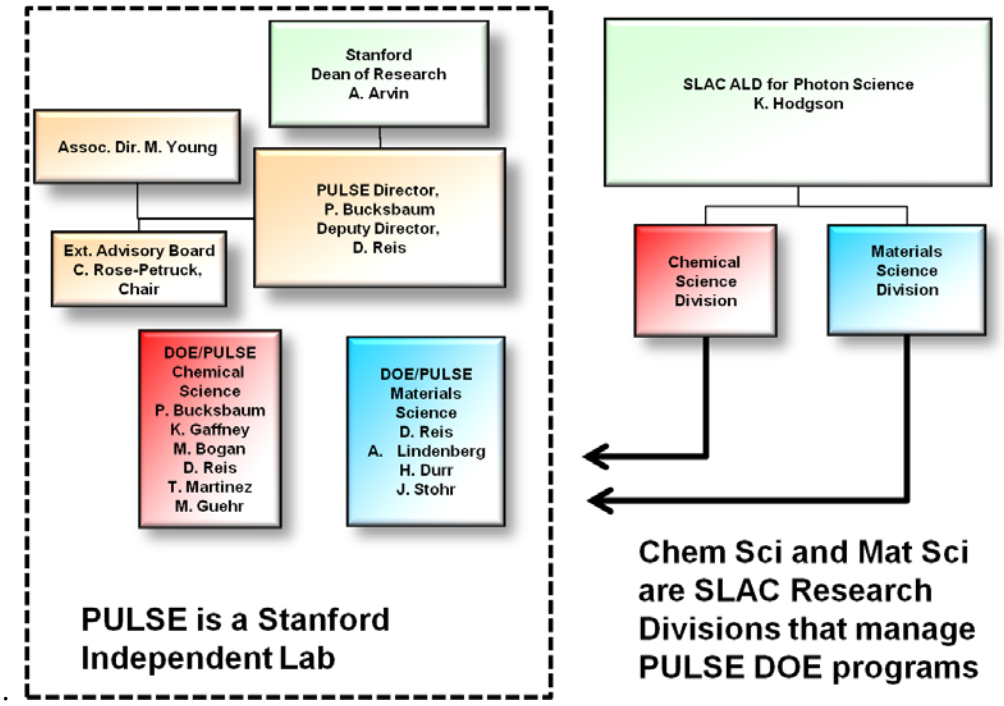

Organization Chart for the PULSE Institute

Tasks supported by the Materials Sciences X-ray Scattering Program of BES: The PULSE tasks in this program are aimed at observing, understanding and controlling ultrafast processes in materials. The emphasis is on grand challenges for energy science that can be addressed using the capabilities of the PULSE Institute and the SLAC National Accelerator Laboratory. The research utilizes our core strengths in magnetic materials (Durr and Stohr), non-equilibrium and nonlinear electronic and phonon interactions (Reis), terahertz scattering and nanoscale phase transitions (Aaron Lindenberg). All tasks that have been approved by the BES Materials Science Division are integrated within the SLAC Materials Science Division and managed as a single coherent unit. This research is described in separate abstracts in this book.

Find out more: http://pulse.slac.stanford.edu

Understanding Domain Formation, Interactions and Dynamics

J. D. Budai, J. Z. Tischler, B. C. Larson and G. E. Ice
Materials Science & Technology Division, Oak Ridge National Laboratory
P.O. Box 2008, Oak Ridge TN. 37831-6116
budaijd@ornl.gov

RESEARCH SCOPE

The central research theme is to investigate structural interactions between individual domains in order to understand the underlying origins of physical properties. Domain interactions play a ubiquitous role in materials physics, and consequently, advanced synthesis and processing methods are often based on controlling domain sizes, shapes, strains and orientations. For example, local phase competition and phase separation in strongly-correlated electron systems give rise to exotic macroscopic electronic properties such as colossal magnetoresistance (CMR), metal-insulator transitions (MIT) and superconductivity. In structural materials, strength is largely determined by grain sizes, textures, and defect densities. Thus, understanding how to control local domain morphologies and dynamics can aid our ability to develop advanced materials ranging from novel electronic devices to higher-strength alloys.

In order to probe the local microstructure, composition, strain and defect densities, our research makes use of advances in synchrotron focusing optics and x-ray microscopy techniques. In particular, we use the spatially-resolved, submicron microdiffraction and microfluorescence capabilities developed at the Advanced Photon Source sector 34 to obtain non-destructive, *in-situ* 2D and 3D quantitative measurements of the local lattice structure, orientation (resolution ~0.01°) and strain tensor ($\Delta d/d \sim 10^{-4}$).

Our research emphasizes local structural interactions in three materials areas:
(1) The relationship between structural and electronic domains in strongly-correlated oxides
(2) The effect of grain interactions in polycrystal 3D grain growth
(3) The local structure within individual nanostructures.

In each case, structural features at nanoscale or mesoscopic lengths play a critical role in determining materials properties. *(1)* In complex oxides such as manganite systems, strong electronic correlations lead to rich phase diagrams, inhomogeneous spatial variations, and interesting physical phenomena. The structural inhomogenieties vary from nanoscale composition and strain fluctuations to large phase-separated domains, and fundamental questions involving how the lattice couples with the electronic and magnetic domains remain unanswered. *(2)* In polycrystalline structural materials, controlling grain morphologies and orientations is a key processing goal for thermomechanical treatments. Previous x-ray and neutron studies have characterized only the ensemble-averaged grain sizes and texture development. X-ray microscopy now provides measurements of 3D grain growth with submicron-spatial resolution, and hence enables direct comparisons with computer models of the local grain-by-grain interactions. *(3)* Increasingly sophisticated nanostructures can be synthesized and x-ray microscopy provides quantitative maps of the internal lattice and domain structures. As x-ray beams become smaller and more intense, it is now possible to map the internal domain structure and dynamics of individual nanocrystals and microcrystals. Our future research in this area will overlap with our investigations of complex oxides, as we will perform *in-situ* microdiffraction studies of domain interactions during metal-to-insulator transitions in individual complex oxide microcrystals.

RECENT PROGRESS

X-ray investigations of domain formation interactions and dynamics are being pursued in collaborations with researchers carrying out related work in x-ray optics, materials synthesis and theoretical modeling.

Phase Separation in Manganites –We have investigated the coupling between structural and electronic phase separation in complex oxide manganite systems using both epitaxial thin films and bulk materials. Complex physical phenomena such as CMR are understood as emerging near phase boundaries from the interactions between coexisting conducting and insulating domains. We have used LaPrCaMnO films grown on different substrates ($SrTiO_3$, $LaAlO_3$, $SrLaGaO_3$, $NdGaO_3$) to investigate the effect of stress on domain formation and dynamics. Temperature-dependent synchrotron x-ray measurements showed that substrate-induced stresses can be used to directly control the orientations of orthorhombic perovskite LPCMO domains and can generate anisotropic tensile or compressive in-plane strains. Figure 1 shows x-ray orientation and strain measurements from an epitaxial film grown on $NdGaO_3$.[4] In the same sample, temperature-dependent resistivity measurements along two perpendicular in-plane directions revealed a large anisotropy and significant differences in the percolative metal-insulator transition temperature. We conclude that a preferential orientation of electronic domains is driven by anisotropic long-range strains. These observations suggest that electronic phase domains are more strongly coupled to the lattice strain than to chemical inhomogeneities. We subsequently attempted to directly observe strain domains in LPCMO films using low temperature x-ray microdiffraction to map lattice parameter fluctuations near the transition. Spatially-resolved strain measurements with a ~1 μm diameter x-ray beam did not reveal spatially-separate domains, implying either averaging over nanoscale domains or MIT strain fluctuations less than $\Delta d/d \sim 10^{-4}$.

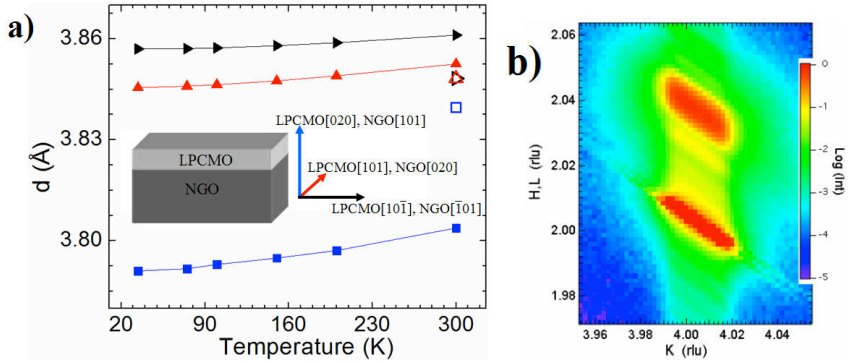

Fig. 1. *(a) Temperature dependent lattice parameters for an epitaxial LPCMO film on a $NdGaO_3$ substrate. (b) Reciprocal-space diffracted intensity at 120K showing that the film is commensurate.*

To directly observe spatially-resolved domains, we have also performed x-ray microdiffraction studies of bulk directionally-solidified, eutectic manganite systems consisting of self-organized patterns of large chemically-separate phases. Both (Y,Eu)MnO and (Lu,LaSr)MnO systems (grown by S-W Cheong, Rutgers) exhibit micron-scale coexistence of separate single-crystal lamellar domains (hexagonal/orthorhombic and hexagonal/rhombohedral respectively). These multiferroic systems provide an opportunity to directly map the 3D domains and strain fluctuations. We find that the orientations of the lamellae are consistent with energetic crystal growth predictions and with the formation of low-energy, semi-coherent interfaces. In addition, we observe a bias for larger strain fluctuations in the hexagonal phase and speculate that a smaller number of slip planes are active to relieve thermal stresses in this phase.

3D Grain Growth in Aluminum – Using 3D micron-resolution x-ray measurements of thermal grain growth in polycrystalline aluminum, we have demonstrated that the evolution of grain orientations, grain morphologies and local defect densities can be obtained.[10] By mapping the same sample volume after each annealing step, we observed the migration of particular boundary types and observed larger more-perfect grains consuming smaller less-perfect grains. Computer modeling comparisons with Tony Rollett (Carnegie-Mellon) showed that simple, isotropic curvature-driven models are not consistent with the x ray data, and that lattice orientations, boundary anisotropies and intragranular defect densities all play significant roles in controlling local grain growth. These results also showed that comparisons between theory and experiment were limited by the invasion of grains originating outside the limited sample volume. Thus, although these results represent the first nondestructive, high-resolution measurements of 3D grain growth and affirm the potential for direct quantitative comparison with computer models, they also reveal the pressing need to collect significantly larger data sets.

Individual Nanocrystals and Microcrystals – Using advanced x-ray focusing, we have investigated the microstructure within individual nanocrystals and microcrystals. Like bulk materials and thin films, nanostructures can incorporate local defects and different domains. However, small sizes and large surface to volume ratios can lead to novel materials behaviors and properties. Figure 2 shows x-ray induced photoluminescence (PL) propagating along an individual EuAlO nanorod lightpipe (fabricated by Z.W. Pan, UGa) and a Laue microdiffraction pattern. With different compositions and synthesis, these novel luminescent materials exhibit PL changes covering the full optical spectra and different lattice structures, growth morphologies and orientations. Structural measurements have been correlated with the optical properties, and x-ray microdiffraction has identified two new lattice structures that are not known to exist in bulk materials.

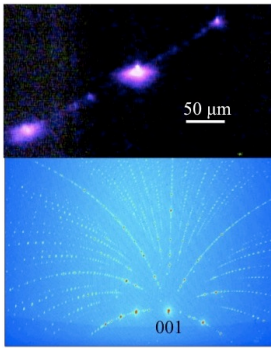

Fig. 2. *(Top) Photo of photoluminescence along individual EuAlO nano-lightpipe. (Bottom) Laue microdiffraction reveals new crystal structure.*

FUTURE PLANS

Our goal in this program is to investigate how local domain formation, interactions and dynamics give rise to macroscopic physical properties. The motivation and crucial advance is that spatially-resolved measurements enable us to examine the *local* 3D microstructure and evolution of *individual interacting grains or phases*. This capability presents opportunities for directly testing theoretical models and will guide the development of a predictive understanding of domain structures and dynamics. Scientific progress will make use of ongoing research collaborations to exploit new developments in materials synthesis, x-ray optics and x-ray techniques.

Understanding how local structural domains couple with electronic and magnetic degrees of freedom will remain a major research thrust in our studies of correlated electron materials. We will use 3D x-ray microdiffraction to study the 3D grain morphology and strain fluctuations associated with self-organization into conducting ferromagnetic, and insulating antiferromagnetic domains. In particular, we will examine whether particular domain morphologies, orientations or strain fields give rise to local chemical or electronic effects such as changes in orbital ordering. As nanoscale x-ray beam sizes become available, we will attempt to determine whether or not electronic phase separation induces nanoscale strain domains in epitaxial manganite films. Quantifying the coupling between electronic and structural domains should provide new insight into the mechanisms driving physical behaviors near phase transitions.

We will combine our research interests in complex oxides and nanostructures in microdiffraction studies of domain formation and dynamics associated with the metal–insulator transition (MIT) in VO_2 microcrystals. VO_2 is a strongly-correlated electron material exhibiting a first-order phase transition from a monoclinic M1 insulator to a higher-symmetry tetragonal (rutile R) metal at around 67°C. The underlying mechanisms ("Mott" electron-electron versus "Peirls" electron-lattice) driving this MIT remain controversial for this relatively simple lattice. We have tested our ability to obtain and analyze microdiffraction measurements from individual VO_2 microcrystals at room temperature. As shown in the stereographic projections in Fig. 3, Laue microdiffraction can identify different individual M1 domain orientations and map domain boundaries. We will use temperature dependent, spatially-resolved measurements to investigate how domains evolve and interact as the microcrystal is cycled through the MIT. We will map local boundary strains, investigate conditions under which other possible phases (monoclinic M2 and triclinic T) can occur, and study how particular microcrystal sizes and substrate strains influence the MIT and phase-coexistence. We will compare x-ray

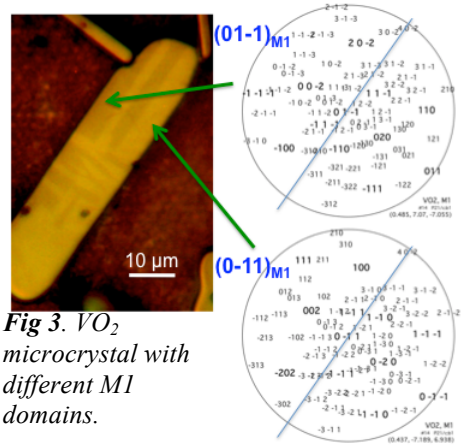

Fig 3*. VO_2 microcrystal with different M1 domains.*

structural measurements with scanning micro-Raman spectroscopy and near-field scanning microwave microscopy results in order to correlate structural and electronic domain behaviors.

We will also pursue our goal of understanding how local interactions drive 3D thermal grain growth by obtaining large-volume, micron-resolution data sets mapping the intergranular and intragranular structural evolution in polycrystalline metals such as aluminum. To accomplish this, we have acquired a faster x-ray detector system and will develop the needed accelerated "on-the-fly" experimental x-ray techniques. The resulting measurements will enable investigations of local grain-by-grain interactions involving lattice anisotropy, boundary mobilities, strain effects, internal dislocation densities, and precipitate pinning. All must be understood in order to develop predictive capabilities for accurately modeling final microstructures and understanding the structural origins of physical properties. In general, the effects of these microstructural features have been compared only with ensemble-averaged measurements; they now can be quantitatively examined in detail. In particular, since the local defect density (e.g. dislocations) associated with the final stages of recrystallization can affect boundary migration, future modeling work will incorporate energy reductions associated with internal defects. The ability to quantitatively measure substructure of this kind will provide a new opportunity to experimentally establish how local microstructure drives 3D grain evolution.

Publications of DOE Sponsored Research 2008-2010

1. S.V. Kalinin, B.J. Rodriguez, J.D. Budai, S. Jesse, A.N. Morozovska, A.A. Bokov, and Z.G. Ye, "Direct evidence of mesoscopic dynamic heterogeneities at the surfaces of ergodic ferroelectric relaxors," *Physical Review B* **81**, 064107 (2010).

2. A. Tselev, E. Strelcov, I.A. Luk'yanchuk, J.D. Budai, J.Z. Tischler, I.N. Ivanov, K. Jones, R. Proksch, S.V. Kalinin, and A. Kolmakov, "Interplay between Ferroelastic and Metal-Insulator Phase Transitions in Strained Quasi-2D VO_2 Nanoplatelets," *Nano Letters* **10**, 2003-2011 (2010).

3. P. Pant, J.D. Budai, et al and J. Narayan, "Nonpolar ZnO film growth and mechanism for anisotropic in-plane strain relaxation," *Acta Materialia* **58**, 1097 (2010).

4. T.Z. Ward, J.D. Budai, Z. Gai, J.Z. Tischler, L. Yin, and J. Shen, "Elastically-Driven Anisotropic Percolation in Electronic Phase-Separated Manganites," *Nature Physics* **5**, 885-888 (2009).

5. G.E. Ice, J.W.L. Pang, B.C. Larson, J.D. Budai, J.Z. Tischler, J.-Y. Choi, W. Liu, C. Liu, L. Assoufid, D. Shu, and A. Khounsary "At the Limit of Polychromatic Microdiffraction," *Mater. Sci. Eng. A* **524**, 3-9 (2009).

6. P. Pant, J.D. Budai, R. Aggarwal, R.J. Narayan and J. Narayan, "Thin film epitaxy and structure property correlations for non-polar ZnO films," *Acta Materialia* **57**, Issue 15 4426-4431 (2009).

7. P. Pant, J.D. Budai, R. Aggarwal, R.J. Narayan and J. Narayan, "Structural characterization of two-step growth of epitaxial ZnO films on sapphire substrates at low temperatures," *Jour. of Physics D: Appl Phys.* **42**, 105409 (2009).

8. L.C. Tien, D.P. Norton and J.D. Budai, "Epitaxial growth of transparent tin oxide films on (0 0 0 1) sapphire by pulsed laser deposition," *Materials Research Bulletin* **44**, 6-10 (2009).

9. Z.W. Pan, J.D. Budai, Z.R. Dai, M.P. Paranthaman, S. Dai, and D.H. Lowndes, "Zinc Oxide Microtowers by Vapor Phase Homoepitaxial Regrowth," *Advanced Materials* **21**, 890-896 (2009).

10. J.D. Budai, W. Liu, J.Z. Tischler, Z.W. Pan, D.P. Norton, B.C. Larson, W. Yang and G.E. Ice, "Polychromatic X-ray Micro- and Nanodiffraction for Spatially-Resolved Structural Studies," *Thin Solid Films* **516**, 8013–8021 (2008).

11. K.H. Kim, D.P. Norton, D.K. Christen, and J.D. Budai, "Formation of oxidation-resistant Cu-Mg coatings on (001) Cu for oxide superconducting tapes," *Surface & Coatings Technology* **202**, 5136 (2008).

12. M. Ivill, S.J. Pearton, S. Rawal, L. Leu, P. Sadik, R. Das, A.F. Hebard, M. Chisholm, J.D. Budai and D.P. Norton, "Structure and magnetism of cobalt-doped ZnO thin films," *New Journal of Physics* **10**, No 6, 065002 (2008).

13. A. Narayanaswamy, J. McBride, L.A. Swafford, S. Dhar, J.D. Budai, L.C. Feldman and S.J. Rosenthal, "Synthesis and characterization of porous TiO_2 with wormhole-like framework structure," *J. Porous Materials* **15**, 21-27 (2008).

14. C. Callender, D.P. Norton, R. Das, A.F. Hebard, and J.D. Budai, "Ferromagnetism in Pseudo-Cubic $BaFeO_3$ Epitaxial Films," *Applied Physics Letters* **92**, 012514 (2008).

Synchrotron Studies of Systems with Strong Correlations

Dr. Clement Burns
Dept. of Physics
1120 Everett Tower
Western Michigan University
Kalamazoo, MI 49008-5252
Ph: 269-387-4921
clement.burns@wmich.edu

1. Research Scope

Our work involves studies of strongly correlated condensed matter systems using synchrotron x-ray sources. Much of the work involves using inelastic x-ray scattering (IXS) to study the electronic and vibrational excitations in these systems. Development of instrumentation for IXS is also a strong priority. IXS offers the ability to probe a variety of excitations at moderate energies and high momentum transfers *q* that cannot be studied with other techniques. High resolution (meV) IXS allows the study of phonon excitations, while moderate resolution (100 meV) is more appropriate for studies of electronic excitations. Resonant inelastic x-ray scattering (RIXS) is used to study electronic excitations, and is a special case which occurs when the incident energy is tuned to the energy of an atomic transition (absorption edge). For our purposes, this will be the excitation of a core electron with an energy on the order of keV. RIXS allow studies with element selectivity and can provide a large increase in the scattering rate for certain excitations.

Recent work has concentrated on implementing of polarization analysis of the scattered x-ray in RIXS. Other work has included 1) low temperature x-ray diffraction on the so-called supersolid state in solid ^{4}He, 2) inelastic x-ray scattering studies of the highly correlated liquid metal systems formed by alkali metals in liquid ammonia, and 4) phonon shifts at the superconducting transition in organic superconductors.

2.0. Recent Progress

2.1 Development of polarization analysis for RIXS

The main goal of the current grant is to add the capability for polarization analysis to RIXS. Polarization is one of the three characteristics of a scattered x-ray (along with energy and momentum), but is currently not measured. Polarization studies offer additional information useful for determining the initial and final states of the electronic excitations which are observed. In addition, under certain circumstances, polarization analysis reduces the elastic background and therefore may allow a study of lower energy excitations. Polarization analysis for inelastic x-ray scattering is also one of the stated goals of the APS Upgrade project.

Currently this work is taking place under a Partner User Proposal (PUP) with the APS which provides dedicated beamtime for the project. Our goal is to create a polarization instrument which we can use for our work but which will also be eventually made available for other users. Workers at other x-ray facilities (i.e., SPring-8) are also proceeding along these lines. The Japanese group working on this uses the 006 reflection of flat graphite for their analyzer. However, the efficiency is only about 2%. Considering the low count rate for inelastic x-ray scattering, we feel that a higher efficiency is needed, and indeed we have designed and tested an optical scheme with a measured efficiency of about 12%; in theory, the scheme can yield 2-3 times higher efficiencies than this.

The basic geometry of inelastic x-ray scattering measurements involves an analyzer crystal and a detector which are both on the Roland circle (the distance from the sample to the analyzer is the same as the distance from the analyzer to the detector). However, this condition cannot be met for the entire analyzer but only a point at the center. An exact solution for the analyzer shape (the so-called Johannson geometry) is known. We designed a shape to provide a good approximation to the required shape and had highly oriented pyrolytic graphite (HOPG) grown on the surface. The initial alignment of the polarization element was time-consuming, but we now have a procedure for aligning that is relatively quick. Fig. 1 shows initial data on the spin Peierls compound $CuGeO_3$ in the sigma-sigma scattering channel. The arrows show the position of peaks we found in our earlier work (without polarization analysis). Even with the short counting time (due to the long setup time) we are able to observe the electronic excitations.

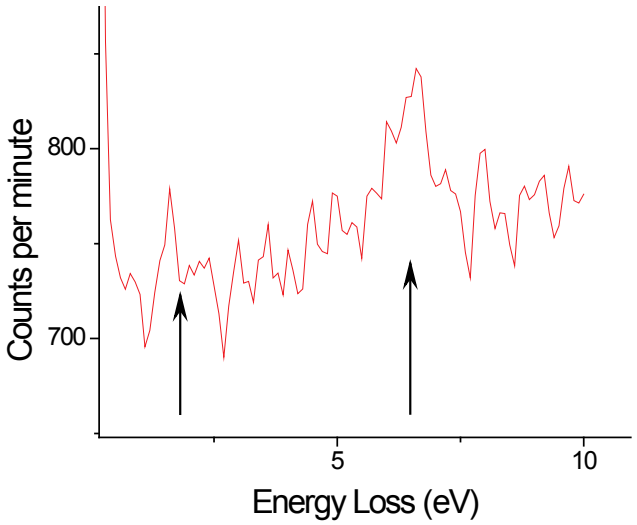

Fig. 1. Initial polarization data on the spin Peierls compound $CuGeO_3$. Incident energy was 8.977 keV, with momentum transfer along the 1-*d* chains.

Several challenges remain. First, the energy resolution is about 600 meV, a factor of two worse than we calculated. We think one of the main causes is a small misalignment of the detector; in our next run we will add motorized motion for the detector. Our setup will then have six motorized motions for alignment of the polarization crystal, which allows a systematic alignment procedure and corrections for small errors in the curvature and position of the optic.

2.1 Low temperature x-ray diffraction in solid ^{4}He

Recent measurements[1] have found non-classical rotational inertia (NCRI) in solid ^{4}He starting at T ~ 200 mK, leading to speculation that a supersolid state may exist in these materials. Differences in the NCRI fraction due to the growth method and annealing history imply that defects play an important role in the effect. Using x-ray synchrotron radiation, we have studied [Publications 4 and 5] the nature of the crystals and the properties of the defects in solid ^{4}He at temperatures down to 50 mK. Measurements of peak intensities and lattice parameters do not show indications of the supersolid transition. Using growth methods similar to those of groups measuring the NCRI we find that large crystals (dimensions ~mm) form. Scanning with a small (down to 10 x 10 μm^2) beam, we resolve a mosaic structure within these crystals consistent with small angle grain boundaries. The mosaic shows significant shifts over time even at temperatures far from melting (see Fig. 2). Our main conclusion is that there are

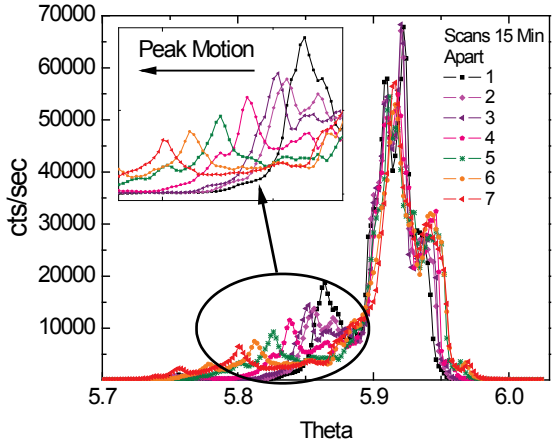

Fig. 2. Intensity vs. crystal angle at T = 1.75 K (T_m ~ 2.6 K) in a crystal of ^{4}He. Scans were taken fifteen minutes apart and show the variation with time of the mosaic structure, indicating that the defects do not become "frozen in" even well below the melting temperature.

a large number of mobile defects in these materials, even far from melting.

We have also studied these materials in restricted geometries such as aerogel and Vycor, where the supersolid phase is also found. Fig. 3 shows the power diffraction in aerogel. The structure in the rings (the variation in intensity) indicates a strong texture in the material and implies correlations in the powder orientation during the growth process.

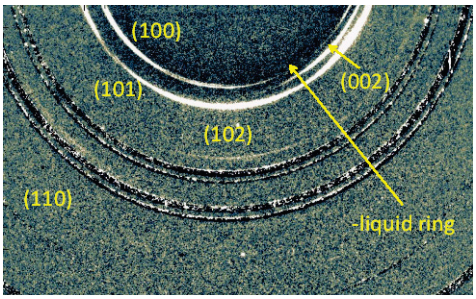

Fig.3. The powder pattern for a solid helium sample in aerogel at 60 bar. The rings corresponding to the first 5 reflections of an hcp structure are indicated.

2.3 **Inelastic x-ray scattering in metal ammonia systems**

Systems created by dissolving elemental metals in liquid ammonia are strongly correlated liquid metals where the electronic correlation strength can be easily changed by altering the electronic density. We have studied [Publication 7] the plasmon in the lithium ammonia system as a function of electronic density using non-resonant inelastic x-ray scattering (IXS), and use this to determine the long wavelength plasmon energy E_0 and the plasmon dispersion α as a function of electronic density. The plasmon becomes broader and its dispersion decreases rapidly as we go to lower concentration. We find the density dependence of the exponent of the dispersion coefficient to be larger by an order of magnitude than predicted by the RPA, suggesting a strong increase in the importance of electronic correlations as the density is decreased. The plasmon width increase at lower concentration is consistent with a reduction in screening and behavior that is further removed from a nearly free electron gas.

Fig. 4 shows data at 16 mole percent metal and illustrates the general properties of the plasmon. The plasmon peak grows in intensity, widens, and disperses to higher energies as the q value increases. Above q_c the plasmon broadens rapidly and quickly becomes difficult to distinguish from the background.

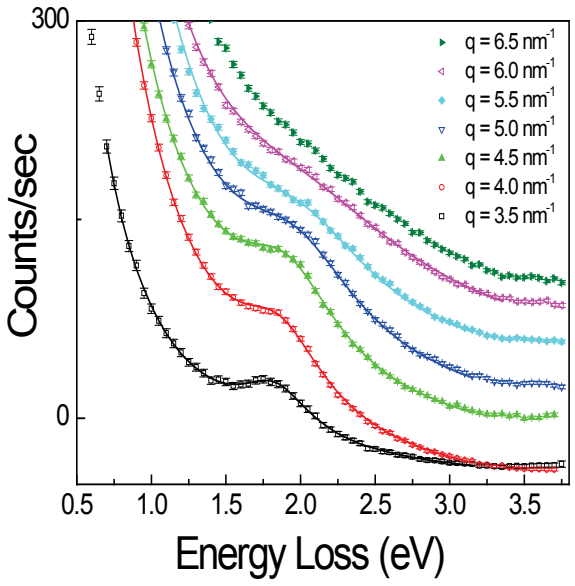

Fig. 4. The plasmon at 16 mole percent metal. The peak disperses to higher energies at higher q values as expected. In addition, the width of the peak increases. Above the cutoff vector q_c ~ 0.61 nm^{-1} the plasmon can decay into electron-hole pairs and broadens rapidly.

2.2.2 Organic superconductors

We have continued our work in the area of phonon shifts at the superconducting transition in exotic organic superconductors. In particular we have studied the shifts in the phonons in κ-(BEDT-TTF)$_2$-Cu(NCS)$_2$ where (BEDT = Bis(ethylenedithio) tetrathiafulvalene. Over the last year we extended our studies to include κ-(BEDT-TTF)$_2$-Cu(N(CN)$_2$)Br. Both of these systems are believed to have *d*-wave superconductivity. We see clear shifts in the phonon spectrum of both samples, with a dependence on the energy of the phonons as well as the direction. These shifts are predicted to depend on the energy of the gap, so in principle we may be able to directly determine the energy gap and its symmetry from these measurements. This would provide a direct means for determining the energy gap along different directions, which is difficult to

do with bulk transport measurements. We are currently analyzing the data. We have also been involved in a similar experiment on an iron arsenic superconductor, but in this case where unable to resolve any shifts.

3.0 Future Plans

1. Further improvements in polarization analysis instrumentation. In particular we will be implementing the use of single crystal silicon for the optic, which should greatly increase the efficiency and energy resolution.
2. Begin detailed studies of the polarization scattering in copper germinate and on systems such as the cuprates.
3. More detailed analysis of the phonon shift in the organic superconducting systems is underway, which we hope will allow us to determine the superconducting gap structure.

4.0 Publications from DOE funded Research

1) A. Alatas, A.H. Said, H. Sinn, G. Bortel, M.Y. Hu, J. Zhao, **C. A. Burns,** E. Burkel, and E. E. Alp, "Atomic form-factor measurements in the low-momentum transfer region for Li, Be, and Al by inelastic x-ray scattering", *Phys. Rev. B* 77, 064301 (2008).
2) **C. A. Burns**, "Is Lithium Ammonia Suitable for a Liquid Lunar Telescope?", *Pub. Astron. Soci. Pac.*, 864, 188 (2008).
3) C. N. Kodituwakku, **C. A. Burns**, A. H. Said, H. Sinn, X. Wang, T. Gog, D. M. Casa, and M. Tuel, "Resonant Inelastic X-ray Scattering Studies of the Organic Semiconductor Copper Phthalocyanine", *Phys. Rev. B* 77, 125205 (2008).
4) N. Mulders, J. West, M. H. W. Chan, C. N. Kodituwakku, **C. A. Burns**, and L. B. Lurio "Torsional oscillator and synchrotron x-ray experiments on solid helium in aerogel", *Phys. Rev. Lett.,* 101, 165303 (2008).
5) **C. A. Burns**, N. Mulders, L. Lurio, M. H. W. Chan, A. Said, C. N. Kodituwakku, and P. M. Platzman, "X-ray Studies of Structure and Defects in Solid ^{4}He from 50 mK to Melting" *Phys. Rev. B*, 78, 224305 (2008).
6) T. Gog, G. T. Seidler, D. M. Casa, M. H. Upton, Jungho Kim, Yu. Shvyd'ko, S. Stoupin, K. P. Nagle, M. Balasubramanian, R.A. Gordon, T. T. Fister, S. M. Heald, T. Toellner, J.P. Hill, D.S. Coburn, Y.-J. Kim, A.H. Said, E. E. Alp, W. Sturhahn, H. Yavas, **C. A. Burns**, and H. Sinn, "Momentum-Resolved Resonant and Nonresonant Inelastic X-ray Scattering at the Advanced Photon Source", Synchrotron Radiation News **22,** 12 (2009).
7) X. Wang, **C. A. Burns**, A. H. Said, C. N. Kodituwakku, Y. V. Shvyd'ko, D. Casa, T. Gog, and P. M. Platzman, "Evolution of a Strongly Correlated Liquid with Electronic Density", Phys. Rev. B **81**, 075104 (2010).

[1] E. Kim, M. H. Chan, Nature 427, 225 (2004).

Understanding the phase diagram of the cuprate superconductors

Juan Carlos Campuzano
Materials Science Division
Argonne National Laboratory
9700 S. Cass Ave.
Argonne, IL 60439

e-mail: campuzano@anl.gov

Scope of research

My collaborators and I aim to understand the electronic excitations in the high temperature superconductors, and their evolution with doping and temperature, using angle resolved photoemission (ARPES) as the main probe. These cuprates evolve from Mott insulators as charge carriers are added. While much effort has been invested in understanding these materials, and certainly great progress has been made, much remains to be learned. Earlier work concentrated on many of the unusual phenomena, such as the d-wave superconducting order, the pseudogap above the superconducting transition in underdoped samples, etc. Fundamental questions remain, such as the nature of the overall phase diagram, the evolution of the material from an insulator to a superconductor at low temperatures, the same evolution at higher temperatures into a normal state which is not yet understood, etc. These questions require far more systematics, such as a large number of doping values, samples with various chemical substitutions, and studies at a large number of temperatures.

Recent progress

What lies before the superconducting phase: The nodal liquid.

This work concerns the electronic excitations of the non-superconducting state that exists between the antiferromagnetic Mott insulator at zero doping and the superconducting state in $Bi_2Sr_2CaCu_2O_{8+\delta}$ (Bi2212). The antiferromagnetic ground state and low-energy excitations in the Mott insulator are well understood. The d-wave nature of the superconducting ground state and its low-lying excitations are also well understood. In between these two phases, for dopings $>0<0.05$ electrons per Cu atom, lies an electronic ground state whose nature is poorly understood.
There is little spectroscopic data at low temperatures in this doping range. A crucial problem has been obtaining samples for these doping values for Bi2212. We have obtained ARPES data on single crystals and thin films whose doping levels range all the way from the insulator to the over-doped superconductor, focusing in particular on non-superconducting thin films with an estimated hole doping of ~ 0.04. These samples have an insulating upturn in resistance $R(T)$ with decreasing temperature that is well described by 2D-variable range hopping. We have measured the diamagnetic susceptibility down to 1.5 K, and found no trace of superconductivity, with a sensitivity of 1% of the volume fraction.

We find that the state for a doping of ~ 0.04 exhibits some highly unusual features, as its Fermi surface exists only at four points in the Brillouin zone. Quite unlike regular metals, the electronic excitations are not coherent, even at low temperatures. This state has been envisioned in some exotic theories, and called the "nodal metal". Notably, despite exhibiting a resistivity characteristic of an insulator and the absence of coherent quasiparticle peaks, this material has the same gap structure as the d-wave superconductor. We observe a smooth evolution of the spectrum across the insulator-to-superconductor transition, which suggests that high temperature superconductivity emerges when quantum phase coherence is established in a non-superconducting nodal liquid.

We also find the surprising result that the maximum spectral gap follow a simple d-wave behavior for *all* samples, superconducting and non-superconducting. This '*d*-wave' gap is universal in nature, and does not distinguish between the *d*-wave superconductor and the low temperature pseudogap phase. The maximal energy gap values monotonically increase with underdoping, although they might decrease near the superconductor-insulator boundary.

Our results confirm an earlier extrapolation, based on ARPES measurements above T_c for underdoped superconducting samples, that the low temperature pseudogap phase should be characterized by a node along the zone diagonal. They are also consistent with thermal conductivity measurements in highly underdoped $YBa_2Cu_3O_{6+\delta}$, which show that the low temperature heat conductivity divided by the temperature of the insulating phase proximate to the superconducting dome is the same as that in the *d*-wave superconducting phase, where it is dominated by nodal excitations.

The $T = 0$ superconductor-to-insulator transition is driven by quantum fluctuations of the phase of the superconducting order parameter. The corresponding thermal fluctuations, which are vortex-like excitations in the pseudogap phase, have been probed by Nernst and diamagnetism experiments.

Our observations imply that the sharp quasiparticles of the d-wave superconducting state exist down to the lowest doping levels while rapidly loosing spectral weight, but are no longer visible on the insulating side. Nonetheless, a low energy d-wave like gap survives the phase-disordering transition. Obviously, the node must disappear as the Mott insulator is approached, as indicated by some photoemission studies. Summarizing, we have found spectroscopic evidence for a d-wave nodal liquid ground state in the narrow doping regime between the high T_c superconductor and the undoped Mott antiferromagnet. This quantum liquid has no superconducting order, the transport characteristics of an insulator, no sharp quasiparticles, and yet it has an energy gap that looks just like that of a *d*-wave superconductor. Since the spectral gap evolves smoothly through the insulator-to-superconductor phase transition, the *d*-wave superconductor appears to be just a phase-coherent version of the *d*-wave nodal liquid.

The phase diagram

In order to understand the origin of high temperature superconductivity in copper oxides, we must understand the normal state from which it emerges. We examined the evolution of the normal state electronic excitations with temperature and carrier concentration in $Bi_2Sr_2CaCu_2O_{8+\delta}$ using ARPES. In contrast to conventional superconductors, where there is a single temperature scale T_c separating the normal from the superconducting state, the high temperature superconductors exhibit two additional temperature scales. One is the pseudogap scale T^*, below which electronic excitations exhibit an energy gap. The second is the coherence scale T_{coh}, below which sharp spectral features appear due to increased lifetime of the excitations. We find that T^* and T_{coh} are strongly doping dependent, and cross each other near optimal doping. Thus the highest superconducting T_c emerges from an unusual normal state that is characterized by coherent excitations with an energy gap.

General features of the phase diagram of the copper oxide superconductors have been known for some time. The superconducting transition temperature T_c has a dome-like shape in the doping-

temperature plane with a maximum near a doping $\delta \sim 0.16$. While in conventional metals the electronic excitations for $T > T_c$ are (i) gapless and (ii) sharply defined at the Fermi surface, the cuprates violate at least one of these conditions over much of their phase diagram. These deviations from conventional metallic behavior are most easily described in terms of two crossover scales T^* and T_{coh}, which correspond to criteria (i) and (ii), respectively.
Our experimental finding that the two crossover lines intersect is not consistent with a **single** quantum critical point near optimal doping, although more complicated quantum critical scenarios cannot be ruled out. Hence, our results are more naturally consistent with theories of superconductivity for doped Mott insulators. We believe these results represent an important step forward in solving the highly challenging problem of high temperature superconductivity.

Future plans

In the normal state of the underdoped high temperature superconductors, instead of a complete Fermi surface above Tc, only disconnected Fermi arcs appear, separated by regions that still exhibit an energy gap. The origin of these arcs is an important question in trying to understand the high Tc superconductors. The arcs could have their origin in the formation of a small Fermi surface, were only part of it is visible due to selection rules, or they could be some novel phenomena. One of the leading contenders to explain the phase diagram is a model proposed by Varma, where the presence of a quantum critical point under the superconducting dome near optimal doping determines the crossover lines observed above T_c. If such a point were present, there should be a scaling of the spectral function with doping and temperature. However, this model has a very unusual requirement, that is, that the divergence of the order parameter take place in only one dimension, perpendicular to the Fermi surface. In this model, the spectral function does not depend on momentum parallel to the Fermi surface. So far in condensed matter physics, such a strange divergence has never been observed. In other words, the spectral function for all values of doping and temperature could be collapsed onto a single curve, independent of momentum parallel to the Fermi surface. However, for underdoped samples, this is unlikely to be satisfied, as there are strong momentum dependences of the spectral function parallel to the Fermi surface. Therefore, the scaling function should be a multidimensional function. Thus, new procedures will be required to find the scaling conditions.Our preliminary work indicates that finding such a multidimensional scaling function is possible.

Publications

Band structure and Fermi surface of heavy Fermion compounds Ce2TIn8 (T = Co, Rh, In) studied by angle-resolved photoemission spectroscopy,
S. Souma, S. Raj, J. C. Campuzano, T. Sato, T. Takahashi, S. Ohara, and S. Sakamoto.
Physcica B 403, 752-754 (2008)

Direct evidence for hidden one-dimensional Fermi surface of hexagonal K0.25WO3,
S. Raj, T. Sato, S. Souma, T. Takahashi, D. D. Sarma, Priya Mahadevan, J. C. Campuzano, M. Greenblatt, and W. H. McCarroll.
Phys. Rev. B 77, 245120 (2008).

Coherent d-Wave Superconducting Gap in Underdoped La2-xSrxCuO4 by Angle-Resolved Photoemission Spectroscopy,

M. Shi, J. Chang, S. Pailhes, M. R. Norman, J. C. Campuzano, M. Mansson, T. Claesson, O. Tjernberg, A. Bendounan, L. Patthey, N. Momono, M. Oda, M. Ido, C. Mudry, and J. Mesot.
Phys. Rev. Lett. 101, 047002 (2008).

Evidence for pairing above the transition temperature of cuprate superconductors from the electronic dispersion in the pseudogap phase,
A. Kanigel, U. Chatterjee, M. Randeria, M. R. Norman, G. Koren, K. Kadowaki, and J. C. Campuzano.
Phys. Rev. Lett. 101, 137002 (2008).

Observation of a d-wave nodal liquid in highly underdoped Bi2Sr2CaCu2O8+δ
U. Chatterjee, M. Shi, D. Ai, J. Zhao, A. Kanigel, S. Rosenkranz, H. Raffy, Z. Z. Li, K. Kadowaki, D. G. Hinks, Z. J. Xu, J. S. Wen, G. Gu, C. T. Lin, H. Claus, M. R. Norman, M. Randeria & J. C. Campuzano.
Nat. Phys. 6, 99 - 103 (2010).

In situ x-ray study of ammonia borane at high pressures

Jiuhua Chen (PI, chenj@fiu.edu), Helene Couvy, Jennifer Girard, Vadym Drozd, Yongzhou Sun, Shah Najiba

Center for the Study of Matter at Extreme Conditions and Department of Mechanical and Materials Engineering, Florida International University, VH140, University Park, Miami FL 33199, USA

Haozhe Liu

Natural Science Research Center, Harbin Institute of Technology, Harbin 150080, China

Luke L. Daemen, Yusheng Zhao (CoPI)

Los Alamos Neutron Science Center, Los Alamos National Laboratory, Los Alamos, New Mexico 87545, USA

Wendy Mao (CoPI)

Geological & Environmental Sciences and Photon Science Department, SLAC Stanford University, Stanford, CA 94305-2115

Chi-Chang Kao (CoPI)

National Synchrotron Light Source, Brookhaven National Laboratory, Upton, NY 11973, USA

Research Scope: Study of behavior of ammonia borane at high pressures

Recent Progress: *In situ* synchrotron x-ray diffraction experiments of ammonia borane synthesized using sonication assisted direct reaction (sodium borohydride and ammonium formate) were performed under high pressures up to 23 GPa at ambient temperature and up to 4 GPa at elevated temperatures (300K – 505K). At ambient temperature, one first-order phase transition (*I*4*mm* to *Cmc*2_1) was observed at 1.3 GPa and one second-order phase transition were observed at about 5 GPa. Fitting the measured volumetric compression data to the third order Birch-Murnaghan equation of state reveals a modulus of K = 9.3 ± 0.4 GPa (K'= 4.8) for the *I*4*mm* phase, K = 11.9 ± 0.5 GPa (K' = 4.6) for the *Cmc*2_1 phase below 5 GPa, and K = 37 ± 4 GPa (K'= 4.6) for pressure above 5 GPa. There is a 6% volume drop at the first order phase transition. Transition pressures from *I*4*mm* to *Cmc*2_1 phases were determined at elevated temperatures. The phase boundary has a negative claperon slope of -1.67MPa/K. The experiments also reveal a new structural transition when temperature increases to 450K at 4 GPa.

Sample synthesis

The ammonia borane was synthesized through a direct reaction between sodium borohydride and ammonium formate in tetrahydrofuran (THF) solvent:

$$NaBH_4 + NH_4HCO_2 \xrightarrow{THF} NH_3\,BH_3 + H_2 + NaHCO_2$$

Ammonium formate (6.3 gram, 0.1 mol) and sodium borohydride (4.0 gram, ~6% excess of 0.1 mol) were added to 100 mL of THF in a beaker. The reaction starts immediately but takes long time (a few hours) to complete by refluxing the mixture. Sonicating the slurry by placing the beaker in an ultrasonic both (150W) could shorten the reaction time to 60 minutes. Applying an ultrasonic horn (250W) further reduced the required time down to 30-40 minutes. The ultrasonic horn method also increased the yield of the reaction. Typical yields of the ultrasonic horn synthesis at 30-40 minutes were 80-85%. After sonication, the sodium formate (and unreacted reagents) could be filtered out due to their very limited solubility in THF. The highly soluble ammonia borane in THF was then recovered from the filtrate on the rotary evaporator at room temperature. During the sonication, the slurry could be heated up if the process was too long. Although the heating facilitated the dissolution of the reagents and speeded up the reaction, over sonication (overheating) could cause thermal decomposition of ammonia borane and decrease yield of the reaction. Chilling the slurry during sonication did not seem to be helpful to preserve the yield.

In situ synchrotron x-ray diffraction using a multi-anvil press (MAP)

The cubic-type multi-anvil apparatus (SAM85) at the X17B2 beamline of the National Synchrotron Light Source (NSLS) was used for *in situ* high pressure x-ray diffraction experiments up to 4.3 GPa at ambient temperature and elevated temperatures for selected pressures. The sample was loaded in a 2 mm diameter chamber of solid pressure transmission medium (made of amorphous boron and epoxy resin, 4:1 in weight) for ambient temperature experiment. A carbon sleeve furnace and BN sample capsule with 1 mm inner diameter were inserted in the chamber for heating experiments. NaCl was placed next to the sample as internal pressure calibrant. The sample pressure was determined by referring the volume change of NaCl measured by x-ray diffraction to the Decker's scale. Sample temperature is directly measured using a W3%Re-W25%Re thermocouple placed in contact with the sample. Energy dispersive x-ray diffraction was performed using 100μm x 100μm cross-section white beam and germanium solid state detector (SSD).

In situ synchrotron x-ray diffraction using a diamond anvil cell (DAC)

A diamond anvil cell (DAC) with 300 μm culet size was used for *in situ* high pressure x-ray diffraction experiments up to 20 GPa at ambient temperature. The sample was loaded in a 200 mm diameter hole of steel gasket. Ruby chips were also loaded in the chamber as a pressure calibrant. Because ammonia borane is very soft, no additional pressure medium was used in the

sample chamber (120μm). The sample pressure was determined based on the pressure-induced shift of ruby fluorescence lines. Angle dispersive x-ray diffraction was performed using a monochromatic x-ray beam (λ = 0.4428 Å, cross section 7x12μm) from the bending magnet beamline of HPCAT at the Advanced Photon Source (APS) and Mar345 imaging plate detector.

Phase transitions at ambient temperature and compressibility

Two sequences of diffraction patterns were collected from the sample in MAP and DAC as a function of pressure. No transition below 1.1 GPa was observed. A significant change in diffraction pattern occurred at 1.3 GPa, corresponding to a structural transformation. Beyond this phase transition, no remarkable change was observed in the x-ray diffraction up to 22.8 GPa except weakening and broadening of diffraction peaks due to pressurization. The energy dispersive and angle dispersive diffraction data were analyzed using Le Bail and Reltveld refinement techniques, respectively, to derive the sample volume as a function pressure. Before the phase transition at 1.3 GPa, all diffraction patterns match the tetragonal structure with space group of *I*4*mm*. After the transition, the diffraction patterns are indentified as the $Cmc2_1$, in consistent with Filinchuk et al's observation. A bulk modulus of K = 9.3 ± 0.4 GPa is obtained for the low pressure phase by fitting the compression data into the third order Birch-Murnaghan equation of state with its pressure derivative fixed at K'= 4.8. For the high pressure phase, although there is no characteristic change in the diffraction pattern when the sample pressure crosses 5 GPa where Raman spectroscopic study indicates a phase transition, the compression data show very different character (compressibility) below and above this pressure. If the compression data are divided into two parts at 5 GPa, the fittings yield much better statistic residuals (random). The derived bulk moduli for the two regions are 11.9 ± 0.5 GPa (in the pressure range 1.3 ~ 5 GPa) and 37 ± 4 GPa (in the pressure range 5 ~ 15 GPa) for K'=4.6.

P-T phase boundary between I4mm and $Cmc2_1$ phases

The transition pressure from *I*4*mm* and $Cmc2_1$ phase was investigated at elevated temperatures using the MAP. At 300K, the $Cmc2_1$ phase appears at 1.5 GPa which is slightly higher than the transition pressure (1.3 GPa) observed in our first run using a difference cell assembly (without heater), indicating a 0.2 GPa pressure uncertainty in these experiments. The transition pressure decreases from 1.5 GPa to 1.1 GPa when temperature increases by 23K (to 323K), and further down to 0.7 GPa when temperature increases to from 323K to 248K (by 25K). The Claperon slope is estimated to be -1.67MPa/K. The negative Claperon slope indicates that the phase transition from *I*4*mm* and $Cmc2_1$ structure is endothermic.

New high temperature phase

Heating experiments on the $Cmc2_1$ phase were conducted at 1.3 GPa and 4 GPa. At 1.3 GPa and a heating rate of ~50K/min, no structural transition was observed until melting at 422 K. No structural transition is observed before melting. The x-ray diffraction peaks of $Cmc2_1$ phase vanished within 0.5 min after the temperature reached 422K. After melting, the sample was

quenched to ambient temperature, and pressure was then increased to 4 GPa. The sample remained amorphous after quenching, and recrystallized at 4 GPa during compression although the diffraction pattern showed relatively poor powder quality with respect to those obtained just after the *I*4*mm* to *Cmc*2_1 transition at 1.3 GPa. Upon heating at 4 GPa, a new diffraction pattern different from that of *Cmc*2_1 phase was observed between 450K and 490K, and melting occurred when the sample temperature was increased to 505K. Due to the weak signals of diffraction and poor powder quality of the sample, crystal structure of the new phase cannot be solved using these diffraction data.

Future Plans: Improve quality of diffraction data at pressures higher than 10 GPa; collect more data at high pressure and high temperature; solve the crystal structure at high pressure and high temperature; explore high pressure and low temperature region; study pressure influence on decomposition of ammonia borane.

References to publications of DOE sponsored research that have appeared in 2008-2010 or that have been accepted for publication

Yu Lin, Wendy L. Mao, Vadym Drozd, Jiuhua Chen, and Luke L. Daemen, Raman spectroscopy study of ammonia borane at high pressure, *Journal of Chemical Physics* 129, 234509 (2008)

Jiuhua Chen, Yunpeng Yang, Tony Yu, Jianzhong Zhang, Yusheng Zhao and Liping Wang, Strength measurement of boron suboxide B_6O at high pressure and temperature using *in situ* synchrotron X-ray diffraction, *High Pressure Research*, 28(3), 423-430 (2008)

Lyci George, Vadym Drozd, Andriy Durygin, Jiuhua Chen, Surendra K. Saxena, Bulk modulus and thermal expansion coefficient of mechanochemically synthesized Mg_2FeH_6 from high temperature and high pressure studies, *International Journal of Hydrogen Energy* 34 (2009) 3410 – 3416.

Artem R. Oganov, Jiuhua Chen, Carlo Gatti, Yanzhang Ma, Yanming Ma, Colin W. Glass, Zhenxian Liu, Tony Yu, Oleksandr O. Kurakevych, and Vladimir L. Solozhenko, Ionic high-pressure form of elemental boron, *Nature* 457, 863-867, doi:10.1038/nature07736 (2009)

Lin, Y., W.L. Mao, and H.-k. Mao, Storage of molecular hydrogen in an ammonia borane compound at high pressure. *Proceedings of the National Academy of Sciences*, 2009. 106(20): 8113-8116.

Chen, J., H. Couvy, H. Liu, V. Drozd, L.L. Daemen, Y. Zhao, and C.-C. Kao, *In situ* x-ray study of ammonia borane at high pressures. *International Journal of Hydrogen Energy*, 2010 doi:10.1016/j.ijhydene.2010.07.085.

Science and Applications of Novel Topological Quantum Materials

Yulin Chen
McCullough Bldg. 230
476 Lomita Mall
Stanford, CA 94305
Email: chenyl@stanford.edu

Zhi-Xun Shen
McCullough Bldg. 342
476 Lomita Mall
Stanford, CA 94305
Email: zxshen@stanford.edu

Introduction:

Topological insulators are a new state of quantum matter with a bulk gap and odd number of relativistic Dirac fermions on the surface (Fig. 1). The bulk of such materials is insulating but the surface can conduct electric current with well-defined spin texture. In addition, the relativistic energy-momentum relationship of electrons in these materials provides a great opportunity to study the physics of relativity in a condensed matter system with the velocity of massless particles about 200 times slower than the light speed in vacuum. This family of new materials is an ideal platform for approaching the grand challenges of designing energy-efficient revolutionary new forms of matter with tailored properties, controlling energy flow at the nanoscale and achieving atomically perfect synthesis..

Unlike other materials where the fragile surface states can be easily altered by details in the surface geometry and chemistry, topological insulators are predicted to have unusually robust surface states due to the protection of time-reversal symmetry. These unique states are protected against all time-reversal-invariant perturbations, such as scattering by non-magnetic impurities, crystalline defects, and distortion of the surface itself, and can lead to striking quantum phenomena such as quantum spin Hall effect (Fig. 2A), an image magnetic monopole induced by an electric charge (Fig. 2B), and Majorana fermions (whose anti-particle is itself) induced by proximity effect from a superconductor (Fig. 2C). These novel quantum insulators thus provide a unique opportunity to broadly address the underlying theme of how quantum mechanical phenomena impact behavior of such novel materials.

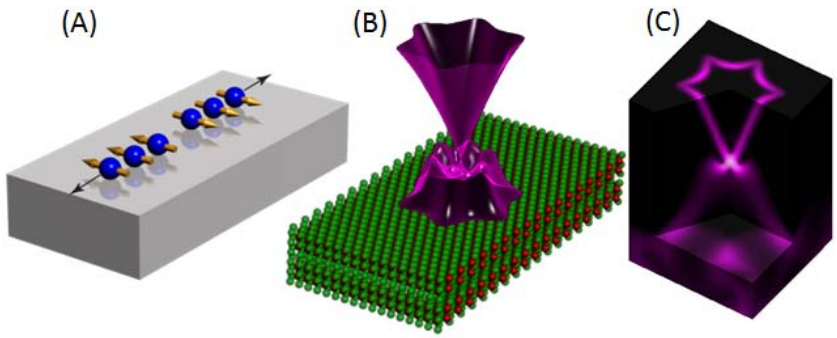

Figure 1: Surface conduction of topological insulators **(A)** The spin of electrons on the surface is correlated with their direction of motion **(B)** The lattice structure of Bi_2Te_3 and the predicted relativistic "Dirac cone" like electronic structure formed by the surface electrons. **(C)** The electronic structure measured by angle-resolved photoemission that confirmed the theoretical prediction and the topological nature of Bi_2Te_3.

Technologically, the robust surface state makes these materials desirable for down scaling of devices where the surface/bulk ratio becomes more important. With the large bulk gap compared to the energy scale of room temperature, some topological insulators (e.g. Bi_2Te_3) could be used for high (room) temperature applications. The surface state with a single linear-dispersing Dirac cone makes it much more convenient to realize the 2D Dirac physics for novel devices, which have attracted a lot of enthusiasm recently due to the discovery of graphene, but without the difficulty encountered by working with the single atomic layer graphene. Furthermore, the dissipationless edge state transport of the topological state and the current flow and spin texture correlation may enable low power spintronics devices.

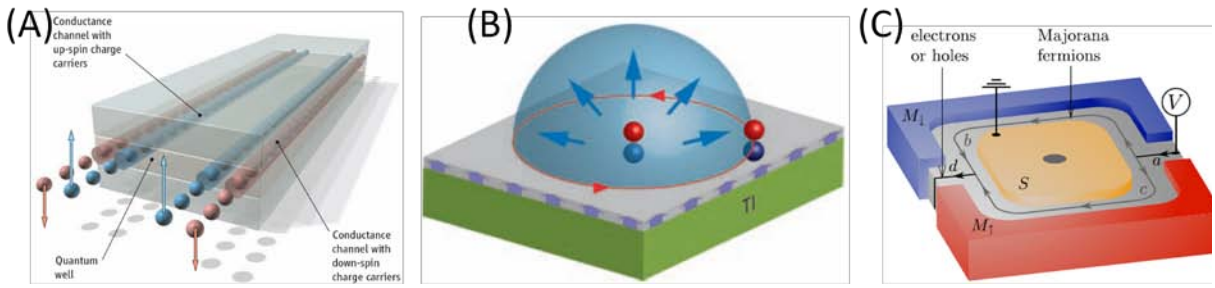

Figure 2. Examples of some unusual properties of topological insulators. **(A)** Schematic of the spin-polarized edge channel in a quantum spin Hall insulator (König, 2007). **(B)** Illustration of the fractional statistics induced by image monopole effect (Qi, 2009). **(C)** Schematic showing the Majorana fermion formed in a topological insulator-superconductor structure (Akhmerov , 2010)

Recent Progresses:

We have initiated several preliminary and complementary experiments on bulk, thin film and nano-scale topological insulators using various techniques, including ARPES, electric and thermal transport and collaborative STM studies. Beside the experimental work, theoretical calculations relevant to these results by collaborative groups are also being developed. These preliminary studies have demonstrated great scientific and technological significance of topological insulators. Four selected recent or preliminary results are summarized in the following:

1. Realization of Bulk Topological Insulator Bi_2Te_3 (Science, 325, 178 (2009))

Following a recent theoretical proposal *(Zhang, 2009)* that predicted a class of stoichiometric materials, Bi_2Te_3, Bi_2Se_3 and Sb_2Te_3, to be the simplest 3D topological insulators whose surface states consist of a single Dirac cone at the Γ point, we performed a series of ARPES measurements on all three compounds. The experimentally determined electronic structures are in broad agreement with the theoretical calculations, and demonstrate that the surface state consists of a single nondegenerate Dirac cone. Furthermore, with appropriate hole doping, the Fermi level can be tuned to intersect only the surface states, indicating a full energy gap for the bulk states. Our results establish that Bi_2Te_3 is a simple model system for the three-dimensional topological insulator with a single Dirac cone on the surface. The large bulk gap of Bi_2Te_3 also points to promising potential for high-temperature spintronics applications.

2. STM/STS Study on Topological Insulators (Physical Review Letter, 104,016401 (2010))

To supplement the ARPES measurement on Bi_2Te_3 electronic structures, STM and STS have also been performed, which exhibit perfect correspondence to ARPES data, hence enabling identification of different regimes measured in the local density of states (LDOS). Oscillations of LDOS near a step are analyzed. Within the main part of the surface band oscillations are strongly damped, supporting the hypothesis of topological protection. At higher energies, as the surface band becomes concave, oscillations appear, dispersing with a wave vector that may result from a hexagonal warping term.

3. Aharonov-Bohm Interference in Topological Insulator nanoribbons (Nature Materials. 9, 225 (2010))

To expand our knowledge of topological insulators and explore the possibility for applications, we studied the transport properties of topological insulators. In order to suppress possible residual bulk carriers coming from defects and increase the surface contribution in the transport measurement, we

fabricated and measured the single crystalline, quasi-1D nanoribbons of Bi_2Se_3. The observation of the AB oscillations in Bi_2Se_3 nanostructures provides important insights into the topological surface states. As although a significant portion of the conduction is carried by the bulk states, the interaction between bulk and surface electrons does not destroy the phase coherence of the surface states. Our result also demonstrates that the surface states not only exist on the top and bottom (0001) surfaces but also propagate coherently through the side walls of the nanoribbon, which are terminated with dangling bonds. the coherent motion of the electrons through the side surface is highly nontrivial, providing further evidence for the topological robustness of the surface states.

4. Realization of the insulating massive Dirac fermion state on topological insulators (Science, 329, 659 (2010))

In addition to a bulk energy gap, topological insulators accommodate a conducting, linearly dispersed Dirac surface state. This state is predicted to become massive if time reversal symmetry is broken, and to become insulating if the Fermi energy is positioned inside both the surface and bulk gaps. We introduced magnetic dopants into the three-dimensional topological insulator Bi_2Se_3 to break the time reversal symmetry and further position the Fermi energy inside the gaps by simultaneous magnetic and charge doping. The resulting insulating massive Dirac fermion state, which we observed by angle-resolved photoemission, paves the way for studying a range of topological phenomena relevant to both condensed matter and particle physics.

Proposed Researches:

Understanding the rich science and exploring the potential applications of topological insulators require a systematic approach to study them under different forms using complementary experimental methods. Continual feedback between synthesis, characterization, and theory are necessary to build a complete picture of the underlying physics of this novel quantum state of matter. Similarly, perfection in materials is also prerequisite to designing and fabricating functional devices for applications. To achieve our objectives, we propose the following studies:

1. In-situ Material Synthesis and Preparation

Successful understanding of the fundamental properties and application potential of topological insulators relies on high quality samples of different forms suitable for various experimental techniques. Taking advantage of the existing experimental setup and collaborative teams in SLAC, we have successfully obtained high quality bulk to nano-scale single crystal samples for our preliminary works.

However, due to the sensitivity of the materials to ambient environments, it is necessary to develop an in-situ sample synthesis/preparation setup in ultra-high vacuum (UHV) environment to ensure the properties studied reflects the true material character. Thus we propose to setup a molecular beam epitaxial (MBE) chamber for in-situ sample growth for the surface sensitive measurements (e.g. photoemission spectroscopy, etc.).

2. Study on Electronics and Structural Properties

Extracting the electronic and structural properties of topological insulators is essential for both the understanding of their underlying physics and potential applications. We plan to use complementary spectroscopic techniques, including photoemission, pump-probe X-ray spectroscopy/scattering, optical spectroscopy and collaborative scanning tunneling microscopy/spectroscopy (STM/STS) experiments for such studies.

Angle resolved photoemission spectroscopy (ARPES) has been proved to be one of the most effective ways to examine the electronic structure of materials, with the state of the art ARPES

beamlines at SSRL and the spin-resolved ARPES spectrometer at SIMES, we can effectively study the electronic (and spin) structure of these materials locally, as demonstrated in our preliminary works.

In addition, at SIMES, we can use the advanced STM/STS equipments for electronic structure study complementary to ARPES and the optical pump-probe ARPES spectrometer for electronic dynamic study; the recently commissioned LCLS further provides the opportunity for pump-probe X-ray scattering for the dynamic study of crystal structures. We will also collaborate with researchers in LBNL for the optical spectroscopy study.

These experiments are the central focus of the proposed program and will be accomplished by leveraging and enriching SLAC's core competency.

3. Study on Electric and Thermal Transport Properties for Applications

The unique properties of topological insulators make them great candidates for many promising applications, such as high efficiency thermoelectric applications, ultra small and low power electronic devices and novel spintronic devices. To bridge the electronic, spin and thermal properties and possible applications, we will perform electric and thermal transport measurements to understand how charges and energy are transported through these topological quantum materials. These are important supplementary activities to enhance the value of core experiments discussed above using SLAC's special photon facilities.

Benefiting from the existing infrastructure of SIMES and Stanford University, we can make use of existing micro-fabrication facilities for device fabrication. The electric and thermal transport will be performed by existing commercial and custom built instruments.

Appendix: Our recent publications on topological insulators:

1 Y. L. Chen, et. al., " *Massive Dirac Fermion on the Surface of a magnetically doped Topological Insulator"* ***Science, 329, 659 (2010)***

2 Y. L. Chen, et. al., *"Observation of Single Dirac Cone Topological Surface State in Compounds TlBiTe2 and TlBiSe2 from a New Topological Insulator Family"*
Preprint available at: http://arxiv.org/abs/1006.3843

3 J. G. Analytis, et. al., *"Bulk Fermi surface coexistence with Dirac surface state in Bi2Se3: a comparison of photoemission and Shubnikov-de Haas measurements"* ***Physical Review B, 81, 205407 (2010)***

4 D. S. Kong, et. al., *"Topological Insulator Nanowires and Nanoribbons"* ***Nano Letters. 10, 329 (2010)***

5 Z. Alpichshev, et. al., "*STM Imaging of electronic waves on the surface of Bi2Te3"****Physical Review Letter, 104,016401 (2010)***

6 H. L. Peng, et. al., *"Aharonov-Bohm Interference in Topological Insualtor Nanoribbons"* ***Nature Materials. 9, 225 (2010)***

7 K. K. Gomes, et. al, *"Quantum Imaging of Topologically Unpaired Spin-Polarized Dirac Fermions"*
Preprint available at: http://arxiv.org/abs/0909.0921

8 Y. L. Chen, et. al., "*Experimental Realization of a Three Dimensional Topological Insulator, Bi_2Te_3"* ***Science, 325, 178 (2009)***

Quantum Confinement, Pseudogaps, and Topological Order in Thin Films

Tai C. Chiang
Department of Physics, University of Illinois, 1110 West Green Street, Urbana, IL 61801
Email: tcchiang@illinois.edu

Research Scope: This research project is a study of the electronic structure and atomistic behavior of selected surface-based nanoscale systems prepared by deposition, artificial layering, self-assembly, and self-organization. Electrons confined in nanoscale systems form discrete states, or quantum well states, which are sensitive to the physical dimensions and boundary conditions. As a result, the electronic properties of such systems including the total energy, electronic charge distribution, and density of states can exhibit substantial quantum variations (or oscillations) as a function of system size and environment. The lattice structure of the system in turn responds to these changes as a result of electron-lattice and electron-phonon coupling, possibly leading to distortions and new structures. These interactions allow modification or tailoring of the physical properties of nanoscale systems by controlling the physical and chemical structures at the atomic scale. At elevated temperatures, entropy and kinetic effects come into play, and morphological evolution, structural transformation, and melting can occur, with possibly little semblance to the corresponding bulk behavior. These effects and phenomena are of basic importance to *nanoscale science and technology*, a prevailing national research theme. This project aims at a fundamental understanding of the underlying physical principles with a focus on simple model systems mostly based on thin films. Limited by space, just a few highlights will be presented in this report. A complete publication list is provided at the end of this document.

Recent Progress: (1) Using electronic coherence to probe a deeply embedded quantum well in bimetallic Pb/Ag films on Si(111): Characterizing quantum-electronic behavior in buried layers of thin-film systems constitutes an outstanding issue in condensed-matter physics and electronic materials engineering. Though the study of buried structures is of basic importance to thin-film applications, surface-sensitive measurement techniques such as angle-resolved photoemission spectroscopy (ARPES) probe electrons within just the first few Ångströms of a material's surface, rendering them unable to access underlying structures directly. Moreover, the incommensurate interfaces and roughness of intervening films in multilayer systems can obscure the electronic properties of the submerged media. Consequently, investigations of such systems have generally failed to assess the impact of constituent layers on the encompassing system. Using results obtained with ARPES we remedy this shortcoming by examining the manifestation of interfering electrons in atomically uniform Ag films on Si(111) covered by Pb films of various thicknesses. We show that when a Pb slab is joined to an Ag slab, the Ag and Pb electronic structures coherently couple, analogous to a two-layer Fabry-Pérot interferometer. Despite a short photoelectron escape depth, the initial-state wave function sensed by photoemission propagates throughout both the Pb and Ag films due to a long phase coherence length. The large lattice mismatch at the Ag/Si and Pb/Ag interfaces notwithstanding, this long electron coherence length promotes quantum interference and gives rise to an electronic structure characteristic of the entire system. Figure 1 shows that the Ag subband structure caused by quantum confinement can be detected under a thick Pb film. A detailed theoretical modeling based on wave mechanics yields

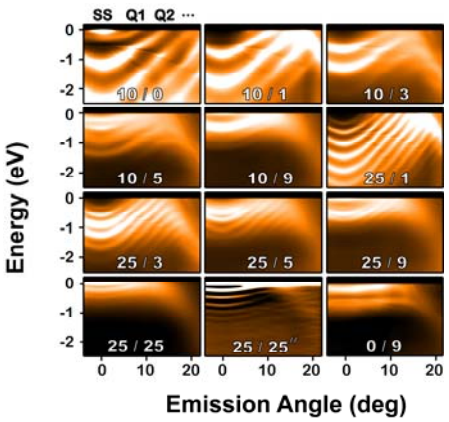

Figure 1. ARPES spectra of Pb films on Ag films on Si(111). The notation p/q indicates a coverage of q ML (monolayer) of Pb on p ML of Ag, and the double-prime (″) denotes a second derivative with respect to the energy. The results show that the Ag quantum well structure can be detected under a thick layer of Pb.

calculated spectral functions in good agreement with the experiment.

(2) Pseudogaps in Pb islands mediated by quantum confinement and electron-phonon coupling: This work is based on a collaboration with the group of Prof. Xiao of the Chinese University of Hong Kong. His group performed the measurements, and our group performed the theoretical analysis based on our expertise in quantum confinement effects. Briefly, scanning tunneling spectroscopy measurements of Pb islands on Si(111) at high energy resolution reveal a novel pseudogap, or a pseudopeak for special island heights, around the Fermi level in addition to the usual quantum well states. These pseudogap or peak features persist to temperatures as high as ~80 K. Figure 2(a) shows the tunneling spectra taken from a 19 ML Pb island; the superconducting gap at temperatures below the transition temperature (~7.2 K, nearly the same as the bulk transition temperature) evolves into a pseudogap at higher temperatures. For comparison, the pseudogap behavior of an underdoped Bi2212 high-temperature superconductor is presented in the same figure. The results are very similar. A systematic analysis indicates that electron-phonon scattering is responsible for the observed electronic structure. The pseudogap is observed for many different island thicknesses. Figure 3(a) shows a Pb island with a "crater" in the middle that consists of terraces with thicknesses ranging from 12 to 19 ML. The corresponding tunneling spectra (Fig. 3(b)) show quantum well peaks; the zoomed-in spectra near the Fermi level (Fig. 3(c)) reveal a pseudogap for all thicknesses except 18 and 27 ML for which a pseudopeak is observed instead. At 18 ML and 27 ML, a quantum well peak is almost exactly centered at the Fermi level. The pseudopeak appears as a small bump atop the much broader quantum well peak. The thin curves in Fig. 3(b) are results from our model calculations; a detailed view near the Fermi level is presented in Fig. 3(d). The agreement between experiment and theory is excellent. All of the essential features including the pseudogaps or peaks and quantum well peaks are seen in the calculation.

(3) Passage from spin-polarized surface states to unpolarized quantum well states in topologically nontrivial Sb films: Topological insulators, which possess robust gapless surface states as a result of strong spin-orbit coupling, have attracted much interest because of their unusual surface spin structures. When such materials are reduced to ultrathin films, the spin-split surface states must connect, by analytic continuation, to quantum well states, which are spin-unpolarized in centrosymmetric systems. We have performed a combined experimental and

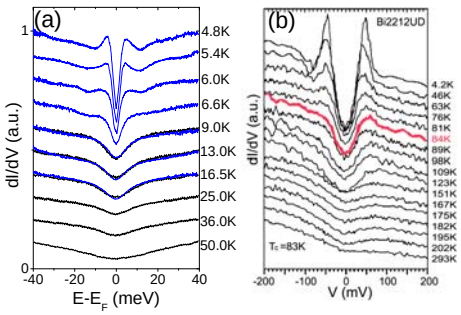

Figure 2. (a) Tunneling spectra taken from a 19 ML Pb island on Si(111) at various temperatures. Bulk Pb has a superconducting transition temperature of 7.2 K. (b) Tunneling spectra taken from an underdoped Bi2212 at various temperatures. This material's superconducting transition temperature is 84 K. The results are taken from Ø. Fischer et al., Rev. Mod. Phys. **79**, 353 (2007). There is a strong similarity between the two cases.

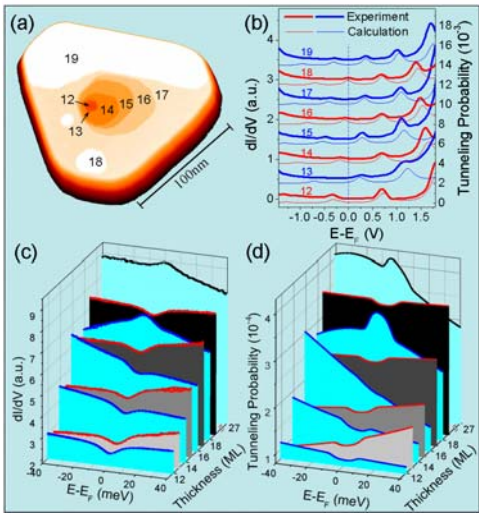

Figure 3. (a) STM image of an island with a "crater" in the middle. (b) Experimental tunneling spectra for various terrace heights. Also shown, for comparison, are theoretical tunneling probabilities. (c) Detailed view of the tunneling spectra near the Fermi level. (d) Calculated tunneling probabilities for comparison.

theoretical study of this passage from polarized to unpolarized states in Sb films. Bulk Sb is semimetallic with a negative band gap; nevertheless, it shares the same topological order as $Bi_{1-x}Sb_x$ ($0.07 < x < 0.2$), the first material identified as a three-dimensional topological insulator. ARPES from Sb films, aided by first-principles calculations, shows smooth dispersion relations associated with this passage; the spin polarizations of the two surface states fade away, while the energy splitting is maintained through the emergence of different charge density patterns of the resulting quantum well states. Our work illustrates the interplay between quantum confinement and topological order.

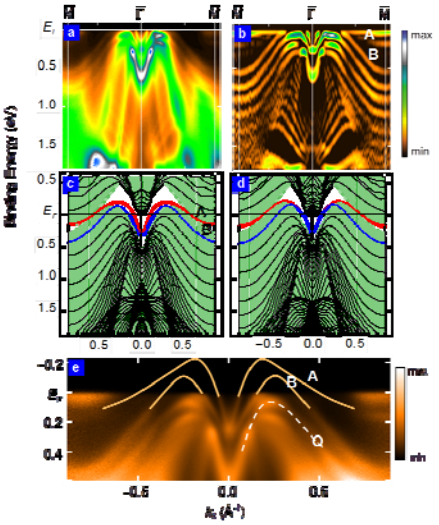

Figure 4. (a) ARPES data taken with 22 eV photons from a 20 bilayer (BL) Sb film. (b) Second derivatives of the data. (c) Calculated band structure for a freestanding 20 BL Sb slab with spin-orbit coupling included. (d) Calculated band structure with spin-orbit coupling excluded. (e) Data near the Fermi level showing the two spin-split surface states A and B and the top occupied quantum well state Q.

Future Plans: (1) We will continue our study of the pseudogap/peak feature in Pb films (and other systems) using ARPES. While STM measurements provide unmatched energy resolution, it is important to perform ARPES studies to extract the angular (or in-plane momentum) dependence of the pseudogap/peak feature. This should shed additional light on electron-phonon coupling in a confined geometry. (2) Quantum confinement effects in films should depend on the size of the substrate band gap. Most work today has been based on Si, which has a relatively small gap. We plan to explore the use of substrates with larger band gaps (such as oxides and insulators). Oxide-metal interfaces are of interest to device applications. (3) We will continue to explore modulation effects in films caused by periodic arrays of steps on the substrate surface. The influence of miscut angles on the growth properties and electronic structure will be studied. Specifically, diffraction effects associated with periodic steps and localization effects associated with strong step potentials are of interest. (4) The work on spin-polarized surface states and topologically nontrivial films will continue. We are currently performing experiments and calculations for surface alloys and multilayers involving Bi, Sb, Te, Pb, Ag, and Au. (5) We are expanding our research program on inelastic x-ray scattering (IXS) and thermal diffuse scattering (TDS) studies of (quantum) phase transitions under extreme conditions. A PUP proposal is being assembled for work on f-electron materials, complex oxides, and charge density wave systems. My group is working with a team from the University of Illinois (Abbamonte, Cooper, and Fradkin) and a team from the Advanced Photon Source (Said, Upton, Hong, and Xu) to set up a diamond anvil cell system for high pressure studies at Sector 30. While we are currently focusing on bulk materials, future developments should allow us to examine small systems, grains, and domains.

Publications (2008-)

1. Ruqing Xu, Joe Wong, Paul Zschack, Hawoong Hong, and T.-C. Chiang, "Soft phonons in δ-phase plutonium near the δ-α' transition," EuroPhys. Lett. **82**, 26001 (2008).
2. Y. Liu, N. J. Speer, S.-J. Tang, T. Miller, and T.-C. Chiang, "Interface-induced complex electronic interference structures in Ag films on Ge(111)," Phys. Rev. B **78**, 035443 (2008).
3. T.-C. Chiang, "Quantum physics of thin metal films," Bulletin of AAPPS (Association of Asia Pacific Physics Societies), **18**, No. 2, 2-10 (2008).
4. S.-J. Tang, Wen-Kai Chang, Yu-Mei Chiu, Hsin-Yi Chen, Cheng-Maw Cheng, Ku-Ding Tsuei, T. Miller, and T.-C. Chiang, "Enhancement of subband effective mass in Ag/Ge(111) thin film quantum wells," Phys. Rev. B **78**, 245407 (2008).
5. R. Xu, H. Hong, P. Zschack, and T.-C. Chiang, "Direct mapping of phonon dispersion relations in

copper by momentum-resolved x-ray calorimetry," Phys. Rev. Lett. **101**, 085504 (2008).
6. H. Hong, R. Xu, A. Alatas, M. Holt, and T.-C. Chiang, "Central peak and narrow component in x-ray scattering near the displacive phase transition in $SrTiO_3$," Phys. Rev. B **78**, 104121 (2008).
7. Y. Liu, J. J. Paggel, M. H. Upton, T. Miller, and T.-C. Chiang, "Quantized electronic structure and growth behavior of Pb films on highly oriented pyrolytic graphite," Phys. Rev. B **78**, 235437 (2008).
8. Kedong Wang, Xieqiu Zhang, M. M. T. Loy, T.-C. Chiang, and X. Xiao, "Pseudogap mediated by quantum-size effects in lead islands," Phys. Rev. Lett. **102**, 076801 (2009).
9. R. Xu, H. Hong, and T.-C. Chiang, "Probing phonons and phase transitions in solids with x-ray thermal diffuse scattering," Chapter 10 in *Diffuse Scattering and the Fundamental Properties of Materials*, edited by Rozaliya I. Barabash, Gene E. Ice, and Patrice E.A. Turchi (Momentum Press, Highland Park, NJ, 2009) pp. 161-178.
10. S. S. Ferng, S. T. Wu, D. S. Lin, and T.-C. Chiang, "Mediation of chain reactions by propagating radicals during halogenation of H-masked Si(100): implications for atomic-scale lithography and processing," J. Chem. Phys. **130**, 164706 (2009).
11. N. J. Speer, M. K. Brinkley, Liu, C. M. Wei, T. Miller, and T.-C. Chiang, "Surface versus bulk electronic structure of silver determined by photoemission," EuroPhys. Lett. **88**, 67004 (2009).
12. T. Miller, M. Y. Chou, and T.-C. Chiang, "Phase relations associated with one-dimensional shell effects in thin metal films," Phys. Rev. Lett. **102**, 236803 (2009).
13. D. A. Ricci, Y. Liu, T. Miller, and T.-C. Chiang, "Analyticity of the phase shift and reflectivity of electrons at a metal-semiconductor interface," Phys. Rev. B **79**, 195433 (2009).
14. C.-T. Lou, H.-D. Li, J.-Y. Chung, D.-S. Lin, and T.-C. Chiang, "Electronic reconstruction at a buried ionic-covalent interface driven by surface reactions," Phys. Rev. B **80**, 195311 (2009).
15. M. K. Brinkley, Y. Liu, N. J. Speer, T. J. Miller, and T.-C. Chiang, "Using electronic coherence to probe a deeply embedded quantum well in bimetallic Pb/Ag films on Si(111)," Phys. Rev. Lett. **103**, 246801 (2009).
16. Y. Liu, T. Miller, and T.-C. Chiang, "Coherent electronic grating cavity modes in corrugated ultrathin metal films," Appl. Phys. Lett. **95**, 243114 (2009).
17. G. Bian, T. Miller, and T.-C. Chiang, "Electronic structure and surface-mediated metastability of Bi films on Si(111)-7x7 studied by angle-resolved photoemission spectroscopy," Phys. Rev. B **80**, 245407 (2009).
18. R. Xu and T.-C. Chiang, "Studying structural phase transitions with x-ray thermal diffuse scattering," Phase Transitions **83**, 99 (2010).
19. T. Miller and T.-C. Chiang, "Quantum electronic stability of atomically uniform films," Chapter 2 in "Thin film growth: physics, materials science and applications" edited by Zexian Cao (Woodhead Publishing) (accepted).
20. M. K. Brinkley, N. J. Speer, Y. Liu, T. Miller, T.-C. Chiang, "Quantum-number bifurcation in Ag quantum wells on Si(111)," (submitted).
21. Hawoong Hong, A. Gray, and T.-C. Chiang, "Real time reciprocal space mapping of nano-islands induced by quantum confinement," Met. Mater. Trans. A (DOI: 10.1007/s11661-010-0329-9 on line first).
22. M. Krisch, D. L. Farber, R. Xu, D. Antonangeli, C. M. Aracne, A. Beraud, T.-C. Chiang, J. Zarestky, D. Y. Kim, E. Isaev, R. Ahuja, and B. Johansson, "Lattice dynamics of cerium metal across the γ-α transition," (submitted).
23. Hawoong Hong, Aaron Gray, Ruqing Xu, Longxiang Zhang, and T.-C. Chiang, "Quantum growth of a metal/insulator system: lead on sapphire," (submitted).
24. Guang Bian, Thomas Miller, and Tai-Chang Chiang, "Passage from spin-polarized surface states to unpolarized quantum well states in topologically nontrivial Sb films," (submitted).
25. Hawoong Hong, Mary Upton, Ayman Said, Hyun-Sook Lee, Sung-Ik Lee, Ruqing Xu, and T.-C. Chiang, "Phonon dispersions and anomalies of $MgCNi_3$ determined by inelastic x-ray scattering," (submitted).

Direct X-ray Studies of Emergent Behavior at Epitaxial Interfaces: from 2DEG to Quantum Dots

Roy Clarke

Department of Physics, University of Michigan,
Ann Arbor, MI 48109-1040
royc@umich.edu

Research Scope

Unusual and unexpected physical properties are known to emerge from the complex interplay of ionic and electronic rearrangements occurring at interfaces. This opens up a new frontier in materials research with endless possibilities for energy critical applications. Examples include the perovskite family of structures which, in bulk form, exhibit an astonishing variety of correlated electron effects, including high-temperature superconductivity, multiferroic phenomena, exotic magnetic phases, charge density waves and a host of other interesting collective behavior. A major focus of this program is on the behavior of epitaxial thin films and nanostructures in which the interface structure plays a dominant role. This can enable entirely new properties as a result of novel structural arrangements at the heteroepitaxial interface. For example we have provided a structural basis [PRL**99**, 155502 (2007)] for the microscopic origin of the novel 2D electron gas at the interface between $LaAlO_3$ and $SrTiO_3$ using a direct x-ray phasing technique known as COBRA (Coherent Bragg Rod Analysis). A significant achievement resulting from this work is the development of a solution to the x-ray phase retrieval problem in two-dimensional (i.e. epitaxial) materials and its first application to epitaxial materials, including perovskite oxides and III-V semiconductor materials [Nature Nanotechnology 4, 835 (2009)]. Of particular interest are materials characterized by the appearance of spontaneous order parameters such as remnant electric or magnetic dipole moments. These effects are well known in bulk ferroelectric and ferromagnetic materials, but the equivalent behavior in reduced dimensionality systems is only now being studied in some detail. An exciting prospect is the manipulation of such structures to provide a platform for novel materials applications relevant to energy harvesting and storage. Ultrafast spectroscopy experiments (laser pump/ laser probe and laser pump/ x-ray probe) provide complementary dynamics information on the relevant energy transport processes.

Recent Progress

Functionalized perovskite interfaces for ultrathin ferroelectrics- Recent research has focused mainly on epitaxial ferroelectric thin films with the goal of investigating the role of electrical boundary conditions. Specifically we wished to test whether a two-dimensional electron gas, formed at the interface between the substrate ($SrTiO_3$) and an ultrathin $LaTiO_3$ film (see Fig. 1], would serve as a conducting electrode to neutralize the depolarization field resulting from the planar ferroelectric structure. Furthermore we were interested to see if the insertion of the conducting electrode layer based on a $LaSrTiO_3$-$SrTiO_3$ interface would maintain the lattice matching conditions necessary for growth of coherent, dislocation-free $BaTiO_3$. The coherence of the growth is essential for producing the biaxial

strain which first-principles theory predicts to be responsible for stabilizing the ferroelectric structure and producing an enhancement of the spontaneous polarization.

Our first experiments on this system were performed on a sample in which 5 unit cells of $LaAlO_3$ were deposited by PLD on a TiO_2-terminated (100) $SrTiO_3$ substrate followed by 3 unit cells of $BaTiO_3$ and a polycrystalline capping layer of gold. An atomic electron density map of multilayer ferroelectric structure, obtained using the direct x-ray phasing technique, COBRA, is shown in Fig. 1a. Small (~0.2 Å) off-center displacements (Fig. 1b) of Ti measured in both the $BaTiO_3$ and nominal $LaAlO_3$ layers indicate the presence of spontaneous polarization.

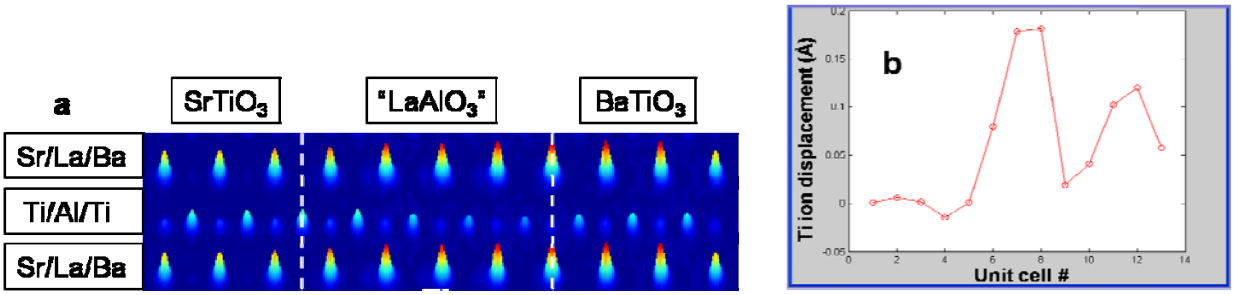

Fig.1: (a) COBRA electron density map of a $BaTiO_3$/$SrTiO_3$ heterostructure containing functionalized $SrTiO_3$/$LaAlO_3$ 2-D electron gas interface grown by PLD. The plane shown here is normal to the $SrTiO_3$ substrate and contains lines of Sr/La/Ba atoms as well as Ti and Al alternated by oxygen atoms. Note the formation of a $LaTiO_3$-like layer at the STO-LAO interface, consistent with earlier structural studies ; (b) Ti ion displacement in each unit cell, starting from the left ($SrTiO_3$) in Fig. 1a.

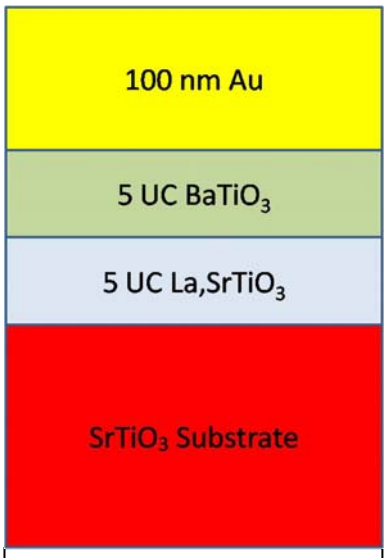

Fig. 2: Ultrathin $BaTiO_3$ on $SrTiO_3$ with functionalized La,SrO_3 electrode.

These findings illustrate the importance of heterointerfaces for the design of epitaxial oxide multilayers with novel electronic and dielectric properties.

The layered electrode structure was further refined by forming an alloy structure at the interface between the substrate and the $BaTiO_3$ film. The alloy composition, $La,SrTiO_3$, was specifically chosen to mimic the form of the actual interface that we had earlier observed at the $LaAlO_3$-$SrTiO_3$ conducting interface. Using this as an epitaxial electrode we find a very interesting result: the Ti-O displacements in the $BaTiO_3$ film are considerably enhanced relative to those seen in the bulk ferroelectric (by as much as a factor of 4) and are even larger than those observed with the $LaAlO_3$ electrode layer that we first tried (see Fig. 1).

A summary of these results is shown below. The most exciting part of these measurements is the unusually large c/a ratio (1.06) that is observed in the $BaTiO_3$ layer as a result of the fully developed spontaneous polarization.

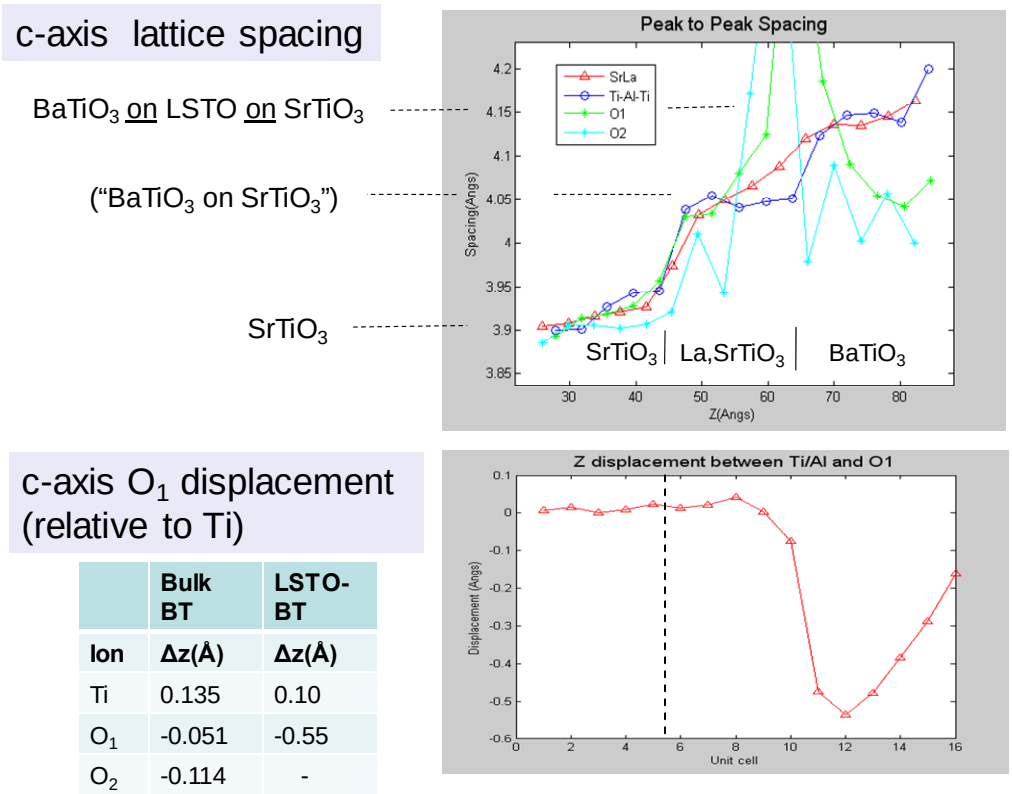

	Bulk BT	LSTO-BT
Ion	**Δz(Å)**	**Δz(Å)**
Ti	0.135	0.10
O_1	-0.051	-0.55
O_2	-0.114	-

Fig. 3: Summary of results from direct x-ray studies of epitaxial ferroelectric heterostructures. Top panel: c-axis layer spacing for $BaTiO_3$ layers grown on $SrTiO_3$ with basal LSTO epitaxial conducting electrode. Bottom panel: Ti-O_1 displacement as a function of distance from substrate interface (dashed line).

Future Work

Atomic-level Mapping of $SrTiO_3$ on Si (001) Using Surface X-ray Diffraction and Direct Methods

Christian M. Schlepütz, Naji S. Husseini, Divine P. Kumah1, and Roy Clarke, University of Michigan, Ann Arbor, MI 48109

Yizhak Yacoby, Hebrew University, Jerusalem, Israel

Philip R. Willmott, Matts Bjoerck, and Stephan A. Pauli, Paul Scherrer Institut, Villigen, Switzerland

Maitri P. Warusawithana, and Darrell G. Schlom, Cornell University, Department of Materials Science and Engineering, Ithaca, NY 14853

We have recently begun a new collaboration to study the surface x-ray diffraction from $SrTiO_3$ layers grown epitaxially on silicon (001) wafers by Darrell Schlom's group at Cornell. In this epitaxial oxide-on-semiconductor system, the $SrTiO_3$ was reported to exhibit ferroelectric nanodomains at temperatures well above ambient. X-ray synchrotron radiation measurements, obtained at Advanced Photon Source and

the Swiss Light Source, combined with direct phase-retrieval methods, are used to determine quantitatively the atomic structure and lattice spacings as a function of position relative to the substrate interface. The epitaxial strain is crucial to explaining the stabilization of a spontaneously polarized state of $SrTiO_3$, which is not present in the bulk material. An in-plane 45 degree rotation of the film relative to the silicon substrate, together with ~1.7 % compressive strain, brings the $SrTiO_3$ into approximate registry with the substrate. We recently confirmed that 5 unit cells of $SrTiO_3$ on Si exhibit good epitaxial registry, whereas thicker films of 10 unit cells are partially relaxed. The resonant response of the complex x-ray scattering factor, measured by tuning the x-ray energy to the absorption K-edge of Sr, is used to deconvolute the effects of interface roughness, chemical mixing and strain. Control of the structure at the Si-$SrTiO_3$ interface will be essential for engineering ferroelectric-semiconductor hybrid devices. We also wish to take advantage of new laser pump- x-ray probe approaches for the study of the soft mode and pseudospin dynamics in this system.

References

1. D.P. Kumah, S. Shusterman, Y. Paltiel, Y. Yacoby, R. Clarke , Atomic-scale mapping of quantum dots formed by droplet epitaxy, Nature Nanotechnology **4** 835-838 (2009).

2. Structural Changes Induced by Metal Electrode Layers on Ultrathin $BaTiO_3$ Films, Y. Yacoby, C. Cionca, N. Husseini, A. Riposan, J. Olmsted Cross, C. Brooks, D. Schlom, and R. Clarke, Phys. Rev. B 77, 195426 (2008).

3. Strain and Composition Mapping of Epitaxial Nanostructures, C.N. Cionca, A. Riposan, D.P. Kumah, N.S. Husseini, D.A.Walko, Y. Yacoby, J. Mirecki Millunchick, and R. Clarke, Applied Physics Letters **92**, 151914 (2008).

4. In Situ Imaging of High Cycle Fatigue Crack Growth in Single Crystal Nickel-Base Superalloys by Synchrotron X-Radiation, Liu Liu, Naji Husseini, Christopher Torbet, Divine Kumah, Roy Clarke, Tresa Pollack, and J. Wayne Jones, J. Mtls. Eng. & Technology 130 (2008).

5. Mapping single-crystal dendritic microstructure in nickel-base superalloys with synchrotron radiation, Naji S. Husseini, Divine P. Kumah, Jian Z. Yi, Christopher J. Torbet, Dohn A. Arms, Eric M. Dufresne, Tresa M. Pollock, J. Wayne Jones, Roy Clarke, Acta Materialia, 56, 4715-4721 (2008).

6. Wideband detection of transient solid-state dynamics using ultrafast fiber lasers and asynchronous optical sampling, Vladimir A. Stoica, Yu-Miin Sheu, David A. Reis, and Roy Clarke, Optics Express **16**, 2322 (2008).

7. Structure determination of monolayer-by-monolayer grown $La_{1-x}Sr_xMnO_3$ thin films and the onset of magnetoresistance, R. Herger, P. Willmott, C. Schlepuetz, M. Bjoerck, S. Pauli, D. Martoccia, B.D. Patterson, D. Kumah, R. Clarke, Y. Yacoby, M. Doebeli, Phys. Rev. B **77**, 085401 (2008).

High Pressure X-Ray Absorption Studies on Correlated-Electron Systems

Principal Investigator
Dr. Andrew L. Cornelius
University of Nevada, Las Vegas
Department of Physics and Astronomy
4505 S. Maryland Pkwy
Campus Box 454002
Las Vegas, NV 89154-4002
e-mail: cornel@physics.unlv.edu

National Laboratory Partner
Dr. Corwin H. Booth
Lawrence Berkeley National Lab
Chemical Sciences Division
1 Cyclotron Road
MS 70A-1150
Berkeley, CA 94720
e-mail: chbooth@lbl.gov

Research Scope

The project is funded by a DOE/EPSCoR University/National Laboratory partnership. Itrevolves around collaboration between the PI, Andrew Cornelius at University of Nevada, Las Vegas (UNLV) and National Laboratory Partner (NLP) Corwin Booth at Lawrence Berkeley National Laboratory (LBNL). The PI has significant expertise in the study of materials at high pressure, low temperature and high magnetic fields. The NLP is a well-known expert in the field of x-ray absorption measurements.

Correlated-electron systems are so named because there are strong interactions between electrons unlike traditional metals such as copper that have weakly interacting "free electrons." Studies on correlated-electron systems have wide ranging interest from defense related issues to future use in nanoscale devices. Experimental results are a necessity for understanding these complicated materials and allow critical tests to theory.

We strive to further the understanding of two important aspects of correlated-electron materials: energy and length scales. One of the most studied areas in correlated-electron systems is how one energy scale (superconductivity) emerges out of the suppression of another (magnetism) at a quantum critical point (QCP) that is inextricably linked to yet another (Kondo). Another area of wide interest is the Kondo effect on the nanoscale. Understanding this could lead to major breakthroughs in the future of nanoscale magnetic devices.

The study of materials at a QCP has shown a breakdown of standard theories. Recent studies of numerous energy scales near quantum critical points have complicated the situation further. As stated in a recent review by Nigel Hussey, "The physics associated with this new energy scale is a conundrum; it violates not only Landau's theory, but also the conventional view of quantum criticality and the standard theory of phase transitions." [N.E. Hussey, Nature Physics **3** (2007) 445.] Clearly, the study of multiple energy scales and quantum criticality are of central importance in our understanding of correlated-electron systems.

In summary, the research would continue our quest for a much needed thorough understanding of correlated-electron systems. The combining of will allow for a thoroughness that will lead to a better understanding of superconductivity, coherence and band formation in correlated-electron materials.

Recent Progress

This project has just started. We have obtained some preliminary results on $CeCu_2(Si_{1-x}Ge_x)_2$. X-ray absorption data were collected in transmission mode on beamline 2-3 at the Stanford Synchrotron Radiation Light source, using Kirpatrick-Baez focusing optics to achieve a beam approximately 2 μm in diameter. Double Si(111) monochromator crystals were detuned 50% to remove unwanted higher harmonic energies. Samples were prepared by grinding them under acetone, then passing through a 20 μm sieve. A small collection of the sieved particles were placed into a Be gasket filled with silicone fluid as a pressure medium and clamped into a DAC. The applied pressure was determined by measuring the laser induced fluorescence energy from a ruby chip that was also loaded into the DAC with the sample.

Data were reduced by fitting a line between 5474 eV and 5670 eV and then subtracting this line over the whole data range. Typically, 16 20 minute scans were collected at each pressure. The averaged data shown in Fig. 1 are also normalized to the step height by extrapolating a line through the data above the main absorption edge to the threshold energy. Given the various errors in this procedure, an offset and a normalizing factor are included in the fits.

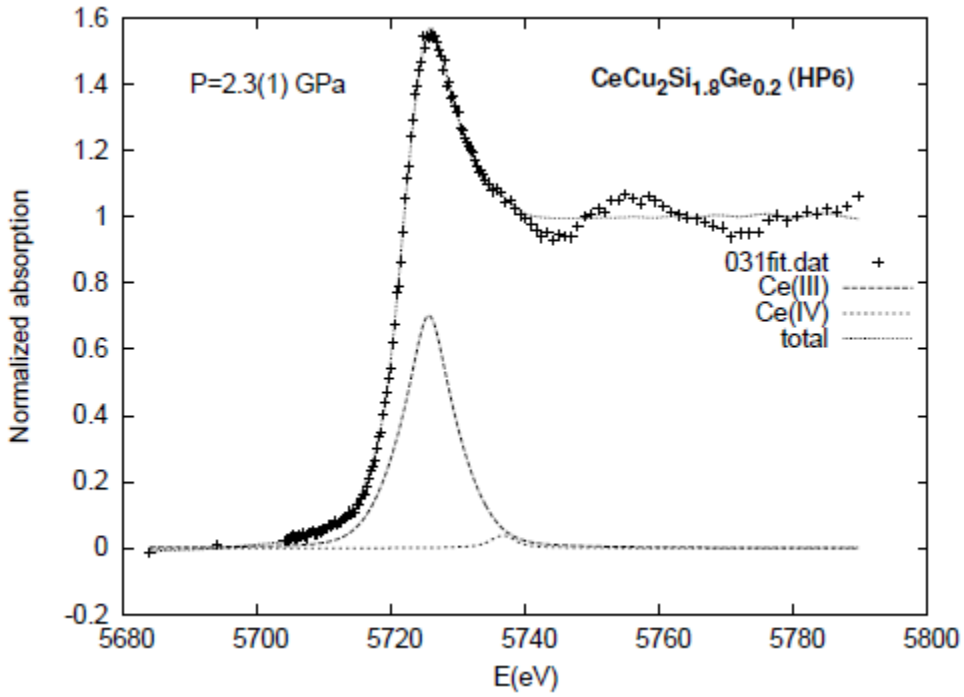

Figure 1 – High pressure XANES measurement on a Ce compound at 2.3 GPa and room temperature. The fitting details for this nearly trivalent material are given in the text.

To fit the data, we make the usual assumption that the main peak at about 5725 eV is due to the Ce(III), f1, configuration, and the shoulder at about 5735 eV is due to the Ce(IV), f0, configuration. The data were fit with a simple model using pseudo-Voigt functions with half Gaussian and half Lorenzian character for the Ce(III) and Ce(IV) peaks, together with an integrated pseudo-Voigt (arctan-like) function for the main

absorption step. For $CeCu_2(Si_{0.8}Ge_{0.2})_2$ shown in Fig. 1, the tetravalent component is very small. Higher pressure causes little change to the valence.

Future Plans

YEAR 1: The project would start with the purchase of a glove box designed to mount air sensitive samples. This is necessary for the molecular systems of interest. A postdoc would be recruited and hopefully arrive by midyear. A graduate student, the PI and Dr. Booth would test and calibrate the high-pressure system (this includes making mounts for the pressure cells for x-ray absorption measurements, testing of the portable ruby fluorescence system for measuring *in situ* pressure in the diamond anvil cell). Optimization of the high pressure technique will be optimized at the various synchrotron sources.

YEARS 2-3: High-pressure x-ray absorption measurements would be completed. In addition, ancillary high-pressure as well as ambient pressure, temperature dependent measurements would be performed. This coupling of various measuring techniques is vital for a comprehensive understanding of the results. A major goal of this project is to make reliable high-pressure x-ray absorption measurements routine at various synchrotron sources. This will allow us to tackle the new, exciting problems that are bound to arise in correlated-electron systems as well as other fields in materials physics.

References to Publications of DOE Sponsored Research

Note – none of these publications come from the listed project. The funding for these publications comes from UNLV High Pressure Science and Engineering Center was supported by the U.S. Department of Energy, National Nuclear Security Administration, under Co-operative agreement number DE-FC52-06NA26274.

1. "Pressure induced structural changes in the potential hydrogen storage compound ammonia borane: A combined X-ray, neutron and theoretical investigation." R.S. Kumar, X. Ke, J. Zhang, Z. Lin, S.C. Vogel, M. Hartl, S. Sinogeikin, L. Daemen, **A.L. Cornelius**, C. Chen, and Y. Zhao, *Chem. Phys. Lett.* **495**, 203 (2010). 5 pages
2. "High-resolution neutron scattering study of $Tb_2Mo_2O_7$: A geometrically frustrated spin glass." G. Ehlers, J.E. Greedan, J.R. Stewart, K.C. Rule, P. Fouquet, **A.L. Cornelius**, C. Adriano, P.G. Pagliuso, Y. Qiu, and J.S. Gardner, *Phys. Rev. B* **81**, 224405 (2010). 8 pages
3. "Inelastic X-ray scattering experiments on B_4C under high static pressures." R.S. Kumar and D. Dandekar, A. Leithe-Jasper, T. Tanaka, Y. Xiao, P. Chow, M.F. Nicol, and **A.L. Cornelius**, *Diamond and Related Mater.* **19**, 530 (2010). 3 pages
4. "Magnetic Ordering in Solid Oxygen up to Room Temperature." S. Klotz, T. Strassle, **A.L. Cornelius**, J. Philippe, and T. Hansen, *Phys. Rev. Lett.* **104**, 115501 (2010). 4 pages

5. "High-pressure structural study of fluoro-perovskite CsCdF3 up to 60 GPa: A combined experimental and theoretical study." G. Vaitheeswaran, V. Kanchana, R.S. Kumar, **A.L. Cornelius**, M.F. Nicol, A. Svane, N.E. Christensen, and O. Eriksson, *Phys. Rev. B.* **81,** 075105 (2010). 6 pages
6. "Structural phase transitions in the potential hydrogen storage compound $RbBH_4$ under compression." Ravhi S. Kumar and **Andrew L. Cornelius**, *J .Alloys and Comp*. **476,** 5 (2009) 4 pages
7. "Pressure-induced valence change in $YbAl_3$: A combined high-pressure x-ray scattering and theoretical investigation" Ravhi S. Kumar, Axel Svane, G. Vaitheeswaran, V. Kanchana, Eric D. Bauer, Michael Hu, Malcolm F. Nicol, and **Andrew L. Cornelius**, *Phys Rev. B* **70**, 075117 (2008). 7 pages
8. "Effect of Pressure and Temperature on Structural Stability of Potential Hydrogen Storage Compound Li_3AlH_6." Ravhi S. Kumar, Xuezhi Ke, **Andrew L. Cornelius**, and Changfeng Chen, *Chem. Phys. Lett.* **460**, 442 (2008). 5 pages
9. "High pressure structural studies on $SrRuO_3$." M.K. Jacobsen, R.S. Kumar, G. Cao, J.J. Neumeier, and **A.L. Cornelius**, *J. Phys. Chem. Solid* **69**, 2237 (2008). 3 pages
10. "*In situ* observations of temperature- and pressure-induced phase transitions in TiH_2: Angle-dispersive and synchrotron energy-dispersive X-ray diffraction studies." P.E. Kalita, **A.L. Cornelius**, K.E. Lipinska-Kalita, Cedric L. Gobin, H. Peter Liermann, *J. Phys. Chem. Solid* **69**, 2240 (2008). 5 pages
11. "Structural Phase Transitions in the Potential Hydrogen Storage Compound KBH_4 under Compression." R. Kumar, E. Kim, and **A.L. Cornelius**, *J. Phys. Chem. C* **112** (2008) 8452. 6 pages
12. "Frustrated spin correlations in $Ho_{2-x}\ La_xTi_2O_7$." G. Ehlers, E. Mamontov, M. Zampoin, A. Farone, Y. Qiu, **A.L. Cornelius**, C.H. Booth, K.C. Kam, R. Le Toquin, A.K. Cheetham, and J.S. Gardner, *J. Phys.: Condens. Matter* **20**, 235206 (2008). 7 pages
13. "Magnetic ordering in UCu_2Si_2 at high pressure." **A.L. Cornelius**, R.S. Kumar, M.K. Jacobsen, E.D. Bauer, J.S. Sarrao, and Z. Fisk, *Physica B* **403**, 940 (2008). 3 pages

Dynamics of electronic interactions in superconductors and related materials.

Dan Dessau, Dept of Physics, University of Colorado, Boulder, CO 80309
Dessau@Colorado.edu 303-492-1607

- Research Scope or Definition

We primarily utilize high resolution angle-resolved photoemission (ARPES) and are building up to perform pump-probe ARPES with ultrafast lasers in the time domain. The intellectual overlaps and goals of our proposed time-resolved studies are perfectly aligned with and complementary to those of our direct-ARPES experiments.

- Recent Progress

- **New method for extracting superconducting gaps and scattering rates - the ATS or ARPES Tunneling Spectra.** We have devised a new method for extracting superconducting gaps and scattering rates from ARPES, giving us a true quantitative method – something which had been sorely lacking up to now. For example, we find that the true scattering rates are an order of magnitude smaller than inferred from previous ARPES measurements, and the gaps much more accurately follow the d-wave predictions. We have been applying this to the study of the near-nodal states of the high T_c superconductor Bi2212. These states have been almost ignored previously because they are more difficult to study, but these states are critical for studying the superconductivity (the antinodal states are contaminated by the pseudogap).

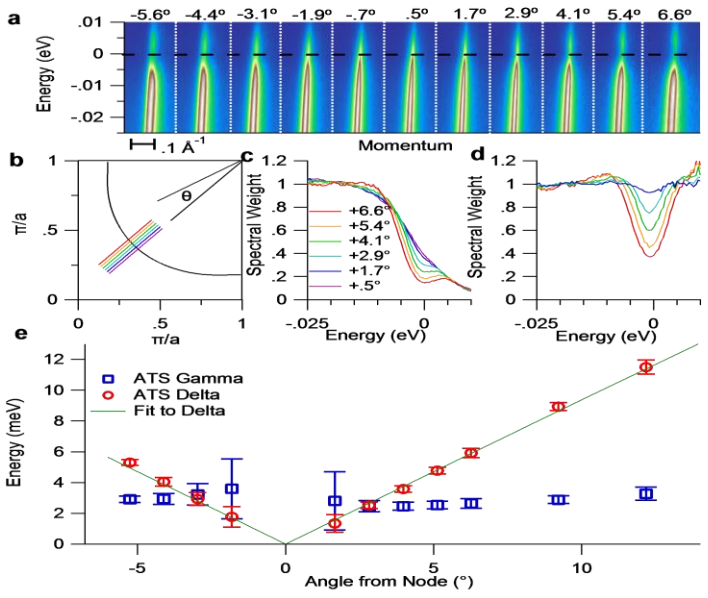

Fig 1. Near nodal gaps Delta and scattering rates Gamma from Bi2212 extracted using our new ATS method (unpublished).

- **New low energy (<10 meV) kink in the nodal states of Bi2212.** We have found a new low energy kink in the near-nodal

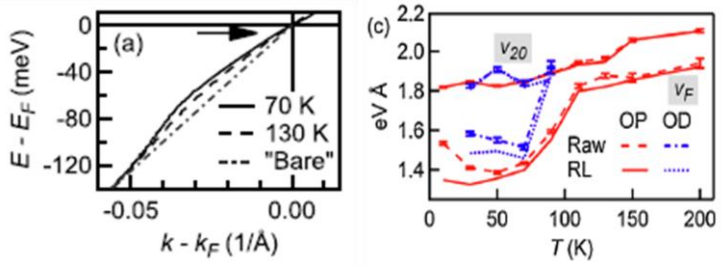

Fig 2. New low energy (< 10 meV) nodal kink below T_c in Bi2212 (Plumb et al., PRL 2010).

dispersion of Bi2212, distinct from the higher energy (~ 70 meV) kink in these materials (fig 2). This kink has a strong temperature dependence, causing the Fermi velocity v_F to dip strongly below T_c while the velocity 20 meV below E_F has only minimal T dependence (right panel). The causes and implications are still under investigation.

- **Uniaxial or "nematic" electronic structure of untwinned single crystals of the parent pnictide superconductor $CaFe_2As_2$.** Obtaining the electronic structure of the newly discovered iron-based superconductors is the key to understanding the mechanism of their high-temperature superconductivity. We used ARPES to make direct measurements of the electronic structure and Fermi surface (FS) of the untwinned uniaxial state of $CaFe_2As_2$. We observed unequal dispersions and FS geometries along the orthogonal Fe-Fe bond directions. More importantly, unidirectional straight and flat FS segments are observed near the zone center, which indicates the existence of a unidirectional nematic charge density wave order, strengthening the case for a quantum electronic liquid crystalline "nematic" phase. Further, the doping dependence extrapolates to a possible quantum critical point of the disappearance of this order in the heavily overdoped regime of these materials.

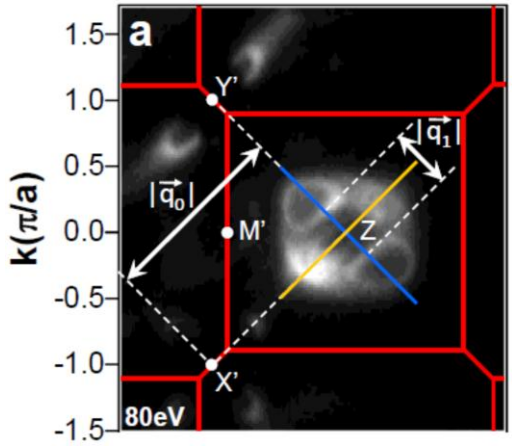

Fig 3. Uniaxial Fermi surface of untwined $CaFe_2As_2$. The nesting vector q_1 matches that observed in STM measurements by the Davis group (unpublished).

- Future Plans

We will continue our direct-ARPES studies of high T_c superconductors, especially those involving our new ATS method for the study of nodal states as the accuracy this method affords is greatly needed. We also will continue developing our ultrafast laser-based pump-probe ARPES capabilities, as this will be a powerful complementary way to get at the electron dynamics.

- References of DOE sponsored research.

N. C. Plumb, J. D. Koralek, J. F. Douglas, T. J. Reber, Z. Sun, Y. Aiura, K. Oka, H. Eisaki, and D. S. Dessau "Low-energy (< 10 meV) feature in the nodal electron self-energy and strong temperature dependence of the Fermi velocity in $Bi_2Sr_2CaCu_2O_{8+\delta}$" arXiv:0903.4900 Phys. Rev. Lett. 105, 046402 (2010)

Q. Wang, Z. Sun, E. Rotenberg, F. Ronning, E. D. Bauer, H. Lin, R. S. Markiewicz, M. Lindroos, B. Barbiellini, A. Bansil, and D. S. Dessau Uniaxial "nematic-like" electronic structure and Fermi surface of untwinned $CaFe_2As_2$ (arXiv:1009.0271v1)

Q. Wang, Z Sun, E Rotenberg, H. Berger, D.S. Dessau "Energy-dependent scaling of incoherent spectral weight and the origin of the waterfalls in high-T_c cuprates" arXiv:0910.2787

K. Sato, H. Iwasawa, N. C. Plumb, T. Masui, Y. Yoshida, H. Eisaki, H. Bando, A. Ino, M. Arita, K. Shimada, H. Namatame, M. Taniguchi, S. Tajima, Y. Nishihara, D. S. Dessau, and Y. Aiura, "Enhancement of oxygen isotope effect due to out-of-plane disorder in $Bi_2Sr_2Ln_{0.4}CuO_{6+\delta}$ superconductors" Phys. Rev. B 80, 212501 (2009)

S. Danzenbacher, D.V. Vyalikh, Yu. Kucherenko, A. Kade, C. Laubschat, N. Caroca-Canales, C. Krellner, C. Geibel, A.V. Fedorov, D.S. Dessau, R. Follath, W. Eberhardt, and S.L. Molodtsov, **"**Hybridization Phenomena in Nearly Half-Filled f Shell Electron Systems: Photoemission Study of $EuNi_2P_2$" Phys. Rev. Lett. 102, 026403 (2009)

H. Iwasawa, J. F. Douglas, K. Sato, T. Masui, Y. Yoshida, Z. Sun, H. Eisaki, H. Bando, A. Ino, M. Arita, K. Shimada, H. Namatame, M. Taniguchi, S. Tajima, S. Uchida, T. Saitoh, D.S. Dessau, Y. Aiura "An isotopic fingerprint of electron-phonon coupling in high temperature superconductors" Phys Rev Lett 101, 157005 (2008)

Z. Sun, J.F. Douglas, A. Fedorov, D.S. Dessau, H. Lin, Sahrakorpi Seppo, Bernardo Barbiellini, Bob Markiewicz, A. Bansil, H. Zheng, J.F. Mitchell, "Electronic structure of $La_{2-2x}Sr_{1+2x}Mn_2O_7$ (x=0.59) and its comparison with $La_{2-2x}Sr_{1+2x}Mn_2O_7$ (x=0.36, 0.38) revealed by ARPES" Phys. Rev. B. **78**, 075101 (2008)

Philip A. Casey, J. D. Koralek, Nick Plumb, D.S. Dessau and Philip W. Anderson **"**Accurate theoretical fits to laser-excited photoemission spectra in the normal phase of high temperature superconductors" Nature Physics **4**, 210 (2008).

Time dynamics of oxides and related materials

T. P. Devereaux, W.-S. Lee, Z.-X. Shen, Z. Hussain, W. Mao, D. Reis, A. Lindenberg
Stanford Institute of Materials and Energy Sciences
SLAC National Accelerator Laboratory
2575 Sand Hill Rd.
Menlo Park, CA 94025
tpd@stanford.edu

Research Scope:

The Time Dynamics of Oxides & Related Materials research area within the Stanford Institute for Materials and Energy Sciences (SIMES) at SLAC is largely a LCLS-focused effort using ultrafast and spectroscopy techniques, along with computational simulations, to address and probe electron dynamics in oxide and related materials that display a variety of relaxational behaviors across many timescales, reflecting the couplings of charge, spin, orbital, and lattice degrees of freedom so prevalent in transition metal oxide materials. The understanding of electron dynamic processes is related to a number of grand scientific challenges, as well as a number of use-inspired research focus areas.

The main project is to extend resonant x-ray scattering into the time domain using LCLS & multi-scale simulations. This project has three specific goals: 1) to offer a direct probe of the time evolution of out-of-equilibrium charge transfer processes in correlated, quantum phases of materials; (2) to explore and probe charge and spin dynamics across thermal and quantum phase transitions; 3) to compliment quasi-particle evolution with time-resolved ARPES.

The components include carrying out time-dependent spectroscopies and scattering measurements via pump-probe methods on superconducting, magnetic, semiconducting, as well as ferroelectric materials including numerical simulations and theory, complemented by x-ray studies of materials under pressure using diamond anvil cell techniques. In addition, x-ray scattering and terahertz activities are carried out at FLASH, SSRL and other synchrotron light sources.

We seek to study the nonequilibrium dynamics of materials on ultrafast time scales and atomic length scales, associated with atomic vibrations and making and breaking of chemical bonds. These efforts will lead to a better understanding the fundamental processes relevant for energy relaxation and transport as well as phase transitions occurring on the nanoscale and under extreme conditions, with a goal of understanding and controlling materials properties from the bottom-up.

Recent Results:

We have recently completed a series of successful LCLS runs where the team members joined forces to make the first materials science LCLS run a highly successful one. This includes pump-probe x-ray resonant scattering studies of atoms, charge and spin ordering in stripe ordered nickelates as well as charge ordering across the Verway transition in magnetite and in the tri-tellurides. The time dynamics indicates that the charge order and spin order evolve when pumped under different time scales, each separate from the dynamics of the lattice Bragg peaks.

In addition, a number of benchmarking experiments using resonant soft x-ray inelastic scattering (RIXS) have been performed under equilibrium conditions for the cuprate & pnictide

superconductors, and under diamond anvil cells to explore high spin/low spin and metal-insulator transitions in correlated materials. A review article on RIXS has been submitted to Rev. Mod. Phys. that gives a snapshot of the current state-of-art experiments and theory.

We also have obtained the first images of nonequilibrium phonons throughout the Brillouin zone in photoexcited III-V semiconductors, indium-phosphide (InP) and indium-antimonide (InSb), using picosecond time-resolved diffuse scattering. In each case, we find that the lattice remains out of equilibrium for several hundred picoseconds up to nanoseconds after laser excitation. The non-equilibrium population is dominated by the delayed emission of transverse acoustic phonons that in InP are directed along high-symmetry directions.

Complementary progress has been achieved in calculating time-domain response functions for correlated electron systems using massively parallel multi-scale computing. We have developed a formalism for calculating pump-probe photoemission spectra in correlated systems using a combination of Keldysh and dynamical mean field theory techniques. We have shown how Block oscillations are damped with increasing interactions, and have investigated how the pumped system display spectra which are not simply characterized in terms of equilibrium spectra at elevated temperatures. In particular, we have shown that Mott gaps do not collapse when pumped.

Future Plans:

Multi-scale numerical simulations of time-domain spectroscopies:

We are developing a complete tool set that combines the best aspects of many different computational techniques to provide the most complete picture of systems in- and out-of-equilibrium. Our efforts include developing massively parallel codes & algorithms, usable on our local cluster, Tier 1 computing facilities at NERSC, and new GPU-based clusters, that combine crystal field/atomic multiplet, quantum cluster, density functional theory, and dynamical mean-field theory methods. Simulations directly relevant to the experimental projects listed below are in progress now.

Charge and spin dynamics of striped nickelates and other cuprates:

In stripe ordered nickelates and cuprates, neutron scattering measurements have observed an anomalous softening of the phonon branch for bond-stretching modes near the charge-ordering wave-vector. It has been a long-standing question regarding the relation between the stripe phase and this phonon anomaly. To shed a new light to this problem, we will perform a mode-selective THz pump and resonant x-ray scattering probe experiments on stripe ordered nickelates and cuprates. We would like to manipulate the population of the bond-stretching phonons by pumping the system using a THz laser, and study the response of the stripes using resonant x-ray scattering (diffraction).

Collective modes in charge density wave and superconducting systems:

Similar to the proposed work on charge ordered states in transition metal oxides, resonant x-ray scattering will be first performed on $TbTe_3$ and other chalcogenides to monitor the time evolution of the charge modulation after the CDW state has been "melted" or perturbed by the pump laser. Followed by time-resolved RIXS at the CDW wavevector, the dynamics of the CDW in both time and energy domain will be studied. As the formation of the CDW state is related to electron-phonon coupling, an interesting experiment involves THz pumping at the appropriate phonon energy to determine the reaction of the charge during the relaxation process. Of particular interest would be to pump the system with THz radiation at the frequency of its amplitude mode (i.e., the collective mode that directly modulates its order parameter amplitude), thereby studying how the collective "resonance" of the system might be a metric of "emergence".

Studying cathode materials for lithium batteries at extreme conditions:

While the above projects are focused on determining relaxational dynamics in the ordered state, and states driven by laser fields, we are also interested in quantum critical dynamics in systems driven across phase boundaries via pressure. Experimental study of the mechanisms and transformation pathways involved in phase transitions at high pressure is an important but challenging problem. Extreme environments (e.g. pressure) give us a much broader field to search for new phases with desirable properties, and improving our understanding of the structural modifications that occur in materials can help us design improved materials. One example is studying cathode materials for lithium batteries. $LiMn_2O_4$ transforms from its ambient condition cubic, spinel structure to a tetragonal structure at high pressure and that this structural transition is tied to the Jahn-Teller effect. We are currently investigating the effect of nanostructuring (i.e. looking at nanorods and other morphologies) on this transition. Besides static high pressure studies, we also plan to tune a material close to a phase transition using static high pressure and then investigating the dynamic behavior under optical or shock excitation using ultrafast time resolution techniques x-ray scattering techniques. To this end, we have begun tests to investigate phase transitions using high pressure using pump–probe spectroscopy by looking at bismuth (specifically the well known Bi(II) to Bi(III) transition). The pressure dependence of the amplitude and frequency of the coherent phonons and the photo-excited carrier relaxation can give information on electronic band structure.

Non-equilibrium phonons in II-V semiconductors:

The interaction of hot carriers and phonons in solids is a fundamental problem with important implications for energy applications. If the scattering of electrons by phonons and subsequent lattice thermalization is sufficiently fast, the nonequilibrium dynamics minimally impacts the transport and other properties. It is generally assumed that lattice thermalization is relatively fast, effectively occurring on the time-scale of a few optical phonon periods to several picoseconds. However, bottlenecks for the decay of certain modes due to kinematic limitations or small anharmonic coupling can lead to nonequilibrium phonon populations that, for example in polar semiconductors, can affect device performance. Prior experiments on nonequilibrium phonons were limited by time-resolution or to studying relatively long wavelength excitations. In the current experiments, performed at the Advanced Photon Source, we cannot resolve earliest stages of energy transfer between the carriers and the lattice or even the first decay processes of the phonons. The LCLS will allow us to probe these dynamics on their fundamental time-scale. The results have broader implications for the detailed understanding of properties of materials where specific phonons play a defining role in the underlying physics.

Polarization switching in ferroelectric & multiferroic materials:

We are investigating the ultrafast dynamics of ferroelectric and multiferroic oxide materials using femtosecond x-ray diffraction techniques as well as ultrafast optical spectroscopy. We are developing methods for controlling the polarization state in ferroelectrics and recording limits for how fast these materials can switch, while visualizing the flow of energy between light, structural and electronic degrees of freedom, using light spanning the range from THz to x-ray frequencies. We are also exploring the photovoltaic response of these materials, trying to understand the coupled structural and electronic response that leads to charge separation and enhanced photo-voltages in the bulk on ultrafast time-scales.

Selected Publications:

- **High pressure evolution of Fe_2O_3 electronic structure revealed by x-ray absorption,** Shibing Wang, Wendy L. Mao, Adam P. Sorini, Cheng-Chien Chen, Thomas P. Devereaux, Yang Ding, Yuming Xiao, Paul Chow, Nozomu Hiraoka, Hirofumi Ishii, Yong Q. Cai, Chi-Chang Kao, to appear in Phys. Rev. B.
- **Temporal response of nonequilibrium correlated electrons,** B. Moritz, T. P. Devereaux, J. K. Freericks, to appear in the Proceedings of the Conference on Computational Physics 2009, Taiwan.
- **Unraveling the nature of charge excitations in La_2CuO_4 with momentum-resolved Cu *K*-edge resonant inelastic x-ray scattering,** C.-C. Chen, B. Moritz, F. Vernay, J. N. Hancock, S. Johnston, C. J. Jia, G. Chabot-Couture, M. Greven, I. Elfimov, G. A. Sawatzky, T. P. Devereaux, to appear in Phys. Rev. Lett.
- **Resonant inelastic x-ray scattering studies of elementary excitations**, Luuk J. P. Ament, Michel van Veenendaal, Thomas P. Devereaux, John P. Hill, Jeroen van den Brink, to appear in Rev. Mod. Phys.
- **Time-resolved photoemission of correlated electrons driven out of equilibrium**, B. Moritz, T. P. Devereaux, J. K. Freericks, Physical Review B 81, 165112 (2010).
- **Evidence for weak electronic correlations in Fe-pnictides**, W. L. Yang, P. O. Velasco, J. D. Denlinger, A. P. Sorini, C-C. Chen, B. Moritz, W.-S. Lee, F. Vernay, B. Delley, J.-H. Chu, J. G. Analytis, I. R. Fisher, Z. A. Ren, J. Yang, W. Lu, Z. X. Zhao, J. van den Brink, Z. Hussain, Z.-X. Shen, T. P. Devereaux, Phys. Rev. B **80**, 014508 (2009) [see also Physics **2**, 60 (2009)].
- **Resonant inelastic x-ray scattering in electronically quasi-zero-dimensional CuB_2O_4**, J. N. Hancock, G. Chabot-Couture, Y. Li, G. Petrakovskii, K. Ishii, I. Jarrige, J. Mizuki, T. P. Devereaux, M. Greven, Phys. Rev. B **80**, 092509 (2009).
- **Femtosecond electronic response of atoms to ultra-intense x-rays.** L. Young, E. P. Kanter, B. Krassig, Y. Li, A. M. March, S. T. Pratt, R. Santra, S. H. Southworth, N. Rohringer, L. F. DiMauro, G. Doumy, C. A. Roedig, N. Berrah, L. Fang, M. Hoener, P. H. Bucksbaum, J. P. Cryan, S. Ghimire, J. M. Glownia, D. A. Reis, J. D. Bozek, C. Bostedt, and M. Messerschmidt. Nature **466** (7302):56–61 (2010).
- **Probing unfolded acoustic phonons with x rays**, M. Trigo, Y. M. Sheu, D. A. Arms, J. Chen, S. Ghimire, R. S. Goldman, E. Landahl, R. Merlin, E. Peterson, M. Reason, and D. A. Reis, Phys. Rev. Lett. **101**, 025505 (2008).
- **Time-resolved pump-probe experiments at the LCLS,** J. M. Glownia, J. Cryan, J. Andreasson, A. Belkacem, N. Berrah, C. I. Blaga, C. Bostedt, J. Bozek, L. F. DiMauro, L. Fang, J. Frisch, O. Gessner, M. G¨uhr, J. Hajdu, M. P. Hertlein, M. Hoener, G. Huang, O. Kornilov, J. P. Marangos, A. M. March, B. K. McFarland, H. Merdji, V. S. Petrovic, C. Raman, D. Ray, D. A. Reis, M. Trigo, J. L. White, W. White, R.Wilcox, L. Young, R. N. Coffee, and P. H. Bucksbaum, Opt. Express **18**, 17620–17630 (2010).
- **Ultrafast electron cascades in semiconductors driven by intense femtosecond terahertz pulses**, Wen H, Wiczer M, Lindenberg AM, Phys. Rev. B **78**, 125203 (2008).
- **X-ray diffuse scattering measurements of nucleation dynamics at femtosecond resolution**. A. M. Lindenberg, S. Engemann, K. J. Gaffney, K. Sokolowski-Tinten, J. Larsson, P. B. Hillyard, D. A. Reis, D. M. Fritz, J. Arthur, R. A. Akre, M. J. George, A. Deb, P. H. Bucksbaum, J. Hajdu, D. A. Meyer, M. Nicoul, C. Blome, T. Tschentscher, A. L. Cavalieri, R.W. Falcone, S. H. Lee, R. Pahl, J. Rudati, P. H. Fuoss, A. J. Nelson, P. Krejcik, D. P. Siddons, P. Lorazo, and J. B. Hastings, Phys. Rev. Lett. **100**, 135502, (2008).

Ultrasmall-Angle X-ray Scattering (USAXS) Studies of the Effect of Transition Metal (Ti2+, Ti3+, V3+, Fe3+, and Zr4+) Dopants in NaAlH4 Powders

Tabbetha A. Dobbins
Institute for Micromanufacturing, Louisiania Tech University, Ruston, LA 71272

Transition metal dopants added to complex metal hydrides, specifically to sodium aluminum hydride (NaAlH4), by high energy ball milling enhances dehydrogenation kinetics and induces dehydrogenation reaction reversibility. This study uses ultrasmall angle x-ray scattering (USAXS) to elucidate differences in NaAlH4 particle morphology as dopant type and mill time is varied. Five dopant types were used. Two dopant types were used to represent the best kinetic enhancements having high desorption rates (e.g. TiCl2, TiCl3) and were compared with two dopant types which do not perform as well (e.g. ZrCl4, FeCl3 and VCl3). USAXS data for the doped hydrides were compared with undoped and milled NaAlH4 powders. Mill times used were 0 minutes (blended), 1 minute, 5 minutes, and 25 minutes. As indicated by USAXS power-law scattering data, the undoped NaAlH4 powders are comprised of primary particles having a high surface area (surface fractal geometries) and of smooth colloidal particles. The powders, when catalyzed with a single transition metal cation, and milled for 1 minute, 5 minutes, and 25 minutes show uniformly decreasing hydride particle surface area with mill time. In co-doped systems, USAXS was used to track changes in powder surface area using measured particle sizes and volume fractions. The variation in desorption rates in those co-doped systems were correlated with changes in powder surface area.

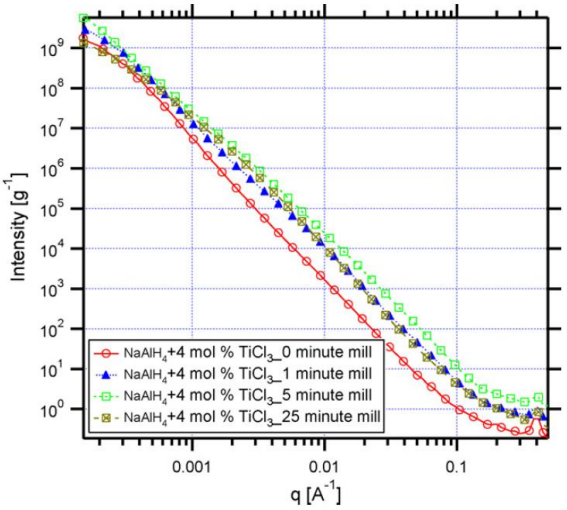

USAXS data: 4 mol % $TiCl_3$ doped $NaAlH_4$ powders blended for 2 min in dry N_2 glovebox and milled for (a) 0 min; (b) 1 min; (c) 5 min; and (d) 25 min.

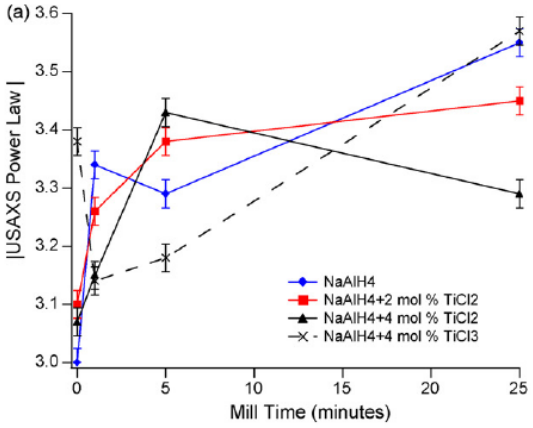

USAXS power-law sloped, p, for the $TiCl_x$-doped $NaAlH_4$ powders

From Kinky Physics to Transuranics: f-Electron ARPES at LANL

Tomasz Durakiewicz, John Joyce, George Rodriguez

Los Alamos National Laboratory, MPA Division, Los Alamos, NM87545, USA

Email: tomasz@lanl.gov

Field Work Proposal: Complex Electronic Materials

Principal Investigator: Joe D Thompson

Research Scope

The photoemission team at Materials Physics and Applications Division at LANL is involved in the investigation of the electronic structure of f-electron materials. This work is divided between three major sub-tasks: (1) work on cerium, ytterbium and uranium materials at public synchrotron facilities, (2) transuranic (mostly plutonium) research performed with the unique and dedicated Angle Resolved Photoemission (ARPES) setup at LANL and (3) ultrafast experiments on uranium systems with the novel time-resolved ARPES capability at LANL . Below we describe the recent progress in all three sub-tasks covering the period of 2008-2010, and future plans.

Recent Progress

***Work at Synchrotron Facilities*.** Band renormalization effects, especially in strongly correlated systems, lead to significant differences between calculated and measured electronic structures. The origin of band renormalization is linked to many-body effects and some novel theories attempt to reproduce experimental findings by calculating the renormalized band dispersion taking into account such interactions. The most commonly recognized mechanism involves flattening of bands related to increase of the quasiparticle effective mass. We have shown that in addition to band flattening, in 5f systems one may also find band shifts and onset of additional periodicity in band dispersion.

Specifically, we have found and characterized two novel band renormalization mechanisms in a 5f system, USb_2. First, in the ARPES data collected in-plane at the Synchrotron Radiation Center (SRC), we have identified the point-like Fermi surface renormalization effect. A single hole-like parabolic band is predicted by LSDA calculation to touch the Fermi level at Γ point of high symmetry. This band, due to interband scattering process involving a boson, is renormalized below the Fermi surface in a way that induces flattening of the band and shift in the Fermi energy. Two combined effects result in a formation of a kink structure at the energy scale of 21meV and a gap of 17meV, while the Luttinger's condition of $S_1 = S_2$ is maintained, where S_1 and S_2 represent the Fermi volume before and after renormalization. The second renormalization mechanism was observed in the perpendicular direction, using the normal emission ARPES technique. Here one needs to consider the Fermi surface of USb_2 consisting of several uniaxial cylindrical sheets. We have found that the bare band LSDA calculation over-counts the number

of sheets by one. Our high resolution normal emission experiments showed that one of the calculated surfaces actually shrinks below the Fermi level. In a normal emission setup, we measured the dispersion of the bands in the Γ-Z direction. We have shown that the bare LSDA bands in this direction can be renormalized numerically using a low-order self-energy expansion in a three-band interband scattering model, and a very good fit between experiment and renormalized calculation is obtained. We conclude that inter-band scattering in USb_2 influences the fermiology of this system in terms of changing the shape and number of Fermi sheets. We proposed that similar band renormalization effects may significantly influence the band structure of other f-electron systems, and need to be considered.

***Work at LANL - transuranics*.** Plutonium materials from Mott insulators to strongly correlated metals exhibit a wide range of 5f electron characteristics. This indicates that the 5f response may be more than a division between localized and itinerant configurations, but it may be discussed in terms of adaptation to the local environment. The electronic structure of Pu materials is investigated using ARPES, and calculated with advanced models accommodating strong electron correlations. The ARPES results are combined with conventional photoemission to reveal details of the electronic structure evolution including bonding and hybridization between 5f electrons and conduction states. The balance in these strongly correlated materials between the central and periodic potentials is experimentally probed by ARPES providing some insight into 5f adaptive character. Model calculations based on dynamical mean field theory are used for strongly correlated metals, while hybrid functionals cover the Mott insulators. The first ARPES results for $PuCoGa_5$, $PuSb_2$ and PuO_2 have been obtained.

The 18.5 K superconductor $PuCoGa_5$ and correlated metal $PuSb_2$ were investigated using ARPES at 10 K. For these strongly correlated metals, the quasiparticle peak at the Fermi energy shows crystal momentum dispersion, providing details into the Fermi surface development and ground state properties. For $PuSb_2$, the ARPES data at a photon energy (hv) of 21.2 eV indicates a peak that disperses through the Fermi energy. At hv=40.8 eV, $PuSb_2$ shows spectral intensity somewhat flat in reciprocal space. The ARPES data for $PuCoGa_5$ show a dispersive feature crossing the Fermi energy at 21.2 eV with a more pronounced response than $PuSb_2$ to the periodic potential at hv=40.8 eV. Photoemission results for the Fermi level as well as the more localized 5f states well-removed from the Fermi energy are used to quantify the 5f and conduction state character. For the Mott insulator actinide oxides, the focus is on identification of the 5f states compared to the valence states. PuO_2 is predicted to represent a unique point of convergence for the 5f and ligand states leading to substantial covalent bonding while the light actinide oxide series is otherwise dominated by ionic bonding. The angle-integrated photoemission results for the series of actinide oxides showed a trend toward convergence between the 5f states and the oxygen 2p states predicted by hybrid functional calculations. Testing the covalency prediction for PuO_2 directly required ARPES to check for dispersion in the spectral features. The data for PuO_2 indicate a substantial dispersion consistent with model calculations. The PuO_2 ARPES results may be compared to previous UO_2 ARPES results demonstrating the range of 5f character in the Mott insulators from ionic to covalent. With the addition of ARPES to the experimental capabilities for Pu research, it is possible to make a more direct assessment than previously available regarding the balance between localized/itinerant, ionic/covalent, or central/periodic potential arguments for the 5f electrons in Pu materials. Combining Pu ARPES and the wider range of materials with conventional photoemission, the

separation of 5f character into two partitions might well benefit from considering the 5f states as showing an adaptive rather than a dual nature with variations dependent on crystal structure, ligands, and lattice constant.

***Work at LANL – time-resolved ARPES*.** A laser-based apparatus suitable for visible pump/VUV probe time-, energy-, and angle-resolved photoemission spectroscopy utilizing high-harmonic generation from a noble gas was recently constructed at LANL using LDRD -DR funding. Tunability in a wide range of energies, currently 20–36 eV, is achieved by using a time-delay compensated monochromator, which also preserves the ultrashort (below 20fs) duration of the XUV pulses. Using an amplified laser system at 10 kHz repetition rate, approximately 10^9 photons/s per harmonic are made available for photoelectron spectroscopy. Simultaneous energy and momentum measurement is carried out in a hemispherical electron analyzer coupled to a 2D imaging detector.

We have demonstrated the capabilities of the new instrument in terms of selection of the probe wavelength of choice, obtaining angle-integrated photoemission data for UO_2 and providing angle-resolved data for URu_2Si_2. The pump-probe experiment was also conducted on URu_2Si_2 and results are used to explain the band renormalization processes happening at its hidden order transition. Specifically, the second-order phase transitions are characterized by a quantity called order parameter, which may be identified e.g. with a gap in the excitation spectrum. However, the transition at 17.5K in URu_2Si_2 is of unknown origin, and the order parameter remains hidden. In recent years about 30 different theories have been proposed to explain the nature of the hidden order transition in this correlated f-electron system. We have proposed a model based on a convolution of hybridization gap and the hidden order gap in one multi-peak structure near the Fermi level in URu_2Si_2. The evidence for individual components within this structure comes from different experiments, where the most important part, the upper edge of the hidden order gap, is evidenced by the time-resolved measurement of the temperature dependent quasiparticle decay dynamics. The tr-ARPES measurement provided evidence for a long lived feature arising at the Fermi level at temperatures below the hidden order transition in URu_2Si_2. This finding allows us also to explain apparently contradicting previous measurements of the electronic structure in this compound.

Future Plans

We will continue exploring the self-energy approach to f-electron correlated systems at synchrotron facilities. At home, we will focus on measuring the quasiparticle behavior in Pu compounds, especially $PuCoGa_5$ and in Pu metal in the context of duality and adaptive nature, as well as comparing the temperature –dependent measurements with predictions of many-body theories. The time-resolved setup will be used to investigate f-quasiparticle dynamics, especially in the context of direct measurements of the gap size, and by comparing the dynamics for different types of coupling.

Acknowledgements

Work supported by the U.S. Department of Energy, Office of Basic Energy Sciences, Division of Materials Sciences and Engineering and the LANL LDRD program. SRC funded by NSF.

References related to the program (2008-2010)

1. Electronic structure theory of the hidden order material URu_2Si_2, P.M. Oppeneer, J. Rusz, S. Elgazzar, M-T Suzuki, T. Durakiewicz, J. Mydosh (2010) **accepted by PRB**.
2. Temperature dependence of hybridization gaps in metallic heavy fermion systems, X. Yang, P.S. Riseborough, T. Durakiewicz (2010) **accepted by J.Phys.C**.
3. Ultrafast Hopping Dynamics of 5f Electrons in the Mott Insulator UO2 Studied by Femtosecond Pump-Probe Spectroscopy, Yong Q. An, Antoinette J. Taylor, Tomasz Durakiewicz, and George Rodriguez (2010) **submitted to PRL** .
4. Band renormalization effects in correlated f-electron systems, T. Durakiewicz, J.J. Joyce, Y. Li, P. S. Riseborough, P.M. Oppeneer, E.D.Bauer, K.S. Graham, (2010) **accepted by J. Phys:Conf. Ser**.
5. Pu Electronic Structure and Photoelectron Spectroscopy, J.J. Joyce, T. Durakiewicz, K.S. Graham, E.D. Bauer, D.P. Moore, J.N. Mitchell, J.A. Kennison, R.L. Martin, L.E. Roy, and G.E. Scuseria (2010) **accepted by J. Phys:Conf. Ser**.
6. Pump-probe reflectivity study of ultrafast dynamics of strongly correlated 5f electrons in UO_2, Yong Q. An, Antoinette J. Taylor, Tomasz Durakiewicz, and George Rodriguez (2010) **accepted by J. Phys:Conf. Ser**.
7. Tunable ultrafast extreme 5f Electronic Structure and Fermiology of Pu Materials, John J. Joyce, Tomasz Durakiewicz, Kevin S. Graham, Eric D. Bauer, David P. Moore, Jeremy N. Mitchell, John A. Kennison, T. Mark McCleskey, Quanxi Jia, Anthony K. Burrell (2009) **submitted to MRS Proceedings**.
8. Ultraviolet source for time- and angle-resolved photoemission spectroscopy, G. L. Dakovski, Y. Li, T. Durakiewicz, and G. Rodriguez, **Rev. Sci. Instr. 81 (2010) 073108.**
9. Quest for band renormalization and self-energy in correlated f-electron systems, T. Durakiewicz, P.S. Riseborough, C.D. Batista, Yi-feng Yang, P.M. Oppeneer, J.J. Joyce, K.S. Graham, **Acta Physica Polonica A, 117 (2010) 264.**
10. Effect of Electronic Correlations on the Quasiparticle Dispersion of USb_2, X. Yang, P. S. Riseborough, T. Durakiewicz, P. M. Oppeneer and S. Eigazzar, **J. Phys:Conf. Ser. 200 012164, 1-4 (2010).**
11. Unusual quasiparticle renormalizations from angle resolved photoemission on USb_2, X. Yang, P.S Riseborough, T. Durakiewicz, C.G. Olson, J.J. Joyce, E.D. Bauer, J.L. Sarrao, D.P. Moore, K.S. Graham, S.Elgazaar, P. Oppeneer, E. Guziewicz, M.T. Butterfield, **Phil. Mag. 89 (2009) 1893-1911.**
12. Observation of a kink in the dispersion of f-electrons, T. Durakiewicz, P.S. Riseborough, C.G. Olson, J.J. Joyce, E. Bauer, J.L. Sarrao, S. Elgazzar, P.M. Oppeneer, E. Guziewicz, D.P. Moore, M.T. Butterfield, K.S. Graham, (2008) **Europhys. Lett. 84 (2008) 37003.**
13. Theoretical studies of spectral properties of d-plutonium, J.X. Zhu, A.K. McMahan, M.D. Jones, T. Durakiewicz, J.J. Joyce, J.M. Wills and R.C. Albers, **MRS Proc. (2008) 1104, 59-64.**
14. Strong coupling approach to actinide metals, C.D. Batista, J.E. Gubernatis, T. Durakiewicz, J.J. Joyce, **Phys Rev Lett 101 (2008) 016403.**
15. Dispersion in the Mott insulator UO_2: A comparison of Photoemission Spectroscopy and screened Density Functional Theory," Lindsay E. Roy, Richard L. Martin, Juan E. Peralta, Gustavo E. Scuseria, Tomasz Durakiewicz, Cliff G. Olson, John J. Joyce, and Ela Guziewicz, **Journal of Computational Chemistry 29 (2008) 2288-2294.**
16. Physical properties of the new Uranium ternary compounds $U_3Bi_4M_3$ (M=Ni, Rh) T. Klimczuk, Han-oh Lee, F. Ronning, T. Durakiewicz, N. Kurita, H. Voltz, E. D. Bauer, T. McQueen, R. Movshovich, R. J. Cava and J.D. Thompson, **Phys. Rev. B 77 (2008) 245111.**
17. Additional **38** conference abstracts not listed here.

The X-Ray View of Ultrafast Electron and Spin Dynamics in Ferrimagnets
(FWP 'Ultrafast Magnetization Dynamics')

Hermann A. Dürr, Andreas Scherz, Joachim Stöhr

SLAC National Accelerator Laboratory,

2575 Sand Hill Road, Menlo Park, CA 94025

hdurr@slac.stanford.edu

Scope of research: This project focuses on manipulation and control of long-range magnetic and electronic order by optical, electric and magnetic field pulses. On the one hand, such studies are of direct relevance for establishing the ultimate time scale for magnetic switching in future data storage devices. On the other hand, they serve to disentangle the complex interactions between electronic, spin and lattice degrees of freedom at the heart of modern solid-state physics. The relevant interactions in magnetic solids such as Coulomb, exchange, spin-orbit and electron-phonon interaction are of various strength and lead to different characteristic time scales for energy and angular momentum transfer between orbital, spin and lattice degrees of freedom. Of particular interest for magnetic solids is to understand how and on what timescale the relatively weak spin–orbit coupling can be used to manipulate ferromagnetic order in extreme electromagnetic fields.

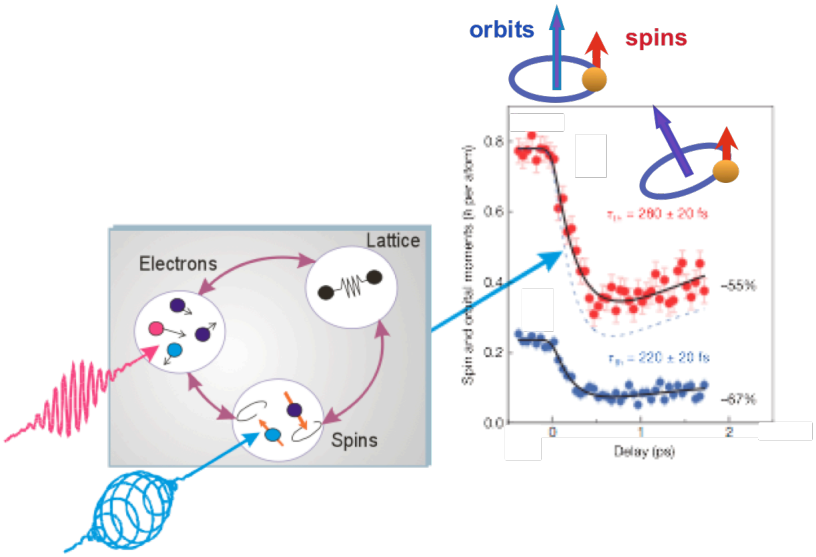

Fig. 1: Temporal evolution of spin, S (top curve), and orbital, L (bottom curve), angular momentum following fs laser excitation (1.5 eV photon energy) of a CoPd film with out-of-plane spin orientation. The data clearly demonstrate that the orbital moment precedes the spin moment leading to non-collinear arrangements as indicated in the insets [Boeglin10].

Fig. 1 shows the first example demonstrating the power of fs soft x-ray pulses to probe the different temporal evolution of spin and orbital angular momentum in CoPd following fs laser excitation [Boeglin10]. While the spins carry the dominant part of the total angular momentum, the electron orbits provide a link to the lattice that can act as an angular momentum reservoir [Wietstruk10]. Here we focus on ferrimagnetic materials consisting of two ferromagnetic sublattices that are exchange

coupled antiferromagnetically. Element specific x-ray scattering and spectroscopy is employed to separate and determine electron and angular momentum exchange between the sublattices on fundamental length and timescales.

Recent progress (subtasks: 'high field magnetism' & 'lattice vs. charge dynamics in magnetite**'):**

Angular momentum exchange in ferrimagnetic FeCoGd: Exchange interaction, being the strongest force in magnetism, is responsible for ferromagnetic or antiferromagnetic spin ordering. We provide unexpected insights into the physics of magnetism, showing that ultrafast spin reversal in a material with antiferromagnetic coupling of spins occurs via a transient ferromagnetic state. In particular, optical excitation of ferrimagnetic GdFeCo on a time-scale pertinent to the characteristic time of exchange interaction between the rare earth (RE) and transition metal (TM) spins pushes the spin dynamics into a yet unexplored regime, where the two exchange coupled magnetic sublattices demonstrate substantially different dynamics. As a result, the reversal of spins appears to proceed via a novel transient state characterized by a ferromagnetic alignment of the Gd and Fe magnetic moments, despite their ground-state antiferromagnetic coupling. The net magnetic moment of the RE (Gd) sublattice is found to reverse within 1.5 ps, which is substantially slower than the TM (Fe) reversal time of 300 fs. These surprising observations supported by atomistic simulations present a novel concept of manipulating magnetic order on a timescale of the exchange interaction. [Radu10]

Ultrafast melting of charge/orbital order in magnetite: Magnetite is not only the oldest ferrimagnet know to mankind with new applications in modern spintronics it is also the first strongly correlated electron material where a metal–insulator transition was observed. The almost degenerate nature of emerging new states in such materials leads to phase fluctuations on many length and time scales during phase transitions. Our goal is to demonstrate how to separate such phenomena in the time domain. We have studied simultaneously the femtosecond (fs) laser induced melting dynamics of the magnetite charge/orbital order and the evolution of the electronic gap in real time using resonant soft x-ray diffraction with fs free electron laser x-ray pulses. The observation of distinctly different timescales between 300 fs and several ps respectively, demonstrates the interplay between lattice symmetry and electronic order that determines the charge transport in magnetite.

Future work:

The above examples represent proof-of-principle studies demonstrating the capability of probing the flow of energy and angular momentum in solid-state materials in real time. The question remains: On what length scale do these processes evolve? While for charge dynamics we can assume that this is typically set by the size of charge/orbital order domains (ca. 100nm) in correlated materials ultrafast spin dynamics should be governed by the exchange length (ca. 10nm). The coherent fs x-ray flux now available at the Linac Coherent Light Source will enable access to such length scales. Initially we plan to do this using (resonant) x-ray scattering techniques. Our vision is to ultimately 'image' snapshots of the evolving spin and charge distribution as indicated schematically in Fig. 2.

The above studies clearly aim at combining fs temporal and nm spacial resolution at LCLS to probe the fastest processes. In addition also 'slower' processes take place on the ps time scale. While, for instance, during magnetic switching the initial stimulus is 'fast' the subsequent energy dissipation occurs much slower but is essential in completing the whole switching process. In this latter regime near equilibrium angular momentum transfer between spins and lattice can ideally be probed using synchrotron radiation especially in the so-called 'low alpha' mode operation, i.e. with reduced bunch length down to several ps [Wietstruck10]. Our preliminary results obtained on magnetite (not shown) indicate that also during laser induced metal-insulator transitions long-lived intermediate

states appear that can be ideally probed with ps temporal resolution available at synchrotron radiation sources such as SSRL.

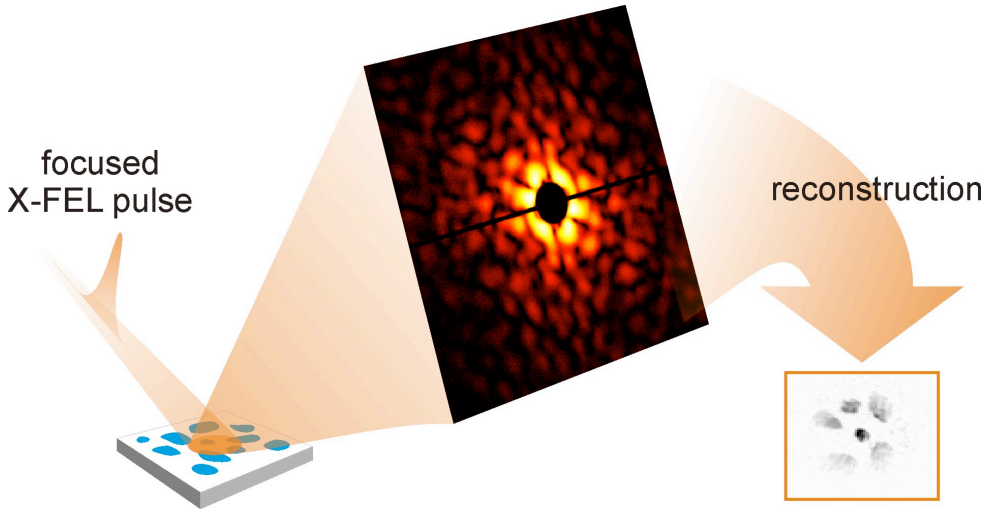

Fig. 2. Schematics of coherent scattering from fluctuating charge/orbital order domains (blue areas). Real space image reconstruction will be possible using the available XFEL flux and by exploring the samples' electronic and structural damage thresholds.

We ultimately plan to extend such studies to the use of extremely strong electromagnetic field pulses on magnetic thin films. The goals are to observe and understand how the response of 3d transition metals and oxides to the ultrashort magnetic and electric fields of unprecedented magnitude differs from the response in a more conventional low field regime. The intense field pulses are created with the highly relativistic electron bunches. Peak electric field values up to the gigavolts/meter range and peak magnetic fields in the tens of Tesla are expected and lead to novel effects such as electric field induced magnetic switching [Gamble09]. We will also utilize intense THz electro- magnetic field pulses generated by relativistic electron pulses initially at FLASH and when available also at LCLS. In THz pump - x-ray probe measurements the electric field induced spin dynamics will be probed in the most direct way, i.e. by measuring the valence band photoelectron spin polarization.

DOE sponsored publications:

[Boeglin10] C. Boeglin, E. Beaurepaire, V. Halté, V. Lopez-Flores, C. Stamm, N. Pontius, H. A. Dürr, J.- Y. Bigot, *Distinguishing the ultrafast dynamics of spin and orbital moments in solids*, Nature **465**, 458 (2010).

[Wietstruk10] Marko Wietstruk, Alexey Melnikov, Christian Stamm, Torsten Kachel, Niko Pontius, Muhammad Sultan, Cornelius Gahl, Martin Weinelt, Hermann A. Dürr, Uwe Bovensiepen, *Strong photo-induced enhancement of spin-lattice coupling in 4f ferromagnets*, submitted (2010).

[Radu10] I. Radu, K. Vahaplar, C. Stamm, T. Kachel, N. Pontius, H. A. Dürr, T. A. Ostler, J. Barker, R. F. L. Evans, R. W. Chantrell, A. Tsukamoto, A. Itoh, A. Kirilyuk, Th. Rasing, A. V. Kimel, *Non-equilibrium spin dynamics of magnetic sublattices in ferrimagnetic GdFeCo,* submitted (2010).

[Gamble09] S. J. Gamble, Mark H. Burkhardt, A. Kashuba, Rolf Allenspach, Stuart S. P. Parkin, H. C. Siegmann, J. Stöhr, Electric Field Induced Magnetic Anisotropy in a Ferromagnet, Phys. Rev. Lett. **102**, 217201 (2009).

Proximity Effects in Conducting Oxide Heterostructures

PIs: J.A. Eastman, D.D. Fong, P.H. Fuoss, P. Zapol
Materials Science Division
Argonne National Laboratory
9700 S. Cass Ave., Bldg 212
Argonne, IL 60439
630-252-5141, jeastman@anl.gov

Research Scope: This program focuses on the growth behavior and characterization of oxide thin film heterostructures exhibiting novel conduction and/or ferroelectric properties. By exploiting proximity effects induced by heterointerfaces through space charge, elastic strain, and interfacial atomic structure, we create new materials with controllable and previously unattainable properties. These proximity effects are amplified in heterostructures when layer spacings are reduced below distances where electronic charges strongly interact or strain fields overlap. We exploit the unique capabilities of in-situ synchrotron x-ray techniques at the Advanced Photon Source (APS) to determine depth-resolved atomic-level structure and film composition in real-time, in the non-vacuum, elevated temperature environments that are integral to growth and transport behavior. Closely integrated first-principles simulation studies provide understanding of the factors that control strain, composition, and structure during growth, play a key role in identifying and elucidating charge transport mechanisms, and facilitate the development of predictive models for the design of oxide heterostructures with emergent properties.

We emphasize synthesis science, using in-situ synchrotron x-ray techniques to understand and control thin film growth behavior during metal-organic chemical vapor deposition (MOCVD), atomic layer deposition (ALD), or oxide molecular beam epitaxy (MBE). A second emphasis is on structure-property correlations, using and developing forefront x-ray scattering and spectroscopy techniques, combined with in-situ electrical characterization, to investigate behavior in elevated temperature, controlled oxygen partial pressure (pO_2) environments. The complex oxide materials that form the building blocks of the heterostructures of interest include, for example, combinations of fast ion conductors such as cubic Y_2O_3-stabilized ZrO_2 (YSZ) or δ-Bi_2O_3, with the ferroelectrics $PbTiO_3$ or $BiFeO_3$.

Recent Progress: In the following, we describe two brief highlights of our recent progress in synthesizing and characterizing oxide heterostructures with unique proximity-induced behavior. These studies demonstrate capabilities and phenomena that will be exploited in our planned studies, which focus on synchrotron x-ray studies of thin film growth science and behavior of oxide thin film heterostructures of conducting and ferroelectric materials.

δ-Bi_2O_3 Epitaxial Stabilization and Oxygen Ordering (in collaboration with D. Proffit, a Ph.D. student co-advised by J.A. Eastman, and Prof. T.O. Mason from Northwestern University)

Oxide ion conductors are critical components in many important energy conversion devices, including solid oxide fuel cells (SOFCs), oxygen separation membranes, and oxidation catalysts. The fluorite-structured δ-phase of bismuth oxide (δ-Bi_2O_3) has attracted significant attention because it exhibits much larger ionic conductivity than all other oxides discovered to date; its conductivity at 750°C is more than two orders of magnitude larger than that of the most commonly used electrolyte in SOFCs, YSZ, at the same temperature [1]. In bulk materials, however, this high conductivity phase is stable only from 729-825°C and transformation to other Bi_2O_3 polymorphs when cooling to room temperature results in a significant reduction in ionic conductivity and may cause deleterious cracking because of the large changes in volume [1].

We recently discovered that δ-Bi_2O_3 nanostructures [2] and continuous films are stabilized to room temperature by epitaxial growth using MOCVD onto oxide substrates having good lattice match to the δ-phase. Synchrotron x-ray scattering results characterizing the orientation relationships and strain states of Bi_2O_3 nanostructures are shown in Fig. 1(a, b). Our findings, which were published in Applied Physics Letters [2], represent the first observation of δ-Bi_2O_3 epitaxial stabilization on oxide substrates and the first demonstration of a tunable δ-Bi_2O_3 strain state by substrate misfit.

The high ionic conductivity of δ-Bi_2O_3 derives from the fact that 25% of the oxygen sites in the fluorite structure are vacant because of the +3 valence of the Bi cations. Ordering of these vacant sites, and the accompanying reduction in conductivity, occurs when the δ-phase is stabilized to low temperature by cation doping [3]. Previous studies of undoped δ-Bi_2O_3 samples did not report oxygen vacancy ordering [4], but were performed only at high temperatures (>729°C), where bulk δ-Bi_2O_3 is stable. As seen in Fig. 1(c), we recently observed that epitaxial nanoislands of pure δ-Bi_2O_3 grown onto $SrTiO_3$ or $DyScO_3$ substrates exhibit 1/3-order superstructure peaks at room temperature, in addition to the normal Bragg peaks from the film and the substrate. These superstructure peaks are likely indicative of vacant oxygen site ordering, which has been theoretically predicted to occur in pure δ-Bi_2O_3 by Aidhy et al [5]. We are currently determining the detailed ordered structure of stabilized δ-Bi_2O_3 from our diffraction data.

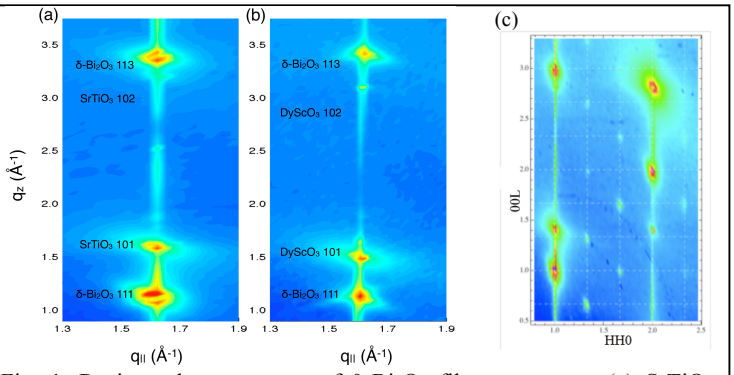

Fig. 1. Reciprocal space maps of δ-Bi_2O_3 films grown on (a) $SrTiO_3$ (001) and (b) $DyScO_3$ $(001)_p$ substrates [2]. As seen, the δ-Bi_2O_3 11*L* CTR is aligned with the substrate 10*L* CTR, indicating (001) δ-Bi_2O_3 // (001) perovskite and [110] δ-Bi_2O_3 // [100] perovskite epitaxy and full lattice match with the substrates. (c) X-ray intensity map of a (110)-type plane in reciprocal space for δ-Bi_2O_3 nanoislands grown epitaxially onto $SrTiO_3$ (001). These observations at 100°C in pO_2 = 10 Torr indicate the presence of superstructure peaks likely due to oxygen ordering, in addition to normal Bragg peaks from the film and substrate.

Reversible Chemical Switching of Ferroelectric Oxide Thin Films (in collaboration with G.B. Stephenson and S.K. Streiffer of ANL, and C. Thompson of Northern Illinois University)

Ferroelectric materials display a spontaneous electrical polarization that can be switched to different orientations, typically through application of an electric field. In this study, we demonstrated for the first time that ferroelectric polarization can also be fully and reversibly switched by changing the chemical environment in contact with the surface of the material. This work was published in Physical Review Letters [6] and was the subject of a Viewpoint commentary in *Physics* [7].

In-situ synchrotron x-ray scattering measurements (Fig. 2) show that high or low pO_2 induces outward or inward polarization, respectively, in ultrathin $PbTiO_3$ films. While x-ray scattering is not sensitive to interfacial charge from polarization, it is very sensitive to the atomic positions in the crystal structure of a ferroelectric film that determine its polarization. By characterizing film structure in-situ, under conditions of controlled pO_2 and temperature, one sees that the oxygen chemical potential determines the electric potential at the film surface, and that the relationship between electrical and chemical potential is complex. In combination with *ab initio*-based modeling performed by our collaborators A.M. Rappe and A. Kolpak (U. Penn.), these experiments show that the chemical

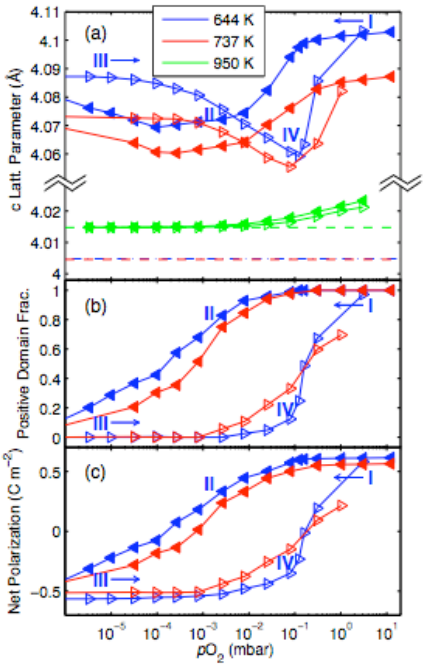

Fig. 2. Lattice parameter, domain fraction, and polarization derived from x-ray scattering measurements during switching of a 10 nm $PbTiO_3$ film by changing the oxygen partial pressure at its surface. In (a), "butterfly" loops observed below T_C indicate switching.

environment can play a dominant role in determining the behavior of nanoscale ferroelectrics.

Future Plans: Our planned research focuses on using synchrotron x-ray scattering and spectroscopy techniques to investigate the growth science of conducting and ferroelectric oxide heterostructures, as well as on understanding the behavior of these heterostructures in elevated temperature, controlled pO_2 environments.

Conducting and ferroelectric oxide thin film growth science

The strength of proximity effects in thin film oxide heterostructures can be tuned through manipulation of the interfacial spacing and morphology during synthesis. We will utilize state-of-the-art in-situ monitoring techniques to enable the creation of specially designed interfaces during the synthesis of layered or nanocomposite epitaxial oxide thin films. Heterostructures will be created using ALD, MOCVD, and MBE, techniques with proven potential for growing high-quality heterostructures. We have already developed unique facilities at the APS for in-situ studies of oxide MOCVD [8] and ALD [9], and are active participants in a new effort to develop the first-ever capability for in-situ x-ray characterization during oxide MBE [10].

A goal of one initial study will be to determine conditions for growth of epitaxial thin films of δ-Bi_2O_3 by ALD, including plasma-assisted ALD. Bi_2O_3 is a material that is known to be difficult to grow by ALD because of issues associated with precursor volatility and thermal stability of the films, particularly in low pO_2, elevated temperature environments [11]. As in our recent in-situ x-ray study of ZnO ALD [9], we will employ a combination of reflectivity, high-angle diffraction, and fluorescence techniques to understand the effects of various processing conditions on growth behavior, and will also determine whether high-quality epitaxial single crystal films can be grown by alternating ALD growth cycles with rapid thermal annealing treatments. In the longer term, we will extend these studies to investigate the growth behavior and properties of Bi_2O_3-containing layered structures and nanocomposites for studies of proximity effects in heterostructures containing combinations of ionic conductors and either ferroelectrics or electronic conductors.

Behavior of Oxide Thin Film Heterostructures of Conducting and Ferroelectric Materials

The behavior of conducting and ferroelectric oxides is simultaneously most complex and most interesting under elevated temperature exposure to gaseous environments. Therefore, *in situ* monitoring techniques are critical for understanding not only synthesis, but also the properties of the materials of interest. In our planned studies we will simultaneously determine environmentally-induced structural changes while monitoring either conduction or ferroelectric behavior.

One planned study focuses on the effects of substrate surface polarity on ferroelectric properties. We will compare and contrast the behavior of $PbTiO_3$ films grown on charge-neutral surfaces (e.g., $SrTiO_3$ (001)) with that of the same material grown on substrates with polar surfaces (e.g., $DyScO_3$ (110)). We will determine the effects of substrate polarity on the paraelectric-to-ferroelectric phase transition temperature, the temperature dependence of the polarization magnitude, and the ferroelectric domain structure and switching characteristics.

Another planned study will investigate the possibility of coupled behavior in heterostructures containing a ferroelectric phase (e.g., $PbTiO_3$ or $BiFeO_3$) in close proximity to an ionic conductor (e.g., YSZ or δ-Bi_2O_3). The polarization in a ferroelectric film is expected to induce a strong effect on the distribution and possibly concentration of oxygen vacancies in an oxide ionic conductor. As the magnitude and direction of the ferroelectric polarization is changed (by either changing pO_2 or an applied electric field), we expect this vacancy distribution to also change. Both experimental and theoretical studies are planned to determine the polarization-induced changes in oxygen vacancy concentration and distribution, and to determine the possible effects on ionic transport behavior. A key question that will be addressed is whether the enhanced vacancy concentrations at the ferroelectric/ionic conductor interface are sufficiently mobile to contribute to altering the oxygen diffusion rate in the ionic conductor. Conversely, we will also explore whether rapid oxygen diffusion through the ionic conductor affects the domain structure and/or switching behavior of the ferroelectric.

References

1) AM Azad, S Larose, and SA Akbar, *J. Mater. Sci*., **29**, 4135 (1994).
2) D.L. Proffit, G.-R. Bai, D.D. Fong et al., *Appl. Phys. Lett*., **96**, (2), 021905 (2010).
3) T Takahashi and H Iwahara, *J. Appl. Electrochem*., **3**, 65 (1973).
4) G. Gattow and H. Schröder, *Zeit. Anorgan. Allgem. Chem*., **318**, 176 (1962); H.A. Harwig, *Zeit. Anorgan. Allgem. Chem*., **444**, 151 (1978).
5) D Aidhy, S Sinnott, E Wachsman et al., *J. Sol. State Chem*., **182**, 1222 (2009); D.S Aidhy, J.C. Nino, S.B. Sinnott et al., *J. Amer. Ceram. Soc.*, **91**, 2349 (2008).
6) R.-V Wang, D.D Fong, F. Jiang et al., *Phys. Rev. Lett.*, **102**, 047601 (2009).
7) J. Hlinka, *Physics* **2**, 8 (2009).
8) M.V.R. Murty, S.K. Streiffer, G.B. Stephenson, J.A. Eastman, G.-R. Bai, A. Munkholm, O. Auciello, C. Thompson, Appl. Phys. Lett., **80**, 1809 (2002).
9) D.D. Fong, J.A. Eastman, P.H. Fuoss, P.M. Baldo, T.T. Fister, M.J. Highland, submitted to *Appl. Phys. Lett.* (2010).
10) J.W. Freeland, D.D. Fong, S.M. Nakhmanson, A. Bhattacharya, H. Hong, J. Jellinek, N. Markovic, J.A. Eastman, "Synthesis Science of Functional Layered Complex Oxides," funded LDRD program (2010).
11) T. Hatanpää, M. Vehkamäki, M. Ritala, M. Leskelä, *Dalton Trans*., **39**, 3219 (2010).

Publications (2008-2010)

"Continuous Switching at the Intrinsic Coercive Field in Ultrathin $PbTiO_3$," M.J. Highland, T.T. Fister, M.-I. Richard, D.D. Fong, P.H. Fuoss, Carol Thompson, J.A. Eastman, S.K. Streiffer, and G.B. Stephenson, to appear in *Physical Review Letters* (2010).

"Phase Stabilization of δ-Bi_2O_3 Nanoislands by Epitaxial Growth onto Single Crystal $SrTiO_3$ or $DyScO_3$ Substrates," D.L. Proffit, G.-R. Bai, D.D. Fong, T.T. Fister, S.O. Hruszkewycz, P.M. Baldo, P.H. Fuoss, T.O. Mason, J.A. Eastman, *Applied Physics Letters*, **96**, 021905 (2010).

"X-ray Probes for *In Situ* Studies of Interfaces," D.D. Fong, C.A. Lucas, M.-I. Richard, and M.F. Toney, *MRS Bulletin* **35**, 504 (2010).

"In Situ Synchrotron Characterization of Complex Oxide Heterostructure," T.T. Fister and D.D. Fong, in *Thin Film Metal-Oxides: Fundamentals and Applications in Electronics and Energy,* ed. S. Ramanathan (New York, NY: Springer Science + Business Media, LLC, 2010).

"Reversible Chemical Switching of a Ferroelectric Film," R.-V. Wang, D.D. Fong, F. Jiang, M.J. Highland, P.H. Fuoss, C. Thompson, A.M. Kolpak, J.A. Eastman, S.K. Streiffer, A.M. Rappe, and G.B. Stephenson, *Physical Review Letters* **102**, 047601 (2009).

"Ferroelectricity in Ultrathin Strained $BaTiO_3$ Films: Probing the Size Effect by Ultraviolet Raman Spectroscopy," D.A. Tenne, P. Turner, J.D. Schmidt, M. Biegalski, Y.L. Li, L.Q. Chen, A. Soukiassian, S. Trolier-McKinstry, D.G. Schlom, X.X. Xi, D.D. Fong, P. Fuoss, J. Eastman, G.B. Stephenson, C. Thompson, and S.K. Streiffer, *Physical Review Letters* **103**, 177601 (2009).

"Phase Transitions in Nanoscale Ferroelectric Structures," S.K. Streiffer and D.D. Fong, *MRS Bulletin*, **34,** 832 (2009).

"In situ characterization of strontium surface segregation in epitaxial $La_{0.7}Sr_{0.3}MnO_3$ thin films as a function of oxygen partial pressure," T.T. Fister, D.D. Fong, J.A. Eastman, P.M. Baldo, M.J. Highland, P.H. Fuoss, K.R. Balasubramaniam, P.A. Salvador, *Applied Physics Letters*, **93**, 151904 (2008).

"Imaging and alignment of nanoscale 180° stripe domains in ferroelectric thin films," C. Thompson, D.D. Fong, R.-V. Wang, F. Jiang, S. K. Streiffer, K. Latifi, J.A. Eastman, P.H. Fuoss, and G.B. Stephenson, *Applied Physics Letters* **93**, 182901 (2008).

"Critical thickness of high structural quality $SrTiO_3$ films grown on orthorhombic (101) $DyScO_3$," M.D. Biegalski, D.D. Fong, J.A. Eastman, P.H. Fuoss, S.K. Streiffer, T. Heeg, J. Schubert, W. Tian, C.T. Nelson, X.Q. Pan, M.E. Hawley, M. Bernhagen, P. Reiche, R. Uecker, S. Trolier-McKinstry, D.G. Schlom, *Journal of Applied Physics*, **104**,114109 (2008).

Looking deeper into buried nanolayers and electronic structure: standing-wave and angle-resolved soft and hard x-ray photoemission

Charles S. Fadley,
Department of Physics, University of California Davis, Davis, CA 95616 USA
Materials Sciences Division, Lawrence Berkeley National Laboratory, Berkeley, CA 94720 USA
E-mail: fadley@physics.ucdavis.edu
with Peter Fischer-LBNL, Jeff Kortright-LBNL, Frances Hellman-UCB&LBNL

⇒ Research Overview: New techniques based on synchrotron radiation photoemission are developed and applied to a variety of magnetic materials and nanostructures [1-11]. In particular, nm-scale standing-wave excitation in multilayer spintronic structures reveals depth-dependent composition, magnetization, density-of-states, and, in our most recent data, k-resolved electronic structure via angle-resolved photoemission (ARPES) [1-3, 5, 8, 9]. Standing-wave excitation has also been shown to add the third dimension in photoelectron microscopy [5,9].

Beyond this, the use of hard x-ray excitation in the 3-6 keV regime permits determining these properties for buried layers and interfaces, as well as assessing more cleanly the bulk properties of novel magnetic and semiconductor materials [4,6-8,10,11]. It is only within the past decade that such experiments have begun with energies in the hard x-ray regime above 2 keV and going up to 10 keV or more. Such hard x-ray photoemission (HXPS or HAXPES) measurements are of high interest because they permit obtaining information from deeper below the surface of a solid sample, due to electron inelastic mean free paths (IMFPs) that increase roughly as (kinetic energy)$^{0.75}$. HXPS is thus rapidly developing worldwide, but not widely practiced in the US. The HXPS data we have obtained include the first use of nm-scale multilayer standing-wave excitation, proof-of-principle valence-band ARPES results, and hard x-ray photoelectron diffraction (HXPD) effects..

⇒ Recent research highlights:

- **Depth resolved electronic structure of an LSMO/STO superlattice via standing-wave excited angle-resolved photoemission [11, and to be published]**

We have determined the depth-resolved composition profiles and electronic structure of a $SrTiO_3/La_{0.67}Sr_{0.33}MnO_3$ superlattice via standing-wave (SW) excited angle-resolved soft and hard x-ray photoemission. The epitaxial superlattice samples consisted of 48 and 120 bilayers of STO (15.6 Å-4 unit cells) and LSMO (15.5 Å-4 unit cells). These were studied using excitation energies of 833.2 eV near the La $3d_{5/2}$ resonance at the ALS, and at 5,946 eV at Spring-8. Analyzing rocking curves at both energies permits determining the precise profile of the bilayers in the superlattice, which varies slightly in thickness from top to bottom, as well as depth-resolved composition profiles and optical constants through the STO/LSMO interface. Some results from this study are shown in Figure 1. Measurements of core-level binding energies through the soft x-ray rocking curve also reveal a shift of the Mn 3p photoemission peak near the interface which is not found for the peaks in any other element; this suggests a change in the Mn bonding near the STO/LSMO interface, and is consistent with Anderson-impurity-model (AIM) calculations incorporating a crystal-field distortion effect. The valence-band density of states also reveals signatures of Mn 3d e_g and t_{2g} and Ti-derived states in the rocking curves, together with their localization character. Finally, some first SW-excited soft x-ray ARPES data shows distinctly different *k*-space maps of the Mn 3d e_g and t_{2g} states, together with changes near the STO/LSMO interface. These last data represent a step towards depth-resolved ARPES.

Co-authors: A. X. Gray, C. Papp, B. Balke, S.-H. Yang, M. Huijben, L. Plucinski, E. Rotenberg, A. Bostwick, S. Ueda, Y. Yamashita, K. Kobayashi, E. M. Gullikson, J. B. Kortright, F. M. F. DeGroot, L. Plucinski, C. M. Schneider, C. S. Fadley (Names in blue are LBNL collaborators.)

- **Hard x-ray photoemission measurement of the electronic structures of an epitaxial, semiconducting $Cr_{0.80}Al_{0.20}$ thin film and of $Fe_{1-x}Si_x$ binary Heusler alloys [Submitted to PRL and to be published]**

We have studied the bulk properties of two magnetic alloys, antiferromagnetic $Cr_{0.80}Al_{0.20}$, together with a pure Cr reference sample, and samples of $Fe_{1-x}Si_x$ near the Fe_3Si composition, with bulk-sensitive hard x-ray photoemission at SPring8. By performing photoemission measurements in the hard x-ray regime, more specifically with an excitation energy of 5956.4 eV, we increase the inelastic mean-free path of the valence-band electrons by a factor of 3-7 compared to conventional soft x-ray photoemission (500 – 1500 eV). With the ability to thus probe on average 25 atomic layers into the sample, the measurements become truly bulk-sensitive.

►**$Cr_{0.80}Al_{0.20}$:** These data reveal among other things a semiconducting energy band gap of 85.5±13.9 meV in $Cr_{0.80}Al_{0.20}$. The valence-band measurements are compared to theoretical density of states calculations, which

agree in predicting the opening of a gap in the alloy. Core-level spectra are also found to exhibit shifts and satellite effects, and these also will be discussed, in comparison to AIM theory.

►**$Fe_{1-x}Si_x$:** We used hard x-ray photoemission spectroscopy at 5,956 eV to investigate the electronic properties of crystalline and amorphous $Fe_{1-x}Si_x$ with x = 0.22 and 0.35. These alloys are considered to be binary Heusler alloys, with theory predicting significant spin polarization at the Fermi energy, and possible spintronic applications. Films in this composition range can be grown metastably in the bcc structure, thus allowing the effect of composition changes to be studied without a change in crystal structure. The shapes and positions of Si (1s, 2s, 2p) and Fe (2p, 3s, 3p) core levels were investigated for the two compositions (x = 0.22 and 0.35) and for both crystalline and amorphous samples. Analysis of the valence bands, dominated by Fe 4s, Si 3s and Fe 3d levels, revealed significant differences between the compounds of the two compositions and degrees of crystallinity. We find excellent agreement with one-step photoemission calculations based on the coherent potential model and including matrix-element effects.
Co-authors: J Karel, AX Gray, C Bordel, Z Boekelheide, DA Stewart, C Papp, B Balke, S Ueda, J Minar, J Braun, H Ebert, K Kobayashi, F Hellman, CS Fadley

• Bulk electronic structure from hard x-ray angle-resolved photoemission: W(110) and a (Ga,Mn)As ferromagnetic semiconductor [11 and to be published]
We have used hard angle-resolved x-ray photoemission spectroscopy (HARPES) to investigate the electronic structure of W(110) as a first proof-of-principle test case and of ferromagnetic $Ga_{1-x}Mn_xAs$ (001) ($x \approx 0.05$) compared to pure GaAs as a system of interest in spintronics, measuring in detail both core-level spectra and angle-resolved valence-band spectra. Data were obtained at both SPring-8 and BESSY, with photon energies of 3.2 keV and 6.0 keV. The $Ga_{1-x}Mn_xAs$ samples were synthesized by ion implantation and pulsed-laser melting. Measuring at these energies should yield about 10-20 times more bulk-sensitivity than traditional ARPES in the 20-130 eV regime. Dispersive bands are clearly seen in the data for W, GaAs, and $Ga_{1-x}Mn_xAs$, particularly after correction for density of states (DOS)-like intensity due to phonon effects and associated XPD effects. Core-level photoelectron diffraction, multiplet splittings and screening satellites also permit better defining the bulk electronic structure. The valence-level data are compared with one-step photoemission calculations, and found to be in excellent agreement. This includes differences between GaAs and $Ga_{1-x}Mn_xAs$. The prospects for future hard x-ray ARPES (HARPES) will be discussed. Some results from this study are shown in Figures 2 and 3.
Co-authors: PR Stone, AX Gray, S Ueda,Y Yamashita, J Fujii, G Panaccione, M Gorgoi, J Minar, J Braun, H Ebert, O Dubon, CS Fadley

• Depth-resolved photoelectron microscopy of nanostructures via soft x-ray standing wave excitation [5,9]
We have demonstrated the addition of depth resolution to the usual two-dimensional images in photoelectron emission microscopy (PEEM), with application to a wedge-profile sample and a square array of circular magnetic microdots. The method is based on excitation with a soft x-ray standing-wave (SW) generated by Bragg reflection from a multilayer-mirror substrate on which the sample is grown. The standing wave is moved vertically through the sample by imaging the wedge with several SW cycles along it, by varying the photon energy around the Bragg condition, or by using the two in concert [5, 9, and video at: http://www.physics.ucdavis.edu/fadleygroup/. The experiment was conducted at the soft x-ray beamline UE49-PGM-a of the storage ring BESSY-II (Helmholtz Zentrum Berlin) that is equipped with an Elmitec PEEM-II including an integrated photoelectron energy analyzer. Depth-resolved PEEM images were obtained for all of the observed elements. Photoemission intensities based on different core peak intensities as functions of photon energy were compared to x-ray optical theoretical calculations in order to quantitatively derive the depth-resolved film structure of the samples. Figure 4 shows some data from the microdot study. This SW approach thus provides complementary information to the usual lateral information provided by PEEM, and should have wide applicability to studies of magnetic and other nanostructures in the future.
Co-authors: F Kronast, AX Gray, C Papp, S H Yang, A Kaiser, S Cramm, IP Krug, F Salmassi, E M Gullikson, DL Hilken, EH Anderson, PJ Fischer, JB Kortright, HA Dürr, W. Eberhardt, CM Schneider, CS Fadley.

⇒ Selected DOE-Funded Publications: *R* = longer review article

1) *R* "Probing Multilayer Spintronic Structures with Photoelectron and X-Ray Emission Spectroscopies Excited by X-Ray Standing Waves", S.-H. Yang, B.C. Sell, and C. S. Fadley, J. Appl. Phys. 103, 07C519 (2008).
2) "Determination of buried interface composition and magnetism profiles using standing-wave excited soft x-ray emission and inelastic scattering", B.C. Sell, S.-H. Yang, M. Watanabe, B.S. Mun, L. Plucinski, N.

Mannella, S.B. Ritchey, A. Nambu, J. Guo, M.W. West, F. Salmassi, J.B. Kortright, S.S.P. Parkin, and C.S. Fadley, J. Appl. Phys. 103, 083515 (2008).
3) *R* "Atomic-Level Characterization of Materials with Core- and Valence-Level Photoemission: Basic Phenomena and Future Directions", C.S. Fadley, invited review, Surf. Interface Anal. 2008, 40, 1579–1605.
4) "Band Mapping in Higher-Energy X-Ray Photoemission: Phonon Effects and Comparison to One-Step Theory", L. Plucinski, J. Minár, B.C. Sell, J. Braun, H. Ebert, C.M. Schneider and C.S. Fadley, Phys. Rev, B 78, 035108 (2008).
5) "Depth-resolved soft x-ray photoelectron emission microscopy in nanostructures via standing-wave excited photoemission, F. Kronast, R. Ovsyannikov, A. Kaiser, C. Wiemann, S.-H. Yang, D. E. Bürgler, R. Schreiber, F. Salmassi, P. Fischer, H. A. Dűrr, C. M. Schneider, W. Eberhardt, and C. S. Fadley, Appl. Phys. Lett. 93, 243116 (2008).
6) "High energy photoelectron diffraction: model calculations and future possibilities", A. Winkelmann, J. Garcia de Abajo and C.S. Fadley, New J. Phys. 10, 113002 (2008).
7) "Report on the Workshop on Hard X-Ray Photoemission in Materials Sciences: Recent Progress and Future Directions", A. Fedorov and C.S. Fadley, Synchrotron Radiation News, 22, 34 (2009), with program and presentations at: http://ssg.als.lbl.gov/ssgdirectory/fedorov/workshops/index.html .
8) *R* "x-ray Photoelectron Spectroscopy : Progress and Perspectives", C.S. Fadley, invited review, Journal of Electron Spectroscopy and Related Phenomena 178–179, 2 (2010).
9) "Standing-wave excited soft x-ray photoemission microscopy: application to nanodot Co magnetic arrays", C. Papp, F. Kronast, A. Gray, A. Kaiser, C. Wiemann, S.-H. Yang, D. E. Bürgler, R. Schreiber, F. Salmassi, P. Fischer, H. A. Dűrr, C. M. Schneider, and C. S. Fadley, Appl. Phys. Lett. 97, 062503 (2010).
10) "Meeting Report: International Workshop for New Opportunities in Hard x-ray Photoelectron Spectroscopy: HAXPES 2009", J. C. Woicik, D. A. Fischer, E. Vescovo, D. A. Arena, D. E. Starr, B. O. Wells, C. S. Fadley, Synchrotron Radiation News, 23, 1 (2010), with program and presentations at: http://www.nsls.bnl.gov/newsroom/events/workshops/2009/haxpes/
11) "Looking Deeper into Buried Nanolayers and Complex Materials: Standing-Wave and Angle-Resolved Hard X-Ray Photoemission", C.S. Fadley, S. Ueda, and K. Kobayashi, SPring8 Research Frontiers 2009, pages 72-73, available as http://www.spring8.or.jp/pdf/en/res_fro/09/072-073.pdf

⇒ **Future plans:** We will continue with the development, refinement, and application of the nm-scale standing wave and hard x-ray techniques in photoemission, with specific systems of interest being oxide multilayer structures, alloys, and Heusler alloys of interest for spintronic applications. We will also construct a facility at the ALS for carrying out HXPS measurements.

⇒ **Figures:**

Fig. 1. **(a)** Standing-wave (SW) rocking-curves from Sr $3p_{3/2}$ and Ti $2p_{3/2}$ core levels excited by 5956 eV photons (data from SPring-8) and 833 eV photons (data from the ALS) from a SrTiO3/$La_{0.67}Sr_{0.33}MnO_3$ multilayer, with both experiment and best-fit X-ray optical theory shown. **(b)** The detailed interface profiles of concentration derived from the best fit. See publication 11.

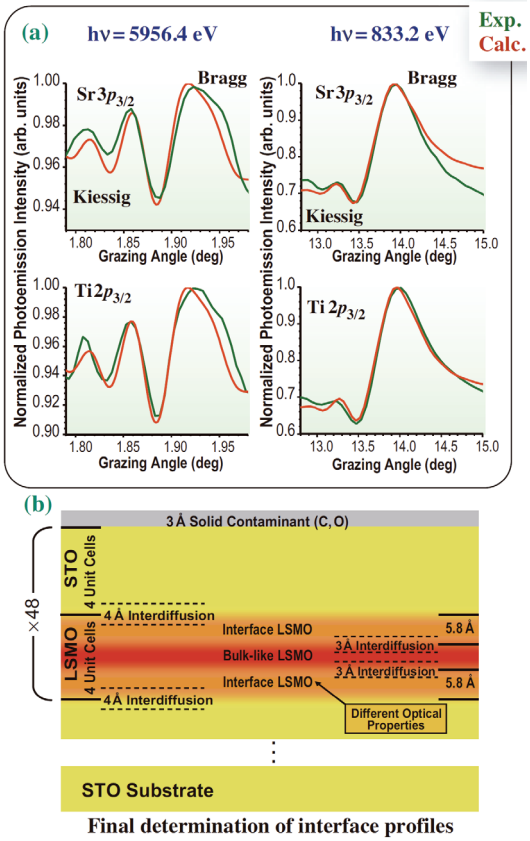

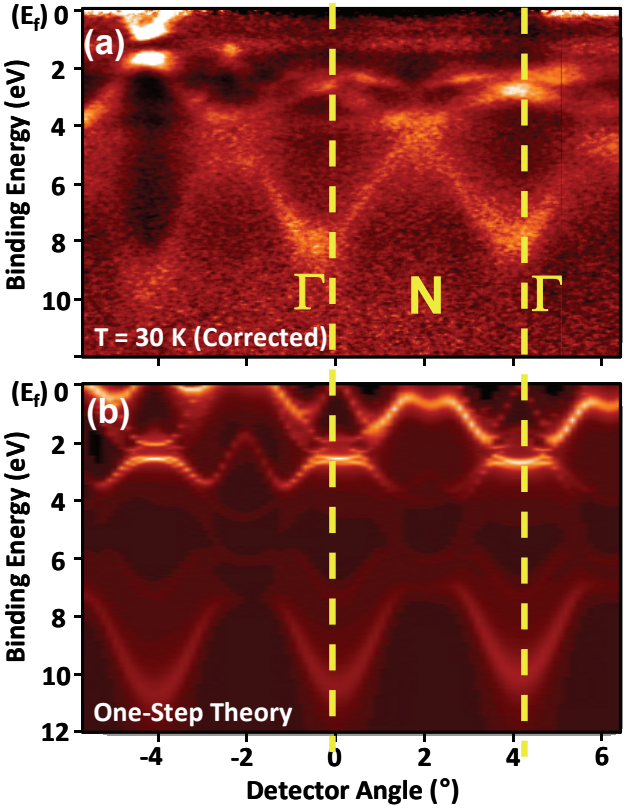

Fig 2. HARPES data from W(110) at 30 K with excitation at a photon energy of 5956 eV. **(a)** The data at 30 K, corrected for DOS and HXPD effects, clearly exhibiting dispersive bands. **(b)** One step photoemission theory, which exhibits good agreement with experiment. (From publication 11.)

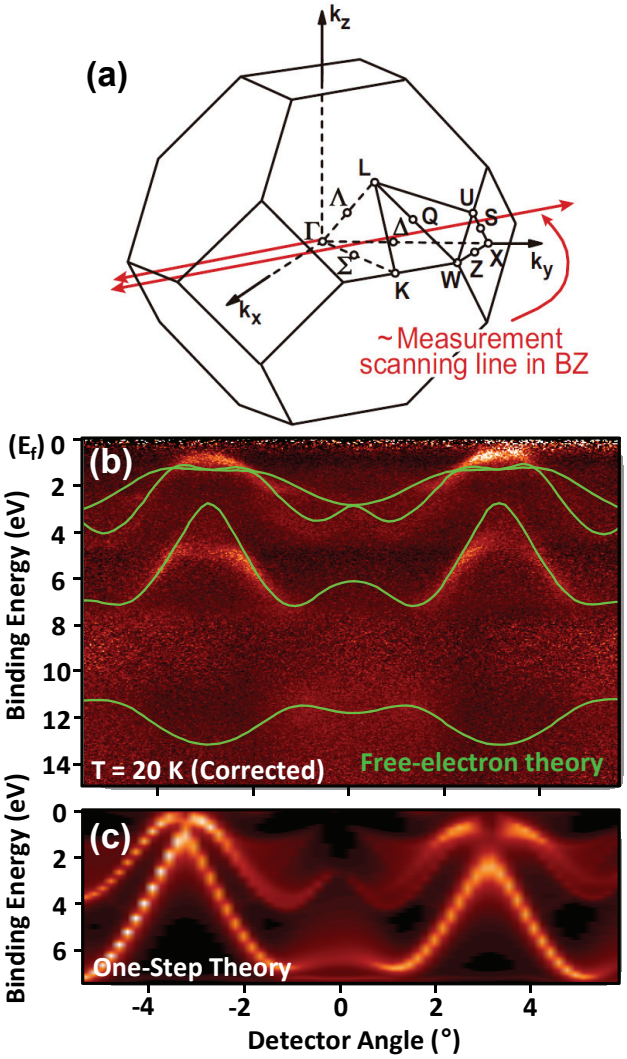

Fig 3. HARPES data from GaAs(001) at 20 K with excitation at a photon energy of 3242 eV. **(a)** The Brillouin zone, with the expected sampling line shown in red. **(b)** The corrected data are overlaid with the band structure region that is predicted by a simple free-electron final-state theory calculation to be involved in direct transitions. The band at *ca.* 13 eV is mostly non-bonding As 4s and so it is core-like, exhibiting HXPD effects. The bands above it are more delocalized, and show dispersion. **(c)** One step photoemission theory, which exhibits good agreement with experiment. (From publication 11.)

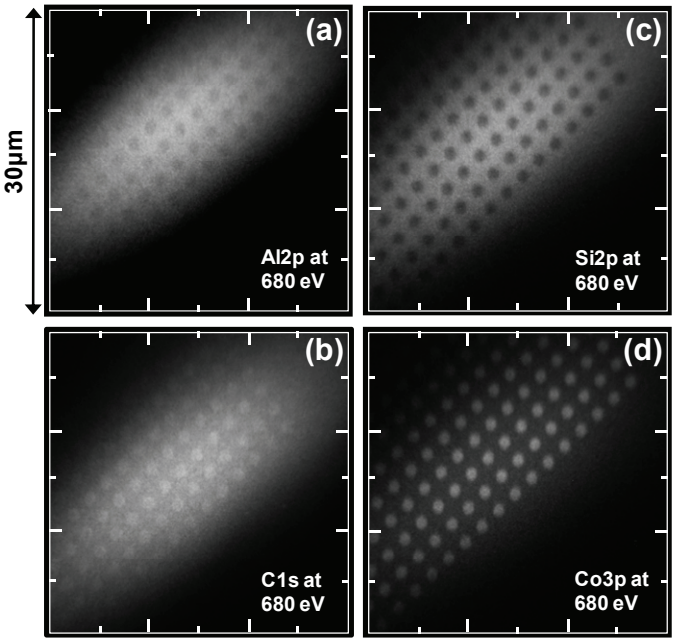

Fig 4. Standing-wave PEEM images at hv-680 eV, for imaging with **(a)** Al *2p*, **(b)** C *1s*, **(c)** Si *2p*, and **(d)** Co *3p* core level intensities. 680 eV is the energy for which the Al image is a maximum off the microdots. (From publication 9.)

Title: *In Situ* Synchrotron X-ray Studies of Reactivity at Polar Oxide Surfaces

PI: Dillon D. Fong
Materials Science Division
Argonne National Laboratory
9700 S. Cass Ave., Bldg 212
Argonne, IL 60439
630-252-3793, fong@anl.gov

Research Scope

Oxide surfaces play an integral role in fields as diverse as heterogeneous catalysis, solid oxide fuel cells (SOFCs), corrosion, and electronic devices. In all of these instances, the surface interacts closely with its gas phase environment, incorporating or losing oxygen, adsorbing or desorbing reactants and products (often transferring charge in the process), and altering its local structure and composition. These modifications in the surface then lead to changes in its interactions with the gas phase. While these interrelationships complicate studies of the underlying physics, they are characteristic of many important surface reactions. One such reaction is oxygen reduction on $La_{1-x}Sr_xMnO_3$, a common SOFC cathode. The reaction involves several distinct atomic mechanisms (some of which are illustrated in Fig.1 (a)), but meeting the longstanding goal of lowering SOFC operating temperature will require understanding how each of the various pathways impacts the surface and thus affects the others [1]. Another example is the reported potential of oxide nanoparticles for water oxidation [2]. Although the specific mechanisms are not well-understood, the Co_3O_4 nanocatalysts demonstrate rates and sizes similar to nature's photosystem II, making them excellent candidates for integrated solar fuel systems.

Aside from their interesting surface properties, many oxides are also electrically active. In some, non-uniform distributions of charge (often point defects in the ionic lattice) lead to local fields, and in others, charged atomic planes contribute to a dipole moment that can be reversed by an applied electric field. With the many advances in oxide heterostructure synthesis, these properties can now be controlled on the near-atomic level. Therefore, although we are only beginning to probe the important interactions between internal field and surface reactivity [3], it is now possible to atomically tailor and dynamically control the catalytic properties of oxide surfaces [4,5]. Needless to say, this has the potential to yield enormous benefits in the areas of energy and environment.

Unfortunately, researchers are still struggling to understand the behavior of “real” oxide surfaces, i.e., surfaces in stable or metastable equilibrium with a reactive environment. The electron-based probes often used for surface characterization cannot function in high pressure environments, and it remains difficult to operate scanning probe microscopes at high temperature or with sufficient time resolution. X-rays, on the other hand, can easily penetrate non-vacuum environments, and the remarkable number of advances in synchrotron-based scattering and

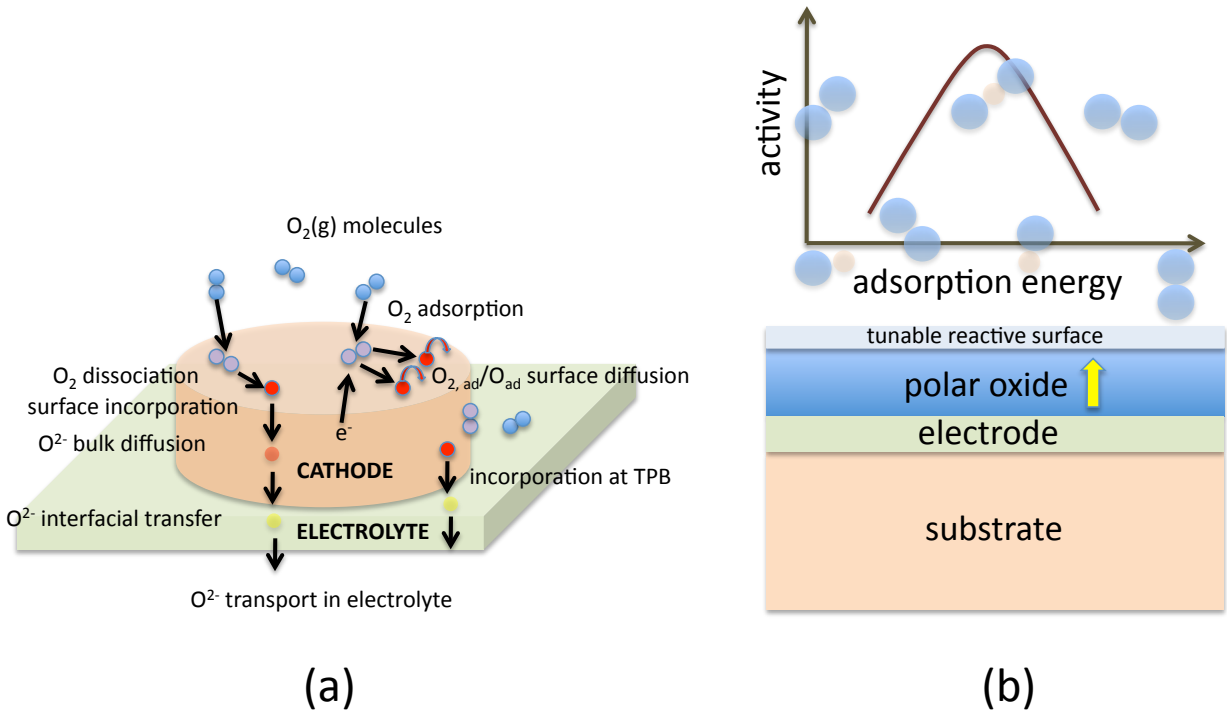

FIG. 1. (a) Schematic of the oxidation reduction reaction on a solid oxide fuel cell cathode. (b) Schematic of oxide thin film with tunable surface properties. Also shown is the "volcano" curve showing that peak catalytic activity occurs at moderate adsorption energies.

spectroscopic techniques advocated by us [6-9] and several other groups [10,11] have made *in situ* synchrotron methods nearly ideal for studying both ensemble-averaged and local structural and chemical information in real time. In this program, we will employ such *in situ* techniques to synthesize novel oxide surfaces and characterize their behavior in reactive environments, with the oxide materials and reactions to be studied typical of those used in a variety of energy applications. A central goal will be taking advantage of the electrical properties of oxides to create tunable surface properties for reactions with the gas phase (Fig. 1(b)).

Recent Progress

This is a new program building on our recent work demonstrating the strong interaction between the ferroelectric surface and the gas phase [3, 12]. As shown in [12], ferroelectric films of $PbTiO_3$ on $SrRuO_3$ (001) can be switched between up and down polarization states by varying the oxygen partial pressure.

Future Plans

Here we outline our plan for synthesizing and characterizing oxide surfaces with controlled reactivities. The work is categorized into three themes, all utilizing *in situ* synchrotron x-ray techniques at the Advanced Photon Source: (1) Environmental effects on oxide surface reactivity,

(2) Synthesis and surface reactivity of polar nanostructures, and (3) Synthesis and surface reactivity of ferroelectric nanostructures. In the first theme, we investigate the effects of various chemical environments on oxide surfaces. As indicated above, substantial changes can occur on oxide surfaces with the variation of oxygen partial pressure, pO_2. In this program, we will not only investigate the effects of pO_2, but also pH_2, pCO_2, pCO, pH_2O, pCH_4, and pCH_3OH, and their reactivity with the surface (and with each other). In the second theme, we will focus specifically on the synthesis and characterization of polar oxide films under similar chemical environments. With sufficiently thick films, both the surface and buried interface will require charge compensation, and methods of compensation will be explored. Finally, in the third theme, we will focus on ferroelectric films both with and without ultrathin electrodes and examine adsorption behavior in various polarization and strain states. The concept of dynamic control of adsorption behavior will be tested and explored. We will also investigate the properties of ultrathin, non-ferroelectric oxides grown on ferroelectric supports to determine whether induced polarization can impact surface reactivity.

The principal system of interest in all cases is the thin film perovskite ABO_3, where A = La, Sr, or Ba and B = Ti, Mn, Fe, Co, and Ni. Alloys comprised of these constituents (e.g., $La_{1-x}Sr_xCo_{1-y}Fe_yO_3$), layered variants of the perovskites (e.g., Ruddlesden-Popper or superlattices), and oxides that can be grown epitaxially onto perovskite substrates (e.g., TiO_2) will also be considered since many of these oxides exhibit important surface properties relevant for energy applications. The samples will be thin films grown by oxide molecular beam epitaxy (MBE) on $SrTiO_3$, the preferred substrate because of the ease of surface preparation with a single termination; for the purposes of manipulating epitaxial strain states, other singly-terminated substrates such as pseudocubic $DyScO_3$ may also be considered. The excellent lattice-match between these (pseudo)cubic perovskites and use of the oxide MBE growth technique will eliminate uncertainties and problems associated with grain boundaries and dislocations, allowing us to focus on single-crystal films with a well-defined orientation and surface termination.

The x-ray studies will be carried out *in situ* at the Advanced Photon Source using a miniature reaction chamber permitting resonant x-ray scattering, x-ray spectroscopy, and temperature programmed desorption studies over a wide range of temperatures and gas pressure environments. The chamber has been designed to optimize the detection sensitivity to reaction products from the sample, using a gas chromatograph / mass spectrometer system. The chamber also allows the *in situ* application of an electric field across the film, which will be important for investigating the effects of ferroelectric polarization on surface reactivity.

References

[1] J. Fleig, *Annu. Rev. Mater. Res.* **33**, 361 (2003).
[2] F. Jiao and H. Frei, *Angew. Chem. Int. Ed.* **48**, 1841 (2009).
[3] D.D. Fong et al., *Phys. Rev. Lett.* **96**, 127601 (2006).
[4] A.M. Kolpak et al., *Phys. Rev. Lett.* **98**, 166101 (2007).
[5] D. Li et al., *Nat. Mater.* **7**, 473 (2008).
[6] D.D. Fong et al., *Phys. Rev. B* **71**, 144112 (2005).
[7] D.D. Fong and C. Thompson, *Annu. Rev. Mater. Res.* **36**, 431 (2006).
[8] T.T. Fister, D.D. Fong, et al., *Appl. Phys. Lett.* **93**, 151904 (2008).
[9] D.D. Fong et al., *MRS Bull.* **35**, 504 (2010).
[10] P. Fenter et al., *Nat. Phys.* **2**, 700 (2006).
[11] M. Björck et al., *J. Phys.: Condens. Matter* **20**, 445006 (2008).
[12] R.V. Wang et al., *Phys. Rev. Lett.* **102,** 047601 (2009).

Publications (2008-2010)

This is a newly funded program.

Title: Ultrafast X-ray Studies of Atomic Scale Dynamics

PIs: Paul. H. Fuoss, G. Brian Stephenson
Materials Science Division
Argonne National Laboratory
9700 S. Cass Ave., Bldg 223
Argonne, IL 60439
630-252-3289, fuoss@anl.gov

Research Scope

While design and characterization are crucial components of the development of new materials, synthesis is an equally important step. Synthesis of new materials for energy related applications typically proceeds through a complicated set of metastable states, and sophisticated processes have been developed that rely on the kinetic properties of these states. While these processes are often well understood on a phenomenological level through indirect and *ex-situ* measurements, many of the underlying mechanisms are still poorly understood. Increases in the brightness of synchrotron x-ray sources have allowed observation of materials dynamics on ever faster timescales, and our research has used this capability to explore basic mechanisms of materials synthesis and processing. As x-ray sources have become brighter, structural transformations occurring on the nanosecond to femtosecond time scale can be studied. The basic interactions that initiate many material processes happen on these time scales in highly local environments (e.g., the creation of a critical nucleus). Thus, in materials applications, ultra-fast phenomena are primarily revealed in nanoscale structures. The emergence of ultra-fast and coherent x-ray sources, both at the Advanced Photon Source (APS) and Linac Coherent Light Source (LCLS), offer new opportunities to explore these fundamental processes by measuring on sub-picosecond time scales and imaging on nanometer length scales.

Materials physics research in this domain is particularly exciting because of the convergence of the time and length scales of optical and acoustic phonons, liquid diffusive modes, and surface transport dynamics. Figure 1 displays the relationship between time and length in these fundamental dynamic processes. We now have the opportunity to study these processes not only as statistical averages, but as events isolated in both time and space.

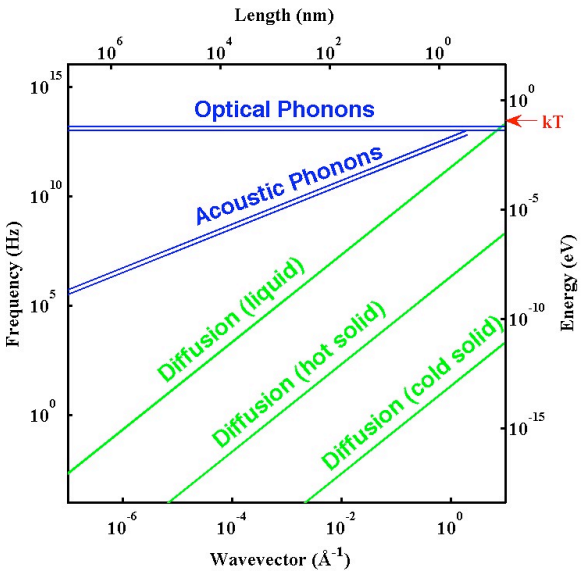

Figure 1: The frequency (energy) dependence of phonons and diffusion on wavevector. The red arrow highlights kT at 1000K.

Recent Progress

The exploitation of these new sources to probe fundamental materials physics requires the development of new, sophisticated technologies to utilize the exceptional x-ray pulses from the LCLS. We made significant progress by utilizing the Sub-Picosecond Pulse Source (SPPS) to explore the initial stages of liquid formation during laser ablation of InSb. Incoherent x-ray diffuse scattering was used to probe the liquid structure [1]. These experiments revealed that there was significant evolution of the structure of the liquid on the picosecond time scale (Figure 2), exactly the temporal region where x-ray photon correlation spectroscopy (XPCS) will be optimized at LCLS.

In preparation for experiments at LCLS studying the ultrafast dynamics of ferroelectric switching, we have performed a series of measurements at the APS exploring the effects of intense laser excitation on the polarization structure of $PbTiO_3$ films. These experiments helped clarify the experimental and theoretical background for future LCLS experiments. In particular, we have developed models for the relationship between polarization and film strain state for the ultrafast case where the substrate lattice parameter may not correspond to the film temperature due to temperature transients, and where the surface charge may not have time to respond to changes in the applied field (see Figure 3).

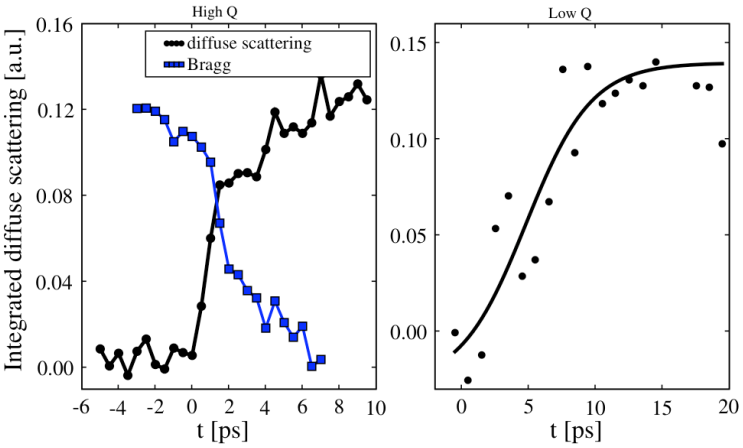

Figure 2: The evolution of diffuse scattering at both high and low Q for InSb being melting with a femtosecond laser pulse.

A third, significant development for probing the nanoscale, ultrafast dimension is the development of multilayer Laue (MLL) optics. MLLs offer a practical avenue to focusing x-rays into spot sizes approaching one nanometer. We have fabricated and tested MLLs, and demonstrated a 16 nm focus [2].

Future Plans

We currently plan a broad range of experiments that build on our APS research, utilize the technologies we've helped develop and expand understanding of materials physics where phonons, diffusion and energy converge. These experiments will utilize both pump-probe and self-synchronized techniques to explore phase transitions and atomic dynamics. Our first efforts will focus on ferroelectric (displacive) phase transitions, XPCS studies of the atomic dynamics of liquids and glasses, and the development of x-ray pump/x-ray probe (XP/XP) measurements.

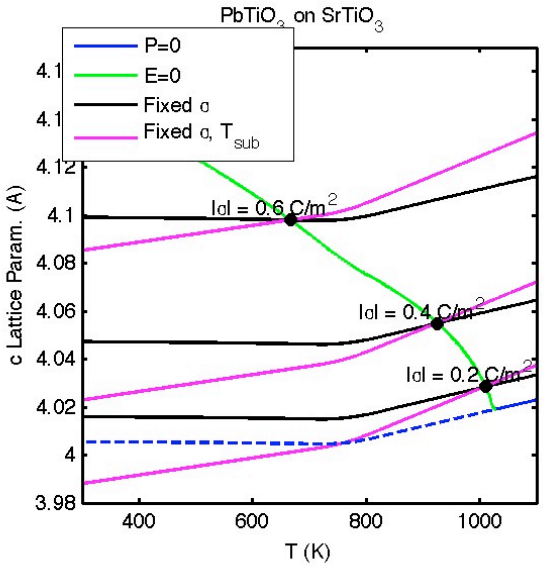

Figure 3: The expected response of the ferroelectric lattice parameter to temperature changes under various electrostatic and strain boundary conditions.

Terahertz Optical Switching of Ferroelectrics: During the last few years, we demonstrated that ultra-thin ferroelectric thin films exhibit unusual behaviors and, recently, that a 10 nm thick $PbTiO_3$ film grown on $SrTiO_3$ could be continuously switched (i.e., without nucleation of domains of the same polarization magnitude, but opposite polarization direction) by controlling the chemical atmosphere to create the required biasing fields. While continuous switching is theoretically possible by directly imposing electric fields, in practice this has never been observed because nucleated switching occurs before a sufficiently large field can be imposed. We will continue to explore the relationships between continuous and nucleated switching in ferroelectrics by using intense, half-cycle terahertz pulses. Based on both theoretical predictions and our experimental results, fields sufficient to bypass nucleation can be generated with the optical lasers available at LCLS. By using the FEL x-ray beam, we will be able to detect the polarization state of the film from lattice parameter measurements. These experiments will be

the first to probe the temporal limits of switching in these technologically important materials, and will probe new regimes of ferroelectric physics that occur before the free surface charge is able to respond to changes in the applied field.

Atomic Dynamics of Liquids and Glasses: Despite decades of concentrated effort, the structure and dynamics of amorphous materials and liquids remain partially, and often poorly, understood. The complexity of amorphous materials and their implicit lack of long-range order have made their description very difficult. Standard scattering techniques only yield the pair correlation function and only crudely describe the structure. Unlike crystals, the higher-order spatial correlation functions necessary to characterize fundamental parameters (e.g., bond angle distributions) and to identify basic structural elements (e.g., icosahedra) are not currently available. The coherent, femtosecond hard x-ray pulses from LCLS provide unprecedented opportunities to observe the structure of liquids and glasses down to the atomic length scale, as well as the dynamics of atomic motion in these systems down to the corresponding femtosecond time scale. We recently initiated experiments at LCLS to probe these correlations. We will measure atomic resolution speckle patterns from bulk metallic glasses, such as Ni_2Pd_2P, using both multi-shot, non-destructive and single shot, destructive modes. These measurements should yield the first higher order atomic correlations from a "simple" glass system. In addition, we will make single-shot measurements from liquids such as Ga and Bi to capture the instantaneous atomic structure. By varying the pulse width (5-500 fs) and monitoring the change in contrast of speckle patterns, we expect to directly observe atomic dynamics in these liquids.

X-Ray Pump/X-Ray Probe Measurements: The development of LCLS with its extremely high peak brightness has created the possibility of practical XP/XP (or x-ray pump/laser probe) experiments. Taking advantage of this possibility requires the development of effective x-ray split-and-delay optics to provide access to the crucial four orders of magnitude of time delay between the maximum LCLS pulse length of 500 femtoseconds and five nanoseconds. We will commission the first such instrument [3] in the near future at LCLS and plan to use it to study fundamental beam-matter interactions. As an example of the exciting possibilities, we plan to use this instrument to study the dynamics of charge ordering in $La_{0.75}Sr_{0.25}MnO_3$ (LSM). LSM exhibits orbital rearrangement and charge ordering at low temperature that can be studied with x-ray diffraction. It has been shown that this charge ordering can be suppressed by irradiation with hard x-rays and recovered by annealing [4,5]. We will perform XP/XP experiments in a temperature range where the charge ordering fully recovers between subsequent LCLS pulses (10 milliseconds), and thus observe the initial stages of the suppression and recovery of charge ordering in LSM.

Finally, these developments at LCLS open up entirely new possibilities for looking at the flow of energy and structural rearrangements in the ultrafast regime. For example, the absorption of a single 24 keV x-ray photon deposits thousands of eV in a very small volume of material. The response of a material to such a localized energy deposition has never been measured. We intend to perform experiments where we locally absorb energy (e.g. in a very small inclusion) and watch the evolution of the inclusion's structure and the strain state of the host lattice with time. Such measurements should give unique insight into the mechanisms of energy flow and heterogeneous nucleation that are crucial in the synthesis of novel materials.

References

[1] Lindenberg, et al., Physical Review Letters, **100**, 135502(2008).
[2] Kang, et al., Applied Physics Letters, 92, 221114(2008).
[3] W. Roseker, H. Fanz, H. Schulte-Schrepping, A. Ehnes, O. Leupold, F. Zontone, A. Robert, and G. Grübel, Optics Letters, **34**, 1768(2009).
[4] V. Kiryukhin et al., Physical Review B, **59**, R6581(1999).
[5] J. Geck et al., Physical Review B, **69**, 104413(2004).

Publications (2008-2010)

"Revealing the Atomic Dance," G. B. Stephenson, A. Robert, and G. Gruebel, invited News and Views article, *Nature Materials* **8**, 702 (2009).

"X-ray Diffuse Scattering Measurements of Nucleation Dynamics at Femtosecond Resolution," A.M. Lindenberg, S. Engemann, K.J. Gaffney, K. Sokolowski-Tinten, J. Larsson, P.B. Hillyard, D.A. Reis, D.M. Fritz, J. Arthur, R.A. Akre, M.J. George, A. Deb, P.H. Bucksbaum, J. Hajdu, D.A. Meyer, M. Nicoul, C. Blome, Th. Tschentscher, A.L. Cavalieri, R.W. Falcone, S.H. Lee, R. Pahl, J. Rudati, P.H. Fuoss, A.J. Nelson, P. Krejcik, D.P. Siddons, P. Lorazo, J.B. Hastings, *Physical Review Letters* **100**, 135502 (2008).

"Multilayer Laue lens: a path toward one nanometer x-ray focusing," H. Yan, H. C. Kang, R. Conley, C. Liu, A. T. Macrander, G. B. Stephenson, and J. Maser, accepted for publication in X-ray Optics and Instrumentation (2010).

"Development of Full Multilayer Laue Lens for Focusing Hard X-rays," C. Liu, B. Shi, J. Qian, R. Conley, H. Yan, M. Wieczorek, A. T. Macrander, J. Maser, and G. B. Stephenson, *Proceedings of 10th International Conference on Synchrotron Radiation Instrumentation,* Melbourne, Australia, Sept. 27 to Oct. 2, 2009.

"Nanofocusing of Hard X-rays with Multilayer Laue Lenses," A. Macrander, H. Yan, H. C. Kang, J. Maser, C. Liu, R. Conley, G. B. Stephenson, Handbook of Optics, 3rd. ed., Vol. V. X-ray and Neutron Optics, Chap. 42 (McGraw Hill, 2010) eds. M. Bass et al.

"A Theoretical Study of Two-Dimensional Point Focusing by Two Multilayer Laue Lenses," H. Yan, J. Maser, H.C. Kang, A. Macrander, and G. B. Stephenson, *Proceedings of SPIE* **7077**, 70770Q (2008).

"Focusing of hard x-rays to 16 nanometers with a multilayer Laue lens," H. C. Kang, H. Yan, R. P. Winarski, M. V. Holt, J. Maser, C. Liu, R. Conley, S. Vogt, A. T. Macrander, and G. B. Stephenson, *Applied Physics Letters,* **92**, 221114 (2008).

"Wedged Multilayer Laue Lens," R. Conley, C. Liu, J. Qian, C. M. Kewish, A. T. Macrander, H. Yan, H. C. Kang, J. Maser, and G. B. Stephenson, *Review of Scientific Instruments* **79**, 053104 (2008).

"Bonded Multilayer Laue Lens for focusing hard x-rays," Chian Liu, R. Conley, J. Qian, C. M. Kewish, A. T. Macrander, J. Maser, H. C. Kang, H. Yan, and G. B. Stephenson, *Nuclear Instruments and Methods A* **582**, 123-125 (2007).

"Characterization of A Multilayer Laue Lens with imperfections," H. Yan, H. C. Kang, J. Maser, A. T. Macrander, C. M. Kewish, C. Liu, R. Conley and G. B. Stephenson, *Nuclear Instruments and Methods A* **582**, 126-128 (2007).

X-ray Studies of Correlations and Competition among Lattice, Electronic, and Magnetic Degrees of Freedom

A. I. Goldman (goldman@ameslab.gov), R. J. McQueeney, A. Kreyssig

Ames Laboratory and Dept. of Physics and Astronomy, Iowa State University, Ames, IA 50011

Program Scope

The physical properties of novel materials, such as high-temperature superconductors and multiferroics, are all sensitively controlled by correlations and competition among the lattice, electronic, and magnetic degrees of freedom. A comprehensive understanding of the necessary conditions for enhancing or tailoring desirable physical properties has been identified as a Grand Challenge to the scientific community. X-ray and neutron scattering are powerful probes that directly investigate the structural, electronic, and magnetic aspects of complex ground states, phase transitions, and corresponding excitations. Any one of the many different scattering techniques alone can reveal detailed information about the underlying physics. At the Ames Laboratory, the varied expertise of the PIs in different scattering methods is employed in a synergistic approach and systems are studied using a wide range of neutron and x-ray techniques. The experimental program is supported by a closely coupled effort in *ab initio* band structure calculations, theoretical modeling, and scattering simulations. The emphasis of close coupling between different scattering techniques and theory is a unique approach of our effort.

Recent Progress

Iron arsenide superconductors

Over the past three years we have focused a significant combined x-ray/neutron/theory effort on the study of high-temperature superconductivity (SC) in the iron arsenide compounds where the interplay between SC, magnetism, and structure has become the major scientific theme. The parent $AEFe_2As_2$ (*AE* = Ba, Sr, Ca) compounds, for example, manifest strong coupling between magnetism and structure illustrated by the observation of a simultaneous transition from a paramagnetic, tetragonal (T) phase to an antiferromagnetic (AFM) ordered, orthorhombic (O) phase. Upon electron-doping through the substitution of Co, Ni, and Rh for Fe, or by applying pressure, both the AFM ordering and structural transition temperatures are suppressed and SC appears. Perhaps most striking is the observation that static AFM order and SC can coexist and compete for the same electrons. The close coupling between structure, magnetism and SC is further established by the surprisingly strong suppression of both the static AFM order *and* the lattice distortion below the superconducting transition for electron-doped compounds. In contrast, hole-doping achieved by the introduction of Mn or Cr for Fe are not superconducting and very different behavior for the magnetic and structural transitions is observed.. Clearly, even beyond their intrinsic interest as a new class of high temperature SC, the iron arsenides provide a nearly ideal family of compounds to explore the fundamental relationships between lattice, electronic and magnetic degrees of freedom. Some of our major results are listed below:

- X-ray and neutron diffraction studies observed coupled first-order magnetic and structural transitions in the $AEFe_2As_2$ parent compounds, revealing strong magnetoelastic coupling.
- Diffraction studies discovered a collapsed tetragonal (cT) phase in $CaFe_2As_2$ under modest hydrostatic pressure. In addition to the astonishing change in the *c*-axis lattice parameter (~10%), the cT phase is also suffers a complete loss of magnetic moment. These results highlight the extreme sensitivity of magnetism to local chemical environments and bonding.
- The comparison of *ab initio* calculations of phonon spectra with inelastic x-ray and neutron scattering measurements is consistent with a strong influence of magnetism on As vibrations.

- The structural evolution of $BaFe_2As_2$ under pressure shares many features with chemical substitution, suggesting that SC results from fine tuning of the electronic band structure.
- Joint x-ray and neutron diffraction studies have shown a striking systematic suppression of both AFM order and the orthorhombic distortion below T_C as a function of composition for $Ba(Fe_{1-x}Co_x)_2As_2$, highlighting the competition between AFM ordering and SC that occurs in the midst of strong magnetoelastic coupling.
- X-ray resonant magnetic scattering measurements of the magnetic structure (at the Fe K-edge) concluded that the AFM structure is, indeed, commensurate for $Ba(Fe_{1-x}Co_x)_2As_2$.

XRMS investigations of novel rare earth magnetism

We have employed XRMS to gain new insights into the magnetic ordering of a wide variety of compounds that are difficult to study via neutron techniques including the $Gd_5(Ge,Si)_4$ magnetic refrigeration materials and incommensurate magnetic order in $EuRh_2As_2$, a compound closely related to the iron arsenide superconductors. XRMS also offers the capability of elemental specificity in magnetic measurements. For example, multiferroic compounds, exhibiting both ferroelectric and magnetic effects within the same phase, have attracted considerable attention due to the possibility of controlling electric polarization by an applied magnetic field or, conversely, magnetic order through an applied electric field. The hexagonal $RMnO_3$ (R = Ho, Dy, Er*)* are particularly interesting compounds, but the nature of the magnetic ordering in this multicomponent system had been a matter of controversy, only recently resolved by our XRMS investigations of the magnetic order for the R sublattice. In the case of hexagonal $HoMnO_3$, it has been proposed that the application of an electric field changes the AFM order of Ho^{3+} to ferromagnetic order. However, our XRMS and x-ray magnetic circular dichroism (XMCD) studies of $HoMnO_3$ found no dependence of the Ho ordering after applying electric fields up to 1 x 10^7 V/m, and concluded that Ho is not responsible for the ferromagnetic response in an applied electric field.

High-energy single-crystal x-ray diffraction measurements

Over the past few years we have advanced high-energy single-crystal oscillation techniques, using two-dimensional area detectors, to image extended planes of reciprocal space. This method has been applied, to a variety of systems including:

- The iron arsenide superconductors, for detailed studies of the tetragonal-to-orthorhombic structural distortion, the characterization of the resultant twinning and domain structure, and methods for detwinning crystals through the application of stress.
- Quasicrystals, providing a map of the reciprocal lattice planes perpendicular to 2-, 3- and 5-fold axes and elucidating the nature of disorder and strain inherent to different growth morphologies.
- Investigations of crystallographic phases phase transitions and defects in novel systems such as the heavy fermion compound, LiV_2O_4.

Future Plans

Iron arsenide superconductors

Our studies in the Co-doped system have revealed that the interplay between magnetism, SC, and the lattice has two major components; 1) the competition between spin-density-wave and SC gaps, and 2) the coupling of spin fluctuations and lattice distortions, possibly occurring via the nematic degrees of freedom. Our understanding of the Co-doped $BaFe_2As_2$ system also provides us with a starting point to investigate the relative importance of these interactions in other systems, specifically the RFeAsO (where single-crystal samples are now available) as well as hole- and isoelectronic-doping of the AFe_2As_2 compounds. Our XRMS studies of the iron arsenides will be extended to study element specific magnetism associated with the transition metal dopants (e.g. Co, Ru, Mn), in

addition to Fe, at higher doping concentrations, to establish the nature of the magnetic and structural perturbations introduced by doping.

Development of high-energy single-crystal methods at the APS

A key distinguishing feature of the Advanced Photon Source (APS) is the capability for high-energy scattering, which has been exploited for numerous applications including pair distribution function studies, high pressure studies, and investigations of the mechanical behavior of materials. Coupled with the new generation of two-dimensional area detectors, high-energy diffraction studies of powder samples provide an important and complementary path to conventional powder diffraction measurements. The capabilities for high-energy single-crystal diffraction measurements at the APS, however, remain somewhat underdeveloped and there is an emerging need for this technique. We have now established a Partner User effort with the APS to expand our work on high-energy single-crystal methods to develop a high-energy x-ray precession camera for single-crystal studies of materials under extreme environments (pressure, temperature, magnetic field).

Selected Publications (FY2008-2010)

1. *Magnetic Structure of Dy^{3+} in Hexagonal Multiferroic $DyMnO_3$*, S. Nandi, A. Kreyssig, J.Q. Yan, M.D. Vannette, J.C. Lang, L. Tan, J.W. Kim, R. Prozorov, T.A. Lograsso, R.J. McQueeney and A.I. Goldman, Phys. Rev. B **78**, 075118 (2008).
2. *The Nature of Ho Magnetism in Multiferroic $HoMnO_3$*, S. Nandi, A. Kreyssig, L. Tan, J.W. Kim, J.Q. Yan, R.J. McQueeney and A.I. Goldman, Phys. Rev. Lett. **100**, 217201 (2008).
3. *First-Order Structural Phase Transition in $CaFe_2As_2$*, N. Ni, S. Nandi, A. Kreyssig, A.I. Goldman, E.D. Mun, S.L. Bud'ko and P.C. Canfield, Phys. Rev. B **78,** 014523 (2008).
4. *Anisotropic Thermodynamic and Transport Properties of Single-Crystalline $Ba_{1-x}K_xFe_2As_2$ (x=0 and 0.45)*, N. Ni, S.L. Bud'ko, A. Kreyssig, S. Nandi, G.E. Rustan, A.I. Goldman, S. Gupta, J.D. Corbett, A. Kracher and P.C. Canfield, Phys. Rev. B **78**, 014507 (2008).
5. *Single-Crystal Growth and Physical Properties of the Layered Arsenide $BaRh_2As_2$*, Y. Singh, Y. Lee, S. Nandi, A. Kreyssig, A. Ellern, S. Das, R. Nath, B.N. Harmon, A.I. Goldman and D.C. Johnston, Phys. Rev. B **78,** 104512 (2008).
6. *Observation of a Spin-Flop Transition in Gd_5Ge_4 by Resonant Magnetic X-Ray Scattering*, L. Tan, A. Kreyssig, S. Nandi, S. Jia, A.I. Goldman, R.J. McQueeney, P.C. Canfield, Y. Lee, B. Harmon, T.A. Lograsso, D.L. Schlagel, V.K. Pecharsky, K.A. Gschneidner, Jr., Z. Islam and J.C. Lang, Phys. Rev. B **77**, 064425 (2008).
7. *Structural Transition and Anisotropic Properties of Single Crystalline $SrFe_2As_2$*, J.-Q. Yan, A. Kreyssig, S. Nandi, N. Ni, S.L. Bud'ko, A. Kracher, R.J. McQueeney, R.W. McCallum, T.A. Lograsso, A.I. Goldman and P.C. Canfield, Phys. Rev. B **78**, 024516 (2008).
8. *Structural Phase Transition in $Ba(Fe_{0.973}Cr_{0.027})_2As_2$ Single Crystals*, S.L. Bud'ko, S. Nandi, N. Ni, A. Thaler, A. Kreyssig, A. Kracher, J.Q. Yan, A.I. Goldman and P.C. Canfield, Phys. Rev. B **80,** 014522 (2009).
9. *Absence of Structural Correlations of Magnetic Defects in the Heavy-Fermion Compound LiV_2O_4*, S. Das, A. Kreyssig, S. Nandi, A.I. Goldman and D.C. Johnston, Phys. Rev. B **80,** 104401 (2009).
10. *Comment on 'Dipolar Excitations at the L-III X-Ray Absorption Edges of the Heavy Rare-Earth Metals*, A.I. Goldman, B.N. Harmon, Y.B. Lee and A. Kreyssig, Phys. Rev. Lett. **102** 129701, (2009).
11. *Lattice Collapse and Quenching of Magnetism in $CaFe_2As_2$ under Pressure: A Single Crystal Neutron and X-Ray Diffraction Investigation*, A.I. Goldman, A. Kreyssig, K. Prokes, D.K. Pratt, D.N. Argyriou, J.W. Lynn, S. Nandi, S.A.J. Kimber, Y. Chen, Y.B. Lee, G. Samolyuk, J.B. Leão, S.J. Poulton, S.L. Bud'ko, N. Ni, P.C. Canfield, B.N. Harmon and R.J. McQueeney, Phys. Rev. B **79**, 024513 (2009).
12. *Unconventional London Penetration Depth in Single-Crystal $Ba(Fe_{0.93}Co_{0.07})_2As_2$ Superconductors* R.T. Gordon, N. Ni, C. Martin, M.A. Tanatar, M.D. Vannette, H. Kim, G.D. Samolyuk, J. Schmalian,

S. Nandi, A. Kreyssig, A.I. Goldman, J.Q. Yan, S.L. Bud'ko, P.C. Canfield and R. Prozorov, Phys. Rev. Lett. **102,** 127004 (2009).
13. *Influence of Magnetism on Phonons in $CaFe_2As_2$*, S.E. Hahn, Y. Lee, N. Ni, A. Alatas, B.M. Leu, D.Y. Chung, I.S. Todorov, E.E. Alp, M.G. Kanatzidis, P.C. Canfield, A.I. Goldman, R.J. McQueeney and B.N. Harmon, Phys. Rev. B **79**, 220511(R) (2009).
14. *Similarities Between Structural Distortions under Pressure and Chemical Doping in Superconducting $BaFe_2As_2$*, S.A.J. Kimber, A. Kreyssig, Y-Z. Zhang, H.O. Jeschke, R. Valenti, F. Yokaichiya, D.N. Argyriou, E. Colombier, J.-Q. Yan, T.C. Hansen, T. Chatterji, R.J. McQueeney, P.C. Canfield, A.I. Goldman and D. Argyriou, Nat. Mater. **8**, 471 (2009).
15. *Nonexponential London Penetration Depth of FeAs-Based Superconducting $RFeAsO_{0.9}F_{0.1}$ (R = La, Nd) Single Crystals*, C. Martin, M.E. Tillman, H. Kim, M.A. Tanatar, S.K. Kim, A. Kreyssig, R.T. Gordon, M.D. Vannette, S. Nandi, V.G. Kogan, S.L. Bud'ko, P.C. Canfield, A.I. Goldman and R. Prozorov, Phys. Rev. Lett. **102,** 247002 (2009).
16. *In Situ High Energy X-Ray Synchrotron Diffraction Study of the Synthesis and Stoichiometry of LaFeAsO and $LaFeAsO_{1-x}F_y$*, R.W. McCallum, J.Q. Yan, G.E. Rustan, E.D. Mun, Y. Singh, S. Das, R. Nath, S.L. Bud'ko, K.W. Dennis, D.C. Johnston, P.C. Canfield, M.J. Kramer, A. Kreyssig, T.A. Lograsso and A.I. Goldman, J. Appl. Phys. **105,** 123912 (2009).
17. *Magnetic Ordering in $EuRh_2As_2$ Studied by X-ray Resonant Magnetic Scattering*, S.Nandi, A. Kreyssig, Y. Lee, Y. Singh, J.W. Kim, D.C. Johnston, B.N. Harmon and A.I. Goldman, Phys. Rev. B **79**, 100407R (2009).
18. *Competition and Coexistence of Antiferromagnetism and Superconductivity in Underdoped $Ba(Fe_{0.953}Co_{0.047})_2As_2$ Compound Using X-Ray and Neutron Scattering Techniques*, D.K. Pratt, W. Tian, A. Kreyssig, J.L. Zarestky, S. Nandi, N. Ni, S.L. Bud'ko, P.C. Canfield, A.I. Goldman and R.J. McQueeney, Phys. Rev. Lett. **103**, 087001 (2009).
19. *Intrinsic Pinning on Structural Domains in Underdoped Single Crystals of $Ba(Fe_{1-x}Co_x)_2As_2$,* R. Prozorov, M.A. Tanatar, N. Ni, A. Kreyssig, S. Nandi, S.L. Bud'ko, A.I. Goldman and P.C. Canfield, Phys. Rev. B **80,** 174517 (2009).
20. *Direct Imaging of the Structural Domains in the Iron Pnictides AFe_2As_2 (A = Ca, Sr, Ba)* M.A. Tanatar, A. Kreyssig, S. Nandi, N. Ni, S.L. Bud'ko, P.C. Canfield, A.I. Goldman and R. Prozorov, Phys. Rev. B **79,** 180508(R) (2009).
21. *Flux Growth at Ambient Pressure of Millimeter-Sized Single Crystals of LaFeAsO, $LaFeAsO_{1-x}F_x$, and $LaFe_{1-x}Co_xAsO$*, J.-Q. Yan, S. Nandi, J.L. Zarestky, W. Tian, A. Kreyssig, B. Jensen, A. Kracher, K.W. Dennis, R.J. McQueeney, A.I. Goldman, R.W. McCallum and T.A. Lograsso, Appl. Phys. Lett. **95**, 222504 (2009).
22. *Solution growth of a binary icosahedral quasicrystal of $Sc_{12}Zn_{88}$*, P. C. Canfield, M. L. Caudle, C.-S. Ho, A. Kreyssig, S. Nandi, M. G. Kim, X. Lin, A. Kracher, K. W. Dennis, R. W. McCallum and A. I. Goldman, Phys. Rev. B **81**, 020201(R) (2010).
23. *Anomalous suppression of the orthorhombic distortion in superconducting $Ba(Fe_{1-x}Co_x)_2As_2$,* S. Nandi, M. G. Kim, A. Kreyssig, R. M. Fernandes, D. K. Pratt, A. Thaler, N. Ni, S. L. Bud'ko, P. C. Canfield, J. Schmalian, R. J. McQueeney and A. I. Goldman, Phys. Rev. Lett. **104**, 057006 (2010).
24. *Suppression of antiferromagnetic order and orthorhombic distortion in superconducting $Ba(Fe_{0.961}Rh_{0.039})_2As_2$*, A. Kreyssig, M. G. Kim, S. Nandi, D. K. Pratt, W. Tian, J. L. Zarestky, N. Ni, A. Thaler, S. L. Bud'ko, P. C. Canfield, R. J. McQueeney and A. I. Goldman, Phys. Rev. B **81**, 134512 (2010).
25. *Unconventional pairing in the iron arsenide superconductors*, Rafael M. Fernandes, Daniel K. Pratt, Wei Tian, Jerel Zarestky, Andreas Kreyssig, Shibabrata Nandi, Min Gyu Kim, Alex Thaler, Ni Ni, Paul C. Canfield, Robert J. McQueeney, Jörg Schmalian and Alan I. Goldman, Phys. Rev. B **81**, 140501(R) (2010).
26. *Uniaxial-strain mechanical detwinning of $CaFe_2As_2$ and $BaFe_2As_2$ crystals: Optical and transport study*, M. A. Tanatar, E. C. Blomberg, A. Kreyssig, M. G. Kim, N. Ni, A. Thaler, S. L. Bud'ko, P. C. Canfield, A. I. Goldman, I. I. Mazin, and R. Prozorov, Phys. Rev. B **81**, 184508 (2010).

Experimental discovery of Topological Order in bulk solids:

Topological Insulators and Superconductors

M Zahid Hasan

Joseph Henry Laboratories, Department of Physics,
Princeton University, Princeton, NJ 08544, USA
Email: mzhasan@Princeton.edu

Discovering new phases of matter with useful electronic or magnetic properties is an important goal in modern physics. In the past few years, theoretical developments have uncovered a new phase of quantum matter dubbed "Topological Insulators". Following our experimental discovery of first 3D topological insulators in 2007(actual observation of topological surface states dates a few years back in connection to our work in thermoelectrics carried out under this DOE grant), we have theoretically predicted (using first-principle calculations) as well as experimentally discovered/demonstrated by directly measuring the topological-order character of the edge-spectrum of single-Dirac-cone topological insulators in 2008. Our discoveries under this DOE grant have open up possibilities for a wide range of novel/exotic experiments with topological quantum phenomena [R1-11].

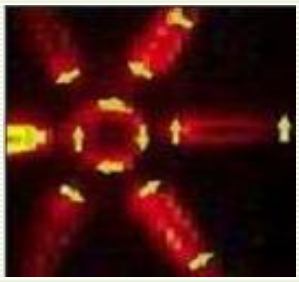

First observation of a 3D topological insulator [Nature '08 (submitted 2007)]

PHYSICS TODAY'09

Under this same DOE grant, we have also pioneered [P2-12] a way to probe the spin degrees of freedom in spin Hall like topological phenomena and demonstrated that topological quantum numbers are completely determined from spin-texture imaging measurements. These spin-sensitive results constitute the first observation of surface electrons collectively carrying a topological-Berry's phase and definite spin chirality. These are the key electronic properties for realizing topological quantum information bits using a topological surface. Recently, we have demonstrated that the topological-order can be maintained at room-temperature without magnetic field, the absence of backscattering or the protected nature of the states and that the materials can be driven to the topological transport regime paving the way for realizing some high-energy-physics-like experiments at table-top settings with wide tunability and systematic quantum control. Following our discovery of single-Dirac-cone topological insulators in binary systems such as the Bi2Se3-class in 2008, we have further discovered several new classes of topological insulators in ternary spin-orbit systems such as the Half-Heuslers, Li-Intermetallics, TlBiTe2-class and in many other compounds. In 2009 we have also discovered Topological-Order in a doped topological

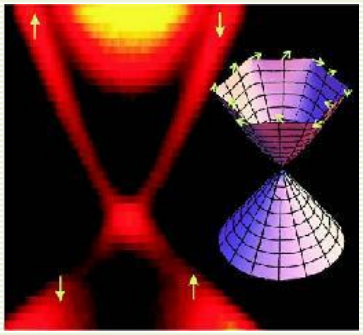

Simplest form of 3D topological insulator : First observation of a spin polarized single Dirac cone providing direct evidence of topologically ordered state) [Nature 2009, Nature Physics 09]

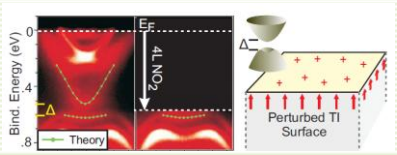

Magnetic Topological Insulator (Nature Physics 2010)

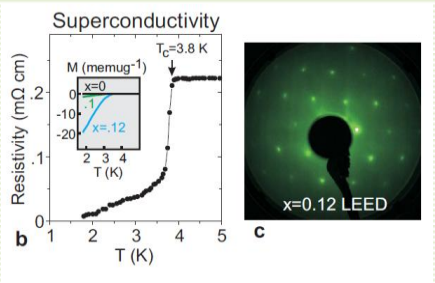

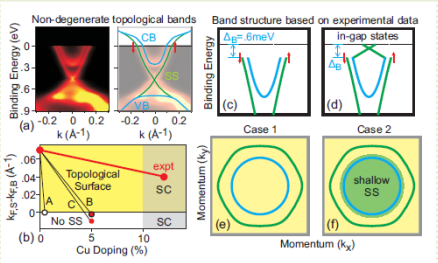

Superconducting doped Topological Insulator (Nature Physics 2010)

insulator as it becomes a superconductor. Following our work, these materials and phenomena are now being studied world-wide by many other groups.

Topological Insulators and Superconductors have been proposed as a possible route to fault-tolerant (topological) quantum computing and related spin-orbit Dirac materials can potentially provide low-power (energy-saving) spin currents for electronic/spintronic applications. On the other hand, doped Mott insulators on triangular lattices not only exhibit exotic superconductivity, spin-liquid behavior but also feature high thermopower figure of merit for applications also being studied under this DOE grant. Currently, there is no obvious application of spin-liquids but some spin-liquids may exhibit "exotic topological order (related to ground-state degeneracy)" and fractionalization which is of much interest.

In an ordinary insulator, such as diamond, the occupied electronic levels are separated from unoccupied levels by a large energy barrier known as an energy gap. The energy gap prevents current flow when an electric field is applied. In topological insulators, electrons can bypass the energy gap by moving out to the surfaces of the insulator. The energy vs. velocity behavior of these unusual electrons moving on the surface is light-like. They exhibit many unusual quantum properties which can be harnessed to improve spin-based electronics, novel forms of quantum computing and energy-efficient devices. This project will focus on studying the details of the novel quantum behaviors of electrons moving on the surface which will in turn not only lead to better understanding of the mechanism for doing so but also likely discover new pathways to applications. Students working on this project will develop expertise in vacuum and nano-technology,

material characterization methodologies, and advanced x-ray optics and electronic spectroscopy techniques preparing them for scientific careers in industry, academia or government laboratories.
Spin-resolved ARPES and related novel spin-sensitive ultra-fast time-resolved X-ray spectroscopic methods and more generally, various state-of-the-art Synchrotron and next-generation X-ray FELs will be used to explore the fundamental physics of topological insulators and topological superconductors.

References:

R1. Surface states in spin-orbit insulators : Conference proceeding (online presentation) : M.Z. Hasan KITP conference (online) proceeding (**2007**).
R2. **Nature Physics** News & Views: "Topological Insulator: An Insulator with a Twist" (2008)
R3. **Science** (February, 2009) Perspective : "Quantum Knots" (Topological Insulator)
R4. **Nature** News &Views (August 2009).
R5. **Physics Today**: "Search & Discovery" (discovery of Topological Insulators) April-2009. Bi-based compounds discovered to be the first bulk (3D) topological insulator under this DOE grant was featured in PHYSICS TODAY's "Search & Discovery" news.
R6. **Physics Today**: News (An insulator's metallic side) August-2009
R7. **Physics Today**: Feature Article on Topological Insulators, January 2010.
R8. **Science News**: "Physics at the Edge", May 2010.
R9. **NATURE NEWS** (nature Home Page): "Topological Insulator: Star Material" (2010). Bi2Se3 discovered to be a topological insulator under this DOE grant was identified to be the "hottest topic" in 2010 APS March meeting.
R10. **Nature Materials** News & Views: "Topological Insulator: Starting a New Family" (May, 2010)
R11. **New Scientist (U.K.)**: Feature Article on Topological Insulators, September 2010.

DOE supported Publications (2008-10):

P1. A Topological Dirac insulator (Bi-based semiconductors) in a Quantum Spin Hall phase, D. Hsieh, D. Qian, L. Wray, Y. Xia, Y.S. Hor, R. J. Cava, M.Z. Hasan
NATURE 452, 970-974 (2008) [Submitted 2007]
P2. Observation of unconventional quantum spin-textures (non-trivial Berry's phase) in topological Insulators (First spin-sensitive study of quantum spin Hall or topological insulator physics) D. Hsieh, Y. Xia, L. Wray, D. Qian, A. Pal, J. H. Dil, F. Meier, J. Osterwalder, C.L. Kane, G. Bihlmayer, Y. S. Hor, R. J. Cava and M.Z. Hasan.
SCIENCE 323, 919-922 (2009) [Submitted 2008]
P3. Observation (discovery) of a large-gap topological-insulator class (Bi2Se3 class) with a single-Dirac-cone on the surface (Much of the topological insulator research is now focused on this class) Y. Xia, L. Wray, D. Qian, D. Hsieh, A. Pal, H. Lin, A. Bansil, D. Grauer, Y. Hor, R.J. Cava, M.Z. Hasan
NATURE PHYSICS 5, 398-402 (2009) [Submitted 2008]

P4. Observation of time-reversal-protected single-Dirac-cone topological states in Bi2Te3 and Sb2Te3 D. Hsieh, Y. Xia, L. Wray, D. Qian, D. Hsieh, H. Lin, A. Bansil, Y. Hor, R. J. Cava, M. Z. Hasan
Physical Review Letters 103, 146401 (2009)

P5. (Demonstration of a topological version of Graphene) A tunable topological insulator ("topological Graphene') in the spin-Helical Dirac transport regime D. Hsieh, Y. Xia, D. Qian, L. Wray, J. H. Dil, F. Meier, L. Patthey, J. Osterwalder, A.V. Fedorov, H. Lin, N.P. Ong, A. Bansil, D. Grauer, Y.S. Hor, R.J. Cava, M.Z. Hasan
NATURE 460, 1101-1005 (2009)

P6. Correlated state in Iron chalcogenide Superconductors: Fermi Surface Topology and Low-Lying Quasiparticle Dynamics of Parent Fe1+ xTe/Se Superconductor, Y. Xia, D. Qian, L. Wray, D. Hsieh, G. F. Chen, J. L. Luo, N. L. Wang, M. Z. Hasan
Physical Review Letters, 103, 037002 (2009).

P7. (Absence of backscattering on topological surfaces) Topological surface states protected from backscattering by chiral spin texture P. Roushan, J. Seo, C.V. Parker, Y. S. Hor, D. Hsieh, D. Qian, M. Z. Hasan, R. J. Cava, A. Yazdani.
NATURE 460, 1106-1009 (2009).

P8. Single-Dirac-Cone topological surface states in TlBiSe2-class of semiconductors: Thallium-based III-V-VI2 Ternary Chalcogenides H. Lin, R.S. Markiewicz, L.A. Wray, L. Fu, M.Z. Hasan, A. Bansil;
Physical Review Letters 105, 03640 (2010).

P9. (A platform for Majorana Fermions) Observation of Topological Order in a Superconducting doped topological insulator L.A. Wray, Y. Xia, S. Xu, S. Jia, R.J. Cava, A. Bansil, M. Z. Hasan
NATURE PHYSICS (in press) Adv. online: doi:10.1038/nphys1762

P10. (Magnetization dynamics of a topological insulator) Observation of Magnetization dynamics of a topological insulator L.A. Wray, Y. Xia, S. Xu, S. Jia, R.J. Cava, A. Bansil, M. Z. Hasan
NATURE PHYSICS (in press)

P11. (A new platform for exploring topological physics) Half-Heusler ternary compounds as new multi-functional experimental platforms for topological quantum phenomena H. Lin, L.A. Wray, Y. Xia, S. Xu, S. Jia, R.J. Cava, A. Bansil, M. Z. Hasan
NATURE MATERIALS 9, 546 (2010)

P12. (Discovery of multi-functional insulating topological insulators) Observation of multifunctional topological insulator classes with long life-time surface states L. Wray, A. Petersen, S.-Y. Xu, Y. Xia, H. Lin, A. Bansil, D. Grauer, R.J. Cava, M.Z. Hasan
NATURE (in review) (2010)

Invited Review Articles:

P13. Three Dimensional Topological Insulators, M.Z. Hasan and J.E. Moore
Annual Review of Condensed Matter Physics (in press) (2010).

P14. Topological Insulators, M. Z. Hasan and C.L. Kane,
Review of Modern Physics (in press) (2010).

Mechanisms of Thin Film Growth by Sputter Deposition and Pulsed Laser Deposition

Randall L. Headrick

Department of Physics and Materials Science Program,
Cook Physical Sciences Building
University of Vermont, Burlington, VT 05405

email address: rheadrick@uvm.edu

Research Scope

Sputter deposition is widely used for making thin films for an enormous range of applications. The objective of this project is to determine the roughening and smoothing mechanisms using real-time x-ray scattering to study the surface evolution of sputter-deposited amorphous films. The results are directly applicable to multilayer structures used in multilayer Laue lenses for nm-scale focusing of x-rays.

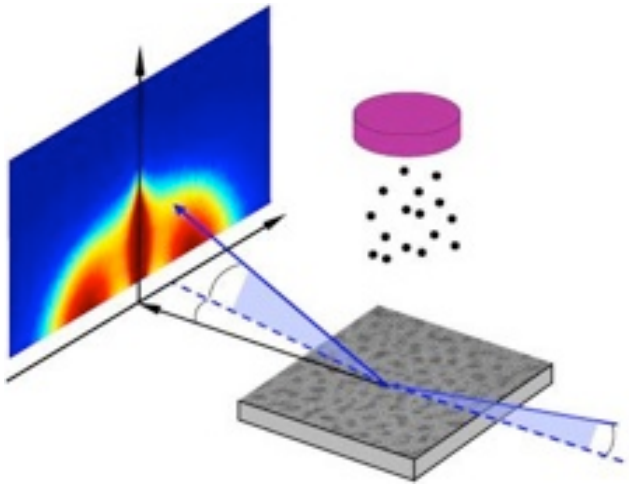

Figure 1. Schematic of the real-time x-ray scattering method to study the surface morphology evolution during thin film growth by sputter deposition. The scattering pattern evolves as the film thickness and roughness spectrum change during deposition.

We have also recently added the capability to perform Pulsed Laser Deposition. These experiments are aimed at studies of mechanisms in epitaxial growth. First results on growth of Ge on Ge(001) in ultra-high vacuum are described below.

Real-time Grazing Incidence Small Angle X-ray Scattering (GISAXS) can reveal fundamental aspects of surface growth phenomena in a straightforward and quantitative way because the GISAXS intensity profile is directly related to the Power-Spectral Density (PSD) of the surface during the thin films growth processes (Fig. 1). The PSD represents the spatial frequency spectrum of the surface roughness. The PSD evolution of the surface thus gives insight into the smoothing and roughening mechanisms inherent to the growth process. We also employ Grazing Incidence X-ray Diffraction for studies of crystalline films. Measurements are performed using the real-time growth apparatus at the National Synchrotron Light Source, beamline X21. A 384 channel fast linear position-sensitive detector (0.125 mm per channel) is oriented in the plane of the surface for the measurements.

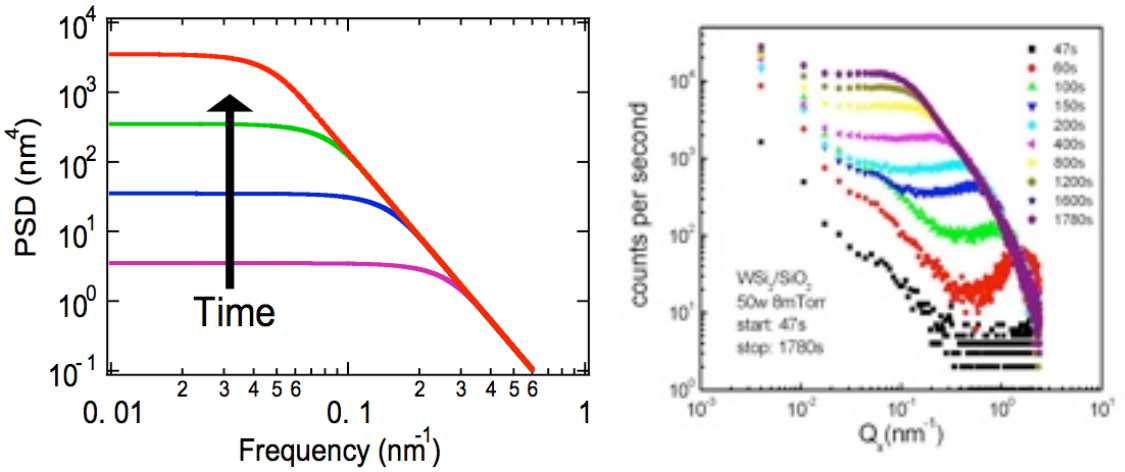

Figure 2. The image on the left shows predicted curves for the evolution of the Power Spectral Density as a function of time for a simple roughening model. The plot on the right shows GISAXS intensity profile evolution for WSi_2 deposited at 8 mTorr. The x-ray energy was 10 keV.

Recent Progress: Roughening and Stress Transitions in Sputter Deposition

Prior in-situ studies of WSi_2/Si multilayer deposition have shown that deposition at 6 mTorr background Ar pressure results in an alternating roughness, i.e. the Si layer is observed to roughen monotonically, while the WSi_2 layer smoothes out when deposited on top of a rough layer. Deposition at higher Ar background pressures has quite a different character, since both Si and WSi_2 layers roughen rapidly. The smoothing of WSi_2 at pressures below 6 mTorr is linked to the energy spectrum of sputtered particles reaching the surface, which can have energies > 100 eV. We know that there are efficient smoothing mechanisms that are operative in this energy range from our recent work on ion erosion of surfaces. The measured PSD is in agreement with the Edwards-Wilkinson model, indicating an impact induced downhill current mechanism.

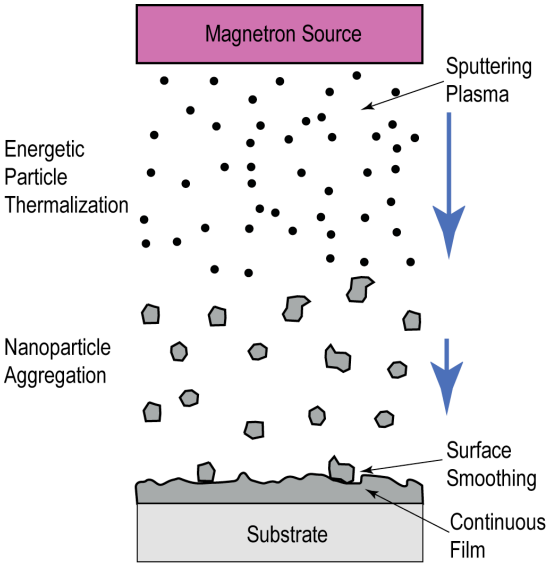

Figure 3. Mechanism of the pressure dependent roughening transition in sputter deposition. The same effect leads to a transition between compressive and tensile stress.

More recently, we have studied WSi_2 deposition in more detail using GISAXS in order to provide insight into the strong roughening effect observed in the high pressure (> 6 mTorr) regime. This study has resolved fundamental questions about the origin of stress and roughness in thin films formed by sputter deposition as the background gas pressure is increased beyond a threshold value. Comparison of real-time GISAXS data with theoretical power spectral density curves shows that the surface roughness spectrum closely resembles the PSD predicted by a simple linear growth model with uncorrelated noise in the deposition flux as the only roughening

mechanism (Fig. 2). However, surprizingly, the noise corresponds to deposited particle sizes significantly larger than individual atoms, as we had originally assumed. The picture that has emerged is illustrated in Fig. 3. Film roughness and tensile stress are caused by formation of nanoparticles in the plasma/gas phase for Ar pressures above the threshold. Particle sizes for WSi_2 inferred from GISAXS spectra increase from ~1 atom at 6 mTorr to hundreds of atoms at 10 mTorr. Particle size determines the roughening rate of amorphous thin films. Stress in WSi_2/Si multilayers deposited above the transition pressure becomes tensile when formed from nanoparticles due to particle coalescence and elimination of nano-voids.

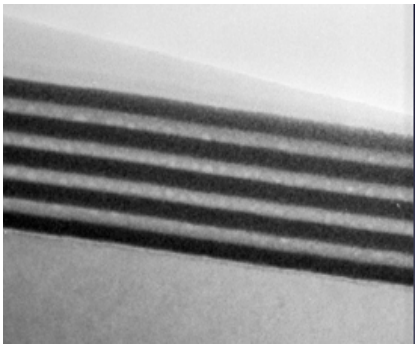

Figure 4. Cross sectional TEM image of a WSi_2/Si multilayer with 5 periods. Acknowledgement: Mark Kirk.

Recent Progress: Assembly of Relaxed 2D Islands in Pulsed Laser Deposition

PLD produces a high nucleation density due to the high peak flux of particles onto the surface during each pulse. Fig. 5 shows GIXD data at (1 1 0.05) during two deposition bursts onto a Ge (001) surface up to a final coverage of 0.3 monolayers. Relaxation between deposition bursts with time constant on the order of 100 - 200 sec is apparent.

One of the main results of this study is that lattice relaxation occurs in the 2D islands due to anisotropic strain induced by the dimers. The islands are fully coherent with the substrate, but they can relax due to the fact that the islands are small (~10 nm). We observe a ~3% contraction of the lattice parameter along the dimer direction and an expansion in the orthogonal direction. This configuration is metastable on modest annealing. Also, further deposition leads to 2D multilevel islands. The results, taken together, suggest that the lattice strain caused by the surface reconstruction plays a role in the transition of the surface from flat to mounded growth, which is known to occur for Ge in MBE growth and also in PLD.

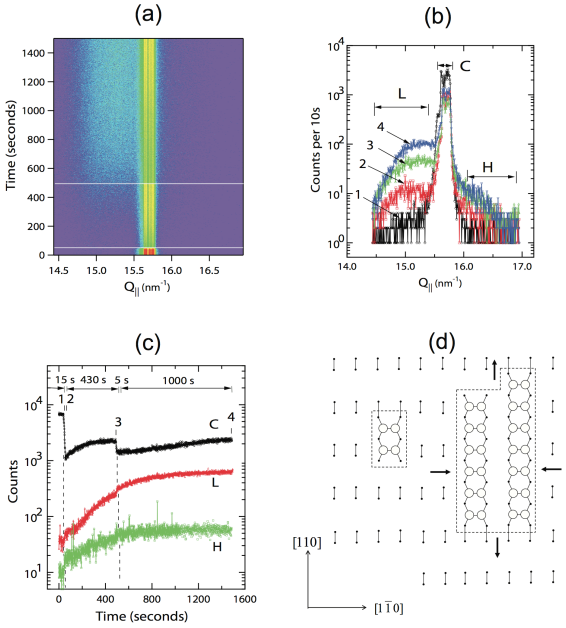

Figure 5. First pulsed laser deposition results for Ge homoepitaxiy on Ge(001). The results show that two dimensional dimer islands are formed on the surface, which continue to evolve after the deposition is halted. (a) Raw time resulved data during deposition at 10 Hz and relaxation, (b) In-plane reciprocal space slices showing evidence for the evoluiton of coherent strain relaxed dimer islands. (c) Time dependence of the specular (C) and relaxed peaks (L, H). (d) Cartoon showing dimer islands on Ge(001). Arrows indicate the directions of anisotropic srain.

Future Plans

Future work will continue in three major directions:

(1) We will continue the real-time x-ray scattering studies of epitaxial growth, but turning our attention to complex oxide materials. Materials of interest include multiferroic $BiFeO_3$, which can be grown as a strained layer on an number of substrate materials. We will compare film growth by Sputter Deposition and PLD processes, which are similar in some respects, but different due to the unique time structure of PLD. Questions will include how to control growth modes such as step flow growth. Very little is known about growth modes in complex oxide growth, largely due to the lack of characterization methods for growth studies during Sputter Deposition or PLD.

(2) Studies of nanoparticle formation in sputter deposition in support of the growth experiments Initially, we plan to investigate elemental Fe sputtering, because Fe is a component of $BiFeO_3$ and we need to understand the conditions under which nanoparticles are formed in the deposition flux. In addition, Fe nanoparticles formed by plasma-gas aggregation are of current interest, partly because the Fe can be oxidized to form Fe_2O_3 or Fe/Fe_2O_3 core/shell structures. This effect is also of interest for the growth of complex oxides because it raises the possibility that the "assembly" step of complex oxide film growth may occur in the plasma-gas phase under some conditions.

(3) Sputter deposition of amorphous silicon films in collaboration with Prof. Karl Ludwig at Boston University. We will investigate roughening and smoothening mechanisms during deposition. The issue here is to determine whether impact induced smoothing is a dominant process under any deposition conditions, and to ultimately explore roughening transitions if they exist.

References

1. "Mechanisms of pattern formation and smoothing induced by ion beam erosion," H. Zhou, L. Zhou G. Ozaydin, K.F. Ludwig Jr., and R.L. Headrick, Phys. Rev. B **78** 165404 (2008)
2. "Ripple formation and smoothening on insulating surfaces," R.L Headrick and Hua Zhou, J. Phys.: Condens. Matter **21**, 224005 (2009).
3. "Pressure-dependent transition from atoms to nanoparticles in magnetron sputtering: Effect on WSi_2 film roughness and stress," Lan Zhou, Yiping Wang, Hua Zhou, Minghao Li, Randall L. Headrick, Kimberly Mac Arthur, Bing Shi, Ray Conley, and Albert T. Macrander Phys. Rev. B **82**, 075408 (2010).
4. "Lattice relaxation of two-dimensional islands on Ge(001)-(2x1) during homoepitaxy by pulsed laser deposition," Lan Zhou, Yiping Wang, Minghao Li, and Randall L. Headrick, Submitted to Phys. Rev. B (2010).

X-ray Scattering Studies of Strongly Correlated Electron Systems

John Hill, Mark Dean, Xuerong Liu, Raanan Tobey and Stuart Wilkins

hill@bnl.gov, mdean@bnl.gov, xliu@bnl.gov, rtobey@bnl.gov, swilkins@bnl.gov

Condensed Matter Physics and Materials Science Department, Brookhaven National Laboratory, Upton NY 11973-5000

Program Scope

This program is organized around the goal of understanding the role of electron correlations in determining the materials properties of strongly correlated electron systems such as high-temperature superconductors and related materials. The principal technique used is x-ray scattering, with experiments performed at the NSLS at BNL, and at other facilities in the US and abroad. Inelastic scattering and resonant scattering techniques are used to probe the ground state and excitation spectrum of the electronic degrees of freedom. Problems to be addressed include the role of electron-lattice coupling in determining the physics of these materials, the role of inhomogeneities; their statics and dynamics, in determining the materials properties and the effect that breaking translational symmetry through the presence of a surface or interface has on the electronic properties of the system.

Recent Progress

Electronic Excitations in cuprates. We have used resonant inelastic x-ray scattering (RIXS) to study the momentum-resolved excitations in a variety of low-dimensional cuprates in the energy range 0 – 10 eV [1,2,22]. By comparing RIXS data to EELS and optical spectroscopy, we have shown that the loss function may be measured, modulo a resonant prefactor, to a good approximation for certain cuprates [13]. In studies of $La_{2-x}Sr_xCuO_4$, new excitations were observed in the mid-IR range around 500 meV. The momentum, doping and temperature dependence of these excitations revealed them to be magnetic in origin, in particular two-magnon excitations [4,20]. Measurements of such high energy magnetic excitations can reveal details of the spin-Hamiltonian in an energy range that is difficult for inelastic neutron scattering to reach. A review of this technique and the enormous advances that have been made in this area over the last decade will be published in Rev. Mod. Phys. [17].

Electron-phonon coupling in superconductors. The discovery of Fe-based superconductors has provided a new route to explore mechanisms for high temperature superconductivity. We have studied $SmFeAsO_{0.6}F_{0.35}$ which has the highest Tc(= 55 K). Extant single crystals of this family are small (100 x 100 x 20 μm) and we have carried out inelastic x-ray scattering experiments to measure the phonons in SmFeAsO and superconducting $SmFeAsO_{0.60}F_{0.35}$. Particular attention was paid to the dispersions along the (100) direction of three optical modes close to 23 meV, polarized out of the FeAs planes. Remarkably, two of these modes –those that couple to the Fe moment - are strongly renormalized upon fluorine doping. These results provide significant insight into the energy and momentum dependence of the coupling of the lattice to the electron system and point to the importance of spin-phonon coupling [23].

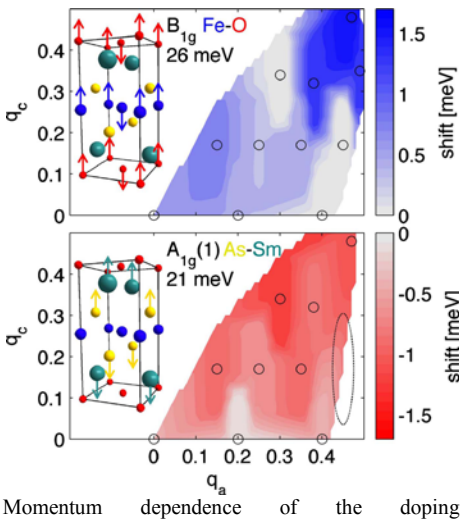

Momentum dependence of the doping renormalization of the two modes around 23 meV that couple to the Fe moment in SmFeAs(O,F) [23].

Spin-lattice coupling in multiferroics.. In multiferroics, the coupling of the lattice to the electron system is manifest between the ferroelectric and magnetic order parameters – a potentially highly useful combination. One model for this coupling requires an incommensurate cycloidal magnetic structure to induce a spontaneous electric polarization. This has been proposed to be the relevant mechanism in $TbMnO_3$. We have used soft x-ray resonant scattering to discover that instead of being driven by a collinear to a noncollienar magnetic transition, as had been previously supposed, the ferroelectric transition is a transition between two non-collinear structures. The essential

difference in the ferroelectric phase is then indeed the cycloidal component of the magnetic structure which forms in the Γ_2 component [3,15]. In contrast, in $TbMn_2O_5$, there is a much larger magnetoelectric coupling, but the magnetic structure is commensurate and almost collinear. This suggests that an entirely different mechanism is active here. Studies at the O K-edge revealed a long range ordered spin polarization at the oxygen site that appears simultaneously with the onset of ferroelectricity. This spin polarization was shown from *ab calculations* to result from hybridization with the Mn^{3+} sites [5,18]. These observations lend support to a second mechanism for multiferroicity, due to Moskvin and co-workers, in which the coupling is driven by coupled magnetic moments on the Mn and O sites.

Construction of soft x-ray diffraction and imaging chamber. This new instrument will carry out diffraction measurements at 3d transition metal L-edge resonances which are extremely sensitive to spin, charge and orbital ordering. The chamber has capabilities for performing diffraction in surface scattering geometries and for carrying out real space imaging utilizing diffraction signals as a contrast mechanism. The resolution of the latter is expected to be ~ 100 nm. Initial commissioning experiments have begun Ultimately, this chamber will move to the NSLS-II, where the resolution will be ~ 10 nm for such experiments, and where Coherent Diffraction Imaging will also be possible. The goals of the instrument are to address the role of dimensionality and of interfaces in determining the controlling physics of these materials, and to study the morphology and dynamics of inhomogeneities..

Future Plans

Electronic Excitations. Work will continue in this area with particular focus on magnetic excitations measured in a regime complementary to that accessible with neutron scattering, i.e. systems for which only small sample volumes are obtainable, and at very large energy transfers.

Nanoscale inhomogeneities. Real space imaging and coherent diffraction imaging experiments will be pursued to explore the morphology and dynamics of nanoscale domains in systems such as CMR manganites and multiferroics, with emphasis on their behavior under thermal excitations and in applied fields.

Electron-phonon coupling. Studies will continue on the Fe-based superconductors, in particular carrying out phonon and diffuse scattering measurements of the [R]FeAs(O,F) and Fe(Te,Se) families as a function of temperature and doping to search for anomalies associated with antiferromagnetism, orbital order or superconductivity.

Future Beamlines. The group is active in defining beamlines under development or proposed at the APS and NSLS-II. At NSLS-II, we are members of the Beamline Advisory Teams .for the inelastic scattering and the soft x-ray coherent scattering beamlines and are PIs on several of the approved beamlines in the next round.

Selected DOE Sponsored Publications 2008-2010

FY08

[1] Ellis, D.S., Hill, J.P., Wakimoto, S., Birgeneau, R.J., Casa, D., Gog, T., and Kim, Y.-J. Charge-transfer exciton in La2CuO4 probed with resonant inelastic x-ray scattering,. Phys. Rev. B 77, 060502 (2008).

[2]Ellis, D.S., Hill, J.P., Wakimoto, S., Birgeneau, R.J., Casa, D., Gog, T., and Kim, Y.-J. Comparison of electronic excitations in single-layer and bi-layer cuprates. Physica B 403, 1053-1055 (2008).

[3] Forrest, T.R., Bland, S.R., Wilkins, S.B., Walker, H., Beale, T.A.W., Hatton, P.D., Prabhakaran, D., Boothroyd, A.T., Mannix, D., Yakhou, F., McMorrow, D.F. Ordering of localized electronic states in multiferroic TbMnO3: a soft x-ray resonant scattering study. J. Phys.: Condens. Matter 20, 422205 (2008).

[4] Hill, J.P., Blumberg, G., Kim, Y.-J., Ellis, D., Wakimoto, S., Birgeneau, R.J., Komiya, S., Ando, Y., Liang, B., Greene, R.L., Casa, D., and Gog, T. Observation of a 500meV collective mode in La2-xSrxCuO4 and Nd2CuO4. Phys. Rev. Lett. 100, 097001 (2008).

[5] Johnson, R.D., Bland, S.R., Mazzoli, C., Beale, T.A.W., Du, C.-H., Detlefs, C., Wilkins, S.B., and Hatton, P.D. Determination of magnetic order of the rare-earth ions in multiferroic TbMn2O5. Phys. Rev. B 78, 104407 (2008).

[6] Turner, J.J., Thomas, K.J., Hill, J.P., Pfeifer, M., Chesnel, K., Tomioka, Y., Tokura, Y., and Devan, S. Orbital domain dynamics in a doped manganite. New J. of Phys. 10(5), 053023 (2008).

[7] Turner, J.J., Jordan-Sweet, J.L., Upton, M., Hill, J.P., Tokura, Y., Tomioka, Y., and Kevan. S.D. Domain mapping of a Ca-doped manganite. Appl. Phys. Lett. 92, 131907 (2008).

[8] Upton, M., Klie, R., Hill, J.P., Gog, T., Casa, D., Ku, W., Zhu, Y., Sfeir, M., Misewich, J., Eres, G., and Lowndes, D. Effect of number of walls on plasmon behavior in carbon nanotubes. Carbon 47, 162-168 (2008).

FY09

[9] Bland, S.R., Detlefs, B., Wilkins, S.B., Beale, T.A.W., Mazzoli, C., Joly, Y., Hatton, P.D., Lorenzo, J.E., and Brabers, V.A.M. Full polarization analysis of resonant superlattice and forbidden x-ray reflections in magnetite. J. Phys. Condens. Matter 21, 485601 (2009).

[10] Hase, T., Raanaei, H., Lidbaum, H., Sanchez-Hanke, C., Wilkins, S., Leifer, K., and Hjorvarsson, B. Spin and orbital moment in amorphous $Co_{68}Fe_{24}Zr_8$ layers. Phys. Rev. B 80, 134402 (2009).

[11] Hatton, P.D., Johnson, R.D., Bland, S.R., Mazzoli, C., Beale, T.A.W., Du, C.-H., and Wilkins, S. Magnetic structure determination using polarized resonant x-ray scattering. J. Magnetism and Magnetic Materials 321, 810-813 (2009).

[12] Jacques, V.L.R., Le Bolloc'h, D., Ravy, S., Giles, C., Livet, F., and Wilkins, S.B. Spin density wave dislocation in chromium probed by coherent x-ray diffraction. Eur. Phys. J. B 70, 317-325 (2009).

[13] Kim, J., Ellis, D.S., Zhang, H., Hill, J.P., Chou, F.C., Gog, T., Casa, D., and Kim, Y.-J. Comparison of resonant inelastic x-ray scattering spectra and dielectric loss functions in copper oxides. Phys. Rev. B 79, 094525 (2009).

[14] Walker, H.C., Ewings, R.A., Fabrizi, F., Mannix, D., Mazzoli, C., Wilkins, S.B., Paolasini, L., Prabhakaran, D., Boothroyd, A.T., and McMorrow, D.F. X-ray resonant scattering study of the magnetic phase diagram of multiferroic $TbMnO_3$. Physica B 404, 3264-3266 (2009).

[15] Wilkins, S.B., Forrest, T.R., Beale, T.A.W., Bland, S.R., Walker, H.C., Mannix, D., Yakhou, F., Prabhakaran, D., Boothroyd, A.T., Hill, P.D., Hatton, P.D., and McMorrow, D.F. Nature of the magnetic order and origin of induced ferroelectricity in $TbMnO_3$. Phys. Rev. Lett. 103(2), 207602 (2009).

[16] Wilkins, S.B., Di Matteo, S., Beale, T.A.W., Joly, Y., Mazzoli, C., Hatton, P.D., Bencok,P., Yakhou, F., and Brabers, V.A.M. Critical reexamination of resonant soft x-ray Bragg forbidden reflections in magnetite. Phys. Rev. B 79, 201102R, (2009).

FY10

[17] Ament, L.J.P., van Veenendaal, M., Devereaux, T.P., Hill, J.P., and van den Brink, Jeroen. Resonant inelastic x-ray scattering studies of elementary excitations. Reviews of Modern Phys. (accepted).

[18] Beale, T.A.W., Wilkins, S., Johnson, R., Bland, S., Joly, Y., Forrest, T., McMorrow, D.F., Yakhou, F., Prabhakaran, D., Boothroyd, A.T., and Hatton, P.D. Antiferromagnetically spin polarized oxygen observed in magneto-electric $TbMn_2O_5$. Phys. Rev. Lett. **105**, 087203 (2010).

[19] Dean, M.P.M., Walter, A.C., Howard, C.A., Weller, T.E., Calandra, M., Mauri, F., Ellerby, M., Saxena, S.S., Ivanov, A., and McMorrow, D.F. Neutron scattering study of the high-energy graphitic phonons in sperconducting CaC_6. Phys. Rev. B 82, 014533 (2010).

[20] Ellis, D.S., Kim, J., Hill, J.P., Wakimoto, S., Birgeneau, R.J., Shvyd'ko, Y., Casa, D., Gog, T., Ishii, K., Ikeuchi, K., Paramekanti, A., and Kim, Y.-J. Magnetic nature of the 500 meV peak in $La_{2-x}Sr_xCuO_4$ observed with resonant inelastic x-ray scattering at the Cu K-edge. Phys. Rev. B 81, 085124 (2010).

[21] Gog, T., Seidler, G., Casa, D., Upton, M., Kim, J., Shyvd'ko, Yu., Stoupin, S., Nagle, K., Balasubramanian, M., Gordon, R., Fister, T., Heald, S., Toellner, T., Hill, J.P., Coburn, D.S., Kim, Y.-J., Said, A.H., Alp, E.E., Sturhahn, W., Yavas, H., Burns, C., and Sinn, H. Momentum-resolved resonant and nonresonant inelastic x-ray scattering at the advanced photon source. Synch. Radiat. News (submitted).

[22] Kim, Y.-J., Hill, J.P., Yamaguchi, H.,Gog, T., and Casa, D. Resonant inelastic x-ray scattering study of the electronic structure of Cu_2O. Phys.Rev. B **81** 195202 (2010).

[23] Le Tacon, M., Forrest, T.R., Rüegg, Ch., Bosak, A., Walters, A.C., Mittal, R., Ronnow, H.M., Zhigadlo, N.D., Katrych, S., Karpinski, J., Hill, J.P., Krisch, M., and McMorrow, D.F. Inelastic x-ray scattering study of $SmFeAs(O_{1-x}F_y)$ single crystals: evidence for strong momentum-dependent doping-induced renormalization of optical phonons,. Phys. Rev. B **80**, 220504R (2009) (*Editors suggestion)*

[24] Springell,R., Langridge, S., Wildes, A., Wilkins, S.B., Sanchez-Hanke, C., Moore, K.T., Butterfield, M., Chivall, J., Ward, R.C.C., and Lander, G.H. Chemical and magnetic structure of uranium/gadolinium multilayers studied by transmission electron microscopy, neutron scattering, and x-ray reflectivity. Phys. Rev. B 81, 134434, (2010).

Time resolved x-ray microdiffraction and phase contrast imaging studies of rapidly propagating reactions in metallic multilayers

Todd C. Hufnagel,[1] Stephen T. Kelly,[1] Sara C. Barron,[1] Timothy P. Weihs,[1]
Eric M. Dufresne,[2] and Kamel Fezzaa[2]
[1]*Department of Materials Science and Engineering, Johns Hopkins University*
[2]*Advanced Photon Source, Argonne National Laboratory*

Program scope

The use of pump-probe x-ray scattering techniques with femtosecond-level temporal resolution for studies of reversible transitions in materials is well established. Many transformations, however, are irreversible and not amenable to multi-shot pump-probe techniques. Particularly challenging to study are transformations that are both rapid and highly localized, requiring simultaneous temporal and spatial resolution. For instance, self-propagating exothermic reactions in nanoscale multilayers can occur as localized reaction fronts approximately 100 μm wide propagating at $\sim$ 10 m s^{-1}, reaching temperatures in excess of 1500 °C in less than 1 ms, followed by rapid cooling. Probing reactions under these extreme conditions requires techniques with spatial resolution of at least 100 μm and temporal resolution of 100 μs or better.

As part of a larger combined modeling and experimental effort, we are developing x-ray techniques to study these transformations. We describe here two such techniques. In the first, we perform x-ray microdiffraction experiments on the microsecond time scale by using a focused broad-spectrum x-ray beam in combination with either a fast detector or a fast shutter. Our most recent experiments at the Advanced Photon Source achieved temporal resolution of 15 μs and spatial resolution of 7 μm. This is sufficient to allow us to track the sequence of phase formation during the initial rapid heating stage of transformation in Al/Ni and Al/Zr multilayers.

To observe the morphology of the advancing reaction front, we use x-ray phase contrast imaging. We observe a transition from uniform to stepwise propagation of the reaction front, depending on the chemistry and layer spacing of the multilayer foil. Simultaneously, we record x-ray diffraction information, allowing us to correlate the advance of the reaction front with the appearance of particular phases.

Recent progress

Time-resolved x-ray microdiffraction

Figure 1 shows the experimental arrangement for our most recent microdiffraction experiments at the Advanced Photon Source (APS). Working with the undulator source at Sector 7 ID-B, we used dynamically bent Kirkpatrick-Baez mirrors to focus the pink ($\sim$ 12 keV with $\sim$ 2 % bandwidth) x-ray beam, producing a 7×6 μm spot with $\sim 3 \times 10^{13}$ ph s^{-1}. We then used a fast shutter to produce x-ray pulses of $\sim$ 15 μs duration from this beam. The shutter uses commercial laser scanning galvanometer heads to rapidly move tungsten shutter blades in response to a voltage level signal input. We collected the diffraction pattern from this short pulse of x-ray s on a fiber-optic-coupled x-ray CCD camera (MAR

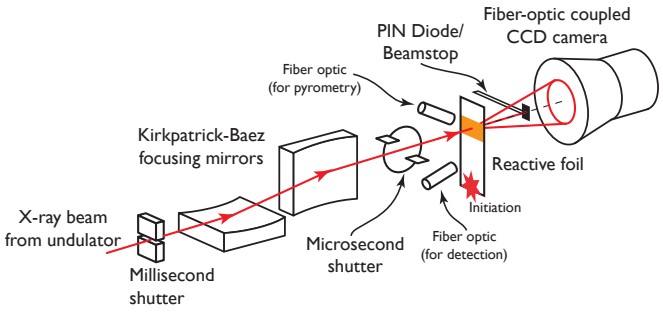

Figure 1: Illustration depicting the experimental setup for the time-resolved microdiffraction measurements. The water cooled millisecond shutter protects the Kirkpatrick Baez mirrors from the power of the white beam incident on the first mirror, which is not water cooled.

165). Simultaneously, we performed *in situ* two-color ratio pyrometry to monitor the foil temperature as the reaction front passed the x-ray beam position.

Earlier versions of this experiment used a fast pixel array detector (PAD), rather than a shutter, for obtaining the required time resolution. Although the PAD allows collection of several diffraction patterns in sequence from a single specimen, its small size creates problems with covering a sufficiently wide region of reciprocal space. In the more recent experiments, we use a slower but much larger detector, allowing us to capture scattering data covering both a wider range of scattering angles and a larger fraction of the powder rings. The trade-off is that we can only record a single diffraction patterns from each specimen.

Because this is a single-shot technique, we build up the temporal sequence of events from experiments on multiple specimens. This requires us to be able to collate the resulting diffraction patterns, putting them into the proper sequence with respect to the advancing reaction front. To do this, we timed the incident x-ray pulse with respect to the reaction by sensing light from the approaching reaction front with a photodiode, and used that signal to trigger the action of the microsecond shutter after a predetermined delay time. The sharp rise in the pyrometer signal provides a time (t_0) which we use as a reference for collating the diffraction patterns. By monitoring the x-ray pulse with a small Si PIN diode positioned on the beam stop, we can know the timing of the x-ray pulse with respect to t_0 with an uncertainty comparable to the duration of the x-ray pulse.

Figure 2 shows a series of integrated x-ray diffraction patterns collected with this technique for multilayer samples with overall composition Al_3Zr and 95 nm bilayer period. For patterns taken at $t = t_0 - 0.058$ ms or earlier the multilayer appears unreacted, with only peaks from fcc-Al and hcp-Zr appearing. Patterns taken at $t = t_0 - 0.052$ ms or later, on the other hand, show partial or complete transformation to the stable intermetallic Al_3Zr without any intermediate phases and over a time scale of ~ 50 μs. This is in contrast with results from other systems, such as Al_3Ni_2, which display more complex phase transformation sequences.

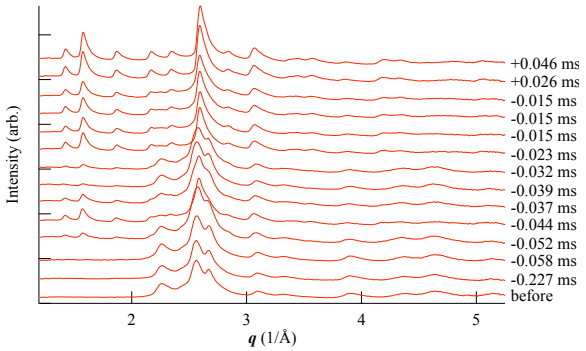

Figure 2: Time-resolved x-ray microdiffraction patterns taken from advancing reaction fronts in Al_3Zr multilayer foils. The labels on the right hand side represent the timing of the x-ray pulse relative to the reference time t_0 from the pyrometer.

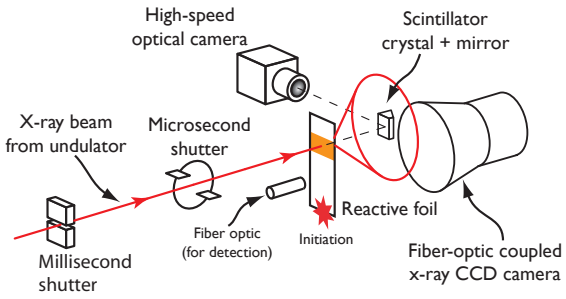

Figure 3: Illustration of the experimental setup (left) for the simultaneous phase-contrast x-ray imaging and diffraction experiments. The water-cooled millisecond shutter reduces the heat load on the other experimental components.

X-ray phase contrast imaging

In order to observe the morphology of the advancing reaction front, we employ x-ray phase contrast imaging while simultaneously recording diffraction data. We illuminated the sample with an unfocused white ($\sim$ 12.4 keV with $\sim$ 5 % bandwidth and $\sim 6 \times 10^{14}$ ph s^{-1} in the fundamental emission peak) x-ray beam from the undulator source at Sector 32 ID-B at APS and imaged the sample by using a high-speed optical camera to record the light from scintillator crystal oriented perpendicular to the x-ray beam and coupled to the camera with a mirror rotated 45° to the beam. Diffraction data was collected with a fiber-optic-coupled x-ray CCD camera over a total 1-2 ms x-ray exposure. Although diffraction data have neither the spatial resolution nor the temporal resolution of the microdiffraction experiments describe above, they provide at least some information about the phase(s) present during the image sequence. The two data sets therefore provide complementary information about the advancing reaction front. We timed the data collection with respect to the advancing reaction in a similar manner to that used in the time-resolved microdiffraction technique outlined in the previous section.

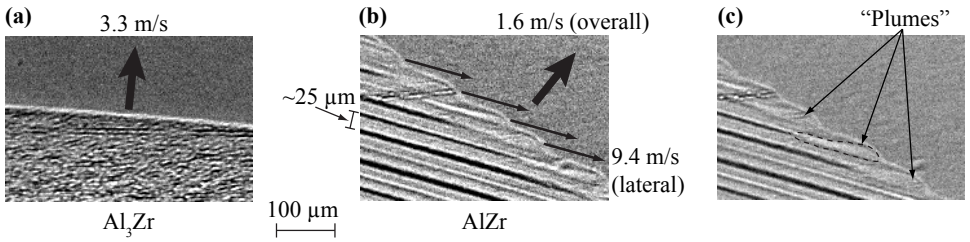

Figure 4: Contrast adjusted images of the propagating reaction fronts in an Al_3Zr (a) and an AlZr (b) foil. The scalloped reaction front in the AlZr foil moves with an overall velocity of 1.6 m/s, while the longitudinally propagating zones move at 9.4 m/s in thin, $\sim$ 25 μm bands. The resulting striped microstructure remains for the duration of the 2 ms exposure time. Distinct "plumes" ahead of the advancing thin bands (c) also appear in the images of reacting AlZr foils.

By adjusting the timing of the microsecond shutter opening with respect to the signal from the photodiode, we obtained image sequences which show the reaction front as it propagates across the field of view. Figures 4a and b show images of the advancing reaction front in a foil with composition Al_3Zr and 95 nm bilayer period and in a foil with composition AlZr and 85 nm bilayer period, respectively. The reaction front in the Al_3Zr foils is essentially planar and propagates uniformly. In contrast, the reaction front in the AlZr foils is more complex, with transverse steps propagating laterally to the over direction of propagation. Similar effects have been seen (by others) in Co/Al multilayers using optical cinematography, but the x-ray technique holds the additional promise of revealing details of the structure inside the advancing reaction front. Note, for example, the "plumes" that appear in advancing steps (Fig. 4c). Additional *ex situ* microscopy and structural analysis combined with modeling efforts will bring us closer to understanding the origin of these features.

Future plans

We are continuing to refine the x-ray microdiffraction technique. The principal limitation on temporal resolution is uncertainty in timing between the x-ray pulse and the arrival of the reaction front at the x-ray beam, which results from uncertainties in the initiation of the reaction and its velocity. We plan to overcome this by sensing the reaction front at a position closer to the x-ray spot and with a focusing optical setup. Our second major area is the development of a new time-resolved x-ray reflectivity technique, based on specular reflectivity from a dynamically bent specimen. We anticipate that this will allow us to collect reflectivity data with sub-millisecond temporal resolution.

References to publications of DOE-sponsored research

Two manuscripts describing the results to date (described above) are in preparation, but neither has yet been submitted.

Neutron Microfocusing Optics and Applications

Gene E. Ice and Judy W. L. Pang
Bldg 4500S Oak Ridge National Laboratory, Oak Ridge TN 37831-6118
IceGE@ORNL.Gov, PangJ@ORNL.Gov

Research Scope

The goal of this research is to field high-efficiency achromatic neutron microfocusing optics capable of resolving heterogeneities in materials with 25-50 μm spatial resolution. The scope also includes demonstrations of new applications made possible by combining the *unique properties of neutron diffraction* with *unprecedented neutron spatial resolution*. Our approach is based on Kirkpatrick-Baez mirrors widely-used by the X-ray community. The focusing properties of various mirror combinations are studied to understand their theoretical limits using ray-tracing programs. Desirable devices are then fabricated using bent-mirror methods and advanced neutron supermirror surfaces. This effort is an integral part of our larger programmatic vision, to clarify the role of *local* structure and defects on materials properties (see abstracts by Larson et al., Budai et al., Pang et al., Barabash et al., Specht et al. and Tischler et al.).

At first glance, this project should be straightforward. X-ray *nanofocusing* mirrors are now almost routine, with bent KB mirror systems below 1000 nm commercially available and with state-of-the-art figured KB mirror systems commercially available with guaranteed 40 nm focusing. However, as described below, neutron microfocusing optics are particularly challenging due to the need to collect the largest-possible divergence onto the sample, and the need for very large mirrors with long working distances. This drives designs toward extremes that are not yet practiced with X-ray mirror systems. Indeed, the approaches pioneered here are inspiring a new generation of X-ray optics that will push the diffraction limit for achromatic total-external-reflection mirrors beyond the current state-of-the-art.

Recent Progress

We have done extensive ray-tracing of achromatic Kirkpatrick-Baez mirror systems based on neutron supermirrors, and find that under most microfocusing conditions, ideal elliptical mirrors can preserve beam brilliance (phase-space density) within the emittance (product of size and divergence) that can be collected onto the sample. This approach was used for example, to successfully focus neutrons to an ~100 μm beam at Chalk river in 2005 with a demonstration of Laue diffraction from small sample volumes.

Based on the success of these experiments, we recently demonstrated Montel or nested optics (Fig. 1b) for achromatic microfocusing on SNAP[1,2]. These experiments have focused to ~80 μm (Fig. 3,4). Compared to traditional Kirkpatrick-Baez optics, Montel optics, have the advantage of collecting 2-3 x more beam onto the sample for the same spot size and are much more compact. However, Montel optics are complicated by the need to produce a nearly ideal aspherical mirror surface near the edge of one mirror, and by extremely different local mirror curvature at upstream and downstream ends. These two challenges are being overcome with new technical developments as described below.

The performance limits of Montel and KB optics (Fig. 1) were compared in ref 3 where we re-evaluated the limits to mirror performance to understand the critical design parameters and the limits to mirror bending schemes. It was recognized that the angle of the supermirror (at the downstream edge θ_D) and the ratio, n, of the mirror length, l, to the clearance distance, F_D, largely determine the maximum divergence that can be focused onto the sample (Fig. 2). Based on this understanding, mirror systems with n~2-3 are desirable[3], but standard KB

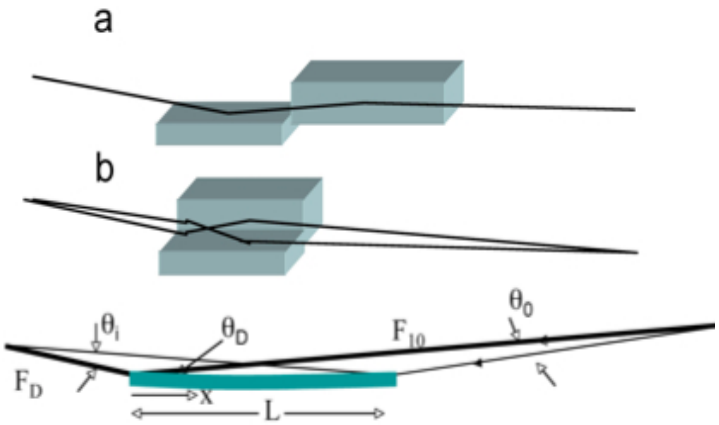

Fig. 1 (a). Standard Kirkpatrick-Baez mirror with sequential elliptical mirrors. (b). Montel mirror pair with parallel reflections of rays. Below- elliptical mirror with various parameters.

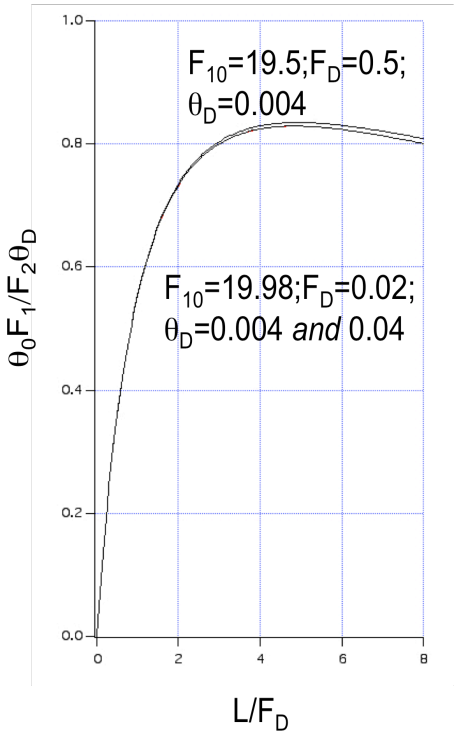

Fig. 2. Figure-of-merit for highest beam intensity as a function of mirror length to clearance ratio n=L/F_D. Note that the function is insensitive to the exact mirror parameters.

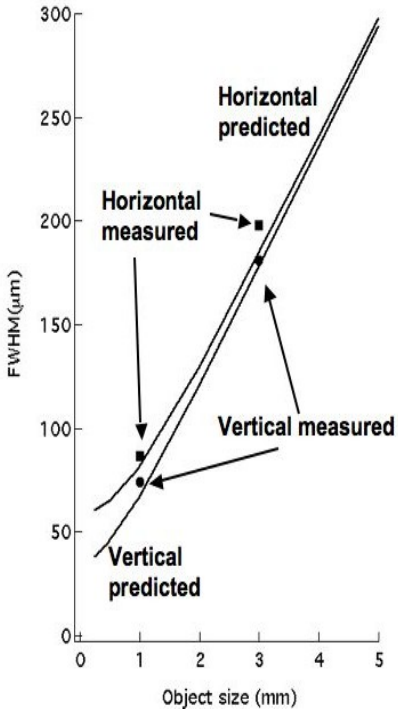

Fig. 3 Nested mirror performance on SNAP for a n~2.2 Montel mirror pair.

mirror systems with n>1 are impractically large. This understanding justifies the efforts at developing Montel mirror optics and sets our ultimate design goals.

Once the n number of the mirror system is set, the problem becomes how to produce such mirrors. Our first attempts at Montel optics, concentrated on obtaining mirrors with good

surface properties at the mirror edge. We were able to locate left-over mirrors from a high-energy physics experiment that were polished on 4 sides with very good roughness and figure right up to the mirror edge. These mirrors were slightly thicker than optimum but were otherwise close to ideal in dimensions. Using a special long-trace-profiler optimized for our neutron studies[4], we optimized the figure of both the vertical and horizontal focusing mirrors. With these mirrors however, we were unable to produce a good figure over the entire mirror surface using a simple unequal bending moment arrangement that had worked well with our first set of sequential KB mirrors.

Modeling of the various bending schemes explained why our initial approach was unsuccessful, and provided new strategies for more precise focusing. In short, the extreme range of local radii from the upstream to the downstream end of a high n elliptical mirror cannot be accurately matched by the linear approximation provided by two unequal bending moments (Fig. 4). A much better approximation is possible with an additional degree of freedom or by optimized mirror shapes (Fig. 4). Using a simple spring to provide an additional degree of freedom we significantly improved the focal spot size. We note that the design principles for these optics are now being adopted by others. For example, IMAGINE a new long-wavelength Laue diffraction beamline on HFIR will use KB optics to focus the beam onto the sample. Ray tracing shows that this approach will produce higher flux density and is far more cost effective than elliptical beam guides. In addition, a Montel prototype (first championed in this program) has recently achieved a 150 nm spot size at the Advanced Photon Source and offers an important path forward for more stable nm scale achromatic optics.

Future Plans

We have specially-designed mirrors on order from Swiss Neutronics, that should enable near theoretical thermal-neutron focusing down to 25-50 μm. The mirrors have a cube-root thickness dependence that will allow nearly ideal bending to an elliptical shape. In addition, they are cut from a pre-polished surface and prepared with an elliptical edge profile to nest against the neighbor mirror. We are also designing a more sophisticated bender for uniform-thickness mirrors that should achieve near ideal performance below 50 μm.

We have at least four experiments already planned for the microfocusing mirrors. For example, we will study the full strain tensor of intra-granular volumes in a polycrystalline Ni sample (see Pang abstract). These measurements will be combined with ensemble-average neutron measurements and submicron X-ray measurements to clarify the role of average, inter- and intra-granular strains in polycrystalline networks. We also propose to make intra-granular full strain tensor measurements on a Ni tri-crystal for comparison to a detailed theoretical calculation that cannot be reproduced by EBSD or X-ray near surface measurements (see Pang abstract). We will also use the unprecedented spatial resolution to probe the strain state of batteries to understand how the materials response changes with position inside an operating battery. Finally-and most importantly- we will use microfocusing mirrors to study pressure sensitive magnetic structure in 3d alloys. This long-standing problem of materials physics (see abstracts by Pang and Specht) is a challenge that is only now addressable due to major advances in first-principles theory and neutron instrumentation-including the focusing mirrors.

Once the *microfocusing* mirrors are demonstrated, we will develop a four-mirror *imaging* system based on nested designs and advanced Kirkpatrick-Baez mirrors (AKB). AKB optics are a hybrid of Kirkpatrick-Baez and Wolter type I optics; with AKB optics two elliptical and two hyperbolic mirrors are used to focus the beam. We propose to use nesting to produce a more compact system. As AKB mirror systems are already in use for plasma diagnostics, a nested approach may have implications beyond neutron optics. We also plan to demonstrate special tricks that will enable ~25 μm focusing of broad-bandpass long-wavelength neutrons and will demonstrate deflected-beam focusing with an order of magnitude greater flux potential.[5]

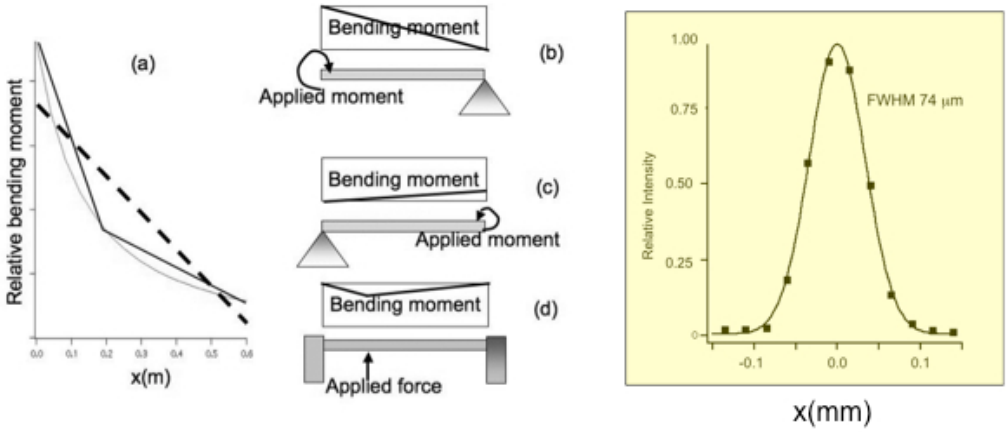

Fig.4. (Left) Schematic showing how the local bending moment changes along an ideal ellipse, and illustrating various approximations to this moment distribution. (Right) Focus on SNAP.

Publications and Patents (FY08-FY10)

1. Ice G.E., J.-Y Choi, P.Z. Takacs, A Khounsary, Y. Puzyrev, J.J. Molaison, C. A. Tulk, K. H. Andersen and T. Bigault, "Nested Neutron Microfocusing Optics on SNAP", Applied Physics A: 99 635 (2010).

2. Ice, G. E., J. W. L. Pang, C. Tulk, J. Molaison, J.-Y. Choi, C. Vaughn, L. Lytle, P. Z. Takacs, K. H. Anderson, T. Bigault, and A. Khounsary, "Design Challenges and Performance of Nested Neutron Mirrors for Microfocusing on SNAP", *J. Appl. Crystallogr.* **42** 1004-1008(2009).

3. Ice, G. E., Rozaliya I. Barabash, and Ali Khounsary, "Nested mirrors for X-rays and Neutrons", in *Proceedings of the SPIE Conference*, San Diego, California (2009).

4. Y. S. Puzyrev, G.E. Ice and P.Z. Takacs,"Long-trace profiler for neutron focusing mirrors", *Nucl. Inst. and Meth*. A: **598** 515-517 (2009).

5. Ice, G. E., U.S. Patent 7,439,492, "Nondispersive neutron focusing method beyond the critical angle of mirrors", October 21, 2008.

6. G.E. Ice, "The Future of Spatially-Resolved Polychromatic Neutron and X-ray Microdiffraction", *Metall. Mater. Trans. A*. **39A** 3058-3064 (2008).

Coherent diffraction imaging: reconstructing rapidly, reconstructing accurately

Chris Jacobsen
Dept. Physics & Astronomy, Northwestern University, Evanston, IL
X-ray Science Division, Advanced Photon Source, Argonne National Laboratory, Argonne, IL
cjacobsen@anl.gov

Coherent x-ray diffraction imaging, or x-ray diffraction microscopy, involves the reconstruction of an image from a far-field diffraction pattern. It offers the advantage of no optic-imposed limits on resolution, no losses in the use of the scattered signal from radiation-sensitive specimens, and no requirement for placing short focal length optics close to the specimen. With support from the Department of Energy, our team at Stony Brook University (now at Northwestern University) has been developing methods to increase the speed at which data can be recorded and reconstructed, and has been exploring the factors that affect the accuracy of reconstructed images. Highlights of this work include the following:

- Because of the q^{-4} dependence of diffraction intensities, one needs to record a series of far-field diffraction patterns with different beamstop positions and exposure times. This leads to a challenging data merging problem so that one can obtain a high dynamic range measure of the diffraction pattern. We have developed an automated merging program AMP [1] that leads to higher quality reconstructed images and more rapid reconstructions (Fig. 1), and which has allowed us to obtain rapid reconstructions of nanoporous glass specimens within 24 hours of data acquisition (Fig. 2).
- We have developed a criterion for measuring the signal-to-noise ratio of images when the object is unknown, and we have used this to examine the relationship between exposure and signal-to-noise in CDI versus conventional imaging (Fig. 3) [2].
- The phase retrieval transfer function (PRTF [3], which is essentially the square root of the intensity ratio [4, 5]) provides a measure of the reliability of a reconstruction after iterate averaging. However, there is a wide variation on the use of the PRTF among CDI practitioners, with some groups using PRTF thresholds as low as 0.05 to measure image resolution even though this corresponds to almost no phase reproducibility. We have shown that a Weiner-filtered Phase Retrieval Transfer Function (wPRTF) provides a more robust measure of reconstructed image quality and resolution (Fig. 4) [1].
- In the far-field geometry, a key step in obtaining a reconstructed image is the determination of the finite support of the object, which is the outline of its shape. We have explored the effects of errors in the determination of the support for various reconstruction algorithms, as well as the effects of failing to record the center, low spatial frequency signal due to detector saturation limits (Fig. **??** [6]).

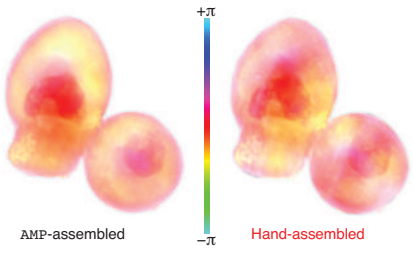

Figure 1: Final averaged reconstructions of both AMP-assembled diffraction intensities and hand-assembled diffraction intensities obtained in experiments on gold-labeled freeze-dried yeast [8]. Magnitude is represented as brightness and phase as hue according to the inset color bar. The hand-assembled reconstruction shows streaks and other variations in intensity that would not be expected in the cell; the AMP-assembled reconstruction provides an improved visual appearance [1].

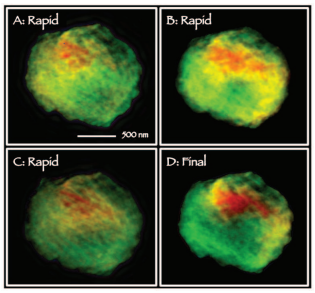

Figure 2: Four independent reconstructions of a nanoporous glass particle. Reconstructions A-C were obtained by three different experimenters (two at the beamline, and one remote) within 24 hours of data collection, while reconstruction D involved use of a complete set of analysis tools including iterate averaging. J. Turner *et al.*, unpublished.

This DoE-supported work has allowed us to better understand the capabilities and limitations of coherent diffraction imaging, so that we have confidence in our experimental work [7, 8].

References

[1] J. Steinbrener, J. Nelson, X. Huang, S. Marchesini, D. Shapiro, J. J. Turner, and C. Jacobsen. Data preparation and evaluation techniques for x-ray diffraction microscopy. *Optics Express*, 18:18598–18614, 2010.

[2] X. Huang, H. Miao, J. Steinbrener, J. Nelson, D. Shapiro, A. Stewart, J. Turner, and C. Jacobsen. Signal-to-noise and radiation exposure considerations in conventional and diffraction x-ray microscopy. *Optics Express*, 17(16):13541–13553, Jul 2009.

[3] H.N. Chapman, A. Barty, S. Marchesini, A. Noy, S. P. Hau-Riege, C. Cui, M.R. Howells, R. Rosen, H. He, J.C.H. Spence, U. Weierstall, T. Beetz, C. Jacobsen, and D. Shapiro. High resolution *ab initio* three-dimensional x-ray diffraction microscopy. *Journal of the Optical Society of America A*, 23:1179–1200, 2006.

[4] D. Shapiro, P. Thibault, T. Beetz, V. Elser, M. Howells, C. Jacobsen, J. Kirz, E. Lima, H. Miao, A. M. Neiman, and D. Sayre. Biological imaging by soft x-ray diffraction microscopy. *Proceedings of the National Academy of Science*, 102(43):15343–15346, 2005.

[5] P. Thibault, V. Elser, C. Jacobsen, D. Shapiro, and D. Sayre. Reconstruction of a yeast cell from x-ray diffraction data. *Acta Crystallographica A*, 62:248–261, 2006.

[6] X. Haung, J. Nelson, J. Steinbrener, J. Turner, and C. Jacobsen. Incorrect support and missing center tolerances of phasing algorithms. *Optics Express*, 0:(submitted), 2010.

[7] X. Huang, J. Nelson, J. Kirz, E. Lima, S. Marchesini, H. Miao, A.M. Neiman, D. Shapiro, J. Steinbrener, A. Stewart, J.J. Turner, and C. Jacobsen. Soft x-ray diffraction microscopy of a frozen hydrated yeast cell. *Physical Review Letters*, 103(19):198101, Nov 2009.

[8] J. Nelson, X. Huang, J. Steinbrener, D. Shapiro, J. Kirz, S. Marchesini, A. M. Neiman, J. J. Turner, and C. Jacobsen. High-resolution x-ray diffraction microscopy of specifically labeled yeast cells. *Proceedings of the National Academy of Sciences*, 107(16):7235–7239, 2010.

Figure 3: Plot of the signal-to-noise ratio SNR as a function of incident photons per pixel $\bar{n}$ for two simulated objects [2]. The results for both x-ray diffraction microscopy (XDM) and transmission x-ray microscopy (TXM) are shown. For both objects the SNR for x-ray diffraction microscopy is about 7 times higher than it is for transmission x-ray microscopy, as expected for the assumption of a 10% efficient zone plate and an integrated area under a modulation transfer function curve of about 0.2 $(1/\sqrt{50} \simeq 7)$.

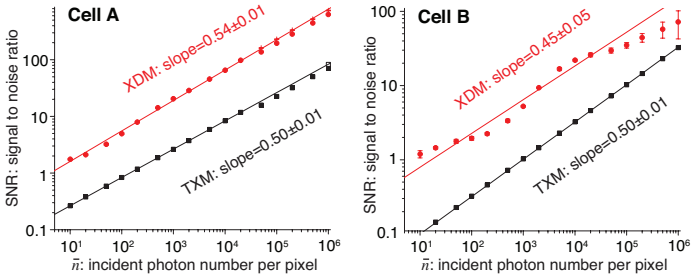

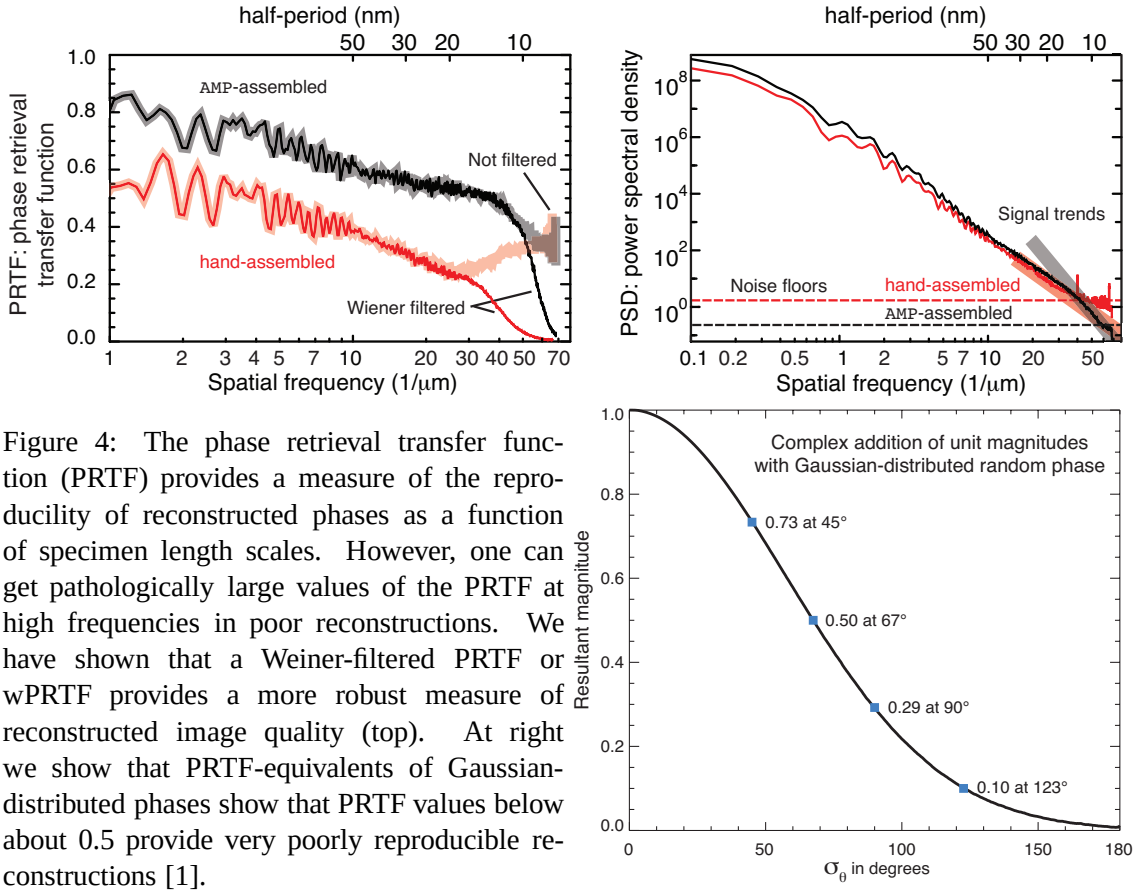

Figure 4: The phase retrieval transfer function (PRTF) provides a measure of the reproducility of reconstructed phases as a function of specimen length scales. However, one can get pathologically large values of the PRTF at high frequencies in poor reconstructions. We have shown that a Weiner-filtered PRTF or wPRTF provides a more robust measure of reconstructed image quality (top). At right we show that PRTF-equivalents of Gaussian-distributed phases show that PRTF values below about 0.5 provide very poorly reproducible reconstructions [1].

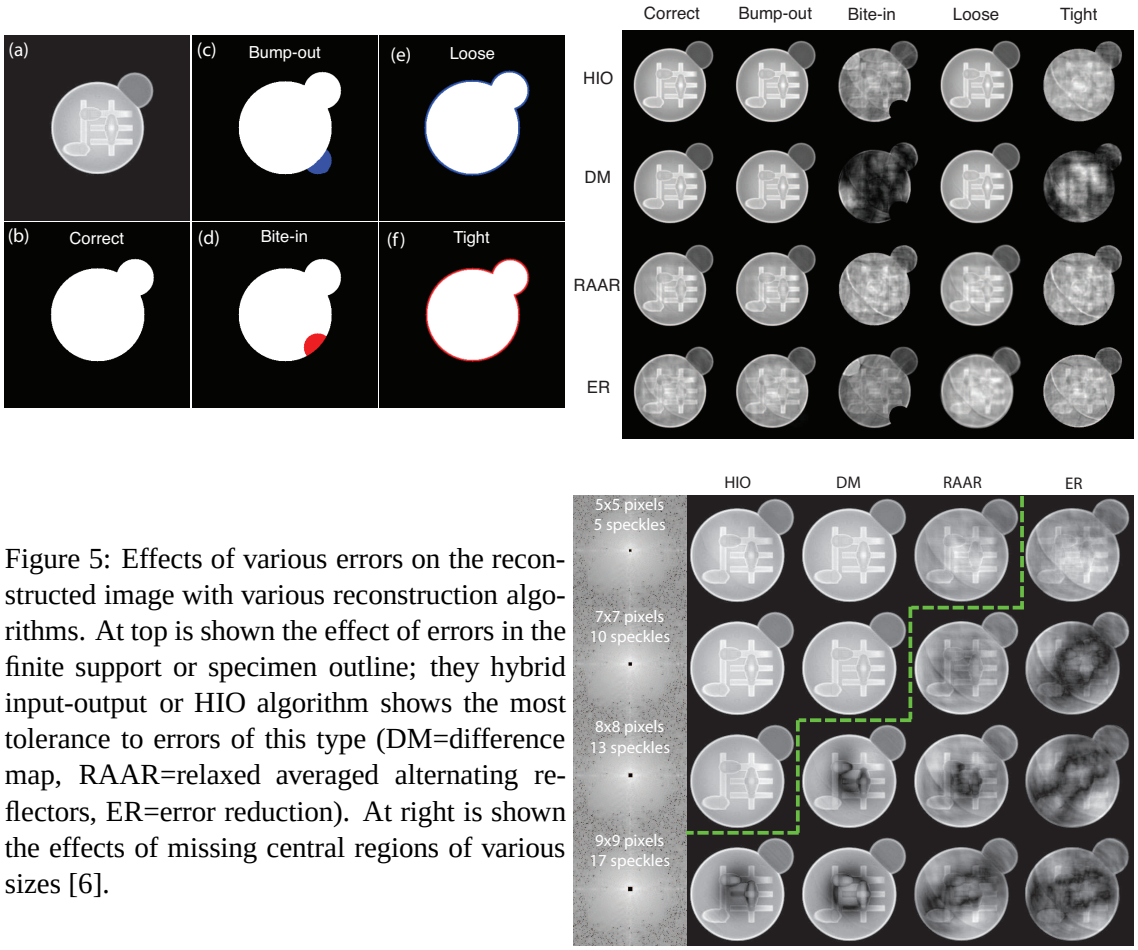

Figure 5: Effects of various errors on the reconstructed image with various reconstruction algorithms. At top is shown the effect of errors in the finite support or specimen outline; they hybrid input-output or HIO algorithm shows the most tolerance to errors of this type (DM=difference map, RAAR=relaxed averaged alternating reflectors, ER=error reduction). At right is shown the effects of missing central regions of various sizes [6].

Competition between ordered states and unconventional superconductivity

Adam Kaminski, Joerg Schmalian, Paul C. Canfield, Sergei L. Budko,

Ames Laboratory and Department of Physics and Astronomy,
Iowa State University, Ames, IA 50011, USA
kaminski@ameslab.gov

Genda Gu

Condensed Matter Physics and Materials Science Department,
Brookhaven National Laboratory, Upton, New York 11973, USA

Eli Rotenberg, Aaron Bostwick

Advanced Light Source, Lawrence Berkeley National Laboratory,
Berkeley, California 94720, USA

Abstract

Many of the unconventional superconductors have complex phase diagrams, where the superconducting phase is often adjacent, or partially overlaps with an ordered state. Two best examples are cuprates and pnictides high temperature superconductors, where superconductivity partially coexists with pseudogap and antiferromagnetic state respectively. Understanding the relation between superconductivity and those other states may be the key to uncover the pairing mechanism in those exciting systems.

Pseudogap state in cuprates is one of most interesting topics in modern condensed matter physics. This state is characterized by anisotropic energy gap that leads to seemingly disconnected segments of the Fermi surface, so called "Fermi arcs". The relationship between the pseudogap and superconductivity is one of the central issues in physics of cuprates. One of the leading theories explaining it is so called "pre-formed'' pair scenario, where pseudogap is thought to be a state of paired electrons that lack the long range coherence. Another class of theories attributes the pseudogap to an ordered state that would naturally compete with superconductivity. By studying the spectral weights associated with pseudogap and superconductivity using Angle Resolved Photoemission Spectroscopy (ARPES) we found that there is a direct correlation between the loss of the low energy spectral weight due to the opening of the pseudogap and a decrease of the spectral weight associated with superconductivity as a function of momentum and doping. High accuracy data lead us to conclude that the pseudogap competes with the superconductivity by depleting the spectral weight available for pairing in the region of momentum space, where the superconducting gap is largest. We also conducted detailed studies of the temperature dependence of the spectral weight at the chemical. We found evidence for a spectroscopic signature of pair formation and demonstrated that in a region

of the phase diagram commonly referred to as the "pseudogap'', two distinct states coexist: one that persists to an intermediate temperature T_{pair} and a second that extends up to T*. The first state is characterized by a doping independent scaling behavior and is due to pairing above T_c, but significantly below T*. The second state is the "proper'' pseudogap - characterized by a "checker board" pattern in STM images, the absence of pair formation, and is likely linked to Mott physics of pristine CuO_2 planes.

The newly discovered iron arsenic high temperature superconductors exhibit particularly rich and interesting phase diagrams. In $Ba(Fe_{1-x}Co_x)_2As_2$ the simultaneous structural/magnetic phase transition that occurs at elevated temperature in the undoped material, splits and is suppressed by carrier doping, and superconductivity emerges at higher doping. Superconductivity exists with apparent equal ease in the orthorhombic / antiferromagnetic (AFM) state as well as in the tetragonal state that has no long range magnetic order. We found that dramatic changes in the Fermi surface coincide with the onset of superconductivity in electron-doped $Ba(Fe_{1-x}Co_x)_2As_2$. The presence of the AFM order leads the appearance of the petal-like hole pockets at the Fermi level. These hole pockets vanish (undergo a Lifshitz transition) at the onset of superconductivity. In the presence of the petal-like hole pockets superconductivity is fully suppressed, while in their absence the two states can coexist.

1. A. D. Palczewski, T. Kondo, R. Khasanov, N. N. Kolesnikov, E. Rotenberg, T. Ohta, Y. Sassa, A. Fedorov, S. Pailhes, A. F. Santander-Syro, J. Chang, M. Shi, J. Mesot, H. M. Fretwell and A. Kaminski, *Origins of large critical temperature variations in single layer cuprates,* Phys. Rev. B **78**, 054523 (2008)

2. T. Kondo, C. Liu, G. D. Samolyuk, Y. Lee, N. Ni, T. Kondo, A. F. Santander-Syro, S. L. Bud'ko, J. L. McChesney, E. Rotenberg, T. Valla, A. V. Fedorov, P. C. Canfield, B. N. Harmon and A. Kaminski, *Momentum dependence of the superconducting gap in $NdFeAsO_{0.9}F_{0.1}$ single crystals measured by angle resolved photoemission spectroscopy,* Phys. Rev. Lett. **101**, 147003 (2008).

3. C. Liu, G. D. Samolyuk, Y. Lee, N. Ni, T. Kondo, A. F. Santander-Syro, S. L. Bud'ko, J. L. McChesney, E. Rotenberg, T. Valla, A. V. Fedorov, P. C. Canfield, B. N. Harmon and A. Kaminski,
The Fermi surface of $Ba_{(1-x)}K_xFe_2As_2$ and its evolution with doping , Phys. Rev. Lett. **101**, 177005 (2008)

4. R. Khasanov, Takeshi Kondo, S. Straessle, D.O.G. Heron, A. Kaminski, H. Keller, S.L. Lee, Tsunehiro Takeuchi, *Partially superconducting Fermi surface in (Bi,Pb)2(Sr,La)2CuO(6+x),: evidence for competition between superconductivity and pseudogap from superfluid density studies,* Phys. Rev. Lett. **101**, 227002 (2008)

5. Takeshi Kondo, R. Khasanov, Tsunehiro Takeuchi, Jörg Schmalian and Adam Kaminski, *Competition between the pseudogap and superconductivity in cuprates,* Nature **457**, 296-300 (2009)

6. S. Straessle, R. Khasanov, T. Kondo, D. O. G. Heron, A. Kaminski, H. Keller, S. L. Lee, T. Takeuchi, *Superfluid Density and Angular Dependence of the Energy Gap in Optimally Doped $(Bi,Pb)_2(Sr,La)_2CuO_{(6+x)}$.* Journal of Superconductivity and novel magnetism, **22**, 189-193 (2009)

7. Chang Liu, Takeshi Kondo, Ni Ni, A. D. Palczewski, A. Bostwick, G. D. Samolyuk, R. Khasanov, M. Shi, E. Rotenberg, S. L. Bud'ko, P. C. Canfield, and A. Kaminski, *Three- to Two-Dimensional Transition of the Electronic Structure in $CaFe_2As_2$: A Parent Compound for an Iron Arsenic High-Temperature Superconductor*, Phys. Rev. Lett. **102**, 167004 (2009)

8. R. Khasanov, Takeshi Kondo, S. Strässle, D. O. G. Heron, A. Kaminski, H. Keller, S. L. Lee, and Tsunehiro Takeuchi *Zero-field superfluid density in a d-wave superconductor evaluated from muon-spin-rotation experiments in the vortex state,* Phys. Rev. B **79**, 180508 (2009)

9. Chang Liu, Takeshi Kondo, A.D. Palczewski, G.D. Samolyuk, Y. Lee, M.E. Tillman, Ni Ni, E.D. Mun, R. Gordon, A.F. Santander-Syro, S.L. Bud'ko, J.L. McChesney, E. Rotenberg, A.V. Fedorov, T. Valla, O. Copie, M.A. Tanatar, C. Martin, B.N. Harmon, P.C. Canfield, R. Prozorov, J. Schmalian and A. Kaminski, *Electronic properties of iron arsenic high temperature superconductors revealed by angle resolved photoemission spectroscopy (ARPES),* Physica C **469**, 491-497 (2009)

10. Takeshi Kondo, R. Khasanov, Y. Sassa, A. Bendounan, S. Pailhes, J. Chang, J. Mesot, H. Keller, N. D. Zhigadlo, M. Shi, Z. Bukowski, J. Karpinski, and A. Kaminski , *Anomalous asymmetry in the Fermi surface of the high-temperature superconductor YBa2Cu4O8 revealed by angle-resolved photoemission spectroscopy.* Phys. Rev. B **80**, 100505 (2009)

11. Takeshi Kondo, R. M. Fernandes, R. Khasanov, Chang Liu, A. D. Palczewski, Ni Ni, M. Shi, A. Bostwick, E. Rotenberg, J. Schmalian, S. L. Bud'ko, P. C. Canfield, and A. Kaminski *Unexpected Fermi-surface nesting in the pnictide parent compounds $BaFe_2As_2$ and $CaFe_2As_2$ revealed by angle-resolved photoemission spectroscopy,* Phys, Rev, B **81**, 060507 (2010)

12. A. D. Palczewski and Takeshi Kondo, J. S. Wen, G. Z. J. Xu, and G. Gu, A. Kaminski, *Controlling the carrier concentration of the high-temperature superconductor Bi2Sr2CaCu2O8+δ in angle-resolved photoemission spectroscopy experiments*. Phys. Rev. B **81**, 104521 (2010)

13. Chang Liu, Takeshi Kondo, Rafael M. Fernandes, Ari D. Palczewski, Eun Deok Mun, Ni Ni1, Alexander N. Thaler, Aaron Bostwick, Eli Rotenberg, Jörg Schmalian, Sergey L. Bud'ko, Paul C. Canfield and Adam Kaminski, *Evidence for a Lifshitz transition in electron-doped iron arsenic superconductors at the onset of superconductivity.* Nature Physics **6**, 419-423 (2010)

15. R. Khasanov, Takeshi Kondo, M. Bendele, Yoichiro Hamaya, A. Kaminski, S. L. Lee, S. J. Ray, and Tsunehiro Takeuchi, *Suppression of the antinodal coherence of superconducting (Bi,Pb)2(Sr,La)2CuO(6+x) as revealed by muon spin rotation and angle-resolved photoemission.* Phys. Rev. B **82**, 020511 (2010)

16. Chang Liu, Yongbin Lee, A. D. Palczewski, J.-Q. Yan, Takeshi Kondo, B. N. Harmon, R. W. McCallum, T. A. Lograsso, and A. Kaminski, *Surface-driven electronic structure in LaFeAsO studied by angle-resolved photoemission spectroscopy.* Phys. Rev. B **82**, 075135 (2010)

17. Takeshi Kondo, Y. Hamaya, A. D. Palczewski, Tsunehiro Takeuchi, J. S. Wen, Z. J. Xu, Genda Gu, Jörg Schmalian and Adam Kaminski*, Disentangling Cooper-pair formation above Tc from the pseudogap state in the cuprates*, Nature Physics - accepted (2010)

Nanoscale Intermittency and Emergence in Complex Materials

Stephen D. Kevan
Physics Department
1274 University of Oregon
Eugene, OR. 97403-1274
kevan@uoregon.edu

Intermittent microscopic behaviors appear to play a key role in diverse emergent phenomena, including earthquakes,[1] molecular switches,[2, 3] polymer melts,[4] colloidal suspensions,[5] magnetic Barkhausen cascades,[6] and 'blinking' in virtually all single-center fluorophores.[7, 8] Many such intermittent systems exhibit self-organized criticality, where power law behaviors and the absence of a particular length or time scales are key features. Ensemble dynamics of such systems often exhibit complex emergent behaviors, e.g., glassy behaviors, stretched exponential kinetics, and violation of the fluctuation-dissipation theorem, though this connection is rarely well understood.

Given their high sensitivity to local environment, many nanoscale devices and nanostructured materials are will show intermittent behaviors, and these behaviors are likely a key ingredient of emergent behavior. For example, fluctuations in the environment are a commonly proposed to understand the intermittency of single-center fluorophores.[7, 8] A nanostructured material – the microphase separated domain structure in a manganite oxide, for example - is itself a complex environment, and intermittent domain percolation is evidently an important ingredient in colossal magnetoresistance.[9-12] The ability to control microscopic intermittency will in turn afford the ability to control complex and useful macroscopic behaviors.

A prerequisite to controlling complexity is the ability to measure microscopic intermittency and to correlate it with macroscopic properties. The power law behaviors mentioned above suggest that this will require probing phenomena over a broad range of both length and time scale. Coherent hard and soft x-ray beams offer particular advantages in this regard. The figure on the left shows schematically how the internal complexity, in this case of domains in an orbital-ordered phase in $Pr_{0.5}Ca_{0.5}MnO_3$, is projected into a soft x-ray speckle-diffraction pattern, making use of resonant scattering at the Mn L-edge off the lowest order orbital Bragg peak.[13] In principle speckle patterns like this can be analyzed to image the domains on the scale of a few nanometers through several microns, or to measure the dynamics of the domains on a time scale that is limited by signal and apparatus stability.

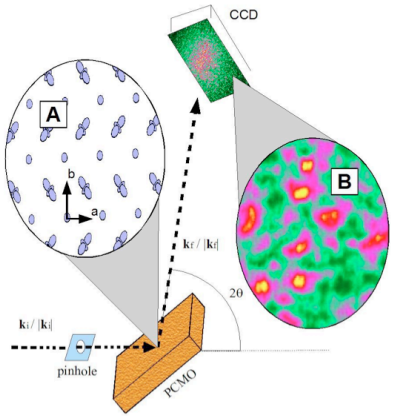

Our focus at the ALS is to apply coherent soft x-ray scattering techniques to probe intermittent and emergent phenomena in complex magnetic materials.[14] I will show three different kinds of experimental protocols to measure different aspects of complex behavior:

1) *Domain memory in magnetic thin films*: Nanoscale intermittency appears in magnetic systems in the form of Barkhausen cascades in which the magnetization changes abruptly as the applied field is tuned continuously. Among other things, these highly irreversible events control the extent to which domain patterns are reproduced from one magnetization cycle to the next; we refer to this as magnetic domain memory. We employ a soft x-ray speckle metrology technique to measure domain memory in magnetic thin films.[15-19] Most recently we have been studying exchange biased CoPd:IrMn multilayers in which the domain memory can be controlled by varying the sample cooling protocol.[18] We are particularly interested in extracting the q-dependence of domain memory to interpolate between macro-scale repeatability of the magnetization loop, which is generally perfect, and micro-scale domain memory, which is often imperfect. In the future, we plan to simultaneously image the domain reversal process using the diffractive imaging variant explained below to correlate the range of real-space events with domain memory measured statistically in q-space. Ultimately, we seek measure and understand the functional forms for domain memory as a function of applied field, temperature, and scattering wave vector.

2) *Magnetic and orbital fluctuations near phase boundaries*: As discussed above, intermittent fast dynamical events often lead to unusual slow nanoscale kinetic phenomena. Soft and hard x-ray photon correlation spectroscopy are starting to make important contributions in illuminating this connection. For example, we have recently measured thermally driven magnetic fluctuations in Au:Co:Au heterostructures near the spin-reorientation transition.[20] We found that the temporal correlations decay according to a stretched exponential rate law with a stretching exponent greater than one. Possibly this indicates thermally driven intermittency related to field-driven Barkhausen events. We have analyzed the results in terms of a simple Landau free energy model based on the two lowest order magnetic anisotropy constants. Our results suggest that we should be able to tune these anisotropies with small structural variations, thereby producing unusual phase behaviors. We have also measured orbital domain fluctuations in $Pr_{0.5}Ca_{0.5}MnO_3$ and plan to pursue related oxide systems in the future.

3) *Soft x-ray diffractive imaging in a reflection geometry*: The potential for x-ray diffraction imaging has been widely discussed and is a key component of the scientific case for emerging and planned facilities. An important limitation of the technique for our purposes is that to date nearly all experiments have been accomplished by diffuse scattering off a spatially limited object in a transmission geometry. Many of the systems we wish to study are extended crystals or films supported in a substrate. The lack of a robust support constraint makes application of phase retrieval algorithms problematic (even ptychography,[21] which we have tried) In collaboration with Sujoy Roy at the ALS, we have recently developed a new variant of x-ray diffraction imaging that appears to overcome this limitation. In this approach we place a small aperture after the scattering object in the near field regime and record the resulting diffraction pattern in the far field. Using iterative algorithms we recover the wave field in the aperture, which is straightforward since the aperture provides a strong support constraint. We then back propagate this recovered Fresnel diffraction pattern to the sample plane to produce an image of the scattering object. While adding the complexity of the post-scattering aperture, this approach appears to be robust and should be applicable to transmission, low-angle reflection, and Bragg scattering geometries. It also offers useful flexibility in

choosing the size and shape of the aperture. We have not yet used the technique to image any interesting material structures, but are actively pursuing that at present.

The experiments discussed above have been performed on ALS beamline 12.0.2.2. This station was optimized to produce the highest coherent flux consistent with the serious constraint imposed by being appended to an existing undulator beamline. Experiments like those discussed above will benefit markedly from beamlines under construction that have been optimized from the ground up for coherent soft x-ray experiments: COSMIC at the ALS and the coherent soft x-ray beamline at the NSLS-II. We are actively involved in both of these and plans for the COSMIC project will be presented in some detail. These experiments are also helping to motivate design and construction of new detectors that handle large data streams with high efficiency. Two different XYt time-stamping detectors have been designed and one of these will soon be delivered; this will also be presented.

References

1. Bak, P. and C. Tang, *Earthquakes as a Self-Organized Critical Phenomenon.* J. Geophys. Res., 1989. **94**: p. 15635.
2. Liu, F., M. Bao, H.-J. Kim, K.L. Wang, C. Li, X. Liu, and C. Zhou, *Giant Random Telegraph Signals in the Carbon Nanotubes as a Single Defect Probe.* Appl. Phys. Lett., 2005. **86**: p. 163102.
3. Chang, S., J. He, L. Lin, P. Zhang, F. Liang, M. Young, S. Huang, and S. Lindsay, *Tunnel Conductance of Watson–Crick Nucleoside–Base Pairs from Telegraph Noise.* Nanotechnology, 2009. **20**: p. 185102.
4. Russell, E.V. and N.E. Israeloff, *Direct Observation of Molecular Cooperativity near the Glass Transition.* Nature, 2000. **408**: p. 695.
5. Weeks, E.R., J.C. Crocker, A.C. Levitt, A. Schofield, and D.A. Weitz, *Three-Dimensional Direct Imaging of Structural Relaxation near the Colloidal Glass Transition.* Science, 2000. **287**: p. 627.
6. Kim, D.-H. and S.-C. Shin, *Intermittency of Barkhausen Avalanche in Co Nanothin Flms* J. Appl. Phys., 2004. **95**(11): p. 6971.
7. Verberk, R., A.M. van Oijen, and M. Orrit, *Simple Model for the Power-Law Blinking of Single Semiconductor Nanocrystals.* Physical Review B, 2002. **66**(23): p. 233202.
8. Issac, A., C. von Borczyskowski, and F. Cichos, *Correlation between Photoluminescence Intermittency of Cdse Quantum Dots and Self-Trapped States in Dielectric Media.* Physical Review B, 2005. **71**(16): p. 161302.
9. Alers, G.B., A.P. Ramirez, and S. Jin, *1/F Resistance Noise in the Large Magnetoresistance Manganites.* Appl. Phys. Lett., 1996. **68**: p. 3644.
10. Hardner, H.T., M.B. Weissman, M. Jaime, R.E. Treece, P.C. Dorsey, J.S. Horwitz, and D.B. Chrisey, *Non-Gaussian Noise in a Colossal Magnetoresistive Film.* J. Appl. Phys., 1997. **81**: p. 272.

11. Podzorov, V., C.H. Chen, M.E. Gershenson, and S.-W. Cheong, *Mesoscopic, Non-Equilibrium Fluctuations in Inhomogeneous Electronic States in Manganites.* Europhys. Lett., 2001. **55**: p. 411-7.
12. Raquet, B., A. Anane, S. Wirth, P. Xiong, and S. von Molnár, *Noise Probe of the Dynamic Phase Separation in $La_{2/3}ca_{1/3}mno_3$.* Phys. Rev. Lett., 2000. **84**: p. 4485.
13. Turner, J.J., J. Thomas, J.P. Hill, M. Pfeifer, K. Chesnel, Y. Tomioka, Y. Tokura, and S.D. Kevan, *Orbital Domain Dynamics in a Doped Manganite.* New J. Phys., 2008. **10**: p. 053023.
14. Chesnel, K., J.J. Turner, M. Pfeifer, and S.D. Kevan, *Probing Complex Materials with Coherent Soft X-Rays.* Appl. Phys. A, 2008. **93**: p. 431.
15. Pierce, M.S., C.R. Buechler, L.B. Sorensen, S.D. Kevan, E.A. Jagla, J.M. Deutsch, T. Mai, O. Narayan, J.E. Davies, K. Liu, G.T. Zimanyi, H.G. Katzberger, O. Hellwig, E.E. Fullerton, and J.B. Kortright, *Disorder Induced Magnetic Memory: Experiments and Theories.* Phys. Rev. B, 2007. **75**: p. 144406.
16. Pierce, M.S., C.R. Buechler, L.B. Sorensen, J.J. Turner, S.D. Kevan, E.A. Jagla, J.M. Deutsch, T. Mai, O. Narayan, J.E. Davies, K. Liu, J. Hunter Dunn, K.M. Chesnel, O. Hellwig, E.E. Fullerton, and J.B. Kortright, *Disorder-Induced Magnetic Memory.* Phys. Rev. Lett., 2005. **94**(1): p. 017272.
17. Pierce, M.S., R.G. Moore, L.B. Sorensen, S.D. Kevan, O. Hellwig, E.E. Fullerton, and J.B. Kortright, *Quasistatic X-Ray Speckle Metrology of Microscopic Magnetic Return-Point Memory.* Phys. Rev. Lett., 2003. **90**: p. 175502.
18. Chesnel, K., E.E. Fullerton, M.J. Carey, J.B. Kortright, and S.D. Kevan, *Magnetic Memory in Ferromagnetic Thin Films Via Exchange Coupling.* Phys. Rev. B, 2008. **78**: p. 132409.
19. Seu, K.A., R. Su, S. Roy, D. Parks, E. Shipton, E.E. Fullerton, and S.D. Kevan, *Microscopic Return Point Memory in Co/Pd Multilayer Films.* New J. Phys, 2010. **12**: p. 035009.
20. Seu, K.A., S. Roy, J.J. Turner, S. Park, C.M. Falco, and S.D. Kevan, *Cone Phase and Magnetization Fluctuations in Au/Co/Au Thin Films near the Spin-Reorientation Transition.* Physical Review B, 2010. **82**(1): p. 012404.
21. Rodenburg, J.M., A.C. Hurst, A. Cullis, G., B.R. Dobson, F. Pfeiffer, O. Bunk, C. David, K. Jefimovs, and I. Johnson, *Hard-X-Ray Lensless Imaging of Extended Objects.* Phys. Rev. Lett., 2007. **98**: p. 034801.

Resonant Soft X-Ray Scattering in Hard Condensed and Magnetic Systems

J. B. Kortright
Materials Science Division, Lawrence Berkeley National Laboratory, Berkeley, CA 94720, jbkortright@lbl.gov

Scope

Resonant, elastic soft x-ray scattering offers rich potential to study the spatial distribution of electronic structure and chemical bonding properties, as opposed to simple electron density, by tuning to sharp core levels that proliferate in the soft x-ray spectral range. This vision of RSXS is somewhat distinct from anomalous phasing in direct methods, and rather results from strong resonant sensitivity to the lowest lying empty states that correlate closely with functional materials properties. RSXS has been applied mostly to magnetic systems, where resonant magnetic effects are large, and to investigate electronic ordering in correlated systems, where isolated superlattice peaks provide information on structural registry. We aim to extend the applicability of RSXS to a broader range of materials and their properties. While the concept of combining *q*-resolved scattering with resonant optical effects is straight forward in principle, in practice we are increasingly faced with situations where questions exist about the spectral details of the resonant optical properties themselves in addition to their spatial distribution. Questions about resonant spectral properties are non-trivial because absolute absorption spectra, let alone their possible spatial variation, are very difficult to measure in the soft x-ray range and because of their direct relationship to functional properties.
Developing quantitative modeling approaches that put spectroscopy and structure on equal footing will best answer such questions and allow resonant scattering to be applied most fully.

Recent Progress

Probing native surface layer on $SrTiO_3$ (001) with reflectivity spectroscopy near Ti $L_{2,3}$ edge

$SrTiO_3$ (STO) surfaces and thin films are of fundamental interest and often used as substrates for or active layers in oxide heterostructures. During studies of superlattices containing STO layers we observed unexpected behavior of STO (001) surfaces prompting their extended investigation as perceived by energy- and *q*-resolved resonant soft x-ray reflectivity near the Ti $L_{2,3}$ edges [1]. The results reveal details regarding the STO (001) near surface region that have not been reported previously to our knowledge, including chemically modified, anisotropic surface layers

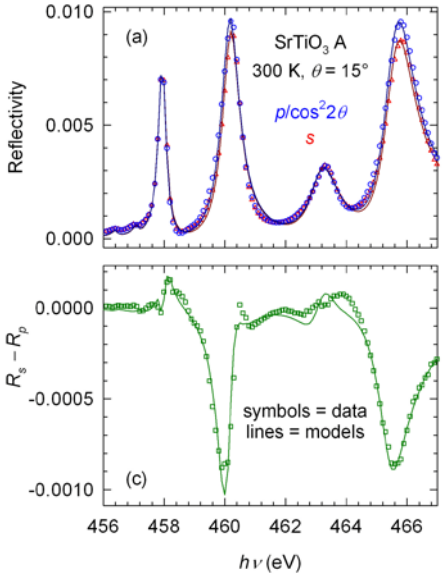

Figure 1. Room temperature $R(h\nu)$ spectra across the Ti L_{23} edges with *s* and *p* incident polarization (top) reveal weak, reproducible linear anisotropy (bottom). Symbols are data points. Lines are fits using optical constants derived assuming a semi-infinite slab optical model.

several nanometers thick that evolve over a range of time scales. These layers appear to result from reaction with the ambient and can thus be thought of as native STO surface layers.

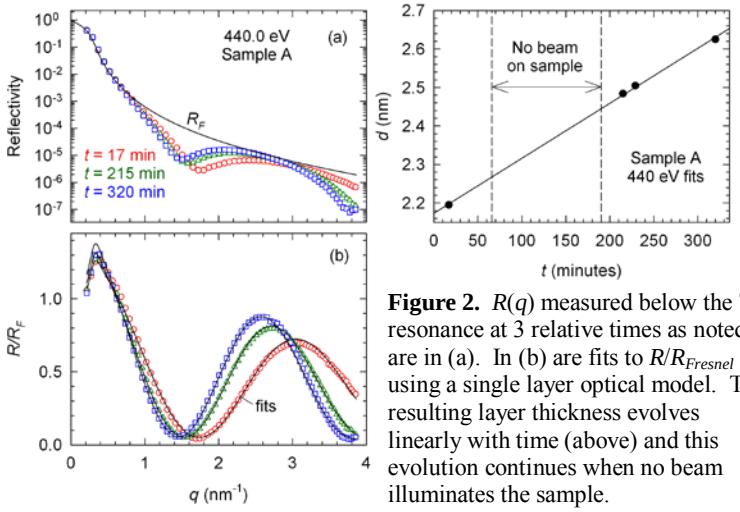

Figure 2. $R(q)$ measured below the Ti resonance at 3 relative times as noted are in (a). In (b) are fits to $R/R_{Fresnel}$ using a single layer optical model. The resulting layer thickness evolves linearly with time (above) and this evolution continues when no beam illuminates the sample.

Five polished STO crystals received four different surface treatments and were exposed to ambient conditions prior to and between soft x-ray measurement sessions; all samples exhibit the general features described here. Room temperature reflectance anisotropy, $R_s(h\nu) - R_p(h\nu)$, as in Figure 1 was observed, and was unexpected for cubic STO. These $R_{s,p}(h\nu)$ spectra were modeled to obtain absolute values of resonant optical properties ($n = 1 - \delta + i\beta$), initially assuming a semi-infinite slab model and that Lorentzian lineshapes describe the well-known strong, sharp Ti resonant Ti $L_{2,3}$ lines. Excellent fits to measured reflectivity result, and the model $\beta(h\nu)$ spectra have significantly stronger t_{2g} and e_g line strengths than do TEY absorption spectra, as expected. The observed anisotropy is consistent with weak anisotropy observed in TEY spectra from STO crystals [2] and strained STO epi-layers on Si [3], and indicates tetrahedral distortion of TiO_6 octahedra stretched along the surface normal. A surface region different from the bulk is implied by this anisotropy.

Angle-resolved reflectivity measurements reveal pronounced Kiessig fringes consistent with a ubiquitous surface layer ranging from 1.5 – 3.0 nm (roughly 4 – 8 unit cells) thick. For a given sample the Kiessig fringe was observed to change between different measurement sessions, prompting repeated measurements during a given session as in Figure 2. Modeling these $R(q)$ with a single layer model yield a linear temporal evolution in surface layer thickness that persisted even when the x-ray beam was off, indicating that this change is not radiation induced and results from vacuum exposure.

While it is straight-forward to refine optical models by including layers to account for interference effects, it is less obvious how to refine the resonant optical properties of the different layers. We refined a single surface layer and bulk optical properties each starting from the values obtained from the semi-infinite slab model (above) in which both the resonant Ti features and non-resonant Ti, Sr, and O contributions were allowed to vary in refinement of $R(q)$ at 8 energies on and off the strong Ti absorption lines as in Figure 3. At each $h\nu$, Kramers-Kronig consistent δ & β values were obtained for the substrate and surface layer that were subsequently fitted to obtain a self-consistent set of optical properties for the substrate and surface layer. The results indicate that the surface layer is substantially depleted in Sr and enriched in Ti & O

suggestive of TiO_2 enrichment, even though the absorption spectra are more STO-like without distinctive additional multiplet splitting of TiO_2. The picture of the surface layer that emerges from this resonant reflectivity spectroscopy study is consistent with the tendency of STO surfaces toward non-stiochiometry, but it does not conform neatly to existing models of the near-surface region, including those from surface truncation rod studies [4, 5]. The layer apparently forms via room temperature surface reactions with the ambient.

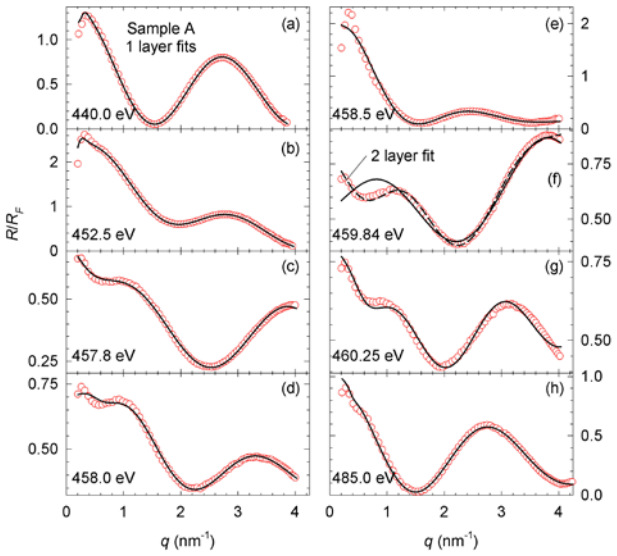

Figure 3. Single layer fits to measured $R(q)$ (symbols) at energies noted obtained by refining optical constants of substrate and surface layer starting from values obtained by fitting $R_{s,p}(h\nu)$ in Figure 1. Single layer fits (solid lines) capture all features except for the lowest q features in (f) where a 2-layer model improves the fit.

This study has implications in several directions. One stems from the fact that we became aware of this surface layer only after observing subtle $R(h\nu)$ anisotropy and then Kiessig fringes in $R(q)$; it would have been easy to miss or dismiss this evidence. On one hand this should serve as yet another warning for those studying oxide surfaces with any soft x-ray spectroscopy to be aware of possible surface layers with different properties from the bulk. On the other hand, the relatively direct sensitivity of $R_{s,p}(q, h\nu)$ to the details of differences between surface layer and bulk properties, obtained through careful modeling, suggests applications of this approach to study the near surface properties of oxides and to study a variety of properties in oxide superlattices.

Future Directions

The quantitative, self-consistent modeling approach yielding simultaneous spectroscopic and structural information developed here is generally applicable and has potential to study near-surface properties of a variety of bulk and thin film systems with a unique combination of depth and chemical/electronic sensitivities within the resonant skin depth of soft x-rays. As demonstrated here this approach benefits from the relative simplicity of the Ti absorption spectrum for which analytical functions (Lorentzians) can reasonably describe spectral features. In general, modeling resonant optical properties is expected to require more flexible algorithms allowing arbitrary variation of resonant spectral features and their anisotropy with depth. We plan to extend variational algorithms commonly used in other spectral ranges that can model arbitrarily complex spectral shapes while maintaining Kramers-Kronig consistency between absorptive and dispersive properties. Combining such flexible spectral modeling self-consistently with structural modeling should be possible to obtain maximum information from such experimental data. We envision many materials directions in which to apply such

approaches, which should extend beyond specular reflectivity studies to resonant diffuse scattering and diffraction as well.

1. M. Valvidares, M. Huijben, P. Yu, R. Ramesh, and J. B. Kortright, "Native $SrTiO_3$ (001) surface layer from resonant Ti $L_{2,3}$ reflectance spectroscopy," submitted for publication.
2. M. Salluzzo, J. C. Cezar, N. B. Brookes, V. Bisogni, G. M. Luca, C. Richter, S. Thiel, J. Mannhart, M. Huijben, A. Brinkman, G. Rijnders, and G. Ghiringhelli, *Phys. Rev. Lett.* **102**, 166804 (2009).
3. J. C. Woicik, E. L. Shirley, C. S. Hellberg, K. E. Andersen, S. Sambasivan, D. A. Fischer, B. D. Chapman, E. A. Stern, P. Ryan, D. L. Ederer, and H. Li, *Phys. Rev. B* **75**, 4 (2007).
4. R. Herger, P. R. Willmott, O. Bunk, C. M. Schlepuetz, B. D. Patterson, and B. Delley, *Phys. Rev. Lett.* **98**, 076102 (2007).
5. A. Fragneto, G. M. De Luca, R. Di Capua, U. S. di Uccio, M. Salluzzo, X. Torrelles, T. L. Lee, and J. Zegenhagen, *Appl. Phys. Lett.* **91**, 3 (2007).

Publications resulting from this work (2008 – 2010)

1. M. B. Holcomb, L. W. Martin, A. Scholl, Q. He, P. Yu, C.-H. Yang, S. Y. Yang, P.-A. Glans, M. Valvidares, M. Huijben, J. B. Kortright, J. Guo, Y.-H. Chu, and R. Ramesh, "Probing the evolution of antiferromagnetism in multiferroics," *Phys. Rev. B* **81**, 134406 (2010).
2. J. C. Lee, J. G. Xiang, B. Ravel, J. Kortright, and K. Flanagan, "Condensed matter astrophysics: A prescription for determining the species-specific composition and quantity of interstellar dust using x-rays," *Astrophysical Journal* ***702***, 970 (2009).
3. S. Roy, E. Blackburn, S.M. Valvidares, M.R. Fitzsimmons, S.C. Vogel, M. Khan, I. Dubenko, S. Stadler, N. Ali, S.K. Sinha, J.B. Kortright, "Delocalization and hybridization enhance the magnetocaloric effect in Cu-doped Ni_2MnGa," *Phys. Rev. B* **79**, 235127 (2009).
4. K. Chesnel, E. E. Fullerton, M. J. Carey, J. B. Kortright, and S. D. Kevan, "Magnetic memory in ferromagnetic thin films via exchange coupling," *Phys. Rev. B* **78**, 132409 (2008).
5. S. Mangin, T. Hauet, P. Fischer, D. H. Kim, J. B. Kortright, K. Chesnel, E. Arenholz, and E. E. Fullerton, "Influence of interface exchange coupling in perpendicular anisotropy $[Pt/Co]_{50}$/TbFe bilayers," *Phys. Rev. B* **78**, 024424 (2008).
6. J. B. Kortright, D. M. Lincoln, R. Shima Edelstein, and A. J. Epstein, "Bonding, backbonding, and spin-polarized molecular orbitals: Basis for magnetism and semiconducting transport in $V[TCNE]_{x\sim2}$," *Phys. Rev. Lett.* **100**, 257204 (2008).
7. B.C. Sell, S.-H. Yang, M. Watanabe, B.S. Mun, L. Plucinski, N. Mannella, S.B. Ritchey, A. Nambu, J. Guo, M.W. West, F. Salmassi, J.B. Kortright, S.S.P. Parkin, and C.S. Fadley, "Determination of buried interface composition and magnetism profiles using standing-wave excited soft x-ray emission and inelastic scattering," *J. Appl. Phys.* **103**, 083515 (2008).

Resonant Soft X-Ray Scattering in Soft Condensed Matter

J. B. Kortright,[1] B. Jerome,[1] and T. Xu[1,2]
[1]*Materials Science Division, Lawrence Berkeley National Laboratory, Berkeley, CA 94720*
[2]*Dept. of Materials Science & Engineering, University of California, Berkeley, CA 94720*
jbkortright@lbl.gov, bjerome@lbl.gov, tingxu@berkeley.edu

Scope

Tuning incident x-ray energy near the carbon, oxygen, and nitrogen *K* edges yields resonant sensitivity to specific bonding motifs allowing us to extend NEXAFS into the angle-resolved resonant elastic scattering regime to study the spatial distribution of organic species with resolution approaching several nanometers [1, 2]. This strong resonant sensitivity complements isotopic substitution in neutron scattering and has potential to impact our understanding of nanometer scale polymeric and molecular systems of increasing fundamental interest for potential applications ranging from bio-sensing to electro-optical devices to materials addressing various energy needs. In addition to addressing experimental challenges encountered when working with soft condensed matter in this soft x-ray spectral region where absorption is quite significant, we are developing viable approaches for interpreting resonant scattering results to obtain desired structural information. We have been targeting two areas as we gain experience with this emerging approach; utilizing the polarization sensitivity to molecular anisotropy to depth-resolve orientational order in polymer films, and addressing questions regarding the structure of hybrid peptide-polymer self-assembled composite systems.

Recent Progress

Molecular orientation in thin polymer films

Our goal is to combine the depth-resolving capability of reflectivity measurements with the polarization dependence of resonant x-ray absorption spectroscopy to obtain depth profiles of molecular orientation in thin polymer films. While polarization dependent NEXAFS can sense molecular orientation within several nanometers of the free surface, techniques able to sense molecular orientation at buried interfaces have been lacking. We have initiated a series of systematic studies aimed at developing this capability.

The initial system chosen for study is a liquid crystalline polymer (LCP) whose rigid side chains (Fig. 1) are known to orient parallel to the surface planes of thin films [3]. A relatively well-understood model system was deemed important considering polarization-dependent measurement artifacts (anisotropic carbon dip) that can complicate anisotropy measurements. LCP samples of differing thickness were spun-cast on Si

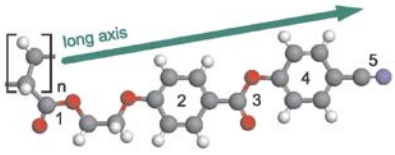

FIG. 1: Sketch of the side chain liquid crystalline polymer poly(2-4-[(4-cyanophenoxy) carbonyl]phenoxyethyl acrylate) containing two ester (COO, 1 and 3), two phenylene (C_6H_4, 2 and 4), and one nitrile group (CN, 5) per monomer. The arrow indicates the long axis of the side chain. In the nematic liquid crystalline phase, the optical axis of the material is defined by the average direction of the long axis of all side chains.

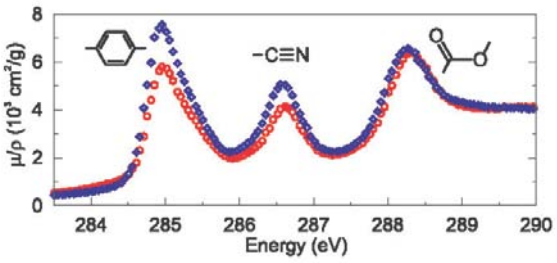

FIG. 2: NEXAFS TEY spectra around the carbon K-edge of a 30 nm thick LCP thin films. Spectra were recorded at 20° incidence for s- (red circles) and p-polarization (blue diamonds).

wafers and carefully annealed to achieve the equilibrium nematic structure. Figure 2 shows NEXAFS spectra by total electron yield revealing dichroism especially in the phenylene and nitrile group peaks confirming that at least the near surface region of this 30 *nm* film shows in-plane ordering of the side chains. Figure 3 shows measured reflectivity using *s* and *p* polarization in the form of $R(h\nu)$ spectra at several fixed angles (top panel) and $R(q)$ scans at a fixed energy $h\nu$ (bottom panel) from a 49.1 *nm* thick film. The energy scans reveal anisotropy extending beyond that apparent in absorption spectra but still limited to the C *K* edge region consistent with resonant refractive effects, and an evolution with incidence angle. The $R(q)$ data exhibit a distinct polarization-dependent phase shift and intensity differences in the Kiessig fringes that reveal anisotropic optical properties extending throughout the film. All LCP films studied exhibit similar signatures of anisotropy and *p* reflectivity well above that predicted by the Lorentz polarization factor in the vicinity of the Brewster angle ($\theta \cong 45°$) resulting from optical activity within the anisotropic samples.

For quantitative modeling of $R(q)$ we adopted Berreman's 4 x 4 matrix method [4] that effectively extends Parratt's formalism to stratified (1D) systems containing anisotropic layers. Modeling accounted for nematic LCP domains with in-plane optic axes taking random orientations with respect to the scattering plane. Fitting the same structural model simultaneously to *s* and *p* reflectivity data yields the 4 components of resonant optical properties describing the refractive and absorptive components along and perpendicular to the optic (nematic) axis at the discrete energies for which $R(q)$ were measured. The resulting optical properties are consistent with, but distinct from, the dichroism in Fig. 2. The resulting model indicates that the degree of orientational order of the LCP side chains relative to the surface is independent of depth in the films studied, as anticipated for this model system. Preliminary studies of polymer films not generally expected to exhibit uniform ordering of main- and side-chain motifs with depth are underway.

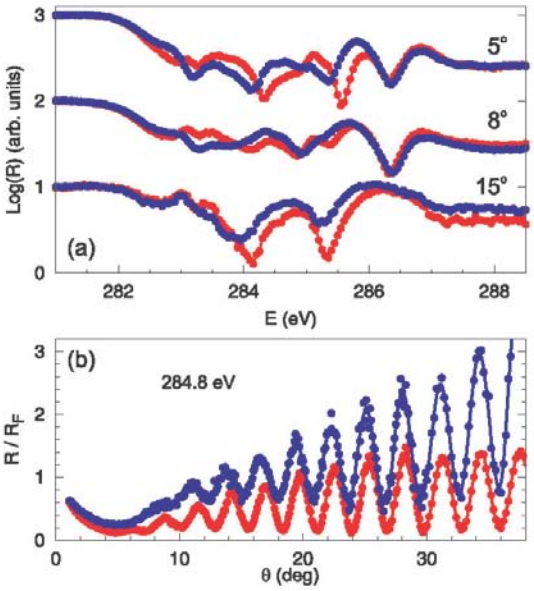

FIG. 3: Reflectivity R of a 49.1 nm-thick LCP100 film in s- (red squares) and p- (blue diamonds) polarization. (a) Energy scans at different incidence angles (horizontal offset for clarity) of 5° (top curves), 8° (middle curves), and 15° (bottom curves). (b) Reflectivity R vs. vertical momentum transfer q divided by the Fresnel reflectivity R_F for silicon at a fixed photon energy of 284.8 eV. The data in p-incidence was normalized by the Lorentz factor $\cos^2 2\theta$.

Locating peptide bundles in phase-separated block copolymer films

This ongoing resonant soft x-ray scattering (RSoXS) project aims to localize 4-helix peptide bundles [5, 6] within a cylinder phase PS-*b*-PEO thin film, as illustrated in Figure 4. Xu's group has shown that peptide bundles conjugated with specific cofactors can self-assemble within block copolymer (BCP) phases without compromising the helical protein structures [7]. Optical circular dichroism confirms that peptide tertiary structure is intact. Hard x-ray GISAXS and RSoXS reveal that the hexagonal packing of PEO cylinders in PS remains intact when peptide is added, and, surprisingly, that the spacing between cylinders *contracts* when peptide is added. This contraction can be understood based on previous studies BCP-homopolymer blends [8] to result from swelling near the BCP interface. But a direct determination of where the peptide bundles reside in this distorted BCP structure has remained elusive using standard structural techniques.

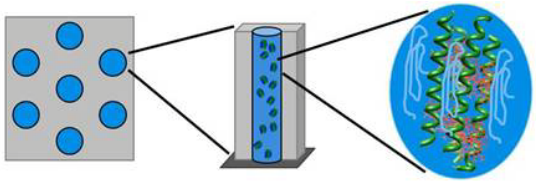

FIG. 4: Intended structure at multiple length scales in which peptide bundles (green) are conjugated with polymers to promote self-assembly within the PEO cylinders (blue) in the phase-separated PS-b-PEO film. Our challenge is to directly locate the peptide bundles within the structure.

We are exploring the potential of resonant soft x-ray scattering to resolve this challenging structural problem. Initial thoughts were that direct methods, such as differential anomalous scattering [9, 10] at the N *K* edge would isolate correlations of just the peptides within the structure since only the peptides contain N. However the total peptide and nitrogen content is too small for this approach to be effective in these samples. Tagging the peptide bundles with strong scattering metal-containing ligands may allow similar approaches to succeed providing a sufficient density of metal scatterers can be added.

We do observe resonant refractive effects that differ markedly in samples with and without peptide bundles. While the resonant integrated intensity spectra of hexagonal peaks in samples with and without peptide are very similar, the resonant refractive spectra (shifts in peak positions) differ markedly. We hypothesize that these resonant refractive effects have similar origin to refractive effects used to measure anomalous scattering factors in the hard x-ray region [11, 12]. Such effects result from strongly inhomogeneous wave fields within samples, have not to our knowledge been reported in diffraction peaks to date, and are not described by simple scattering models that do not fully treat refractive & absorptive effects at internal phase boundaries. By applying more rigorous 2D and 3D EM models we expect to evaluate the sensitivity of these resonant refractive effects to changes in optical properties of the individual phases and, thereby, to gain insight on the location of the polymer within the structure.

Future directions

Regarding the ordering of polymer chain constituents relative to interfaces, we will continue measurements and analysis of systems with no *a priori* knowledge of such order and for which the presence or absence of such order is expected to have important implications on materials properties such as polymer electronics. At least two additional directions for investigation are

suggested by the polarization sensitivity to polymer constituent orientation. One is the extension of this sensitivity into the diffuse scattering regime to study in-plane heterogeneity of orientation order and its evolution with processing. Another is to explore this sensitivity at a more fundamental level. For example, we hypothesize that randomly oriented phenyl groups in polystyrene will cause an incident linearly polarized beam to resonantly depolarize on propagation near the C π^* resonance. Such effects are essential to understand in order to properly analyze polarization dependent reflectance and scattering effects.

In the hybrid peptide-polymer materials we will explore analytical and numerical approaches to understand the resonant refractive effects mentioned above. If such effects can be understood they will open new avenues to utilize resonant scattering in nanostructured materials.

References cited in text

1. G. E. Mitchell, B. G. Landes, J. Lyons, B. J. Kern, M. J. Devon, I. Koprinarov, E. M. Gullikson, and J. B. Kortright, *Appl. Phys. Lett*. **89**, 044101 (2006).
2. J. M. Virgili, Y. F. Tao, J. B. Kortright, N. P. Balsara, and R. A. Segalman, *Macromolecules* **40**, 2092 (2007).
3. M. Mezger, B. Jerome, J. B. Kortright, M. Valvidares, E. M. Gullikson, A. Giglia, N. Mahne, and S. Nannarone, "Molecular orientation in soft matter thin films studies by resonant soft x-ray reflectivity," submitted for publication.
4. D. W. Berreman, *J. Opt. Soc. Am.* **62**, 502 (1972).
5. T. Xu, and J. Shu, *Soft Matter* **6**, 212 (2010).
6. J. Y. Shu, Y. J. Huang, C. Tan, A. D. Presley, J. Chang, and T. Xu, *Biomacromolecules* **11**, 1443 (2010).
7. A. D. Presley, J. J. Chang, and T. Xu, *Soft Matter* (in press).
8. K. I. Winey, E. L. Thomas, and L. J. Fetters, *Macromolecules* **24**, 6182 (1991).
9. P. H. Fuoss, P. Eisenberger, W. K. Warburton, and A. Bienenstock, *Phys. Rev. Lett.* **46**, 1537 (1981).
10. J. B. Kortright and A. Bienenstock, *Phys. Rev. B* **37**, 2979 (1988).
11. A. Fontaine, W. K. Warburton, and K. F. Ludwig, *Phys. Rev. B* **31**, 3599 (1985).
12. W. K. Warburton, and K. F. Ludwig, *Phys. Rev. B* **33**, 8424 (1986).

Publications resulting from this DOE funded program

1. T. Xu, and J. Shu, "Coiled-coil helix bundle, a peptide tertiary structural motif toward hybrid functional materials," *Soft Matter* **6**, 212 (2010).
2. J. Y. Shu, Y. J. Huang, C. Tan, A. D. Presley, J. Chang, and T. Xu, "Amphiphilic Peptide-Polymer Conjugates Based on the Coiled-Coil Helix Bundle", *Biomacromolecules* **11**, 1443 (2010).
3. A. D. Presley, J. J. Chang, and T. Xu, "Directed co-assembly of heme proteins with amphiphilic block copolymers toward functional bimolecular materials," *Soft Matter* (in press).

Fundamental Investigations of Microstructure and Evolution in Materials Using 3D X-Ray Microscopy

Bennett C. Larson and Jonathan Z. Tischler
Materials Science & Technology Division, Oak Ridge National Laboratory
Oak Ridge, TN 37831
Larsonbc@ornl.gov

RESEARCH SCOPE

The physical properties of technologically important materials are based on complex and collective interactions involving spatial correlations on atomic, nano-, micro-, meso-, and macroscopic length scales. Developing materials with desired properties outside known envelopes has long been through the discovery of new and innovative processing methods guided by intuition, the accumulated understanding of physical principles, and previous successes. The nature of this process is not likely to change dramatically; however, the level of knowledge and the level of understanding of the underlying physical principles required for continued technological advances increases inexorably. Accordingly, it is increasingly important that new and innovative materials research directions are pursued that link multiple length scales, fully exploit newly developed structure and microstructure tools and techniques, and address the fundamental physics of materials in concert with first principles based theory and modeling.

The research in this part of the ORNL x-ray program is directed toward obtaining a fundamental understanding of longstanding issues associated with microstructure evolution and deformation in structural materials by combining submicron-resolution 3D x-ray microscopy (3DXM) experimental measurements with first principles based theory and computations. Formulating a predictive understanding of the underlying science of microstructure and evolution during deformation/formation represents a grand challenge ultimately involving the statistical dynamics of dislocations as filamentary interacting structures.

The research is directed (1) toward deformation in the initial stages of crystal breakup and dislocation patterning in large, uniformly deformed single crystals, where (for the first time) direct and absolute mesoscale tests can be made of discrete dislocation dynamics simulations using submicron resolution 3D x-ray microscopy measurements, and (2) toward the use of micro-indentation by spherical tip indenters in order to localize deformation to volumes ~50 μm diameters or less that can be addressed over the full deformed domain by both submicron resolution 3DXM and deformation simulations. Investigations are focused on submicron-resolution, non-destructive measurements of the structure, microstructure, and evolution of materials on mesoscopic length scales. The approach includes direct and absolute comparisons with collaborative first principles based (bottom-up) simulations and constitutive law finite element (top-down) modeling. Non-destructive measurements of dislocation correlations, aggregation, and patterning with submicron 3D resolution have not been possible on mesoscopic length scales previously, nor has it been possible to generate such spatially inhomogeneous distributions of dislocations in top down (constitutive law) modeling. The measurements are performed using the unique, submicron-resolution 3D x-ray microscopy user facility on the XOR/UNI Sector 34 ID-E beamline at the Advanced Photon Source.

RECENT PROGRESS

Direct and absolute comparison between mesoscale deformation in Cu and discrete dislocation dynamics (DDD) deformation simulations – The concept of the geometrically necessary dislocation (GND) density tensor (or dislocation density tensor) for characterizing plastic deformation in deformed materials was introduced more than fifty years ago. We have now made the first quantitative, submicron-resolution, 3D measurements of the geometrically necessary dislocation density tensor over a mesoscopic volume (~11 x 20 x 28 μm^3), and we have used these measurements to make the first direct and absolute mesoscale test of DDD deformation simulations using measurements for 2.3% compressed single crystal Cu and simulations for 1.6% compression (collaboration with A. El-Azab, FSU). The length scales of the measured microstructure and the range of the measured misorientations in Fig 1A are larger than those simulated for a

5 μm cube using DDD; however, considering the strain magnitude differences, the misorientations differ by less than a factor of two. On the other hand, the measured GND densities appear to be more than a factor of two smaller than predicted by the simulations for a 5 μm cube.

Figure 2 shows a quantitative and absolute comparison of the measured and simulated microstructure in terms of radial averaged GND spatial correlation functions. The correlation functions for three positions (A,B,C) in Fig. 2A represent the first such experimental measurements, providing absolute quantifications of the spatial frequency of GNDs (i.e. orientation gradients) in deformed Cu. The radial correlation function obtained within the simulation cube (red dashed line) is similar in form to the measured function, but crosses zero at 1.5 μm compared to the 2.5 μm experimentally measured value. Deformation simulations are in progress using a 10 μm cube with larger strain magnitudes to determine the sensitivity of the microstructure generated by the DDD simulations to the strain magnitude and the size of the simulation cell.

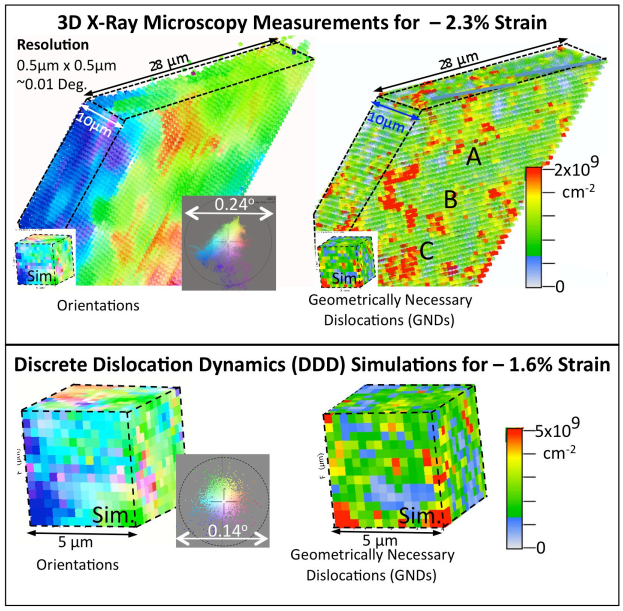

Fig. 1. A quantitative comparison between measured and simulated deformation in compressed Cu. (A) Local orientation measurements with 0.5 μm resolution in 2.3% strained Cu plus local GND densities obtained from the orientation gradients; (B) Local orientation DDD simulations and simulated GND densities over a 5 μm cube for -1.6% strain(A.-El-Azab, FSU). The angular ranges of the measured and simulated misorientations and the GND density color scales are shown.

Although larger simulation cell sizes will be necessary to properly compare DDD with experiment, these results demonstrate the capability of testing DDD simulations quantitatively on critical mesoscopic length scales using submicron resolution 3DXM. We emphasize also that the measured correlation functions in Fig. 2 provide information needed to coarse-grain DDD deformation simulations to statistical dislocation approaches.

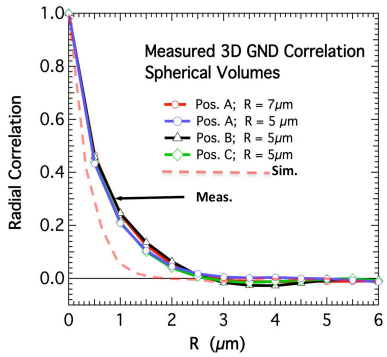

Fig. 2. GND Radial correlation functions for compressed Cu extracted from Fig. 1A experimental measurements (solid lines) and from Fig. 1B DDD simulations (red dashed line).

The Mesoscale Deformation Laboratory Below Indentations – Indentations, especially nano-indentations are increasingly used to investigate some of the most fundamental aspects of dislocation generation and deformation. Overlooked so far because of the perceived complex nature of the stress fields below micro-indents is the fact that their spatially confined distortion fields constitute a mesoscopic deformation laboratory containing a rich array of fundamental deformation information. Submicron resolution 3DXM investigations of the deformation distribution below 100 μm radius spherical indentations have demonstrated that the in-plane deformation symmetry and rotation magnitudes provide new insight into fundamental deformation processes as shown in Fig. 3. While the ϕ rotations in the middle panel of the figure constitute the largest deformation mode as discussed in the abstract of J. Tischler, examining the nature of the R and Z rotation (defined in the left panel) components in the right panel reveals a remarkably well developed symmetry pattern in the plane normal to the indent axis. Moreover, the symmetry pattern is not simply a

reflection of deformation kinetics imposed by the crystal and dislocation slip-system geometries as indicated by the completely different measured and calculated rotation patterns within the dashed white boxes for the ϕ and R in the right panel. Such effects, that have not been reported previously demonstrate the limitations of

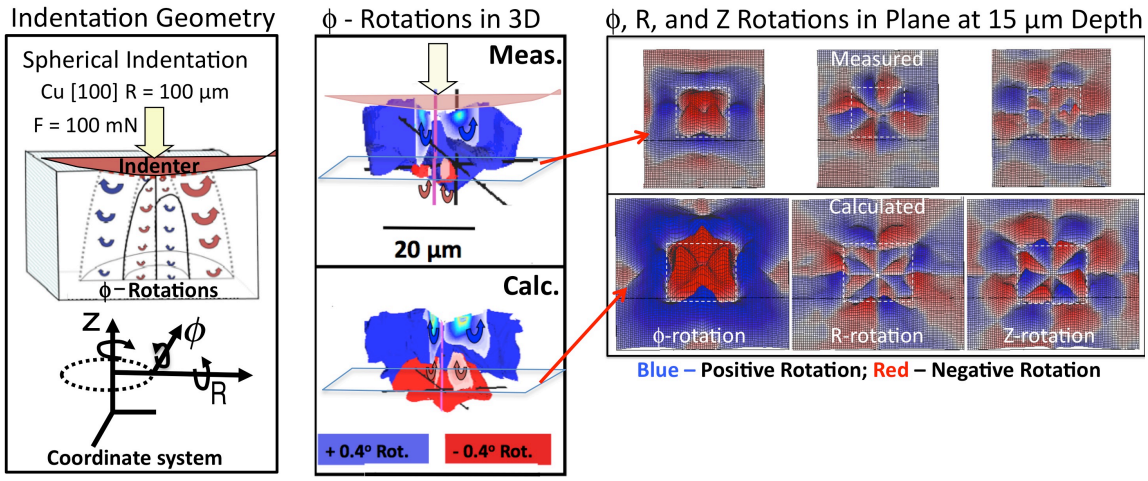

Fig. 3. (left panel) The indent geometry and coordinate system; (middle panel) The ϕ rotations in 3D; and (right panel) The rotations in a plane 15 µm below the sample surface for a 100 mN indent in <001> Cu.

of finite element simulations (Y. Gao, UT-K) using standard crystal plasticity. Not shown is the fact that the local lattice rotations contain copious dislocation patterning near the surface, which is also not generated in the finite element simulations. Accordingly, the confined distortion fields provide a wide range of deformation conditions that critically tests theory and simulations within a single indent

The Nature and Origin of Local Stresses In Deformed Cu – Numerous competing models have been proposed for the dramatic strengthening of metals during deformation, but experimental differentiation between longstanding models of how dislocations multiply and entangle into dense wall structures has been in need of new experimental approaches. We have combined submicron resolution 3D X-ray microscopy with diffracted-beam masking to make the first direct measurements of axial elastic strains (and thus stresses) in individual dislocation cell walls and adjacent cell interiors. As discussed in the abstract by J. Z. Tischler, measurements of lattice strain in individual, high dislocation density cell walls (~0.2 µm width) were accomplished for the first time by separating the diffuse scattering from individual highly dislocated cell walls from the sharply peaked scattering from adjacent more perfect cell interiors. The effective lattice parameters for cell interiors and cell walls obtained in this way produced the two stress distributions shown in Fig. 1. The opposite signs of the wall and interior stresses indicate that the long-range stresses are dominated by dipolar stress fields. This discriminates between the two leading models proposed to describe deformation in ductile materials. The dashed line corresponding to the pile-up model is ruled out in favor of the dipole-character composite model of Mughrabi. Achieving a truly predictive understanding of dislocation evolution and aggregation will depend ultimately on our ability to identify and explore such local behavior.

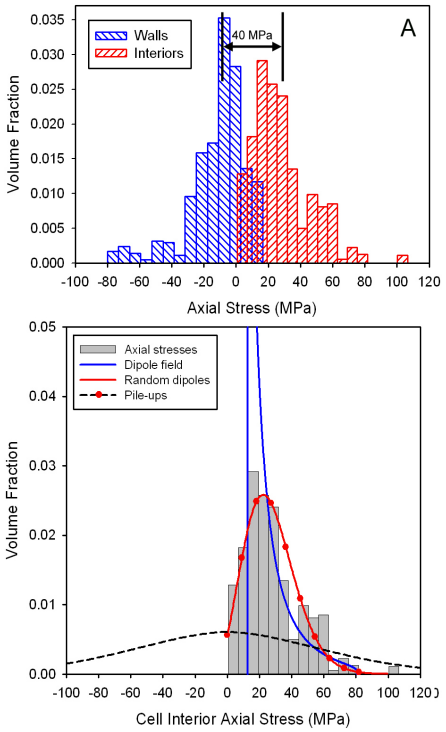

Fig. 1. (A) Stress distribution for dislocation cell walls and cell interiors in compression deformed Cu (upper); (B) comparison of the measured cell interior stress distribution with deformation models.

FUTURE DIRECTIONS

Investigations of deformation and strain localization will be directed toward the development of a fundamental and predictive understanding of deformation in ductile materials. In this context, geometrically necessary dislocations (GNDs) on mesoscopic length scales form a fundamentally important description of deformation and strain localization. GND densities drive local orientation gradients and the net Burgers vector density in turn generates long-range strain fields. 3D x-ray microscopy represents the only nondestructive method for spatially-resolved measurements of GND densities and internal stress/strain distributions on mesoscopic length scales. Both heavy and light deformation investigations will be pursued and the use of spherical microindentation in connection with deformation investigations will provide for an entirely new level of combined experimental and computational investigation of deformation.

Although the large near-surface strains and deformation gradients inherent with indentations present challenges for simulations, they inherently provide an entire range of strain geometries within a single mesoscopically confined volume, and, hence, provide the equivalent of an entire series of uniform deformation conditions. Investigations will be performed in connection with collaborative theory and modeling efforts, including finite element, constitutive law approaches with Y. Gao, UT-Knoxville/ORNL and first-principles based DDD and statistical dislocation density simulations in collaboration with A. El-Azab at Florida State University.

The materials studied will be extended from Cu to Ni, Al, and iron-based alloys, and the measurements will utilize a range of indent forces, varying tip radii, and multiple crystal orientations. In addition to these *ex situ* studies, an in-situ indentation capability under development in another project will be used to probe dislocation deformation and patterning as it evolves. The confined nature of indent deformation will be even more important for a further level of study, which will involve grain-boundaries in polycrystalline materials.

PUBLICATIONS OF DOE SPONSORED RESEARCH 2008-2010

1. T. Hoffmann, J. Kalisch, A. Bertram, S. Shim, J. Z. Tischler, H. Bei, and B. C. Larson, *Technische Mechanik*, 30, 136 – 145 (2010).

3. G.E. Ice, J.W.L. Pang, B.C. Larson, J.D. Budai, J.Z. Tischler, J.-Y. Choi, W. Liu, C. Liu, L. Assoufid, D. Shu, and A. Khounsary, *Mater. Sci. Eng. A* 524, 3-9 (2009).

9. J. Deng, A. El-Azab, and B.C. Larson, *Philosophical Magazine* 88, 3527-3548 (2008).

6. B.C. Larson, J.Z. Tischler, A. El-Azab, and W.J. Liu, *J. Eng. Mater. Technol.* 130 (2), 021024 (2008).

4. L.E. Levine, B.C. Larson, J.Z. Tischler, P. Geantil, M.E. Kassner, W.J. Liu, and M.R. Stoudt, *Zeit. für Kristallogr.* Suppl. 27, 55 (2008).

5. J.D. Budai, W.J. Liu, J.Z. Tischler, Z.W. Pan, D.P. Norton, B.C. Larson, W. Yang, and G.E. Ice, *Thin Solid Films* 516, 8013 (2008).

7. M.E. Kassner, P. Geantil, L.E. Levine, and B.C. Larson, *International Journal of Materials Research* 100, 333-339 (2009).

8. M.E. Kassner, P. Geantil, L.E. Levine, and B.C. Larson, "*Materials Science Forum* 604, 39-51 (2009).

10. B.C. Larson, "X-Ray Diffuse Scattering Near Bragg Reflections for the Study of Clustered Defects in Crystalline Materials," chapter in *Diffuse Scattering and the Fundamental Properties of Materials*, ed. By R.I. Barabash, G.E. Ice and P.E.A. Turchi, Momentum Press, LLC, New York, (2009).

Ultrafast characterization and control of materials: Application to ferroelectric oxides and nanoscale structural dynamics

P.I.: A.M. Lindenberg

Stanford Institute for Materials and Energy Research
PULSE Institute for Ultrafast Energy Science
Dept. of Materials Science and Engineering
Stanford University/SLAC
Stanford, CA 94305

Research Scope: This subtask is focused on exploring and controlling the properties of materials on ultrafast time-scales utilizing real-time probes and atomic-scale resolution techniques. The emphasis is on materials with potential energy applications, including the photovoltaic response of nanoscale ferroelectric materials and their coupled charge and lattice dynamics, and the first steps in nanoscale superionic structural transformations. A broad range of all-optical techniques are applied towards these problems, including femtosecond x-ray diffraction and spectroscopy utilizing the Linac Coherent Light Source, the Advanced Light Source femtosecond slicing beamline, and the Advanced Photon Source, building off of previous femtosecond x-ray work at the Sub-Picosecond Pulse Source at SLAC [1-3]. An important complimentary aspect of this work is focused on high field THz generation as a novel all-optical means of biasing the electronic and structural degrees of freedom in materials in electrode-less geometries, utilizing both laboratory-scale and linac-based sources.

Recent Progress:

1. Nanoscale dynamics of ferroelectric oxides. In recent work we have carried out ultrafast x-ray diffraction experiments probing the optical and THz response of ferroelectric $PbTiO_3$ nanolayers on $SrTiO_3$ substrates. Fundamental questions include: How fast can the polarization in a ferroelectric material be switched? What are the time-scales and atomic-scale pathways for these processes? How do photo-excited carriers couple to the lattice and the polarization of these materials and what is the origin of the photovoltaic response that these samples exhibit? In recent work we have observed an ultrafast modulation of the polarization state of these materials occurring on ultrafast time-scales, corresponding unexpectedly to an optically-induced increase in the polarization.

Time-dependent θ-2θ scans and fluence dependent measurements are recorded as a function of temperature for various temperatures below and near the Curie temperature. Fig. 1 displays the observed optically-induced changes in the diffracted intensity at 550 C within the ferroelectric stripe phase. It is observed that the (004) reflection changes occur on time-scales limited by the time-resolution of the x-ray source used for these measurements (~100 ps). An ultrafast increase in the diffracted intensity on the low-angle side is measured followed by a rapid recovery on ns time-scales. A peak-shift of roughly 0.2 degrees to lower Q and significant reshaping of the diffraction peak occurs at

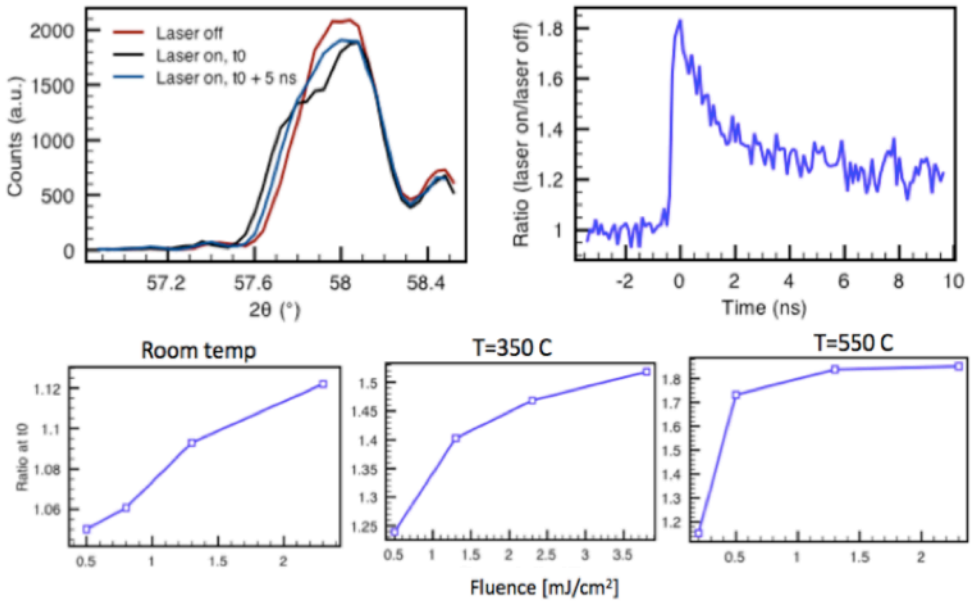

Fig. 1. (top left) Θ-2Θ scan on the (004) diffraction peak of $PbTiO_3$ nanolayers for different times after photoexcitation with 400 nm photons. (top right) Time-scan showing pulse-duration limited structural changes. (bottom) Fluence dependent scans for various temperatures showing enhanced polarization modulation as the Curie temperature is approached.

a temperature of 550 C corresponding to an increase in the c-axis lattice spacing of roughly 0.02 Angstroms and relative changes in the diffracted intensity of order 100% for an incident fluence of 500 μJ/cm^2. These effects are opposite to those that occur under a laser-induced temperature jump, in which a reduction in the tetragonality of the unit cell as the temperature increases leads to decreases in the c-axis lattice spacing. Fluence dependent measurements as shown in Fig. 1 for different temperatures indicate a strong-dependence on temperature, with the sample response increasing as the Curie temperature is approached from below, and exhibiting a saturation response with a temperature dependent saturation fluence strongly decreasing as a function of increasing temperature. These results indicate a dramatic ferroelectric polarization sensitivity to light and a pathway towards direct all-optical manipulation of the ferroelectric polarization in nanoscale films with low intensity light sources. The mechanism underlying this extreme sensitivity to light likely involves an optically-induced screening of the ferroelectric depolarization field associated with free carrier excitation near the $PbTiO_3/SrTiO_3$ interface and the formation of a transient optically-induced electrode. This work is in preparation for submission.

2. Developments in high field THz science. Complementary to the work described above, we are developing techniques for all-optical manipulation of the polarization state in ferroelectrics or multiferroics, or controlling carrier dynamics in materials on ultrafast time-scales. This requires means of biasing materials in electrode-less geometries with shaped and controllable sub-cycle light pulses with femtosecond duration. We have been exploring novel means of generating, modulating, and controlling THz-frequency light pulses which enable coupling to specific vibrational modes and all-optical application of

well-defined electric and magnetic field pulses, employing a plasma-based two-color excitation scheme. In initial measurements we have used these high fields to drive novel THz nonlinear responses in small-bandgap semiconducting materials, which can be associated with an ultrafast field-driven impact ionization process occurring within the THz field envelope [4,5,10]. We have recently shown for the first time that through manipulation of electron trajectories in a plasma with synthetic light pulses, the polarization of the THz emitted pulses can be coherently controlled. This work provides a definitive understanding of the mechanism by which the plasma emission process occurs. It also provides a unique tool for studying electron dynamics through THz emission spectroscopy. Fig. 2 shows two-dimensional plots of the THz polarization as a function of the relative phase of a two-color synthetic optical field at 800 and 400 nm [6].

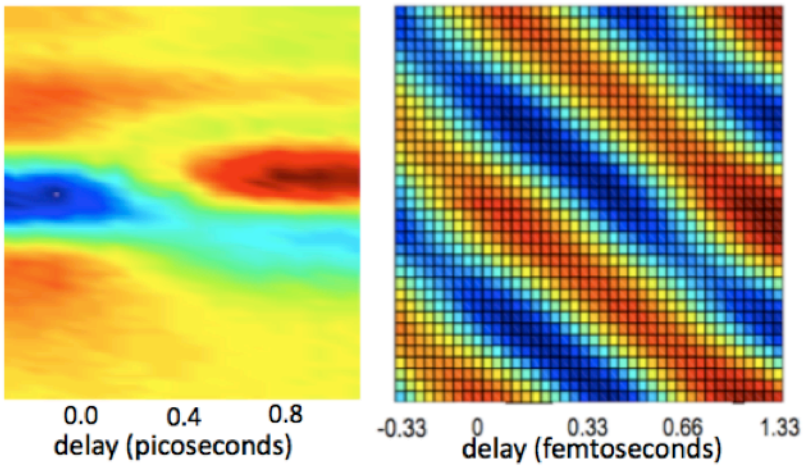

Fig. 2. (left) Plasma-based switching of the polarization state of sub-cycle ultrafast THz pulses on femtosecond time-scales. (right) Demonstration of coherent control of the THz polarization state through sub-femtosecond-time-scale phase shifts in the relative phase of a two-color excitation pulse. These measurements enable the development of ultrafast THz modulators and reversible switching of materials.

In further work [7], we have recently shown that one may employ a two-plasma geometry to create a transient optic, serving as a plasma phase modulator that turns on with a sub-picosecond time-constant and lasts only a few nanoseconds, enabling high speed polarization switching/modulation of broadband THz fields. Fig. 2 (left) shows electro-optic sampling measurements of the THz field profile as a function of time, showing the inversion of the THz sub-cycle pulse occurring on hundreds of femtosecond time-scales. This development will be directly made use of in future experiments at the LCLS in which one needs to reset the sample following ultrafast switching events.

3. Nanoscale structural dynamics in superionic materials. We have begun investigating structural transformations in superionic Cu_2S nanocrystals (in collaboration with Prof. Yi Cui, Stanford) belonging to a class of nanoionic systems which exhibit ultrafast ionic hopping rates in the solid state (comparable to that of liquid water) with important applications to high energy density electrochemical energy storage, next generation battery technology, supercapacitors, and fuel cells. Measurements are being carried out using ultrafast soft x-ray absorption spectroscopy in transmission [7,8], enabling probing of the dynamical local order around each Cu ion and the first steps in the superionic transition, corresponding to hopping of Cu atoms through a rigid S lattice. First measurements, carried out at the ALS, indicate ultrafast structural and electronic changes occuring on few-picosecond time-scales (comparable to the time for an acoustic wave to propagate across the nanocrystal) [Fig. 3]. This work is currently in progress.

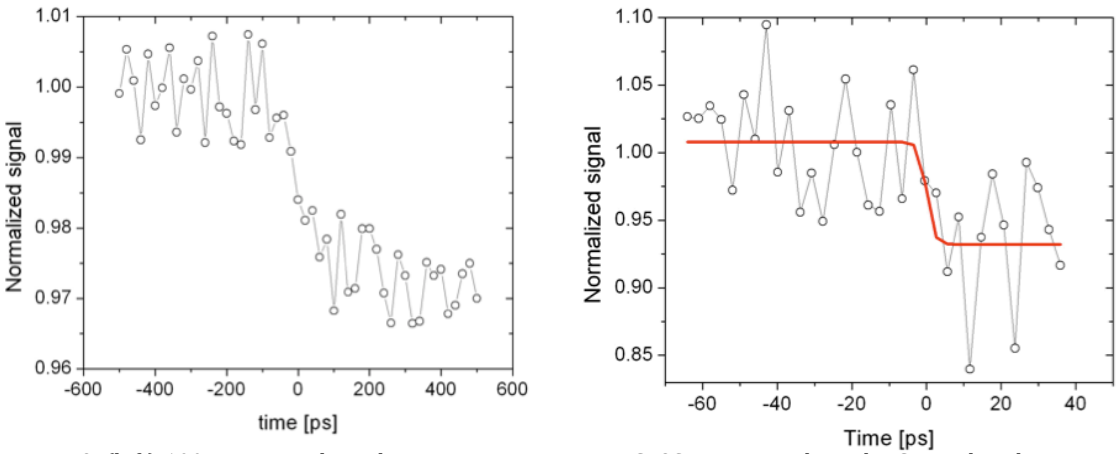

Fig. 3. (left) 100 picosecond resolution measurements in Cu2S nanocrystals at the Cu L-edge showing time-resolution limited changes (935 eV) (right) Slicing mode measurements showing few picosecond time-scale response corresponding to a shift of the Cu-L-edge to lower energies.

Future plans. We will be carrying out first measurements probing ferroelectric dynamic response to optical and THz excitation at the Linac Coherent Light Source in the fall of 2010. In addition to the efforts focused on laboratory-scale development of high field THz pulses, we are pursuing in parallel techniques to extract significantly higher THz fields directly from the electron beam which seeds the LCLS. First measurements using this new source will be carried out in the near future. Measurements on the nanocrystal response will continue at both the Advanced Light Source and at SSRL using both x-ray spectroscopic and scattering techniques.

5. References (DOE-sponsored publications in 2008-2010)

1. "Femtosecond x-ray diffuse scattering measurements of semiconductor ablation dynamics", A.M. Lindenberg et al., *Proc. of SPIE, High-Power Laser Ablation VII* **7005**, 04 (2008).
2. "Formation of secondary electron cascades in single-crystalline plasma-deposited diamond upon exposure to femtosecond x-ray pulses", M. Gabrysch, E. Marklund, J. Hajdu, D.J. Twitchen, J. Rudati, A.M. Lindenberg et al., *J. Appl. Phys.*, **103**, 064909 (2008).
3. "X-ray diffuse scattering measurements of nucleation dynamics at femtosecond resolution", A.M. Lindenberg, S. Engemann, K. Gaffney, K. Sokolowski-Tinten, J. Larsson P.B. Hillyard et al., *Phys. Rev. Lett.*, **100**, 135502 (2008).
4. Ultrafast electron cascades in semiconductors driven by intense femtosecond THz pulses" H. Wen, M. Wiczer, and A.M. Lindenberg, *Phys. Rev. B*, **78** 125203 (2008).
5. "Ultrafast electron cascades driven by intense femtosecond THz pulses" H. Wen, M. Wiczer and A.M. Lindenberg, *Ultrafast Phenomena XVI: Proceedings of the 16th International Conference*, Edited by P. Corkum, S. De Silvestri, K.A. Nelson and E. Riedle (2009).
6. "Coherent THz polarization control through manipulation of electron trajectories", H. Wen and A.M. Lindenberg, *Phys. Rev. Lett.*,**103** 023902 (2009).
7. "High-speed all-optical terahertz polarization switching by a transient plasma phase modulator", H. Wen, D. Daranciang, A.M. Lindenberg, *Appl. Phys. Lett.* **96** 161103 (2010).
8. "Ultrafast conversions between hydrogen bonded structures in liquid water observed by femtosecond x-ray spectroscopy", H. Wen, N. Huse, R.W. Schoenlein and A.M. Lindenberg, *J. Chem. Phys.* , **131** 234505 (2009)
9. "Probing the hydrogen-bond network of water via time-resolved soft x-ray spectroscopy", N. Huse, H. Wen, D. Nordlund, E. Szilagyi, D. Daranciang, T.A. Miller, A. Nilsson, R.W. Schoenlein, and A.M. Lindenberg, *Phys. Chem. Chem. Phys.*,**11**, 3951 (2009) (cover article).
10. "High intensity THz interactions with materials: New aspects and applications", *Proc. Of SPIE, High-Power Laser Ablation VIII* (2010) (in press).

Real-Time X-ray Studies of Surface and Thin Film Processes
DE-FG02-03ER46037

Karl Ludwig
Dept. of Physics; Boston University; Boston, MA 02215
ludwig@bu.edu; (617) 353-9346

Research Scope:

Better understanding complex surface and thin film processes continues to be an important materials science challenge from both fundamental and applied perspectives. Real-time investigations of such processes have natural advantages over *post facto* studies. They provide a complete temporal record of kinetics processes and there is no concern about sample changes in the period between the end of processing and the *post facto* measurement. This attribute is especially important for the study of high temperature surfaces, in which case relaxation can be relatively rapid. To investigate these issues we have been using a facility we developed at the National Synchrotron Light Source (NSLS) insertion-device beamline X21 in collaboration with Prof. Randall Headrick (University of Vermont). The facility uses a permanently installed custom base diffractometer with rails onto which experimental chambers can be rolled after optimization off line. These chambers allow for a very flexible range of *in-situ* thin film growth and modification methods including sputter deposition, plasma-assisted molecular beam epitaxy, atomic layer deposition and ion bombardment. Recently our program has focused on the four areas described below, with a goal of advancing fundamental understanding of thin film and surface processes and developing approaches utilizing the Linac Coherent Light Source (LCLS) to dramatically push down the time scales on which x-ray studies of material dynamics can be performed.

Recent Progress:

Nanoscale thin liquid film adsorption/desorption kinetics and morphology

The behavior of very thin liquid films on surfaces is of significant interest because of the important role that such films can play in solid thin film growth (e.g. as surfactant layers) and because nanodroplets can be used in novel liquid-phase epitaxy nanodot growth [1]. However detailed fundamental understanding of nanodroplet formation and coarsening behavior remains limited. Because of their important role in III-V nitrides under continued development for optoelectronics and energy applications, Ga and In are both important examples of such materials. We have therefore been systematically investigating their film growth behavior and morphology evolution kinetics as a function of temperature, deposition flux (thus examining competition between adatom nucleation of new droplets and diffusion to existing droplets) and substrate orientation (and hence interface energetics) [2,3]. Our work uses real-time x-ray fluorescence to monitor the amount of Ga or In on a sapphire surface during deposition with an effusion cell. The morphology is simultaneously followed with grazing-incidence small-angle x-ray scattering (GISAXS). As an example, Fig. 1 shows the formation of correlated nanodroplets during deposition of Ga on sapphire (0001).

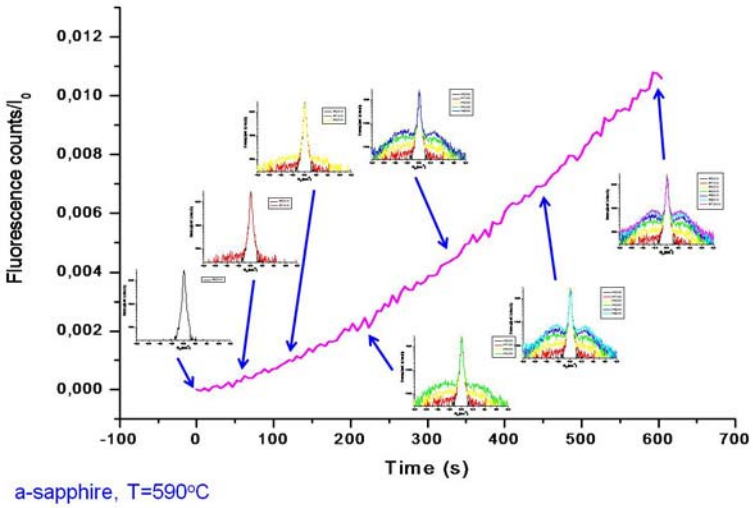

Fig. 1: Growth of thin liquid Ga film on a-plane sapphire showing correlation between coverage (as monitored by fluorescence) and nanodroplet morphology as monitored by GISAXS.

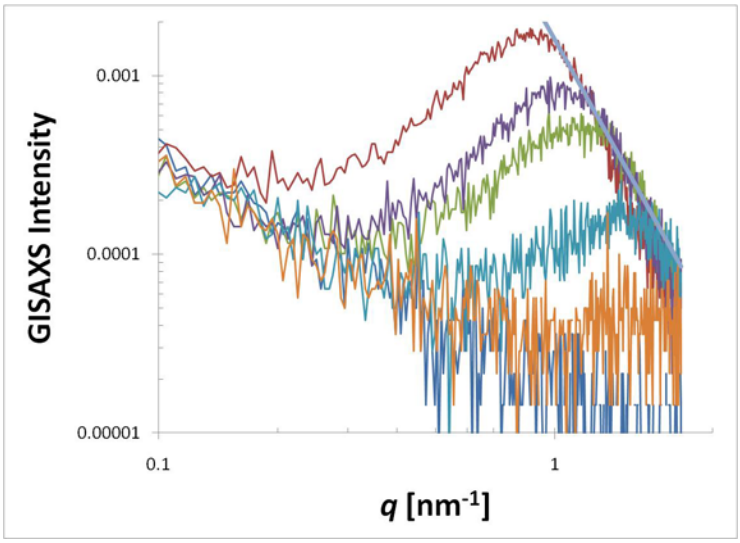

Fig. 2: Evolution of GISAXS pattern during deposition of Al film at room temperature. The blue line shows q^4 behavior expected for surface diffusion to minimize surface energy.

Nanoscale morphology evolution during growth of thin solid films

In thin liquid films, the coarsening of nanodroplets during growth can be understood in terms of droplet impingement and coalescence. The coarsening of nanoscale morphology during the growth of solid thin films is also widely observed, though the driving mechanisms are varied and often not well understood. As an example, Fig. 2 shows the real-time GISAXS evolution during Al thin film growth from an effusion cell at room temperature. The final thickness of the film in this case is approximately 1-2 nm, but the rapid coarsening of nanoscale structure observed leads to lateral correlations of approximately 30 nm. When the deposition is stopped, there is a small relaxation in the surface morphology observed in the x-ray data, but the structure is largely frozen. Thus the morphology evolution observed is fundamentally driven by the deposited atoms, not by significant thermal diffusion at room temperature. The structure factor evolution at each wavenumber shows a strong initial superlinear growth with time, inconsistent with many continuum models for thin film growth, such as the Edwards-Wilkerson or Kardar-Parisi-Zhang approaches [4]. Stress is often cited as a primary driving force for nanoscale coarsening, but existing theory predicts strong wavenumber dependence of the linear-theory growth factor [5] which is in sharp contrast to the relatively modest variation of growth factor obtained from detailed analysis of the real-time data shown here. We are currently examining Monte-Carlo models of the morphology evolution to better understand the physics necessary to explain the observed growth kinetics.

Kinetics of thin film growth by atomic-layer deposition (ALD)

Atomic-layer deposition is continuing to gain importance for its ability to grow highly conformal films with atomic-level thickness control. Because it uses typical pulse pressures in the millitorr range and higher and coats all chamber walls, it is difficult to use many surface-sensitive techniques for real-time studies. However, one of the great powers of hard x-ray techniques is their ability to penetrate ambient environments to examine processes taking place there. To better understand the fundamental growth processes in ALD, we have been collaborating with the group of Prof. Christophe Detavernier (University of Ghent, Belgium) to examine growth of Al_2O_3 and TiO_2 from organometallic precursors and water vapor on both flat substrates and into nanoporous films [6]. As an example, Fig. 3 shows the difference in initial growth kinetics for TiO_2 films on planar SiO_2 versus growth on a porous film (pore size is approximately 4 nm). X-ray fluorescence, reflectivity and GISAXS measurements have tremendous ability to characterize the anomalies in initial stages of film growth, as well as the resulting

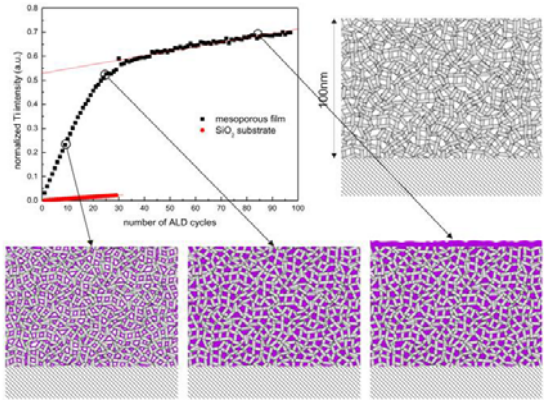

Fig. 3: Real-time x-ray fluorescence during ALD filling of mesoporous film with an initial average pore size of 4nm (top left). Top right is a sketch of the nanoslab organization and overall porosity of the initial film. The bottom figures illustrate three stages of filling, as indicated by the arrows: left, coating of the pore walls; middle: complete filling of mesopores; right: deposition on rough top

thin film morphologies.

Photon correlation spectroscopy, fast dynamical processes and experimental strategies for their study at the LCLS

X-ray photon correlation spectroscopy (XPCS) offers unique insights into fundamental dynamical processes in materials. For instance, Fig. 4 shows examples of the sudden changes in speckle pattern we observe during the martensitic transformation of cobalt from FCC to HCP phases. These experiments are performed in collaboration with Prof. Mark Sutton (McGill University, Canada). The "avalanches" of sudden structural change observed from the figure are telling us much about the heterogeneous dynamics associated with frustration and stress associated with the phase transformation. We have discovered, for instance, that the avalanche frequency and size distribution following the initiation of the transformation obey power laws that we are now seeking to understand.

Many important materials processes occur faster than can be examined with current synchrotron sources. The LCLS is now beginning to offer unique possibilities for their study down to sub-picosecond time scales. However experiments at LCLS face a strong challenge of mitigating radiation damage and adiabatic heating. Successful approaches must optimize signal while minimizing beam power density in the sample. The unfocussed LCLS x-ray beam in the experimental halls is inherently relatively large (of order 300 μm), offering the possibility of keeping the power density low while maintaining a high total flux. However, given practical constraints for sample-to-detector distances, the use of incident hard x-ray beams larger than roughly 50 μm rapidly moves experiments beyond the familiar far-field Fraunhofer limit requiring $R >> d^2/\lambda$, where R is the sample-to-detector distance, d is the incident beam diameter and λ is the photon wavelength. Using calculations and simulations we have therefore investigated scattering outside the far-field condition. We have shown that, for scattering outside the forward direction, there is an "intermediate-field" regime $d\xi/\lambda << R << d^2/\lambda$ (where ξ is the length of structural correlations in the material) in which the scattering is no longer proportional to the structure factor $S(\boldsymbol{q}) = N^{-1}\sum_{ij}\exp(i\boldsymbol{q}\cdot\boldsymbol{r_{ij}})$, but in which ensemble-averaged quantities, such as the intensity-intensity correlation function used in XPCS, yield the same result as in the far field. This potentially opens up the parameter space in which successful dynamics studies can be performed at the LCLS considerably. However, for optimal utilization of larger incident x-ray beams, area detectors with smaller pixels than currently used are needed.

Future Plans

In the near future, our focus is with ongoing data analysis and publication of the results for the projects described above. In the broader perspective, our future work will focus in three directions:

Fundamental Growth Processes in Thin Films

While much effort has been directed toward understanding how processes such as surface diffusion, related step-edge barrier effects, viscous flow, stress, surface/interface energies and the stochastic nature of the deposition process affect thin film growth, in many cases the experimental information available about the detailed kinetics of the growth process has been limited. The ability that we now have to do real-time studies of deposition under a wide range of growth conditions and processes, contrasting, for example, growth from thermal versus energetic sources, offers new important new opportunities for sorting out the contributions of different physical mechanisms to growth and morphology evolution. To obtain a more complete picture of growth processes, we are in the process of designing approaches to include

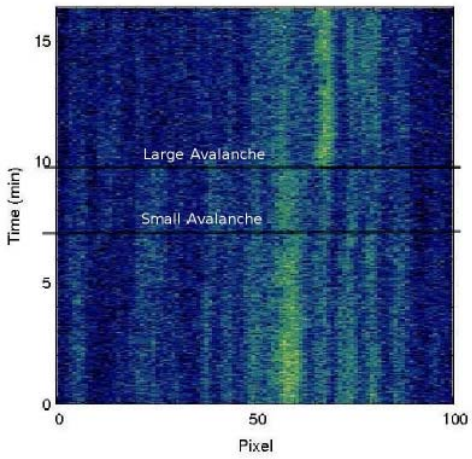

Fig. 4: XPCS pixel intensities as a function of time during the martensitic transformation of Co. The kinetics is dominated by avalanches of sudden structural change.

simultaneous stress measurements with the x-ray studies.

Processes in the Plasma-Assisted Molecular Beam Epitaxial Growth of III-V Nitride Films

Group III-V nitride materials continue to offer exciting technological possibilities while presenting a wide range of interesting growth issues. Key focus areas of our research in the future will be: investigation of the film/substrate interface structure at the atomic level by crystal truncation rod analysis and its effect on subsequent film growth polarity, the structure and kinetics of high-mobility surfactant layers on the growing nitride surface and the possible relationship of this layer and growth kinetics to the complex ordering and phase separation we have discovered in ternary nitrides [7-10]. In this latter area, particular attention will be given to theoretical suggestions about the role of surface steps, and to composition and possible phase separation in the surfactant adlayers on the growing surface.

Fast Structural Processes in Materials and on Surfaces

We will continue to develop techniques utilizing the unique coherence and time resolution available at the LCLS to illuminate fast dynamical processes in materials and on surfaces. In collaboration with scientists from Argonne National Laboratory, first experiments to examine dynamics in glasses are scheduled for November, 2010. With colleagues at Boston University and at SLAC, we are also developing LCLS experiments to investigate dynamics in water (which may be related to the proposed existence of a critical point in the supercooled region of the phase diagram) and glassy aqueous solutions.

References

1. Y. Wang, A.S. Özcan, C. Sanborn, K.F. Ludwig, A. Bhattacharyya, R Chandrasekaran, T.D. Moustakas, L. Zhou and D.J. Smith, J. Appl. Phys. **102**, 073522 (2007).
2. Ahmet S. Özcan, Yiyi Wang, Gozde Ozaydin, Karl F. Ludwig, Anirban Bhattacharyya, Theodore D. Moustakas and D. Peter Siddons, J. Appl. Phys. **100**, 084307 (2006).
3. Y Wang, A. Ozcan, K. Ludwig and A. Bhattacharyya, J. Appl. Phys. **103**, 103538 (2008).
4. For an overview of growth models see, for example, *Fractal Concepts in Surface Growth*, A-L. Barabási and H.E. Stanley (Cambridge University Press, 1995).
5. B.J. Spencer, P.W. Vorhees and S.H. Davis, J. Appl. Phys. **73**, 4955 (1993).
6. "Tailoring nanoporous materials y atomic layer deposition", C. Detavernieer, J. Dendooven, S.P. Sree, K.F. Ludwig and J. Martens, submitted to Chemical Society Review.
7. D. Korakakis, K.F. Ludwig, Jr. and T.D. Moustakas, Appl. Phys. Lett. **71**, 72 (1997).
8. D. Doppalapudi, S. Basu, K. Ludwig and T. Moustakas, J. Appl. Phys. **84**, 1389 (1998).
9. L. Iliopoulos, K.F. Ludwig, Jr. and T.D. Moustakas, J. Phys. Chem. Sol. **64**, 1525 (2003).
10. Y. Wang, A. S. Özcan, K. F. Ludwig, Jr., A. Bhattacharyya, T.D. Moustakas, L. Zhou and D. J. Smith, Appl. Phys. Lett. **88**, 181915 (2006).

Publications 2008-2010

"Real-Time Studies of Gallium Adsorption and Desorption Kinetics by Grazing Incidence Small-Angle X-ray Scattering and X-ray Fluorescence", Yiyi Wang, Ahmet Ozcan, Karl Ludwig and Anirban Bhattacharyya, J. Appl. Phys. **103**, 103538 (2008).

"In Situ X-ray Studies of Native and Mo-Seeded Surface Nanostructuring during Ion Bombardment of Si(100)", G. Ozaydin-Ince and K.F. Ludwig, Jr., J. Phys.: Condens. Matter. **21**, 224008 (2009).

Direct Methods for Surface X-Ray Diffraction: Surfaces of Alloys and Polar Oxides

Paul F. Lyman and Dilano K. Saldin
University of Wisconsin-Milwaukee
1900 E Kenwood Blvd,
Milwaukee, WI 53211
plyman@uwm.edu

Research Scope:

The research project is aimed at unraveling the structure of nanoscopic systems by the use of x-ray scattering techniques and advanced data analysis. Particular emphasis is placed on the arrangement of atoms at the surface of materials or in thin heterofilms (although some theoretical attention has been paid to scattering from small particles). In all cases, the limited extent of the object in real space, and the consequent breadth in reciprocal space, allows one to acquire redundant information that can be used to determine the phases of the scattered x-rays. The effort in the project has a theoretical and an experimental component that work synergistically. Experimentally, diffraction data, primarily from reconstructed surfaces, is acquired and analyzed. Theoretically, direct methods to extract information from these data are applied and refined, and new methods are also developed.

The measured intensities of x-rays scattered from a sample are proportional to the square of the *amplitudes* of the Fourier transform of the electron density distribution, which is itself closely related to the distribution of atoms in the sample. Briefly, the direct methods employed here attempt to assign a set of phases to these measured scattering amplitudes. Because of the limited spatial extent of a 2D (or nanoscopic) sample, the intensity will be distributed continuously over a broad range of reciprocal space. For the case of surface x-ray diffraction (SXRD), the termination of the surface leads to continuous streaks in reciprocal space normal to the surface called *crystal truncation rods* (CTR). Also, any Fourier component arising from a surface reconstruction will, of course, have limited spatial extent in the direction normal to the surface and will give rise to continuous *superstructure rods* (SSR). These streaks may be sampled in the normal direction at a spatial frequency greater than twice the Nyquist sampling rate necessary for describing the contents of a unit cell of the bulk. An iterative algorithm can be applied to assign phases to the measured amplitudes. The algorithm places constraints on the data in real space and reciprocal space. (See Fig. 1.) We term this method Phase and Amplitude Recovery and Diffraction Image Generation Method, or PARADIGM for short. In reciprocal space, the phases are adjusted to ensure agreement between the data and predicted scattering intensities. In real space, the charge distribution is constrained to lie within a *support region* near the vacuum interface. Eventually, the algorithm converges on a self-consistent assignment of phases, and thereby directly provides a model-independent structure. As we have demonstrated repeatedly, this algorithm can recover the charge density on the surface of a reconstructed solid. This charge density can then be used to suggest atomic locations, which may be precisely refined by conventional chi-squared fitting.

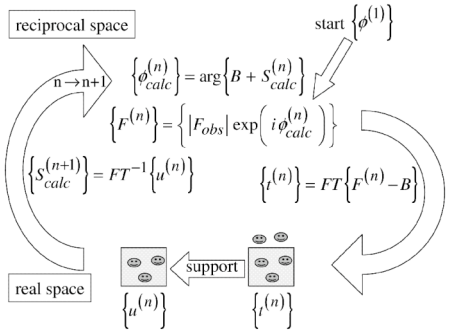

Fig. 1 Schematic flowchart of the PARADIGM iterative phase recovery algorithm described in text.

Our experimental studies commenced on metal surface alloys, including the Sb/Au(110) and Ir/Cu(100) surface systems. Our latest findings for Sb/Au(110) are reported below. The project has taken a recent focus on reconstructed polar oxide surfaces. Polar oxide surfaces result when an oxide crystal is

terminated parallel to the planes of cations and anions in the bulk crystal structure. Due to the accumulated dipole moments, the surface energy of such crystal faces tend to be quite high. Such polar surfaces of ionic materials have been predicted to undergo surface reconstruction to lower this surface energy, and a number of polar oxide surfaces have indeed been found experimentally to reconstruct. An intriguing characteristic of some of these surfaces is that the resultant reconstruction is, remarkably, stable in air. In particular, we have examined the MgO(111)-(√3×√3)R30° reconstruction, as well as the ZnO $(000\,\overline{1})$-(√3×√3)R30° surface that we recently discovered.

Progress:

<u>*Sb/Au(110)*</u> One of the first systems that we had tackled with these methods was the Sb/Au(110) surface system, wherein we found 4 new surface reconstructions, and had solved 2 of them. We have recently resolved the structure of another of these reconstructions, and also investigated the nature of a temperature-induced phase transition we observed. To briefly recapitulate our previous findings, we discovered that upon Sb deposition, the clean-surface (2×1) reconstruction is replaced by a *c*(2×2) pattern (~0.3 ML Sb coverage), which in turn undergoes a continuous transition to a (√3×√3)R54.7° pattern (~2/3 ML). Upon further deposition, a $\begin{pmatrix} 2 & -1 \\ 1 & 2 \end{pmatrix}$ pattern (which is similar to a (√5×√5) pattern on a square lattice) emerges near 0.8 ML. Finally, upon exceeding a ML, a *p*(5×6) pattern is exhibited. With the help of PARADIGM, we were able to ascertain the atomic structure of the *c*(2×2) [1] and (√3×√3)R54.7° [2] reconstructions and to understand the transition between them. The overall phase diagram and the $\begin{pmatrix} 2 & -1 \\ 1 & 2 \end{pmatrix}$ reconstruction were described in a separate publication [3]. This phase may be explained by a substitutional surface alloy where four of every five surface Au atoms are replaced by Sb. (See Fig. 2.) We also probed the thermal stability of the *c*(2×2) reconstruction with diffraction and spectroscopy. Upon heating, the diffracted intensity associated with the superstructure vanished in a power-law phase transition. (See Fig. 3a) However, line scans of the diffraction profile (Fig. 3b) indicate no transfer of diffracted intensity from the Bragg peak to a diffuse peak, which would be the signature of an order-disorder transition. Also, a large and sudden change in surface Sb coverage is observed at a different temperature (not shown). Thus, we infer that a surface miscibility gap transition [4, 5], rather than an order-disorder transition, is responsible for these phenomena [3].

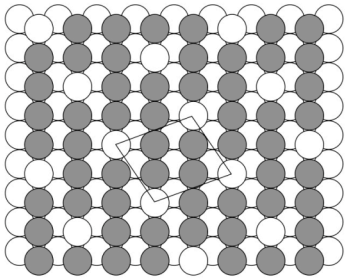

Fig. 2. Structure of the Sb-Au(110)-$\begin{pmatrix} 2 & -1 \\ 1 & 2 \end{pmatrix}$ surface alloy.

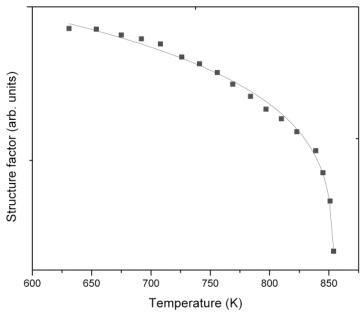

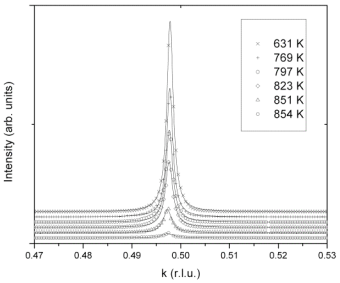

Fig. 3 Critical behavior of the (0.5 0.5 0.3) reflection. (a) integrated intensity vs. temperature. (b) diffraction line profiles at representative temperatures.

<u>*$SrTiO_3$(001)*</u> In another extension, we have applied the method to a non-reconstructed surface. In collaboration with workers at the Swiss Light Source, we applied our method to a data set from the

$SrTiO_3$(001) surface to recover a map of the electron density [6]. While at RT, this surface exhibits a (2×1) and/or (2×2) surface, at high temperatures, it deconstructs to form a (1×1). A major advantage of our technique is that it can handle *both* crystal truncation rods (CTR) and superstructure rods (SR). However, it was enlightening to apply the method for the first time to a dataset containing only CTR.

<u>*MgO(111)*</u> This surface features alternating planes parallel to the surface that are composed entirely of Mg or O ions, leading to a large surface energy [7] and predicted reconstruction [8]. The MgO(111) surface has been seen to reconstruct with several periodicities, including $p(2\times2)$, $(\sqrt{3}\times\sqrt{3})R30^\circ$, and $(2\sqrt{3}\times2\sqrt{3})R30^\circ$ [9]. There have been three reports of the surface structure of the $(\sqrt{3}\times\sqrt{3})R30^\circ$ reconstruction, none of which agree with each other [9, 10, 11]. The weak scattering of MgO presents a real experimental challenge for SXRD investigations. Using a pixel (area) detector [12] not previously available to us, we were able to acquire high-quality data [13]. In particular, the pixel detector posed two important advantages: it allows post-processing to recover the weak MgO signal from the background, and it allows one to capture the entire structure factor in one exposure, greatly speeding up data acquisition. Recently, we have found a new model that may explain these data. The top layer in this model consists of a stacking fault, and this layer is also buckled; there are no atomic vacancies, in contrast with published models. The lack of vacancies helps to explain the extreme robustness of this reconstruction. (It is even stable for weeks under bulk water.) The measured rods show good qualitative agreement with the model; detailed structural refinement is in progress.

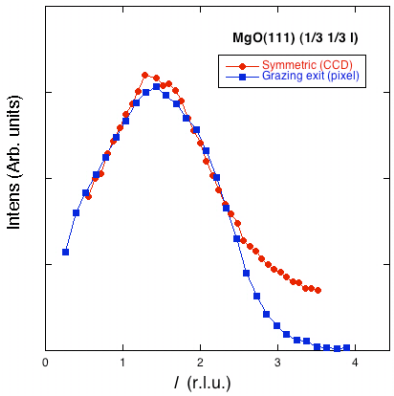

Fig. 4. SXRD data from $\left(\frac{1}{3}\frac{1}{3}l\right)$ *rod from MgO(111)-(√3×√3)R30° surface using two different experimental setups.*

<u>*ZnO(000-1)*</u> Earlier, we discovered a new sharp $(\sqrt{3}\times\sqrt{3})R30^\circ$ reconstruction on this polar surface [14] that only forms (in vacuum) under low levels of residual H gas. We have recently found that extended annealing in air can *also* induce a $(\sqrt{3}\times\sqrt{3})R30^\circ$ reconstruction. Using LEED-IV measurements, we have established that these two surface reconstructions very likely share the same structure. The Pendry R-factor R_P , which allows the quantitative comparison between two such datasets, was measured (Fig. 5) in this case to be $R_P = 0.27$, indicating it is highly probable that the underlying structures are the same. We recently acquired a SXRD dataset from such a surface, but, unfortunately, sample preparation problems rendered these data nearly useless for extracting information on the reconstruction.

References

[1] P.F. Lyman et al., Surf. Sci. **600**, 424-435 (2006).
[2] R. Fung, et al., Acta Crystallographica **A63**, 239-250 (2007).
[3] S.S. Parihar et al., J. Vac. Sci. Tech. A. **26**, 485-493 (2008).
[4] C. R. Helms, Surf. Sci. **69**, 689 (1977).
[5] Y. Liu and P. Wynblatt, Surf. Sci. **290**, 335 (1993).
[6] R. Herger et al., Phys. Rev. B **76**, 195435-1-18 (2007).
[7] F. Bertaut, Compt. Rendu. **246**, 3447-3450 (1958).
[8] D.Wolf, Phys. Rev. Lett. **68**, 3315-3318 (1992).
[9] R. Plass et al., Phys. Rev. Lett. **81**, 4891-4894 (1998).
[10] A. Subramanian et al., Phys. Rev. Lett. **92**, 026101-1-4 (2004).
[11] J. Ciston et al., Phys. Rev. B **79**, 085421-1-13 (2009).
[12] C.M. Schlepütz, et al., Acta Crystall. **A61,** 418-425 (2005).
[13] P. Fenter et al., J. Synchrotron Rad. **13**, 293-303 (2006).
[14] S.T. King, et al., Surf. Sci. Lett. 602, L131-L134 (2008).

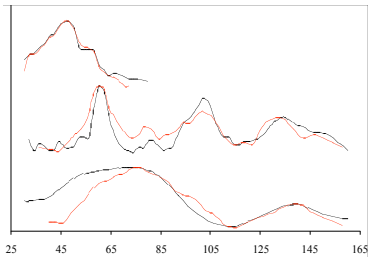

Fig. 5. LEED-IV spectra from ZnO(000-1)-(√3×√3)R30° surfaces: UHV-prepared (black) and air-annealed (red) samples. Top curves are (1/3,1/3), middle are (2/3,2/3) and bottom are (0,1).

Future plans:

Fluid-Solid Interfaces: It has been previously established that the hard-wall interaction of a liquid with a solid develops a nascent ordering in the liquid (at temperatures far above its melting point) in the direction normal to the substrate surface. In a few cases, the lateral corrugation of the substrate was seen to extend this ordering (weakly) in the lateral direction, i.e., in-plane order developed. In the near future, we will interrogate the structure of a water/mineral interface for the special case of a reconstructed oxide substrate. A reconstructed surface will have corrugations on a longer lateral length scale, and may serve as a more effective template for imbuing this nascent lateral order. The lack of a bulk Fourier component corresponding to the surface reconstruction confers added sensitivity to detecting this incipient order. Understanding the factors that contribute to lateral ordering may shed light on phenomena as diverse as lubrication, frost heave, and intracellular transport.

Dissemination of Computer Programs: The PARADIGM method of phasing of SXRD data is both novel and very successful. Consequently, it is likely to be adopted also by others in the field. It is our aim to facilitate this by disseminating the computer programs that produce an electron density map of the surface unit cell directly from measured SXRD data in an accessible form. It is our intention to disseminate these programs by publishing a paper in the journal Computer Physics Communications. Each paper in this journal consists of a description of a computer program, together with a listing of the input data and sample output. The program, and typical input and output, are deposited with the journal and may be obtained by readers directly from the journal. The progress of this part of the project was held back by the recent death of a postdoc working on it. After some delays due to visa issues etc., we have succeeded in hiring a new postdoc, who is now working full time on this, and we expect this part of the project to be completed before too long.

Selected Publications:

"Surface phase diagram and alloy formation for antimony on Au(110)," S.S. Parihar and P.F. Lyman, J. Vacuum Sci. and Technol. A. **26**, 485-493 (2008).

"Direct Methods for Surface Crystallography," D. K. Saldin and V. L. Shneerson, J. Phys.: Condens. Matter 20, 304208 (2008).

"Observation of a $(\sqrt{3}\times\sqrt{3})$R30° reconstruction on ZnO $(000\bar{1})$," S.T. King, S.S. Parihar, K. Pradhan, H.T. Johnson-Steigelman, and P.F. Lyman, Surf. Sci. Lett. **602**, L131-L134 (2008).

"Molecular Shapes from Small Angle X-Ray Scattering," V. L. Shneerson and D. K. Saldin, Acta Cryst. A65, 128-134 (2009). The editor (Schwarzenbach) chose this paper to be Acta Cryst A's highlight in a (quarterly) IUCr Newsletter in 2009.

"Molecular Structure Determination from X-Ray Scattering Patterns of Laser-Aligned Symmetric-Top Molecules," P. J. Ho, D. Starodub, D. K. Saldin, V. L. Shneerson, A. Ourmazd, and R. Santra, J. Chem. Phys. 131, 131101 (2009). This was the most downloaded paper from the journal website in October 2009.

"Reconstruction from a Single Diffraction Pattern of Azimuthally Projected Electron Density of Molecules Aligned Parallel to a Single Axis," D. K. Saldin, V. L. Shneerson, D. Starodub, and J. C. H. Spence, Acta Cryst. A, 66, 32-37 (2010).

"Beyond Small Angle X-Ray Scattering: Exploiting Angular Correlations," D. K. Saldin, H. C. Poon, V. L. Shneerson, M. Howells, H. N. Chapman, R. Kirian, K. E. Schmidt, and J. C. H. Spence, Phys. Rev. B 81, 174105 (2010).

Advancing High-Pressure Synchrotron X-Ray Research at HPCAT

P.I.: Ho-kwang (David) Mao, Russell J. Hemley, & Guoyin Shen

Geophysical Laboratory, Carnegie Institution of Washington, 5251 Broad Branch Rd., NW, Washington DC, 20015-1305

mao@gl.ciw.edu

A plethora of high-pressure (HP) synchrotron radiation (SR) techniques has been developed and established at the HPCAT beamline of APS to explore the rich behavior of materials under pressure. These include *HP x-ray emission spectroscopy* which provides information on the filled electronic states of the HP samples, *HP x-ray Raman spectroscopy* which probes HP chemical bonding changes of the light elements, *HP electronic inelastic x-ray scattering spectroscopy* which accesses the high energy electronic phenomena, including electronic band structure, Fermi surface, excitons, plasmons, and their dispersions, *HP resonant inelastic x-ray scattering spectroscopy* which probes shallow core excitations, multiplet structures, and spin-resolved electronic structure, *HP nuclear resonant x-ray spectroscopy* which provides phonon densities of state and time-resolved Mössbauer information, *HP x-ray diffraction* which determines the fundamental structures and densities of single-crystal, polycrystalline, nanocrystalline, and non-crystalline materials, and *HP radial x-ray diffraction* which yields deviatoric elastic and rheological information. These tools, integrated with hydrostatic or uniaxial media, laser and resistive heating, and cryogenic cooling, have enabled investigations of structural, vibrational, electronic, and magnetic properties over an extensive *P-T* range.

To take full advantage of the rapid advancing SR brilliance, resolutions (in energy, size, and time), polarization, and coherence, a single beamline like HPCAT has its technical and organizational limitations. The extreme synchrotron capabilities, including the maximum energy to hundreds of keV, the maximum spatial resolution in tens of nanometer, the maximum energy resolution to sub-meV, and the maximum time resolution to follow the advances of a shock-wave front, would require specialized beamlines incompatible with the dedicated, HP, multi-purpose beamline. A new infrastructure, HPSynC, has been established to bridge the HP research and most APS specialized beamlines, thus unleashing the full power of the multidisciplinary HP science.

Synchrotron x-ray studies of materials under extreme environments

Wendy Mao
450 Serra Mall
Braun Bldg #320, MC2115
Stanford, CA 94305-2115
wmao@stanford.edu

Extreme conditions in pressure, temperature, and irradiation can induce dramatic changes materials and give us a much broader field to search for new phases with desirable properties, and improving our understanding of the modifications that occur in materials can help us design improved materials. Our group has been investigating a number of strongly correlated systems and hydrogen storage materials using a suite of *in-situ* probes including many x-ray scattering techniques to study changes in properties at extreme conditions in these materials. Concurrently we have also been helping to develop high pressure x-ray capabilities and collaborating with theory groups for interpreting our results. A few of the research highlights and directions include:

<u>High pressure evolution of Fe_2O_3 electronic structure revealed by X-ray absorption</u>
We made the first high pressure measurement of the Fe K-edge in hematite (Fe_2O_3) by X-ray absorption spectroscopy in partial fluorescence yield geometry. The pressure-induced evolution of the electronic structure as Fe_2O_3 transforms from a high-spin insulator to a low-spin metal is reflected in the x-ray absorption pre-edge (Figure 1). The crystal field splitting energy was found to increase monotonically with pressure up to 48 GPa, above which a series of phase transitions occur. Atomic multiplet, cluster diagonalization, and density-functional calculations were performed in collaboration with Tom Devereaux's group at SLAC/Stanford to simulate the pre-edge absorption spectra, showing good qualitative agreement with the measurements. These results represent a novel approach for studying Fe_2O_3 and related compounds under pressure. This is the first use of high resolution pre-edge XAS at high pressure to investigate insulator-metal transition and high spin-low spin transition. Together with the theory we use to help interpret the spectra, our work opens up a new way to study the electronic transitions of transition metal compounds.

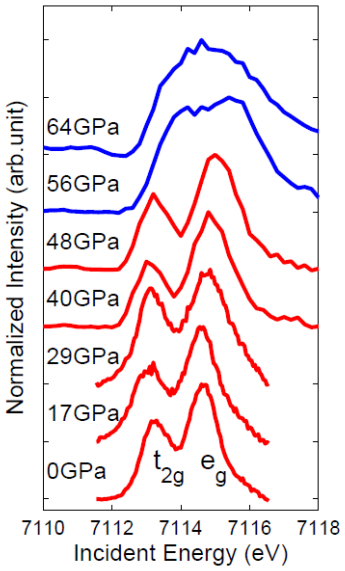

Figure 1. X-ray K-edge pre-edge of Fe_2O_3 at 0, 17, 29, 40, 48, 56 and 64 GPa showing changes in the crystal field splitting with pressure. The red spectra are from the insulating, high spin lower pressure phase and the blue spectra are from the metallic, low spin higher pressure phase.

High-pressure EXAFS study of vitreous GeO_2 up to 44 GPa

We performed high-pressure extended x-ray absorption fine-structure measurements on amorphous GeO_2 over increasing and decreasing pressure cycles at pressures up to 44 GPa. Several structural models based on crystalline phases with fourfold, fivefold, and sixfold coordination were used to fit the Ge-O first shell. The Ge-O bond lengths gradually increased up to 30 GPa. Three different pressure regimes were identified in the pressure evolution of the Ge-O bond distances. Below 13 GPa, the local structure was well described by a fourfold "quartzlike" model whereas a disordered region formed by a mixture of four- and five-coordinated germanium-centered polyhedra was observed in the intermediate pressure range between 13 and 30 GPa. Above 30 GPa the structural transition to the maximum coordination could be considered complete. The present results shed light on the GeO_2 densification process and on the nature of the amorphous-amorphous transition, suggesting that the transition is more gradual and continuous than what has been previously reported. They also demonstrate the potential for using energy-dispersive high pressure EXAFS to studying 3*d* transition metal compounds.

High pressure X-ray Absorption Near Edge Structure (XANES) studies of strongly correlated systems

$CsAuI_3$ presents an intriguing parallel to the better known charge density wave (CDW) compound $BaBiO_3$. Similar to the two distinct Au sites (Au^+ and Au^{3+}) in $CsAuI_3$, $BaBiO_3$ comprises two distinct Bi sites. It has been suggested that the CDW state in this compound might reflect the tendency of Bi to disproportionate ($2Bi^{4+} \rightarrow Bi^{3+} + Bi^{5+}$). Significantly, suppression of the CDW state in $BaBiO_3$ by hole doping leads to superconductivity. The nature of the pairing mechanism in these compounds remains an open question, as does the possibility of finding related higher Tc materials. In this context, understanding the nature of the coupled structural and valence transition under pressure in $CsAuI_3$ is especially important. The CDW state in $CsAuI_3$ is different to that found in $BaBiO_3$ in that the relative difference in bond lengths between the coordinating ligands and the two distinct Au sites are substantially larger, and that the frozen phonon mode associated with the CDW state is different. Understanding the consequences of these differences in terms of the electronic structure, electronic transport, and electron-phonon coupling are key steps in assessing the potential of $CsAuI_3$ to host superconductivity in part of the composition-pressure phase diagram. In addition, there are very few compounds containing Au^{2+} ions, and even fewer exhibiting Au valence transitions, motivating a careful study of the correlation between structural and electronic properties in $CsAuI_3$. This is a collaboration with Ian Fisher's group at Stanford. L-edge XANES is an ideal tool to explore changes in the 5*d* electron configuration associated with the various valence and structural transitions observed, and can be applied to many strongly correlated systems (e.g. Hg L_3 edge in Hg cuprates). Together with additional structural information from separate x-ray diffraction experiments and theoretical calculations (from Tom Devereaux's group), these results will provide a much clearer picture on the correlation between the electronic state of the system and the crystal structure in the various pressure regimes.

Distortions and stabilization of simple-cubic calcium at high pressure and low temperature

Ca-III, the first superconducting calcium phase under pressure, was identified as simple-cubic (sc) by previous X-ray diffraction (XRD) experiments. In contrast, all previous theoretical calculations showed that sc had a higher enthalpy than many proposed structures and had an imaginary (unstable) phonon branch. By using our newly developed submicrometer high-

pressure single-crystal XRD, cryogenic high-pressure XRD, and theoretical calculations, we demonstrate that Ca-III is neither exactly sc nor any of the lower-enthalpy phases, but sustains the sc-like, primitive unit by a rhombohedral distortion at 300 K and a monoclinic distortion below 30 K. This surprising discovery reveals a scenario that the high pressure structure of calcium does not go to the zero-temperature global enthalpy minimum but is dictated by high-temperature anharmonicity and low-temperature metastability fine-tuned with phonon stability at the local minimum. The development of high pressure submicron single-crystal XRD has potential application for addressing many structural problems surrounding new phases which occur under compression.

Compressional behavior of $LiMn_2O_4$ bulk and nanorods under nonhydrostatic stress

The effect of pressure on $LiMn_2O_4$ commercial powders and well-characterized nanorods was investigated using angle-dispersive x-ray diffraction in diamond anvil cells (DACs), indicates spinel $LiMn_2O_4$ is extremely sensitive to deviatoric stress induced by the external applied pressure. Under nonhydrostatic conditions, bulk $LiMn_2O_4$ underwent an irreversible phase transformation at pressure as low as 0.4 GPa from a cubic to an orthorhombic *Fdd*2 structure driven by the Jahn-Teller effect. In contrast, bulk $LiMn_2O_4$ with methanol-ethanol mixture as pressure medium started to experience a reversible structural transformation at approximately 11 GPa. Well-characterized $LiMn_2O_4$ nanorods with an average diameter of 130 nm and an average length of 1.2 μm synthesized by Yi Cui's group at Stanford were further investigated with the same experimental conditions. The observations that nanorods showed a similar behavior as bulk $LiMn_2O_4$ confirms the conclusion that $LiMn_2O_4$ displays an extremely sensitive structural response to deviatoric stress. SEM images of the quenched samples and the starting materials indicate a link between the morphology of the samples and the origin of the phase transition (Figure 2). Our comparative study of $LiMn_2O_4$ bulk and nanorods is useful for improving our understanding of its fundamental structural and mechanical properties which may provide guidance for applied battery technology. In addition, $LiMn_2O_4$ interesting strongly correlated systems whose structural, electronic, and magnetic behavior at high pressure is of broad interest for chemistry and condensed matter physics.

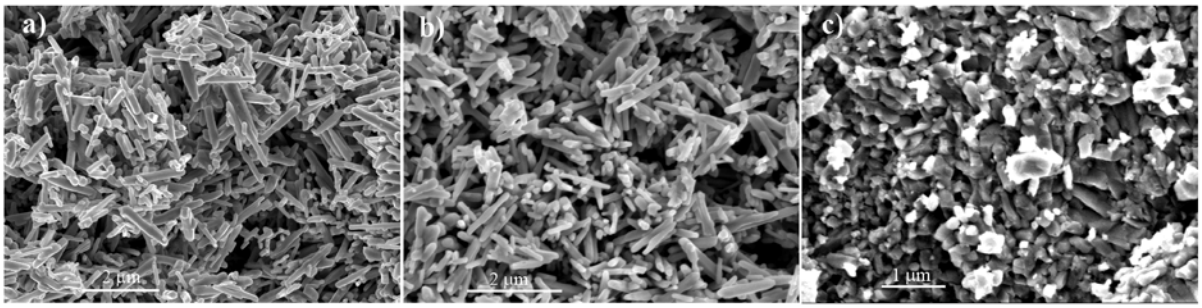

Figure 2. SEM images of a) synthetic $LiMn_2O_4$ nanorods before compression, b) after compression in a mixture of methanol-ethanol, and c) after compression without pressure medium which shows loss of nanorod morphology.

Publications

S. Wang, W. L. Mao, A. P. Sorini, C-C. Chen, T. P. Devereaux, Y. Ding, Y. Xiao, P. Chow, N. Hiraoka, H. Ishii, Y. Q. Cai, and C-C. Kao, High pressure evolution of Fe_2O_3 electronic structure revealed by X-ray absorption spectroscopy, *Phys. Rev. B*, in press.

H-k. Mao, E. L. Shirley, Y. Ding, P. Eng, Y. Q. Cai, P. Chow, Y. Xiao, J. Shu, R. J. Hemley, C-C. Kao, and W. L. Mao, Electron structure of crystalline ^{4}He at high pressures, *Phys. Rev. Lett.*, in review.

X.-Q. Chen, S. Wang, W. L. Mao, and C. L. Fu, Pressure-induced behavior of the hydrogen-dominant compound $SiH_4(H_2)_2$ from first-principles calculations, *Phys. Rev. B*, doi: 10.1103/PhysRevB.82.104115, 2010.

W. L. Mao, L. Wang, Y. Ding, W. Yang, W. Liu, D. Y. Kim, W. Luo, R. Ahuja, Y. Meng, S. V. Sinogeikin, J. Shu, and H-k. Mao, Distortions and stabilization of simple primitive calcium at high pressure and low temperature, *Proc. Nat. Acad. Sci.*, doi: 10.1073/pnas.1005279107, 2010.

M. Baldini, G. Aquilanti, H-k. Mao, W. Yang, G. Shen, S. Pascarelli, and W. L. Mao, High-pressure EXAFS study of vitreous GeO_2 up to 44 GPa, *Phys. Rev. B* **81**, 024201, 2010.

S. Wang, W. L. Mao, and S. T. Autrey, Bonding in boranes and their interaction with molecular hydrogen at extreme conditions, *J. Chem. Phys.* **131**, 144508, 2009.

Y. Lin, W. L. Mao, and H-k. Mao, , Storage of molecular hydrogen in an ammonia borane compound at high pressure, *Proc. Natl. Acad. Sci.* doi:10.1073/pnas.0903511106, 2009.

L. Sun, W. Yi, L. Wang, J. Shu, S. Sinogeikin, Y. Meng, G. Shen, L. Bai, Y. Li, J. Liu, H-k. Mao, W. L. Mao, X-ray diffraction studies and equation of state of methane at 200 GPa, *Chem. Phys. Lett.* **473**, 72-74, 2009.

Y. Lin, V. Dozd, J. Chen, L. Daemen, and W. L. Mao, Raman spectroscopy study of ammonia borane at high pressure, *J. Chem. Phys.* **129**, 234509, 2008.

Structure and dynamics in block-copolymer-nanoparticle nanocomposites

Principal Investigator: Simon Mochrie
Sloane Physics Laboratory
217 Prospect Street
New Haven, CT 06520-8120 P.O. Box 208120
simon.mochrie@yale.edu

Research Scope

The goal of this proposal is to establish and investigate the basic physical principles underlying the equilibrium structures and dynamics within block copolymer-nanoparticle nanocomposites. This new understanding will facilitate the design and creation of robust and stable nanocomposites with desirable properties. In particular, for nanocomposites built from nanoparticles with a size that is smaller than the characteristic size of the block copolymer morphology, and with a surface treatment that yields a strong preference for the interior of one of the blocks, we hypothesize that for low and moderate concentrations of nanoparticles, the block copolymer morphology will be minimally affected by the nanoparticles. Thus, in these cases, the block copolymer morphology will effectively constitute a template that, together with the overall concentration of nanoparticles, will define the nanoparticles' arrangement. We will test this hypothesis and investigate the structure (via SAXS) and dynamics (via XPCS) of nanoparticles in such confined geometries, including in zero, one, and two-dimensional spaces and in curved spaces, such as at the curved interface between different diblocks. In the case of nanocomposites built from larger nanoparticles, whose size approaches or exceeds the characteristic size of the block copolymer morphology, and with a surface treatment that yields a preference for the nanoparticle to be located at the block-block boundary, we hypothesize that the addition of such nanoparticles at sufficient volume fractions will eventually give rise to novel nanocomposite morphologies, different from that of the parent copolymer system. We will carry out SAXS measurements to elucidate how the presence of nanoparticles feeds back onto the block-copolymer morphology, and how the morphology of nanocomposites changes with the addition of an increasing concentration of surface-active nanoparticles. The dynamical properties of the resultant novel structures will be studied via XPCS.

Recent Progress

In preparation for synchrotron-based SAXS and XPCS experiments, we have successfully implemented at Yale the protocols of Ref. [1] to create two distinct nanoparticle-block copolymer motifs. Specifically, a polystyrene-block-poly(2-vinylpyridine) block copolymer (PS-b-P2VP) was purchased from Polymer Source. PS-b-P2VP micelles were formed by solvating in toluene (5 mg/ mL). To carry out the synthesis of CdS nanoparticles, $Cd(OAc)_2$ and Na_2S were each dispersed in methanol. The $Cd(OAc)_2$/methanol solution was then mixed into a PS-b-P2VP/toluene solution to induce the coordination of P2VP and Cd2? ions. After stirring this solution for 24 hours at room temperature, the Na_2S/methanol solution was added. The resulting solution was again stirred for 12 hours to complete the reaction

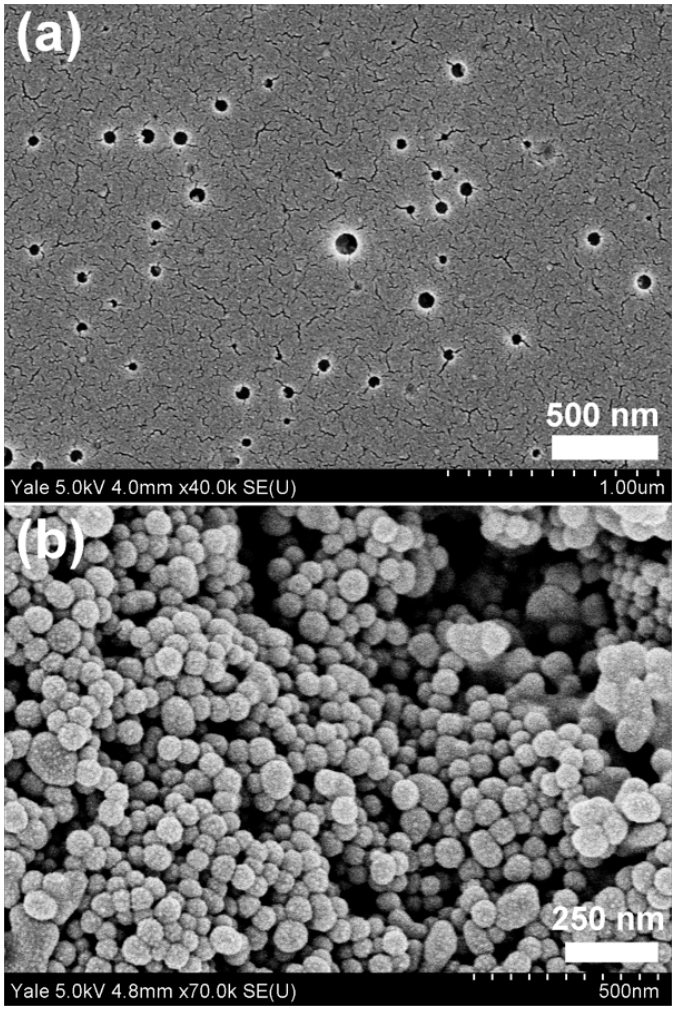

Figure 1: Representative scanning electron microscope (SEM) images of poly(styrene)-block-poly(2-vinylpyridine) (PS-b-P2VP) micellar structure. (a) P2VP core containing cadmium sulfide (CdS) nanoparticles and PS shell formed in toluene. (b)The addition of excess methanol (MeOH), which is a good solvent for P2VP, results in the core-shell inversion of PS-bP2VP. This core-shell inversion leads to micellar-shell embedded CdS nanoparticles.

between Cd^2 and Na_2S. This lead to the creation of CdS nanoparticles, located at the P2VP micellar cores with a polystyrene micellar shell. A transmission electron micrograph of such micelles is shown in Fig. 1(a).

Subsequent inversion of the micellar structure and rearrangement of the CdS nanoparticles was achieved by adding an excess of methanol into the toluene-based micellar solution. This led to the formation of micelles with PS cores and P2VP shells and correspondling shell-embedded CdS nanoparticles. An SEM image of these micelles is shown in Fig. 1(b). Currently, we are implementing methods to prepare more concentrated samples, suitable for x-ray measurements, which will occur in beamtime scheduled for December 2010.

Future Plans

We now have a system in hand that will permit us to invesigate the behavior of nanoparticles with a strong preference for one block, namely the CdS-P2VP-PS system. In the case of a lamellar parent PS-P2VP block copolymer system, we anticipate that the CdS nanoparticles will form a stack of two-dimensional particle arrays, confined within sheets of P2VP, separated and shielded one from another by the presence of sheets of PS.. This system will afford the opportunity to study the collective structure and dynamics in a quasi-two-dimensional situation. (In this case, to achieve a single lamellar orientation, we will repeatedly spin caste onto a flat substrate to built up the film thickness.) For moderate nanoparticle volume fractions, we expect to realize a two-dimensional nanoparticle liquid, and at yet higher volume fractions a quasi-two-dimensional solid.

If instead of a lamellar parent morphology, we choose a hexagonal one, then the nanoparticles, will be confined within one-dimensional cylindrical domains. As is well-known, one-dimensional systems cannot order at any non-zero temperature. Therefore, with increasing nanoparticle volume fraction, we expect that the structural correlations that this system will evolve smoothly. It seems clear, however, that in a certain sense, such a one-dimensional liquid is always "jammed" [2, 3] because of the difficulty of one particle passing another (particle exchange), at least for narrow enough cylinders. We hypothesize therefore that the collective dynamics of such a system will be unusually slow, compared to its two- and three-dimensional analogues, and will be a strong function of the ratio of the nanoparticle diameter to the cylinder diameter.

Our immediate future goals are to characterize the structural arrangement of such 2D- and 1D-confined nanoparticles and their dynamics via SAXS and XPCS, respectively.

References

[1] H.-D. Koh, M. Changez, and J.-S. Lee. Au/CdS hybrid nanoparticles in block copolymer micellar shells. *Macromolecular Rapid Communications*, 31:in press, 2010.

[2] A. J. Liu and S. R. Nagel. Non-linear dynamics: Jamming is not just cool anymore. *Nature*, 396:21, 1998.

[3] V. Trappe, V. Prassad, L. Cipelletti, P. N. Segre, and D. A. Weitz. Jamming phase diagram for attractive particles. *Nature*, 411:772, 2001.

DOE award #DE-FG02-09ER46652: Ultrafast Magnetism Dynamics Measure Using Tabletop Ultrafast EUV Sources

Margaret Murnane, Henry Kapteyn and Thomas Silva
University of Colorado and NIST, Boulder, CO
Margaret.Murnane@colorado.edu; Henry.Kapteyn@colorado.edu; Silva@boulder.nist.gov

Introduction

Magneto-optical measurements of magnetic dynamics currently use either ultrafast lasers and visible-wavelength light, or x-rays from large-scale synchrotron x-ray facilities. The former gives short pulses (~ 50 fs), enabling studies with high time resolution but with low spatial resolution. X-ray probes enable high spatial resolution and high contrast at the elemental absorption edges of ferromagnetic materials. However, until recently the available time resolution has been too low to capture the fastest dynamics involved in demagnetization or domain switching. Ultrafast short wavelength light from high-harmonic generation (HHG) or x-ray free electron lasers (XFELs) has the potential to combine nm spatial resolution with ~< 10 fs time resolution.

Synchrotron x-ray studies typically make use of magnetic contrast near the L-edge of the elements at ~ 700 eV photon energy – outside the wavelength range accessible using HHG light. However, recent work has shown that it is also possible to obtain good magnetic contrast suitable for spectroscopy and imaging at the M-edges of the magnetic materials, at photon energies of 55-65 eV that *are* accessible using HHG light. Moreover, this approach is very sensitive, is element selective, and achieves high time resolution (≈ 50 fs), with much higher time resolution possible in the future.

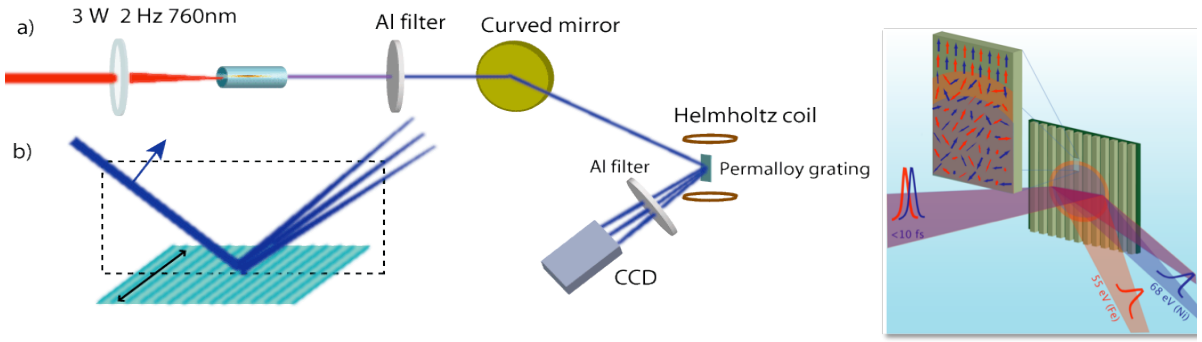

Figure 1. Experimental setup. a) A femtosecond laser beam is focused into a gas-filled hollow waveguide, to generate high harmonics of the fundamental laser in the 35 – 70 eV range. A uniform magnetic field is generated by a Helmholtz coil, and the direction of magnetization of the sample is continuously changed. b) The samples consist of doped and updoped permalloy gratings. The large blue arrow depicts the polarization of the incident EUV light whose plane of incidence is shown by the dashed black box. The small black arrows indicate the direction of magnetization, which is perpendicular to the plane of incidence of the probe beam. The EUV harmonics are spectrally resolved by the sample grating, and then focused onto a CCD camera.

Results to date

In our work to date, we made two significant advances. First we demonstrated element-selective demagnetization dynamics for the first time, with a record time resolution for x-ray probing of 55 fs (see Figs. 2 and 3). Our initial experiments measured the demagnetization

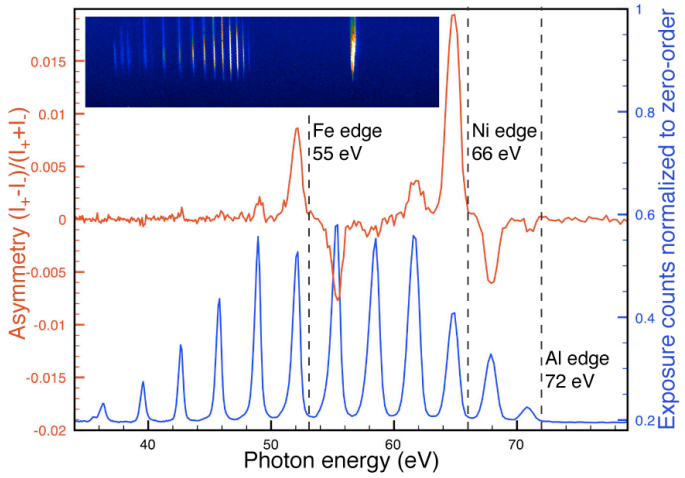

Figure 2. T-MOKE signal from a permalloy sample ($Ni_{80}Fe_{20}$): (red) Asymmetry signal, defined as the difference in reflected intensities after magnetization reversal (normalized). Large asymmetries are measured near absorption edges of Ni and Fe. (blue) Typical harmonic spectra. Inset shows the diffraction pattern recorded on the CCD.

dynamics the alloy Permalloy (Ni80Fe20), in which the two transition metal species are strongly exchange coupled and, therefore, the demagnetization timescales were the same for Ni and Fe (within our measurement accuracy). More recently, we extended our measurements to other alloys with weaker exchange coupling between magnetic species, with which we measured different demagnetization timescales for the different elements in a single material. We also compared our demagnetization timescales in simple materials (Ni) with those measured by visible lasers, and found them to be equal within our measurement accuracy (≈ 150 fs), with the exact time dependent on the heating pump pulse fluence. In other exciting preliminary data, we investigated the magnetization dynamics of buried magnetic layers in a spin-valve type multilayer system.

Our measurements were made using the transverse magneto-optic Kerr effect (T-MOKE) geometry, since the reflectivity of a magnetic material changes with the direction of the magnetization vector of a surface. In our experiment, we periodically reversed the magnetization direction of a grating structure made of Permalloy (Ni80Fe20) using an external magnetic field (Fig. 1). To achieve maximum contrast, we used HHG light spanning the M-shell (3p) absorption edges of Fe and Ni. Our first measurement on a Permalloy sample shows high magnetic asymmetry (up to 2%) at photon energies just above and below the absorption edges at 55 eV and 65 eV, respectively. This result (Fig. 2) is in qualitative agreement with Faraday rotation measurements previously done using a synchrotron source.

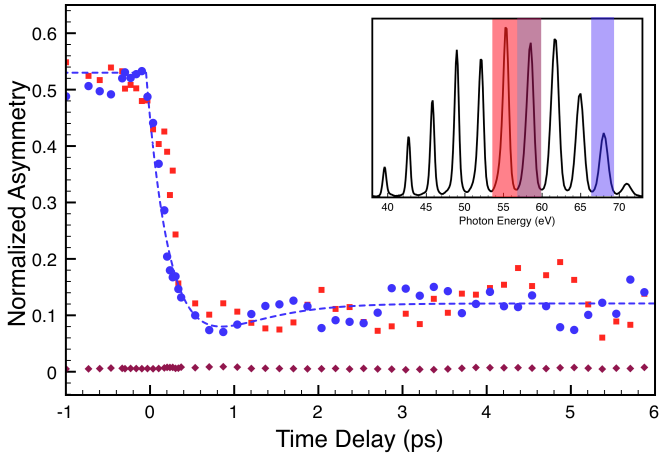

Figure 3. Time-resolved measurement of the femtosecond laser-pulse induced demagnetization of the Permalloy film by high-harmonic photons around the Ni (blue circle), Fe (red square) M-edge, and off-resonance from M-edge (diamond). The dashed line represents a fit to the data.

Figure 3 demonstrates the use of femtosecond EUV beams to probe ultrafast demagnetization processes with elemental selectivity. A Permalloy sample is demagnetized using an ultrafast infrared pump-beam, and the magnitude

of the magnetization is monitored as a function of time-delay between the laser pump pulse and the EUV probe pulse. We measured a demagnetization time of 400 fs for both Fe and Ni in Permalloy. This result shows that the different atomic species in Permalloy are strongly exchange-coupled even during the ultrafast non-adiabatic heating process.

In order to break the coupling between the moments of Fe and Ni in Permalloy, we made further measurements on Cu-doped Permalloy (40% Cu / 60% Permalloy), which exhibits a very Curie temperature Tc of 425 K. Near Tc, the exchange interaction in ferromagnets is known to renormalize. The basic principle is that the collapse of ferromagnetism near the Tc is not just the result of an increased density of thermally excited spin waves, but the commensurate reduction of the exchange interaction as the magnetization approaches zero: the more magnons in the ferromagnetic spin system, the less energy it takes to add yet another magnon.

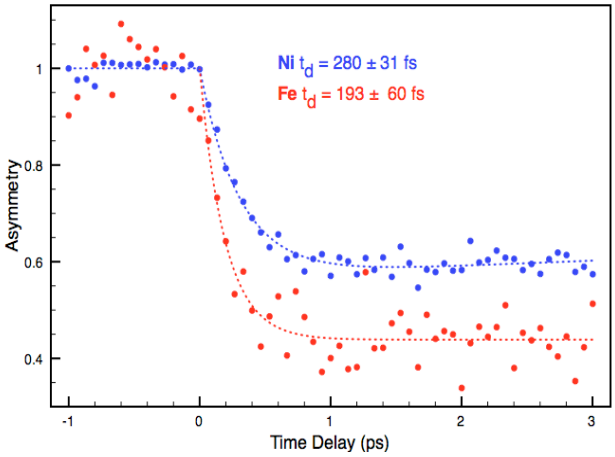

Figure 4. Time-resolved measurement of the femtosecond laser induced demagnetization of Cu-doped Permalloy (Curie temperature of 425 K). There is an evident difference between the two elements Fe and Ni.

As the ferromagnetic order is destroyed during the ultrafast demagnetization process, we expect a weakening of the exchange coupling that otherwise synchronizes the magnetization dynamics for Fe and Ni in the Cu-doped Permalloy film. If completely decoupled, the details of the demagnetization process depend solely on processes localized at each atomic site. Fig. 4 shows a a preliminary result demonstrating this behavior for Fe and Ni in Cu-doped Permalloy, where we see a 45% increase in the demagnetization time for Ni relative to Fe.

Future Plans

In the short term, we will investigate magnetization dynamics in ferro- and antiferromagnetic coupled multilayer devices and Heusler-alloys. We are also making nanoscale heat flow measurements and eventually imaging of magnetic nanostructures in collaboration with industry. In the longer term (≈ 3 years), we are developing a broadband high harmonic ultrafast soft x-ray source that spans the L absorption edges of magnetic materials (around 700-900eV). Image contrast, resolution, and transparency of many materials are all greatly improved at soft x-ray L-edge energies. Thus, imaging of buried magnetic structures, domain interactions, strongly coupled nanolayers, and spin dynamics will all be accessible with femtosecond and possibly even sub-femtosecond time resolution.

Publications

C. La-O-Vorakiat, M. Siemens, M. Murnane, H. Kapteyn, S. Mathias, M. Aeschlimann, P. Grychtol, R. Adam, J. Shaw, H. Nembach, T. Silva, *Ultrafast Demagnetization Dynamics at the M Edges of Magnetic Elements Observed Using a Tabletop High-Harmonic Soft X-Ray Source*, Phys. Rev. Lett. **103**, 257402 (2009).

X-ray Spectroscopy and Scattering Studies of Alloy Fuel Cell Catalysts

Anders Nilsson (Primary Contact), Michael Toney and Hirohito Ogasawara
Stanford Synchrotron Radiation Laboratory Division
Stanford Linear Accelerator Center
Menlo Park, CA 94025
Phone: (650) 926-2233, Fax: (650) 926-4100, nilsson@slac.stanford.edu

Peter Strasser
Dept. of Chemical and Biomolecular Engineering, University of Houston, 4800 Calhoun Ave. S226
Phone: (713) 743-4310, PStrasser@UH.EDU

Research Scope

- Develop new synchrotron radiation based x-ray diffraction and spectroscopy methods that allow in-situ probing of the intermediates in the oxygen reduction reaction (ORR) on the cathode in fuel cells where both species identification, geometric and electronic structure properties can be fully characterized.
- Gain insight into how various catalytic properties on Pt surfaces can be modified due to alloying.
- Perform combinatorial synthesis and high throughput electrochemical screening methodologies of alloy catalyst with different chemical compositions and structures to obtain optimum performance.

Recent Progress

While the oxidation of pure hydrogen is not considered a technical hurdle in fuel cells, the power loss at the cathode during the electroreduction of oxygen is found to be significant. Therefore the identification of a catalyst for the electroreduction of oxygen with improved performance is a major scientific priority. Pt has been the only metal which offers a good compromise in terms of performance and durability, and catalyst costs dominate at high Pt loading. Our goal is to understand the mechanistic pathway of the ORR reaction and to design new low Pt containing catalyst by optimizing the geometric and electronic structure of catalyst along the mechanistic pathway.

Novel alloy catalyst for fuel cell cathode reaction

Dealloying is the preferential dissolution of the electrochemical more reactive component from a bimetallic alloy (precursor) consisting of a less reactive (here Pt) and more reactive metal (here Cu). We have shown that dealloyed Pt-Cu nanoparticles show uniquely high catalytic reactivity for the oxygen reduction reaction (ORR) in fuel cell electrodes (1-3). Dealloyed Pt catalysts, however, meet and exceed the technological activity targets in realistic fuel. Owing to their reactivity, dealloyed Pt catalysts can reduce the required amount of Pt by more than 80%. Despite this importance, the mechanistic origin of their enhanced reactivity remains poorly understood.

We have shown based on a combination of electron microscopy, x-ray photoelectron spectroscopy and anomalous x-ray diffraction studies of dealloyed Pt-Cu catalysts (4) that a core-shell structure is formed during dealloying, which involves removal of Cu from the surface and subsurface of the precursor nanoparticles. X-ray diffraction shows that the resulting Pt-rich surface shell exhibits compressive strain that depends on the composition of the precursor alloy. Based on model electron and x-ray spectroscopy experiments of strained Pt films on Cu(111) the existence of a downward shift of Pt d-band resulting in a weakening of the bond strength of intermediate oxygenated species due to strain (see fig.1). Theoretical simulations of the fuel cell catalytic process also shows that strain enhance the overall reactivity via a weakening of the

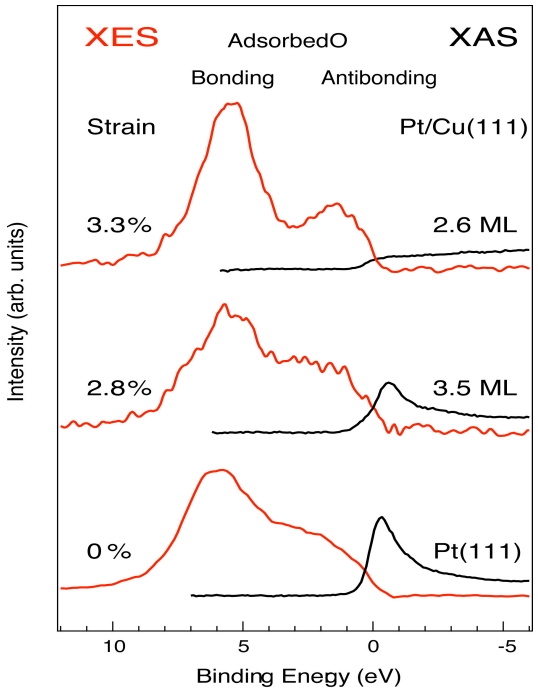

Figure 1 Electronic interactions between p-level of oxygen and the d-band in the metal results in the formation of bonding and antibonding states Thin layer of Pt on Cu(111) results in strained films and x-ray spectroscopy of adsorbed oxygen shows that this results in a weakening of the oxygen-metal bond through increased population of the antibonding states. This allows for oxygen to become more active for reactions with hydrogen at the cathode of the fuel cell.

oxygen adsorption bond strength. The stoichiometry of the precursor, together with the dealloying conditions, provides experimental control over the resulting surface strain and thereby allows continuous tuning of the surface electrocatalytic reactivity – a concept that can be generalized to other catalytic reactions.

To build on the above results and to better understand the structure-activity relationships in dealloyed Pt-alloy electrocatalysts, we have used uniform, single phase, polycrystalline Cu_3Pt thin films and single crystal $Cu_3Pt(111)$ as model catalysts for accurate characterization of structure and the resulting ORR activity enhancement. Anomalous x-ray diffraction (AXRD) is used to study the structure of the dealloyed Pt-Cu thin film (lattice constant and composition) (5). We have obtained a detailed understanding of the structure and composition relationships in these Pt-skeleton structures prepared by dealloying base metal rich alloy. Compositional inhomogeneity of the dealloyed films is observed with a Pt enriched surface region and Cu depleted interior. The composition of Cu depleted interior is different from that of as-deposited Cu_3Pt showing that dealloying of Cu occurs at the surface and proceeds into the interior, leaving a compressively strained Pt-enriched surface region as shown in Fig. 2. Work on single crystal $Cu_3Pt(111)$ is ongoing, but qualitatively consistent with the film studies.

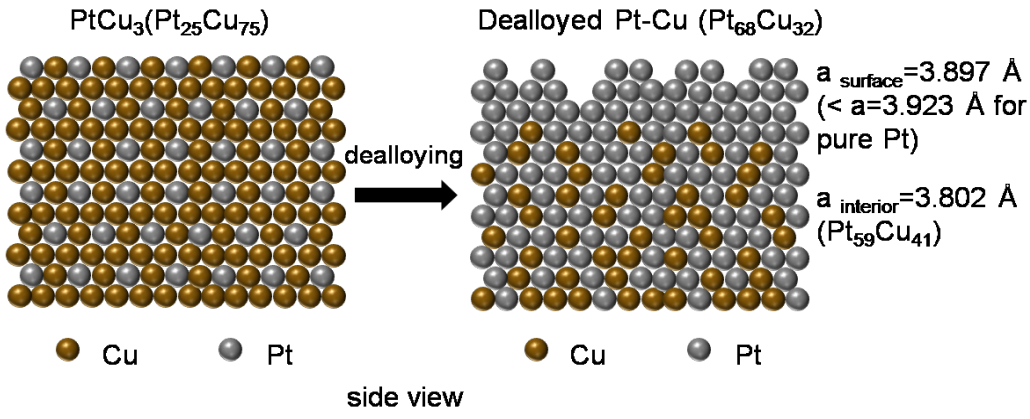

Figure 2. Schematic of the dealloying of $PtCu_3$ film.

Mechanistic understanding of fuel cell cathode reaction

In order to develop more efficient fuel cell catalysts it is essential that we can gain information regarding the nature of intermediate species during oxygen reduction reaction (ORR) that contribute to the sluggish kinetics. Hard x-rays penetrate several millimeters through electrolyte solutions, thus providing a unique capability for *in situ* x-ray absorption spectroscopy (XAS) studies of active fuel cell catalysts under electrocatalytic conditions. Of particular interest is determining the nature of Pt–O interactions at high potentials since this is essential for understanding the origin of the overpotential of the electrochemical oxygen reduction reaction (ORR). We have chosen to study a well-defined, simple model system, consisting of one monolayer Pt on a Rh(111) single-crystal surface. By tuning the energy to the Pt L_3 absorption edge this allows for the – intrinsically bulk sensitive – hard x-ray spectroscopy to probe only surface Pt atoms and their interaction with oxygen.

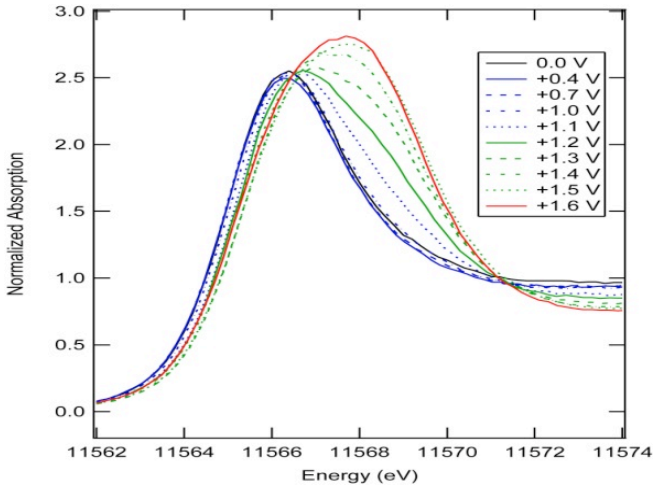

Figure 3. Pt L_3 edge high resolution fluorescence detection XAS spectra of 1ML Pt/Rh(111) in 0.01M $HClO_4$ as a function of increasing potentials.

Fig. 3 shows the L-edge x-ray absorption spectra (XAS) of a Pt monolayer on Rh(111) detected using High Energy Resolution Fluorescence Detection (HERFD), where the life time broadening of the Pt L-edge has been experimentally removed, resulting in much higher resolved spectral features (15). By using the L_3-edge, the unoccupied Pt 5d-states are probed. The intensity increase, broadening, and shift of the spectra with increasing potential have been identified, through theoretical spectral simulations, to result from the development of a Pt surface oxide. Complementary extended x-ray absorption fine structure (EXAFS) measurements have been carried out under identical conditions. Pt-Pt and Pt-O bond lengths and coordination numbers have been derived, confirming the interpretation of the growth of a surface Pt oxide. Weaker changes in the spectral features at lower potentials can be related to adsorbed hydrogen and to the presence of other oxygenated species.

Future Directions

We will continue the in-situ spectroscopy studies of the ORR of a single Pt monolayer to other substrates which are expected to bind oxygen stronger where we expect that the onset of Pt surface oxide formation will occur at lower potentials. We will also extend these studies to nanoparticles of Pt with different sizes since there is a hypothesis that small nanoparticles could induce oxide formation at lower potentials. We will also continue our effort to develop in-situ spectroscopic techniques to the soft x-ray regime. We will extend the studies of the dealloying process to Pt-Cu single crystals. We are currently exploring dealloyed bimetallic Pt systems other than Pt-Cu. Current studies focus on dealloyed PtCo3 and PtNi3. Dealloying behavior of these bimetallic compounds is unknown to date. Preliminary results suggest a similar core shell behavior for PtCo3 as found in PtCu3. PtNi3 showed less susceptibility to leaching. Future experiments will include morphological studies of dealloyed PtCo3 and PtNi3, monitoring of the compositional changes upon extended cycling protocols.

Publications (2008-2010)

1. Strasser, P. in Handbook of Fuel Cells:Advances in Electrocatalysis, Materials, Diagnostics and Durability, Vol. Volumes 5 & 6. (eds. W. Vielstich, H.A. Gasteiger & H. Yokokawa) 30-47 (John Wiley & Sons Ltd, Chichester, West Sussex, UK; 2009).
2. Strasser, P., Koh, S. & Greeley, J. Voltammetric Surface Dealloying of Pt bimetallic nanoparticles: An experimental and DFT computational analysis. *Phys. Chem Chem. Phys.* **10**, 3670-3683 (2008).
3. Koh, S., Hahn, N., Yu, C. & Strasser, P. Effects of Compositions and Annealing Conditions on the Catalytic Activities of Pt-Cu Nanoparticle Electrocatalysts for PEMFC. *J. Electrochem. Soc.* **155**, B1281-1288 (2008).
4. Strasser, P.: Shirlaine, K.: Anniyev, T.; Greeley, J.: More, K.; Yu,C.; Liu, Z.; Kaya, S.; Nordlund, D.; Ogasawara, H.; Toney, M.F.; and Nilsson, A. Lattice-strain control of exceptional activity in dealloyed core-shell fuel cell catalysts *Nature Chem.* **2**, 454 (2010).
5. Yang, R.; Leisch, J.; Strasser, P.; Toney M. F. Structure of Dealloyed PtCu3 Thin Films and Catalytic Activity for Oxygen Reduction, *Chem Mat*. **22**, 4712–4720 (2010).
6. H. Ogasawara L. Å. Näslund, J. McNaughton . Anniyev, and A. Nilsson, Double Role of Water in the Fuel Cell Oxygen Reduction Reaction, *ECS Transactions* **16**, 1385 (2008).
7. Yu, C., Koh, S., Leisch, J., Toney, M., Strasser, P. Size and composition distribution dynamics of alloy nanoparticle electrocatalysts probed by anomalous Small Angle X-ray Scattering (ASAXS). *Faraday Discussions, FD* **140**, 283-296 (2008) (selected as hot article !).
8. Mani, P.; Srivastava, R.; Strasser, P. Dealloyed Pt-Cu Core-Shell Nanoparticle Electrocatalysts for use in PEM Fuel Cell Cathodes. *J. Phys. Chem*. C,**112**, 2770-2778 (2008).
9. Srivasta, R.; Mani, P.; Strasser, P. In-situ Voltammetric Dealloying of Fuel Cell Catalyst Electrode Layer: A combined SEM/EPMA study. *J. Power Sources* **190**, 40-47 (2008).
10. Yamamoto, S;, Bluhm,H.; Andersson,K.; Kettler, G.,; Ogasawara, H.; Salmeron, M.; Nilsson, A.; In-situ X-ray Photoelectron Spectroscopy Studies of Water on Metals and Oxides at Ambient Conditions *J. Phys: Condensed Matter* **20**, 184025 (2008).
11. MacNaughton, J.; Näslund, L. Å; Anniyev, T. C; Ogasawara, H.; Nilsson, A.; Peroxide-like intermediate observed at hydrogen rich condition on Pt(111) after interaction with oxygen, *Phys. Chem. Chem. Phys*. **12**, 5712 (2010).
12. Anniyev, T.; Ogasawara, H.; Ljungberg, M. P.; Wikfeldt, K. T.; MacNaughton, J. B.; Näslund, L.-Å.; Bergmann, U.; Koh, S.; Strasser, P.; Pettersson, L. G.M.; Nilsson, A.; Complementarity Between High-energy Photoelectron and L-edge Spectroscopy for Probing the Electronic Structure of 5d Transition Metal Catalysts, Phys. Chem. Chem. Phys.**12**, 5694 (2010)
13. Schiros, T.; Takahashi, O.; Andersson, K. J.; Öström, H.; Pettersson, L. G. M.; Nilsson, A.; Ogasawara, H.; The Role of Substrate Electrons in Wetting of a Metal Surface, J. Chem. Phys. **132**, 094701 (2010).
14. Schiros, T.; Ogasawara, H.; Näslund, L. Å.; Andersson, K. J.; Ren, J.; Meng, Sh.; Karlberg, G. S.; Odelius, M.; Nilsson, A.; Pettersson, L. G. M.; Cooperativity in Surface Bonding and Hydrogen Bonding of Water and Hydroxyl at Metal Surfaces, J. Phys. Chem. C **114**, 10240 (2010).
15. Friebel, D.; Miller, D. J.; O'Grady, C. P.; Anniyev, T. C., Bargar, J.; Bergmann, U.; Ogasawara, H., Wikfeldt, K. T.; Pettersson, L. G. M.; Nilsson, A. In-situ probing reveals the importance of surface platinum oxide formation, Phys. Chem. Chem. Phys. in press.
16. Miller, D. J.; Öberg, H.; Näslund, L. -Å.; Anniyev, T.; Ogasawara, H. ; Pettersson, L. G. M.; Nilsson, A.; Low O_2 Dissociation Barrier on Pt(111) due to Adsorbate-Adsorbate Interactions, submitted.

Directed Self-Assembly of Soft-Matter and Biomolecular Materials

Benjamin Ocko (ocko@bnl.gov), Antonio Checco (checco@bnl.gov) and
Masa Fukuto (fukuto@bnl.gov)
Brookhaven National Laboratory, Upton, NY 11973

Program Scope: The primary goal of the group is to understand the effects of nanoscale confinement and the role of self-assembly in soft materials through the use of patterned templates and well-defined interfaces. We use synchrotron x-ray scattering, scanning probe and optical microscopy techniques to study fundamental properties of complex fluids, simple liquids, macromolecular assemblies, liquid crystals, polymers, and biomolecular materials. The challenges are (1) to understand liquids under nano-confinement, (2) how templates and confinement can be used to direct the assembly of biomolecular materials and diblock copolymer thin films, (3) to understand the fundamental interactions which give rise to similar self-assembly behavior for a wide variety of systems, (4) how the order correlates with function. Understanding structural aspects of self-assembly and thin organic films underlies many emerging organic based devices and energy technologies. Our approach uses two complementary structural probes, x-ray scattering and AFM. An important aspect of our approach is to use nanopatterned surfaces to confine liquids and complex fluids. To accomplish this, we are using polymer based self-assembly techniques and AFM based local-oxidation nanolithography. The program integrates experimentalists with a dedicated history of collaboration in liquids, wetting, biomaterials, and synchrotron-based structure characterization.

Recent Progress:

A. Biomolecular materials: One of our main efforts is focused on lipid monolayer-mediated 2D assembly of biomolecular nanoparticles (BNPs) at liquid interfaces. A major challenge of nanoscience has been to identify and understand what physical parameters promote long-range order in the assemblies of nanoscale objects. Arrays of BNPs, i.e., proteins and virus particles, formed at the lipid membrane-aqueous solution interface are well suited to investigating ordered assembly in 2D because of the intrinsic monodispersity of BNPs as building blocks, the use of a fluid-phase lipid monolayer to promote the mobility of interface-confined BNPs, and the ability to tune the BNP-BNP and BNP-surface interactions through chemical compositions in the buffer and in the lipid membrane. Our recent progress in this research area includes

- *2D assembly of Tobacco Mosaic Virus (TMV) on cationic and zwetterionic lipid monolayers.* In-situ GISAXS, AFM, and optical microscopy measurements have been carried out at the substrate-liquid and liquid-vapor interfaces. The results demonstrate that the in-plane mobility of the interface-bound TMVs and the presence of divalent cations (Ca^{2+}) are essential to developing structural order, consisting of close packing and alignment of these "nanorods" lying parallel to the interface. Quantitative analysis of the GISAXS data shows that the structure of the TMV arrays in the absence of Ca^{2+} is consistent with purely repulsive, electrostatic inter-particle interaction. By contrast, the structural order within Ca^{2+}-induced TMV assemblies is consistent with the behavior of a fluid of sticky rods, implying the presence of strong attraction between TMVs.
- *2D assembly of streptavidin (SA) on a Langmuir monolayer of biotin-bearing lipids.* The results of in-situ XR, GID, and optical microscopy measurements demonstrate that the adsorption and 2D crystallization of SA depend sensitively on the surface biotin density. The minimum biotin density required for the 2D crystallization of SA is found to be remarkably close to the density of the ligand-binding sites in the protein crystal. Moreover, the measured protein adsorption isotherm is consistent with the predominance of the doubly-bound SA over the singly-bound SA, both above and below the threshold biotin density. These results imply

that even in the low-density noncrystalline phase, the bound proteins share a common, fixed orientation relative to the surface normal, and that dense packing of these already well-oriented proteins is the driving mechanism for the 2D crystallization of SA.

B. Fundamental aspects of surface induced order at liquid interfaces: Understanding interface-induced order is relevant to many fields including those used in molecular electronic and photovoltaic devices. We have had a long-standing program to understand interface-induced ordering of simple molecular and atomic systems. One of the most elegant examples is surface freezing in alkanes where a crystalline phase forms up to 3˚C above the bulk melting transition. We have also investigated interfacial freezing in Langmuir-Gibbs films, surface freezing at the oil/water interface, surface induced ordering at the vapor interface of liquid metals and alloys. More recently we have investigated electrocapillary effects at the mercury/electrolyte interface, surface induced ordering of mercury, ionic liquids and long-chain alcohols at the sapphire interface. Two highlights of these studies are presented below:

- *Surface freezing of long-chain alcohols at the sapphire interface:* X-ray reflectivity measurements have been carried out to determine the structure of the deeply-buried interface between a bulk alcohols (CnOH), for $12 \leq n \leq 20$, and a solid surface, sapphire, (0001). Over a range of temperature (about 30 ˚C) above the freezing point of the alcohol an extremely well defined monolayer is stable at the solid interface, with surface-normal, rather than surface-parallel, molecules. After disordering of the layer at higher temperature, the ordered layer is reformed by cooling. This reversible formation of an interfacial monolayer is reminiscent of surface freezing at the vapor interface where the much larger temperature range for the solid interface is consistent with the much stronger surface interaction.
- *Thin-thick coexistence behavior of liquid crystalline films on silicon:* As the thickness of an adsorbed film is reduced the stresses within the films can lead to stable coexistence of thick and thin films on the surface. We have conducted X-ray reflectivity measurements to study the effect of varying the thickness of 8CB liquid crystalline films on a flat silicon surface. Our measurements show the existence of a temperature-thickness phase diagram with a novel reentrant region, where thick and thin films coexist on the silicon surface.

C. Nanoliquids*: A main research effort of the BNL's Soft Matter Group* focuses on the study of the equilibrium and out-of-equilibrium wetting behavior of nanoscale liquids. Our unique experimental approach to the problem is based on the use of nanopatterned surfaces to confine liquids within nanometer-scale structures. The effects of confinement and long-range interactions between the liquid and the nanostructured substrate may lead to substantial deviations from the macroscopic wetting behavior. In situ X-ray scattering and AFM are then used to study the morphology of the confined nanoliquids which are then compared to recent theoretical models. Our recent progress in this research area includes:

- *Wetting of topologically nanopatterned surfaces.* Silicon surfaces were nanopatterned with an array of parallel, ~20 nm-wide trenches by using state of the art electron-beam lithography (Hitachi collaboration) or with hexagonal array of ~20 nm-sized parabolic cavities using diblock-copolymer lithography. The wetting of simple liquids (perfluoromethylcyclohexane, cyclohexane) on the nanopatterned surfaces was studied using transmission X-ray scattering measurements as a function of the chemical potential (temperature) difference between the substrate and a liquid reservoir contained in a hermetically sealed chamber. These measurements have provided the amount of liquid condensed in the nanocavities with unprecedented accuracy and therefore a stringent test for current theories of wetting on the nanoscale. Our result confirm the validity of continuum, mean field models with dispersive interaction potential for describing wetting phenomena at a ~10 nm length-scale.
- *Wetting of chemically nanopatterned surfaces.* We have studied the wetting of liquid nanodrops of cyclohexane and ethanol on chemically nanopatterned stripes (50-1000 nm

wide) prepared using oxidation nanolithography. The equilibrium shape of the nanodrops was investigated using non-contact AFM. The measured power law dependence of the height of the liquid drops versus the stripe width confirms the long-standing prediction that the shape of the drops is controlled by the dispersive (Van der Waals) potentials.

- *Directed Assembly of Block Copolymers:* These same chemical patterns have also been used to direct the dewetting of polymer thin films into structures of complex shapes in order to study the effect of the lateral confinement on the spatial orientation of diblock copolymer microdomains, so called graphoepitaxy. The combined sectoring and self-assembly provides a unique route towards a guided self-assembly of BCP films with long-range order that may be used to fabricate sectored, high-density arrays of nanoscopic elements suitable as templates for device applications.
- *Deliquescence of model aerosol nanoparticles.* The wetting of nanoscale atmospheric aerosols by water is relevant for improved climate models. To gain insight into this phenomenon we have studied the hygroscopic growth of "model" aerosols particles (cubic NaCl crystals) deposited on a prepared hydrophobic surface using non-contact environmental atomic force microscopy (AFM). Results show that the nanoparticles (sized between 35 and 150 nm) reversibly adsorbed a 2–4 nm thick layer of water at values of relative humidity slightly (~5%) below the deliquescence point. These findings suggest that significant reorganization of mass near the interface of water and solid NaCl occurs at RH-values near 70%. Current physical models of the RH-dependent properties of hygroscopic aerosols may underestimate (i) particle size and (ii) salt-content of the liquid "shell" prior to deliquescence.

Future Plans:

In addition to the projects discussed above, many of which are ongoing, we highlight some additional research plans below. In the area of biomolecular materials, we will extend the approach of the lipid-mediated 2D assembly to sphere-like virus particles, such as cowpea mosaic virus (CPMV), and explore the effects of the chemical environment, such as pH, ionic strength, type of ions, and lipid charge density. In the area of surface induced ordering, we intend to study the surface freezing of alcohols at the sapphire interface to mixtures, both of alcohols of different length and diols (two sided alcohols) with alcohols. At the vapor interface, we will investigate surface induced ordering of ionic liquids. In the area of nanoliquids, we will extend our studies of wetting phenomena to various chemically and topographically patterned surfaces with the aim of reducing the feature sizes so as to better test existing theories. The studies on the effect of lateral confinement on spreading will be extended to complex liquids (such as polymers and liquid crystals) where anomalous behavior is expected. We have started a program to improve our understanding of the structure and phase separation in organic electronic materials and organic photovoltaic devices. Specifically, we will extend our initial studies of temperature-dependent solvent annealing to include nano-imprinted polymer films. The Group has spear headed the proposal for the Soft Matter Interfaces (SMI) undulator beamline at NSLS II. This effort has recently received a very favorable review from the NSLS Science Advisory Committee (SAC) and SAC Study Panel. It is envisioned that the Group's future plans will greatly benefit from this new facility.

DOE Sponsored Publications (2008-2010)

Morphology and phase behavior of ethanol nanodrops condensed on chemically patterned surfaces, Checco, A. and Ocko, B.M., Phys. Rev. E **77,** 061601 (2008).

Extended molecular layering of a pyrrolidinium-based ionic liquid at the sapphire(0001) surface, Mezger, M., Schroeder, H., Reichert, H., Schramm, S., Okasinski, J., Schoeder, S., Honkimaki, Deutsch, M., Ocko, B.M., Ralston, J., and Dosch, H., Science **322**_424-428 (2008).

In-Situ X-ray Reflectivity Studies on the Formation of Substrate-Supported Phospholipid Bilayers and Monolayers, S. T. Wang, M. Fukuto, and L. Yang, Phys. Rev. E **77**, 031909 (2008).

Thin-Thick Coexistence Behavior of 8CB Liquid Crystalline Films on Silicon, R. Garcia, E. Subashi, and M. Fukuto, Phys. Rev. Lett. **100**, 197801 (2008).

Comment on "How Water Meets a Hydrophobic Surface". B. M. Ocko, A. Dhinojwala, and J. Daillant, Phys. Rev. Lett. **101**, 039601 (2008).

Post assembly chemical modification of a highly ordered organosilane multiplayer: New insights into the structure, bonding, and dynamics of self-assembling silane monolayers, Wen, K., Maoz, R., Cohen, H., Sagiv, J., Gibaud, A., Desert, A., and Ocko, B.M. ACS Nano **2**, 579-599 (2008).

Dynamics and critical damping of capillary waves in an ionic liquid, Sloutskin, E., Huber, P., Wolff, M., Ocko, B.M., Madsen, A., Sprung, M., Schon, V., Baumert, J., and Deutsch, M. Phys. Rev. E **77**, 060601 (2008).

Wetting of Liquid-Crystal Surfaces and Induced Smectic Layering at a Nematic-Liquid Interface: An X-ray Reflectivity Study, M. Fukuto, O. Gang, K. J. Alvine, B. M. Ocko, and P. S. Pershan, Phys. Rev. E **77**, 031607 (2008).

Non-linear eleasticity of a liquid contact line. A. Checco, Europhys. Lett. **85**, 16002 (2009).

Liquid spreading under nanoscale confinement, A. Checco, Phys. Rev. Lett., **102,** 106103 (2009).

Grazing incident small angle x-ray scattering: a metrology to probe nanopatterned surfaces, Hofmann, T., Dobisz, E. and Ocko, B, J. Vac. Sci. Technol**. 27**, 3238 (2009).

Lateral ordering of cylindrical microdomains under solvent vapor. Park, S., Kim, B., Xu, J., Hofmann, T., Ocko, B., and Russell, T. Macromolecules **42**, 1278 (2009).

Equilibrating nanoparticle monolayers using wetting films, Pontoni, D., Alvine, K.J., Checco, A., Gang, O., Ocko, B.M., and Pershan, P.S. Phys. Rev. Lett. **102**, 016101 (2009).

Structure and Interaction in 2D Assemblies of Tobacco Mosaic Viruses, L. Yang, S. T. Wang, M. Fukuto, A. Checco, Z. Niu, and Q. Wang, Soft Matter **5**, 4951 (2009).

Effects of Divalent Cations on Phase Behavior and Structure of a Zwitterionic Phospholipid (DMPC) Monolayer at the Air-Water Interface, Kewalramani, S., Hlaing H., Ocko, B.M. Kuzmenko, I., Fukuto, M., J. Phys. Chem. Lett. **1,** 489 (2010).

Atomic-Scale Structure of a Liquid Metal-Insulator Interface, Tamam, L., Pontoni, D., Ocko, B.M., Reichert, H. and Deutsch, M.D.. J. Phys. Chem. Lett. **1,** 1041 (2010).

Effects of surface ligand density on lipid-monolayer-mediated 2D assembly of proteins, Fukuto, M., Wang, S.T., Lohr, M.A., Kewalramani, S., and Yang. L, Soft Matter **7,** 1513 (2010).

Formation and Collapse of Poly(n-Butyl Acrylate) Homopolymer Monolayers at the Air-Water Interface, K. N. Witte, S. Kewalramani, I. Kuzmenko, W. Sun, M. Fukuto, and Y.-Y. Won, Macromolecules **43**, 2990 (2010).

Morphology of Air Nanobubbles *Trapped at Hydrophobic Nanopatterned Surfaces*, Checco, A., Hofmann, T., DiMasi, E.D., Black, C.T., and Ocko, B.M. Nano Letters **10**, 1354 (2010).

Direct self-assembly of Block copolymers in 2D chemical patterns fabricated from Electro-oxidation nanolithography, J. Xu, S. Park, T.P. Russell, A. Checco, and B.M. Ocko, Adv. Mat, **22**, 2268 (2010).

Surface Layering at the Mercury-Electrolyte Interface, Eisen, A., Murphy, B.M.. Ocko, B.M., Taman, L., Deutsch, M.D., Kuzmenko, I., and Magnussen, O.M. Phys. Rev. Lett. **104**, 105501 (2010).

X-ray and neutron microbeam studies of deformation structure and magnetic phases

Judy W. L. Pang, G.E. Ice, E. D. Specht, and J. D. Budai

Oak Ridge National Laboratory, Oak Ridge TN 37831-6118

Pangj@ornl.gov, Icege@ornl.gov, SpechtED@ornl.gov, BudaiJD@ornl.gov

Research Scope

In this research task, we combine x-ray and neutron microbeam methods (see abstract by Ice et al.) to study deformation structures in structural materials. We have already made measurements of bulk, inter- and intra-granular strains and deformation structure and how they are accommodated in polycrystalline materials with anisotropic elastic behavior. These measurements provide new information about stress accommodation at the sub-grain level (see recent progress). We will extend our study by applying 3D neutron microscopy technique to measure the full elastic and plastic strain tensors with ~50μm spatial resolution using energy sensitive neutron detectors.

The availability of focused neutron beams also opens up the possibility of small sample studies in extreme environments. In particular lattice spacing (pressure) is a critical parameter in emerging theories of 3*d* alloy behavior. We are developing a research task to understand the origin of the complex magnetic behavior and its relation to chemical order in 3*d* alloys using state of the art first principles calculations and experimental instrumentations. By utilizing sub-100 μm neutron beams on the high pressure beamline SNAP at the SNS, the volume dependence of the spin states, spin correlation and fluctuation of 3*d* alloys can be investigated directly by applying pressure in the range of tens of GPa. The experimental work will be complemented by first principles electronic structure calculations that are just now practical.

Recent Progress

Deviation of deformation behavior due to intra-granular effects at the near- surface of single crystals and inside the grains of polycrystals have been studied by x-ray microbeam diffraction. Spatial correlation of the local lattice rotations in 8% tensile deformed Cu single crystals oriented with [123], [111] and [001] axes parallel and perpendicular to the tensile axis were investigated. The nondestructive depth-resolved measurements were made over a length scale of one to hundreds of micrometers. Self-affined correlation was found both at the surface and below the surface of the samples. A universal exponent for the power-law (Hurst exponent for fractal structure) is found at the surface of all samples but crystallographically sensitive changes are observed as a function of depth (Fig. 1). These measurements illuminate the transition from surface-like to bulk-like deformation behavior and provide new quantitative information to guide emerging models of self-organized structures in plasticity.

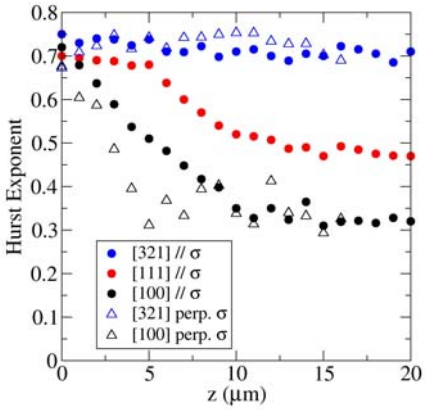

Fig. 1. Hurst exponent H for the three Cu samples as a function of depth z.

Constraints imposed by neighboring grains further complicate deformation behavior of polycrystals compared to single crystals. Although micromechanical simulations of polycrystalline deformation include the role of local grain morphology and elastic anisotropy, ensemble-averaged measurements *do not* provide local environment sensitivity. We have initiated combined neutron and x-ray measurements that investigate the importance of the local grain environment, and illustrate the need for spatially-resolved *full strain tensor* information with intra-granular resolution. Residual strain measurements were performed on 20 and 200 μm grain-size tensile-strained Ni samples with weak cube texture. Fig. 2 shows the neutron diffraction line profile for the 20 μm grain-size, 10% tensile-strained Ni sample. It also shows spatially-resolved 3D x-ray microscopy measurements of intra- and inter-granular strain performed in 10 separate grains. We note that *intra- and inter-granular strain fluctuations are up to 5 times larger than the Δd/d =0.0014 ensemble-average residual strain from the neutron measurements*. These spatially resolved measurements underscore the notion that obtaining a fundamental understanding of polycrystal deformation will require a close connection between such measurements and advanced micromechanical modeling using local grain morphology. Moreover, it will be important to develop techniques for obtaining full strain tensor information with spatial resolution. Although the high-energy, monochromatic, 3DXRD measurement technique provides the capability for grain-average determinations of the full strain tensor, intra-granular strain tensors are not available.

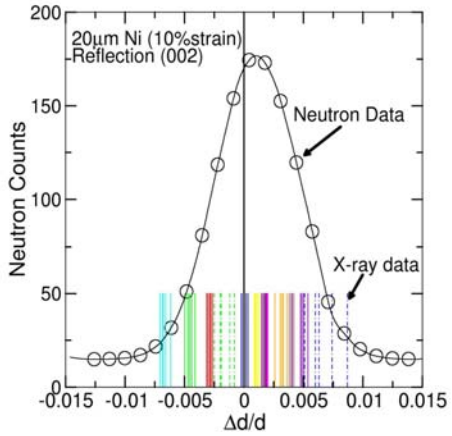

Fig.2. Intra- and inter-granular residual strains measured by x-ray microscopy. Color of the vertical lines denotes a particular grain and the spread in each color denotes intra-granular variation of strain; dashed lines are near grain boundaries.

Future Plans

Neutron microscopy investigation of polycrystalline deformation and structure in 3D:

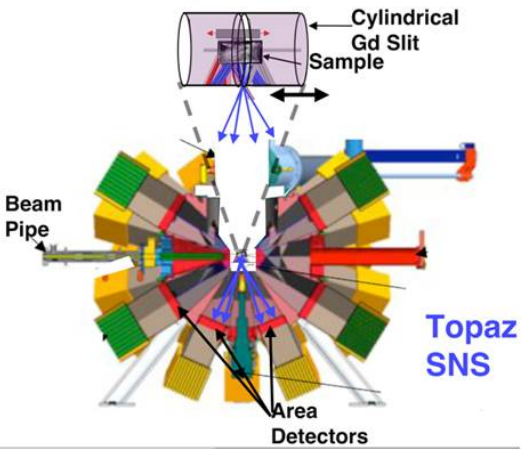

Fig. 3. Geometry for 3D neutron microscopy on the TOPAZ beamline at the SNS.

Measurements of the full elastic and plastic strain tensors within the microstructure of deformed materials are not possible with 3D-XM because energy resolving area detectors do not exist. However, 3D neutron microscopy (3D-NM) under development by Ice et al. at the SNS ,will provide this capability. By surrounding the sample with a cylindrical traveling 50 μm Gd slit at the SNS single crystal diffractometer TOPAZ (Fig. 3), the Laue diffraction pattern from the pulsed, white neutron beam is depth resolved as the cylindrical slit is passed through the Laue

pattern and the pattern is energy-resolved by time-stamped Auger area neutron detectors.

To develop and provide the first demonstration with sub-100 μm, subgrain deformation distributions deep within polycrystalline, 10% tensile-strained Ni with ~200 μm grain size (studied with conventional neutron powder diffraction and 3D x-ray microscopy by Pang et al.) will be investigated. Deformation within and around single grains, including the boundary conditions imposed by the morphology of surrounding grains will be probed. Plastic deformation and elastic strain tensor measurements will be used to make direct quantitative tests of crystal deformation models. These neutron microscopy measurements will be both complementary to and synergistic with present 3D x-ray microscopy deformation investigations.

Investigating the relationship between magnetic and atomic structures of 3d transition alloys:

Magnetic states of transition metals are complex because of the partially-filled d-shells and have been of long-standing research interests both experimentally and theoretically. Indeed, the underpinning of many applications of 3*d* alloys is based on the volume dependence of the correlation functions for magnetic moments and chemical order (atomic configuration), see Fig. 4. The interdependence of magnetization, short-range chemical order, atomic displacements and thermodynamics and their roles in determining phase stability and properties of the 3*d* alloys was investigated in the 70-80s. Although progress was made, conclusions that could be drawn from magnetic diffuse scattering experiments are limited by the absence of first principle (FP) spin dynamics (SD) and molecular dynamics (MD) calculations, albeit such knowledge is essential in the fundamental understanding of the thermal, mechanical, and field-dependent behaviors of 3*d* alloys.

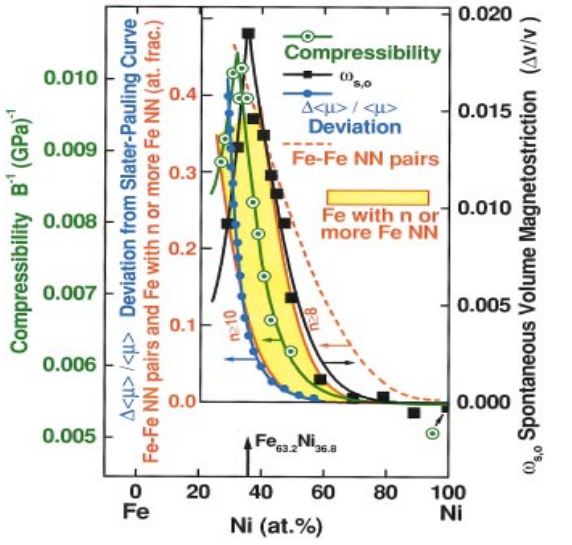

Fig.4. The concentration dependence of the compressibility, volume magnetostriction, and deviation from the Slater-Pauling curve are plotted to show the correlation with the fraction of Fe-Fe NN pairs and even stronger correlation with the fraction of Fe atoms with $n \geq 8$ Fe NN.

The advance of large scale computing in the last two decades has transformed FP-SD simulations. Although there are still limitations in FP-SD simulations, the situation is rapidly changing. For example, the ground state of bcc-Fe has been correctly determined by GGA-DFT (generalized gradient approximation-density functional theory) simulation, but it is not yet possible to correctly simulate the ground state of Cr using the same framework. New theoretical capabilities for calculating magnetic ground states involving quantum Monte-Carlo (QMC) and exact exchange derived functionals are being developed in the *Theoretical Studies of Formation, Stability, and Properties of Low-Dimensional Materials Program at ORNL*. These computational advances together with important experimental advances such as sub-100 μm neutron beam focusing optics, new high-efficiency polarizing optics, and ~100 GPa pressures to be available on the high pressure beamline SNAP at the SNS create the opportunity to seriously address 3*d* transition element materials physics at a new level.

The most direct approach to study the volume dependence of magnetic state and its transition is by performing high-pressure (tens of GPa) neutron experiments to determine the spin correlation and the spin local fluctuation as volume decreases. However the conventional requirement of large samples (~ cm^3) had slowed progress. Magnetic state transitions were usually studied as a function of temperature instead. Use of sub-100 μm focused beam is advantageous for small samples (<10^{-3} mm^3) and also improves the signal-to-noise and reduces multiple Bragg scattering which is important for diffuse scattering.

We will study the magnetic states of 3*d* alloys under high pressure using polarized neutron analysis. All the information of a magnetic structure: total and local moments, spin density, spin orientation, spin-spin and spin-nuclear correlations, and spin fluctuations; can be obtained by magnetic Bragg and diffuse scattering experiments with polarized neutrons. We will begin by studying permalloy $Fe_{80}Ni_{20}$ and Invar $Fe_{65}Ni_{35}$ single crystals, for which the local atomic arrangements have already been determined by our group using x-ray diffuse scattering. These experiments will establish the evolution of spin states as volume changes. Theoretical calculations by Stocks et al. will be used in the data analysis. Large array QMC calculations will be carried out using experimental chemical short-range-order information. This major theoretical undertaking demands a coordinated experimental effort for validation and guidance.

The experimental program will be expanded to other techniques such as small-angle neutron scattering, quasi-elastic scattering, x-ray diffuse and inelastic scatterings as guided by initial measurements on SNAP and theoretical simulations. Other than the ferromagnetic Fe-Ni systems, Fe-based alloys with other 3*d* elements such as Fe-Mn, Fe-Cr, and spin glass Cu-Mn, will also be studied. All these systems have interesting but distinct properties. The task is designed to achieve a broad understanding of the complex magnetic and thermo-mechanical behaviors of a wide range of 3*d* alloys with different chemical orders at the atomic level.

Publications

Judy Pang, G. E. Ice, and W. Liu, "The role of crystal orientation and surface proximity in the self-similar behavior of deformed Cu single crystals," accepted by *Mater. Sci. Eng., A*, August 2010, (available online).

G. E. Ice and Judy Pang, "Polychromatic X-Ray Microdiffraction Studies of 3D Elastic and Plastic Strain Tensors," *Challenges in materials science and possibilities in 3D and 4D characterization techniques*, Eds. N. Hansen, et al., pp. 279-284 (September 2010).

G. E. Ice, and J. W. L. Pang, 'Tutorial on x-ray MicroLaue Diffraction', *Materials Characterization*, **60**, 1191 (2009).

G. E. Ice, J.W.L. Pang, B.C. Larson, J.D. Budai, J.Z. Tischler, J-Y Choi, W. Liu, C. Liu, L. Assoufid, D. Shu[c] and A. Khounsary, "At the limit of polychromatic Microdiffraction," *Mater. Sci. Eng.* **524**, Issue 1-2, pp. 3-9 (2009).

T. Ohashi, R. Barabash, J.W.L. Pang, G.E. Ice, O.M. Barabash, 'X-ray microdiffraction and strain gradient crystal plasticity studies of geometrically necessary dislocations near a Ni bicrystal grain boundary', *International Journal of Plasticity*, **25(5)**, 920 (2009).

Temperature dependent structural heterogeneity in liquids.

J.B. Parise[1,2], J.K.R. Weber[3], C.J. Benmore[4]

[1]Stony Brook University, Stony Brook, NY; john.parise@sunysb.edu, [2]Light Source Division, Brookhaven National Laboratory, Upton NY; jparise@bnl.gov, [3]Materials Development, Arlington Heights, IL; rweber@matsdev.com, [4]Argonne National Laboratory, IL 60439; benmore@anl.gov

Probing the structure of non-equilibrium melts and supersaturated solutions is important to advance the fundamental understanding of liquids and glass formation, materials processing and development of new materials. Bulk liquids are often regarded as structurally homogeneous materials partly due to their inherently disordered nature and also because many of their properties can be modeled by a uniform continuum. However, we show [1] static and fast cooling high-energy synchrotron x-ray structure factor measurements performed on aerodynamically levitated $CaSiO_3$ droplets, which are consistent with the existence of a heterogeneous liquid state. Upon cooling the high temperature liquid, diffraction isosbestic points are observed in the pair distribution function (PDF), and evidence of the polymerization of edge shared Ca octahedral is observed. This behavior is linear in the high temperature melt but exhibits rapid growth just above the glass transition temperature around 1.2Tg. The heterogeneous liquid interpretation is supported by molecular dynamics (MD) simulations, which show the $CaSiO_3$ glass has more edge-shared polyhedra and fewer corner shared polyhedra than the liquid model. On-going work suggests heterogeneity in under-cooled liquids may be a general phenomenon.

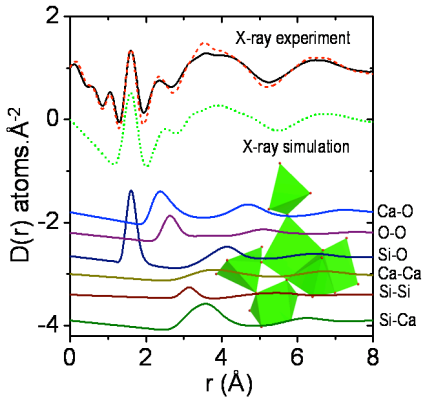

Figure 1. Top: Differential distribution functions, D(r), for liquid $CaSiO_3$ at 1900°C (solid black line) and 1033°C (dashed red line). **Middle:** Molecular Dynamics simulation of $CaSiO_3$ melt at 3700°C (dotted line) Fourier transformed over the identical Q-range to the experiment with same Lorch modification function. **Bottom :** Faber-Ziman x-ray weighted partial distribution functions for the $CaSiO_3$ melt at 3700°C taken directly from the simulation scaled by 0.6 and offset for clarity. A cluster of corner and edge shared Ca polyhedra from the MD simulation are shown in the backdrop.

Approaching the glass transition, dynamic heterogeneity has been observed around the crossover from 'normal' liquid to 'complex' solid like properties [2] which coincides with a similar crossover from mode coupling theory at a temperature of T=1.2Tg between a primarily 'ergodic' liquid to a mainly 'non-ergodic' glassy regime [3]. Unlike dynamic heterogeneity, structural heterogeneity in a liquid at the atomic level is difficult to establish and to our knowledge there has been no definitive evidence for structural heterogeneity occurring in the PDFs of glass forming liquids [3]. This is despite the fact the analysis of some quenched glass structures indicates that atomic to nanometer scale structural heterogeneity occurs in the liquid state [4].

Silica is classified as a strong liquid with an Arrhenius viscosity-temperature relation and only subtle differences occur between the liquid and glass structures [5]. In contrast $CaO\text{-}SiO_2$ liquids can be considered fragile based on viscosity measurements [6] and consequently larger structural re-arrangements are likely to be necessary to form a glass. The real space PDFs $D(r)=4\pi\rho r[G(r)-1]$ with the bulk density removed were measured for liquid $CaSiO_3$ at 1900°C and 1033°C (melting point T_m=1540°C) and are shown in figure 1. Previous x-ray measurements on the glass [6], have established the presence of SiO_4 tetrahedra and the CaO peak at ~2.43±0.02Å. The structure of the glass at a composition close to $CaSiO_3$ (with the addition of 3% Al_2O_3) has been studied in exceptional detail using a double difference neutron isotopic substitution method [4]. Gaskell *et al* [4] provided evidence that the distribution of calcium atoms was not random in the glass, but exhibited a well defined Ca-Ca peak at 3.8Å bearing many characteristics of the crystalline form. The structures of crystalline pyroxenes such as wollastonite can be considered as

a close packed oxygen sub-lattice with Ca occupying octahedral interstices in alternate layers in a fcc model. This structure has distinguishable domains comprising of sheets of edge shared CaO_6 octahedra which are parallel and interleaved with linked SiO_4 tetrahedra. Although the recent model by Mead and Mountjoy [7] and our MD simulations show that the Ca polymerization need not be quasi-crystalline in nature and branched winding chains of CaO polyhedra are also consistent with the diffraction data.

THE HIGH TEMPERATURE LIQUID STATE.

Diffraction isosbestic points (DIPs), introduced by Johnson [8], to explain the linear dependence of the differential distribution function with concentration in Se-rich $Si_xSe_{(1-x)}$ glasses, have been associated with a two state liquid system using optical spectroscopy. DIPs are common points in the diffraction pattern and Tse *et al* [9] have extended Johnson's [8] ideas to argue that a system exhibiting these points as a function of temperature can be interpreted in terms of a two state model. We note that since all of our data were Fourier transformed at the identical value of Q=19 $Å^{-1}$ with a Lorch modification function this does not enter into the analysis. Furthermore, although DIPs for T>1000^{0}C are observed directly in the differential distribution functions, D(r), they become much more apparent in the difference function $\Delta D(r)=D_T(r)-D_0(r)$ shown in figure 2, where the highest temperature $D_0(r)$ at 1900^{o}C has been subtracted. DIPs are observed for liquid $CaSiO_3$ (T>1000^{0}C) at 1.48, 1.63, 2.15, 2.52, 3.13, 4.47, 5.80, 7.28 Å. For calcium silicate liquids we argue that Johnson's clustered unit model applies in this temperature regime in the form of aggregation of Ca-rich atom regions (by analogy with the compositional dependence in [8]). Based on the peaks in the liquid diffraction data for $CaSiO_3$ this implies the existence of two distinct domains on a length scale of ~3-18 Å: One domain comprising of edge shared CaO_6 octahedra and the other a mixture of CaO polyhedra and SiO_4 tetrahedra, these domains are presumably corner-shared by oxygen atoms at the interface. For temperatures Tg<T(^{0}C)<1000 the DIPs are no longer observed, consistent with the transition from normal to complex behavior around T=1.2T_g [2]. The onset of solid glass like behavior is associated with rapid peak growth associated with Ca polymerization with decreasing temperature. It is important to note that the existence of isosbestic points do not definitively prove the system is two phase; the sharpening of intra-molecular correlations in a molecular liquid upon cooling for example, could also produce the same effect due to narrowing zero point motions. However, strong arguments for the heterogeneous clustered unit model can be made due to the observation of the increased number of edge shared CaO octahedra upon cooling liquid $CaSiO_3$ and because of the supporting evidence from MD simulations.

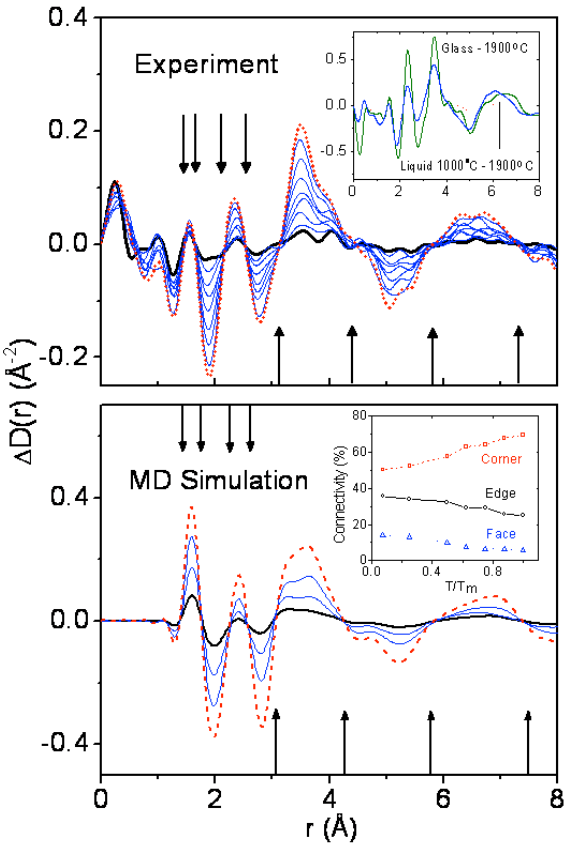

Figure 2. Top : Differences between the experimental liquid D(r)'s for 1033^{o}C minus 1900^{o}C (red dashed line), and 1800^{o}C minus 1900^{o}C (thick black solid line). The thin blue lines in between these extremes represent the D(r) differences in ~100^{o}C increments. The diffraction isosbestic points are marked with arrows (see text). **Insert:** shows the $\Delta D(r)$'s for the liquid at 1033^{o}C minus 1900^{o}C (dashed red line), 800^{o}C minus 1900^{o}C (thin blue solid line) and the room temperature glass minus 1900^{o}C (thick green solid line). **Bottom.** Differences between the model liquid D(r)'s taken from the MD simulations for 0.5 minus T_m (red dashed line), 0.625T_m minus T_m and 0.75T_m minus T_m (thin blue lines) 0.875T_m minus T_m (thick solid black line). **Insert.** Changes in Ca-polyhedral connectivity of the liquid/glass MD model as a function of temperature.

The MD model shows that at the melting temperature a few 3 and 5 fold coordinated Si exist, but 98.5% of these polyhedra remain corner shared and only 1.5% are edge shared. By

$0.75T_m$ all the SiO_4 units are corner shared and in the room temperature glass all Si ions are tetrahedrally coordinated by oxygen. The MD model shows that the number of edge and face shared Ca-polyhedra increase steadily with decreasing temperature indicating Ca-polymerization occurs upon supercooling the melt, see figure 2.

BELOW 1.2Tg.

The main local structural changes that occur upon cooling the melt are at 2.34 Å and 3.50 Å in the x-ray differential distribution function (figure 2) and we interpret the growth of these peaks upon cooling as the increase in size of edge-shared octahedral clusters. Integrating these two peaks in the $\Delta D(r)$ functions between associated isosbestic points we can obtain an estimate of the rate of growth of the CaO_6 and Ca-Ca edge-sharing octahedral units in the melt as a function of temperature, see figure 3. The same integration limits were also used below 1000°C for consistency, although the isosbestic points are no longer present introducing a small error. Given that, for both peaks the integrals can be fitted using a linear term at high temperatures and a non-linear term at low temperatures. This analysis implies that there is a linear growth of chains and/or sheets of CaO_6 in the liquid between 1900°C and 1000°C, but he aggregation increases more rapidly as Tg is approached and is concomitant with a steep rise in viscosity (figure 3). Similar curves were obtained for the data for all the glass forming compositions studied, but only linear behavior is observed for the high CaO content samples which could not be vitrified.

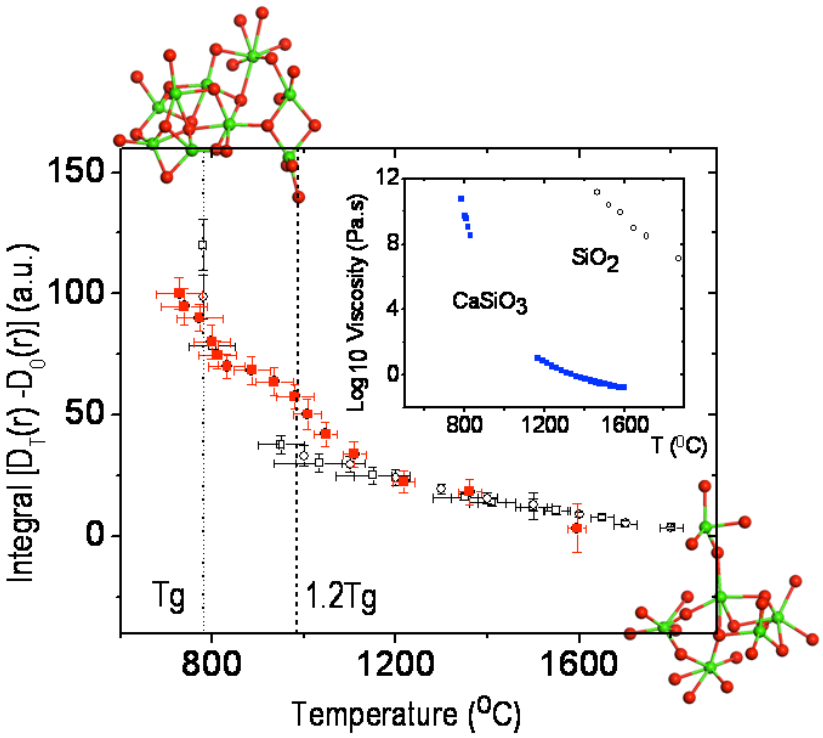

Figure 3. The integrals of the differences between the static state differential distribution functions, $\Delta D(r)$ measurements (see text), shown in figure 2(top) for liquid $CaSiO_3$. The integrals were taken over the region between the isosbestic points for the 3.50Å peak in $\Delta D(r)$. Fast cooling measurements (solid red squares) compared to isothermal measurements (open black symbols) for the integrals of the differences between $\Delta D(r)$ measurements on liquid $CaSiO_3$ around the Ca-Ca pea. The dotted line represents Tg =781°C for $CaSiO_3$ and the dashed line 1.2Tg (992 °C). The 1.2Tg line is calculated in Kelvin but shown in degrees Celsius. **Insert.** Viscosity-temperature relation of liquid $CaSiO_3$ (blue squares) and SiO_2 (circles). Molecular dynamics Snapshots of the polymerization of CaO polyhedra from the predominantly corner shared $CaSiO_3$ melt (bottom right) to more edge shared CaO_6 units in the glass (top left) obtained from MD simulations.

FAST COOLING MEASUREMENTS.

In order to probe the low temperature region a separate set of experiments were performed using the area detector. The $CaSiO_3$ samples were quenched by switching the laser off and sequential measurements were taken every 200ms. The results shown in figure 3 around 1000°C are therefore intriguing since they suggest the small deviation in structure between the isothermal and fast quenched $CaSiO_3$ samples which begins at ~1100°C is real.

The fast cooling measurements also show a distinct plateau as Tg is approached that is absent in the slow cooling measurements. This difference is attributed to the higher fictive temperature expected in the quenched sample compared to one that is vitrified by slow cooling. The differences observed in the present work also provide a possible explanation of the differences in structure measured in prior work by Taniguchi *et al* [6] and Mead and Moutnjoy [7]. Further fast cooling structural studies are needed to see if these features are ubiquitous in quenched glass forming liquid oxides. In the future, it is anticipated that the ability to probe metastable structures of

fragile melts near Tg using a levitator together with high-flux x-ray diffraction with fast, high efficiency 2D detectors and rapid data acquisition, will help clarify the relationship between dynamic and structural heterogeneity in supercooled liquids [4].

DIFFRACTION EXPERIMENTS.

Six compositions between 40 and 75 mole% CaO were investigated in the liquid state. The materials were made from calcium carbonate and silica powders that were mixed, calcined and consolidated into spheres in a laser hearth. Compositions containing less than 60 mole % CaO formed glasses when cooled. In this work we present only the results only for $CaSiO_3$ in detail as the other glass-forming compositions all showed a similar behavior. The high-energy x-ray diffraction experiments on the calcium silicate liquids were performed using an aerodynamic levitator installed on beamline 11 ID-C at the Advanced Photon Source (APS), USA. The temperature of the melts was controlled using a 250 Watt CO_2 laser beam. The experiment was performed in transmission geometry with a 1mm x 1mm x-ray beam of wavelength 0.1088Å and diffraction patterns on isothermal melts were collected using a *Mar345* image plate detector mounted orthogonal to the x-ray beam. Samples of 2-3 mm in diameter were made from binary $(CaO)_x(SiO_2)_{(1-x)}$ compositions containing x=40, 50, 60, 70 and 80 mol % CaO. The sample lost ~1% of its initial mass during the high temperature levitation experiments in pure oxygen. Microprobe analysis on the recovered samples indicated that the composition change was <1%.

Calcium silicate liquids were studied at static temperatures ranging from ~800^{o}C to ~1900^{o}C in approximately 100^{o}C increments. The data were reduced using the software *FIT2D* and the x-ray structure factors, S(Q), obtained up to *Q* ~19 Å^{-1} using the program *PDFgetX2*. The apparent temperature of the levitated sample was measured using an optical pyrometer that operated at a wavelength of 0.650 μm. The estimated errors associated with the temperature measurement arising from the emissivity correction and temperature gradients that occur in the high temperature melts are ±25^{o}C for T>1000^{o}C and ±50^{o}C at lower temperatures approaching the glass transition temperature. Fast, transient cooling measurements were made on selected samples using a Perkin Elmer model 1621 x-ray area detector. This arrangement enabled a measurement of structure to be made in a period of 200 ms and a sequence of measurements were made as the liquid drop cooled from about 2000 to 600 ^{o}C. An optical pyrometer (Chino Corporation, Tokyo, Japan) operating at 10Hz was sighted onto the levitated drop in the region where it was heated by the laser beam and the x-ray beam intersected the droplet.

MOLECULAR DYNAMICS SIMULATIONS.

The contributions of the six partial PDF to the measured $CaSiO_3$ x-ray functions were established using classical molecular dynamics (MD) simulations using Buckingham potentials based on the point charge Born model. The MD simulations were performed using the constant temperature and constant pressure (NPT) ensemble with 1 fs time steps for 80,000 steps. Each cubic simulation cell contained 2500 atoms and with the initial simulation cell size determined based on the experimental density of the glass. At each of the eight simulation temperatures, a constant volume and energy (NVE) run of 80,000 steps followed the NPT simulations. Structure analyses were obtained by averaging 400 structure snapshots of the final 20,000 steps under NVE. For our potential the melting temperature of the model system was 4000K, so structure factors were extracted at T_m, $0.875T_m$, $0.75T_m$ and $0.625T_m$ to provide the same effective T-range as the supercooled liquid experimental data. The simulations confirm that the 2.34 Å arises mainly from the Ca-O peak and shows a high-r contribution from the O-O correlations. Whereas the main contributions to the 3.50 Å peak comes from the Ca-Si and Ca-Ca partial PDFs.

[1] C.J. Benmore, J.K.R. Weber, M.C. Wilding, J. Du and J.B. Parise, Nat. Phys. (submitted).
[2] M. Goldstein, J. Chem. Phys. **51**, 3728 (1969).
[3] M.D. Ediger, Annu. Rev. Phys. Chem. **51**, 99 (2000).
[4] P.H. Gaskell *et al.*, Nature **350**, 675 (1991).
[5] B.O. Mysen, D. Virgo, F.A. Seifert, Rev. of Geophysics **2**, 353 (1982).
[6] T. Taniguchi, M. Okuno, T. Matsumoto, J. Non-Cryst. Solids 211 (1997) 56.
[7] R. N. Mead, G. Mountjoy, J. Phys. Chem. B **110**, 14273 (2006).
[8] R.W. Johnson, J. Non-Cryst. Solids **88**, 366 (1986).
[9] J. Tse *et al.*, Phys. Rev. B **71**, 214107 (2005).

Nonequilibrium Phonon Dynamics

David A. Reis (dreis@slac.stanford.edu) and Mariano Trigo
Stanford PULSE Institute and Material Science Division
SLAC National Accelerator Laboratory MS59
2575 Sand Hill Rd
Menlo Park, CA 94025

In this subtask we are developing ultrafast x-ray scattering as a tool to study the fundamental dynamics of materials with atomic-scale spatial and temporal resolution. The ability to probe atomic and ultimately electronic motion on such short scales can yield important information about nonequilibrium dynamics during energy relaxation as well as phase transformations. Initial experiments are concentrating on generation and detection of nonthermal phonons in semiconductors and on electronic bond softening in semimetals. Here we discuss recent results where we used picosecond x rays from the APS to study phonon relaxation in ultrafast laser excited polar semiconductors (InP and InSb) and found a surprisingly long-lived nonequilibrium state involving delayed emission of large wavevector transverse modes.

The interaction of hot carriers and phonons in solids is a fundamental problem with important implications for energy applications. If the scattering of electrons by phonons and subsequent lattice thermalization is sufficiently fast, the nonequilibrium dynamics minimally impacts the transport and other properties. It is generally assumed that lattice thermalization is relatively fast, effectively occurring on the time-scale of a few optical phonon periods to several picoseconds. However, bottlenecks for the decay of certain modes due to kinematic limitations or small anharmonic coupling can lead to nonequilibrium phonon populations that, for example in polar semiconductors, can affect device performance. Prior experiments on nonequilibrium phonons were limited by time-resolution or to studying relatively long wavelength excitations. In our work, we have obtained the first images of nonequilibrium phonons throughout the Brillouin zone in photoexcited III-V semiconductors, indium-phosphide (InP) and indium-antimonide (InSb), using picosecond time-resolved diffuse scattering. In each case, we find that the lattice remains out of equilibrium for several hundred picoseconds up to nanoseconds after laser excitation. The nonequilibrium population is dominated by the delayed emission of transverse acoustic phonons which in InP are directed along high-symmetry directions.

Experiments were performed at the BioCARS beamline of the Advanced Photon Source (APS) at Argonne National Laboratory. The samples were (001)-cut single crystals of InP and InSb. Photoexcitation of carriers was achieved using $\sim$1ps visible pulses from an optical parametric amplier synchronized to the x-rays from the APS. A dual undulator setup provided an x-ray photon

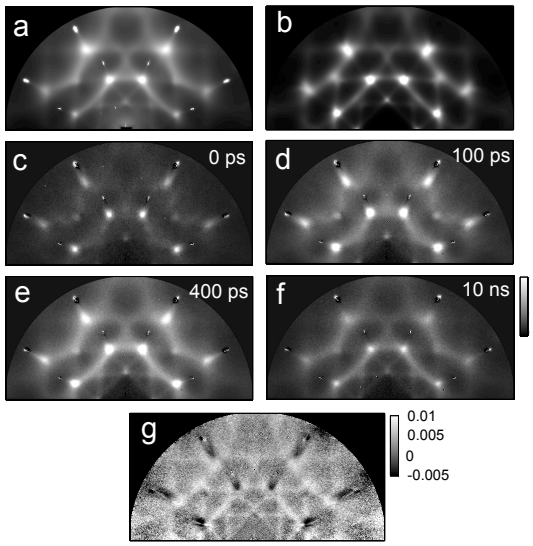

Figure 1: (a) room temperature TDS of InP at 15keV oriented along (100) (b) Calculated TDS convolved with a 2% Gaussian energy spread. (c)-(f)differences between laser-exposed and laser-off frames at Δt=0, 100, 400ps, and 10ns, respectively. (g) normalized difference between frames at 400ps and 100 ps.

ux at the sample of $\sim 10^{10}$ photons/pulse with photon energies in the range 12 –15 keV in a < 4 % bandwidth. Single 100 ps x-ray pulses were isolated by a high-speed chopper at a rate of 40 Hz. The crystals were oriented at grazing incidence to match the laser penetration depth and such that the x-rays were incident primarily along (100). X-ray scattering up to $2\theta \approx 51^{\circ}$. were collected on a 165 mm diameter CCD.

Figure 1a. shows the thermal diffuse scattering image from an InP crystal at room temperature. Using a simple Born model for the forces, we can reproduce the general features (figure 1b). The relative change in the time-resolved diffuse scattering images (approximately 100 frames of 100 shots each, equivalent to a few seconds of LCLS) are shown in figure 1c-f. We find that the diffuse scattering rises within a time of $\sim$100ps limited by the temporal resolution of the APS and then slowly decays on the time-scale of thermal diffusion. However, upon closer inspection, subtle differences in the scattering pattern can be seen which is indicative of a nonthermal lattice. In order to amplify these differences, we plot in figure 1(g) the difference between the signal at 400 ps and 100 ps, normalized to the laser off. The light regions correspond to areas where the nonthermal phonon population is continuing to increase relative to the earlier time, while the dark regions are areas where it decreases. Singular value decomposition of the time resolved images shows that the scattering is primarily due to two components, corresponding roughly to the thermal and nonthermal response of the lattice. The former corresponding to a nearly uniform and rapid rise and slow decay in the population, consistent with lattice heating, and the latter showing a roughly nanosecond delayed heating of transverse acoustic modes along the high symmetry directions concomitant with a decrease in small wavevector longitudinal acoustic modes (see figure 2). A nonequilibrium

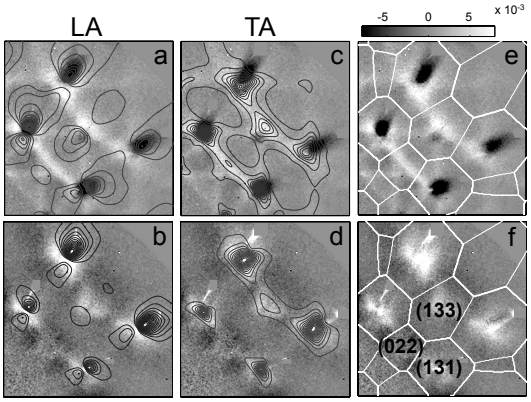

Figure 2: Contribution to the diffuse scattering from TA and LA branches . The images correspond to the first two singular vectors contributions to the time-resolved diffuse scattering images. The contours in (a) and (b) show the calculated contribution from LA phonons in InP and InSb, respectively. (c) and (d) show the contribution from TA phonons for InP and InSb, respectively. (e)and(f) show the singular vectors with the Brillouin-zone boundaries.

response throughout the Brillouin zone is also seen in InSb, although it is much less directional.

In the current experiments, the relatively long pulse width of the APS means that we cannot resolve earliest stages of energy transfer between the carriers and the lattice or even the first decay processes of the phonons. The LCLS will allow us to probe these dynamics on their fundamental time-scale.

DOE supported papers 2008–2010

[1] M. Trigo, Y. M. Sheu, D. A. Arms, J. Chen, S. Ghimire, R. S. Goldman, E. Landahl, R. Merlin, E. Peterson, M. Reason, and D. A. Reis. Probing unfolded acoustic phonons with x rays. *Physical Review Letters*, 101(2):025505, 2008.

[2] P. B. Hillyard, D. A. Reis, and K. J. Gaffney. Carrier-induced disordering dynamics in insb studied with density functional perturbation theory. *Physical Review B (Condensed Matter and Materials Physics)*, 77(19):195213, 2008.

[3] A. M. Lindenberg, S. Engemann, K. J. Gaffney, K. Sokolowski-Tinten, J. Larsson, P. B. Hillyard, D. A. Reis, D. M. Fritz, J. Arthur, R. A. Akre, M. J. George, A. Deb, P. H. Bucksbaum, J. Hajdu, D. A. Meyer, M. Nicoul, C. Blome, T. Tschentscher, A. L. Cavalieri, R. W. Falcone, S. H. Lee, R. Pahl, J. Rudati, P. H. Fuoss, A. J. Nelson, P. Krejcik, D. P. Siddons, P. Lorazo, and J. B. Hastings. X-ray diffuse scattering measurements of nucleation dynamics at femtosecond resolution. *Physical Review Letters*, 100(13):135502, 2008.

[4] D. A. Reis. Squeezing more out of ultrafast x-ray measurements. *Physics*, 2:33, 2009.

[5] M. Trigo and D. Reis. Time-resolved x-ray scattering from coherent excitations in solids. *MRS Bulletin*, 35:514–519, 2010.

[6] J. P. Cryan, J. M. Glownia, J. Andreasson, A. Belkacem, N. Berrah, C. I. Blaga, C. Bostedt, J. Bozek, C. Buth, L. F. DiMauro, L. Fang, O. Gessner, M. Guehr, J. Hajdu, M. P. Hertlein, M. Hoener, O. Kornilov, J. P. Marangos, A. M. March, B. K. McFarland, H. Merdji, V. S. Petrović, C. Raman, D. Ray, D. Reis, F. Tarantelli, M. Trigo, J. L. White, W. White, L. Young, P. H. Bucksbaum, and R. N. Coffee. Auger electron angular distribution of double core-hole states in the molecular reference frame. *Phys. Rev. Lett.*, 105(8):083004, Aug 2010.

[7] J. M. Glownia, J. Cryan, J. Andreasson, A. Belkacem, N. Berrah, C. I. Blaga, C. Bostedt, J. Bozek, L. F. DiMauro, L. Fang, J. Frisch, O. Gessner, M. Gühr, J. Hajdu, M. P. Hertlein, M. Hoener, G. Huang, O. Kornilov, J. P. Marangos, A. M. March, B. K. McFarland, H. Merdji, V. S. Petrovic, C. Raman, D. Ray, D. A. Reis, M. Trigo, J. L. White, W. White, R. Wilcox, L. Young, R. N. Coffee, and P. H. Bucksbaum. Time-resolved pump-probe experiments at the LCLS. *Opt. Express*, 18(17):17620–17630, 2010.

[8] L. Young, E. P. Kanter, B. Krässig, Y. Li, A. M. March, S. T. Pratt, R. Santra, S. H. Southworth, N. Rohringer, L. F. DiMauro, G. Doumy, C. A. Roedig, N. Berrah, L. Fang, M. Hoener, P. H. Bucksbaum, J. P. Cryan, S. Ghimire, J. M. Glownia, D. A. Reis, J. D. Bozek, C. Bostedt, and M. Messerschmidt. Femtosecond electronic response of atoms to ultra-intense x-rays. *Nature*, 466(7302):56–61, 2010.

Nanoscale Imaging and Advanced Spectroscopy of Transient Magnetic States
FWP (Ultrafast Magnetization Dynamics)

Andreas Scherz, Hermann A. Dürr, Joachim Stöhr, SLAC National Accelerator Laboratory, scherz@slac.stanford.edu

Scope of research: Understanding the microscopic mechanisms driving the magnetization dynamics on the femtosecond time scale is of essential importance for manipulating and controlling the macroscopic state in magnetic storage devices. This project aims at a microscopic understanding of the recently demonstrated switching of ferromagnetic thin films by circularly polarized fs optical laser pulses. The essence of magnetization is angular momentum. What are the channels for ultrafast angular momentum transfer to, from and within the spin system? Does the angular momentum come from light or is it provided by other reservoirs (lattice)? Understanding the microscopic mechanisms driving the magnetization dynamics on the fs and ps time scale is essential for manipulating and controlling the macroscopic state in magnetic devices. An example of high current interest worldwide is the emergence of reversed ferromagnetic order after several 10 ps in FeCo Gd alloy films depending on the initial pump photon helicity. The origin of this "memory" of the photon helicity remains elusive and may involve a transient, strongly non-equilibrium state. X-rays provide the ideal tool to investigate the temporary memory loss of electronic spins. While the fs timescale will be addressed at LCLS, the use of element specific x-ray microscopy at SSRL offers unique access to the ps timescale.

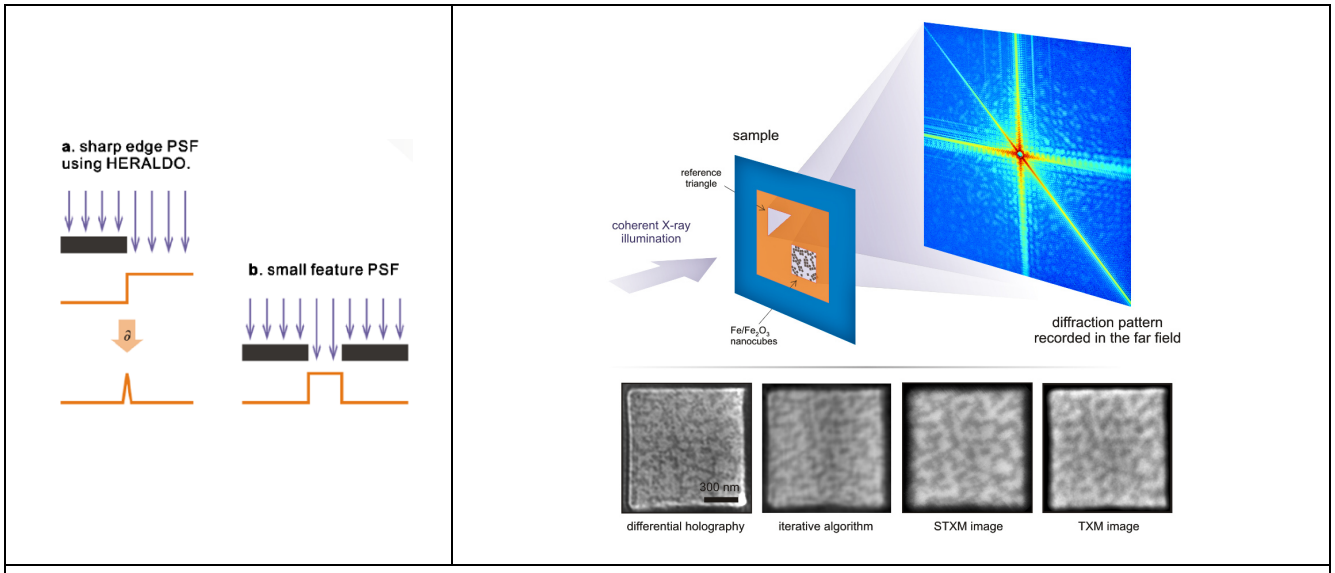

Fig1: Left) The concept is very much similar to the "edge scan" method that is widely used for determining the profile of a small beam. The image reconstruction from conventional Fourier holography can be viewed as a convolution of the ideal image with the reference. For differential holography technique, the convolution happens between the ideal image and a sharp corner that is used as the reference. The additional step of differential operation is able to deliver a much sharper image. Right) In the actual experiment at SSRL, we imaged iron/iron-oxide nanocubes 18 nm in size dispersed on a silicon nitride membrane. A resolution of 16 nm was obtained using a triangular holographic reference. The result is compared with images of the same sample obtained using alternative x-ray imaging methods, including iterative phase retrieval methods, scanning transmission x-ray microscopy (STXM) and transmission x-ray microscopy (TXM).

Recent progress:

Nanoscale Imaging: X-ray Holography is an x-ray microscopy technique that takes advantage of the coherence property of modern x-ray sources and is therefore a powerful technique to address important questions in our project. Fourier transform holography is a particularly straight-forward method for taking single-shot images at X-ray free-electron lasers such as LCLS. Previous Fourier transform holography experiments used small pinholes as the reference. The resolution was determined by the size of the reference pinhole and achieved 30nm resolution. We have recently demonstrated at SSRL Beamline 13-3 that by using extended reference structures with sharp corners, the resolution can be improved by a factor of two with the same reference fabrication tool [Guizar10, Zhu10]. The image reconstruction also compares favorably with alternative x-ray microscopy methods as shown in Figure 1. This will enable nanoscale imaging of the magnetization reversal of individual magnetic bits of a few 10nm in dimension for investigating novel nanoscale phenomena such as dipolar interactions with neighbor 'bits' and controlling the magnetization direction via exchange bias.

Advanced Spectroscopy of Transient Magnetic States: Until only recently, the field of "Femto-magnetism" has naturally been driven by all-optical pump-probe techniques. Femtosecond time-resolved X-ray magnetic circular dichroism spectroscopy has been utilized to unambiguously determine the ultrafast quenching of spin and orbital moments after ultrashort laser excitation. While all-optical pump-probe techniques allow ultrafast excitations (pump) and the study of their evolution (probe) on the macroscopic scale by use of the magneto-optical Kerr or Faraday effect, little is known about the microscopic processes on nano- and sub-nanometer length scales because of the lack of real or momentum space resolution of optical techniques.

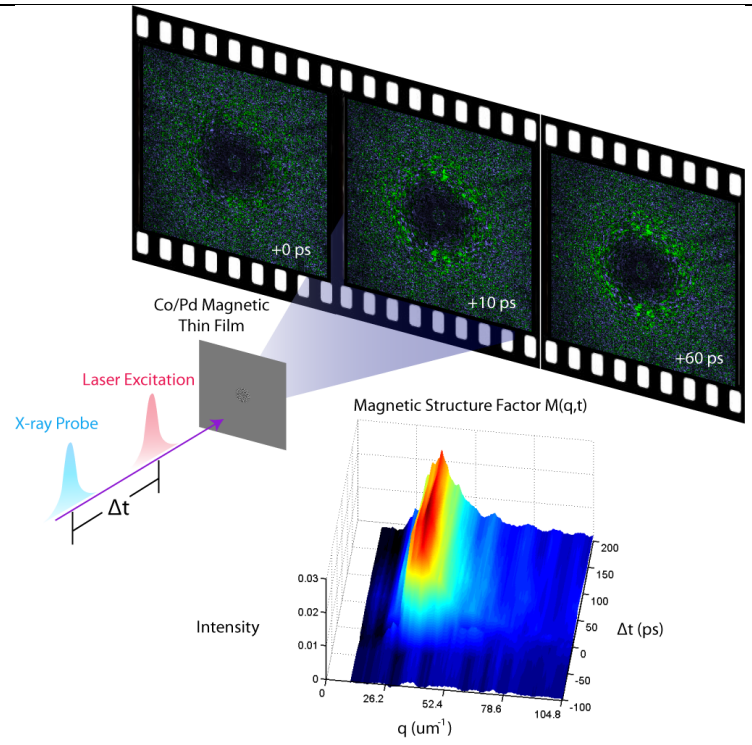

Figure 2: Generic optical pump X-ray probe geometry to probe the ultrafast magnetization dynamics and relaxation processes as a function of momentum transfer at SSRL and LCLS. The inset shows the change of the magnetic structure factor as a function of time delay and momentum transfer (relaxation dynamics measured at SSRL). Experiments at LCLS will allow for recording a single-shot image at delay time Δt after a pump pulse and studying the evolution of the intermediate magnetic states.

We performed first time-resolved coherent x-ray scattering experiments of laser-induced

magnetization dynamics in ferromagnetic multilayer on nanometer length scales, see Fig 2. We overcome coherent flux limitations at SSRL BL13-3 by making use of a larger fraction of the high repetition rate of the synchrotron with an MHz-repetition pump laser. By studying the time correlations in the coherent diffraction patterns we observed that the magnetic worm domain state is reversal on larger length scales while irreversible processes alter the domain configuration on smaller length scales.

While experiments at the synchrotron can serve for studying the relaxation magnetization dynamics on the ps time scale, LCLS offers both the relevant length and time scales to explore the ultrafast processes of laser-induced demagnetization and all-optical magnetization reversal on the nanoscale.

Towards this goal, we performed first time-resolved pump-probe coherent magnetic scattering and single-shot imaging experiments at LCLS. In particular, we demonstrate that nondestructive imaging is possible.

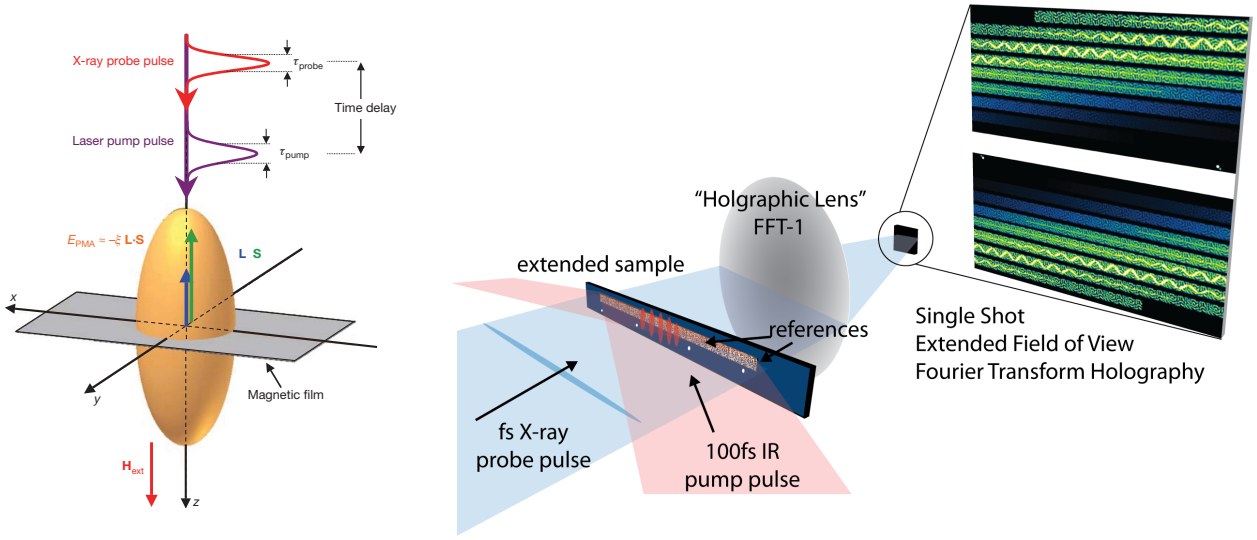

Fig. 3: **Left)** In next generation magnetic data storage devices the spin orientation will be out of the layer plane. This will be achieved controlling the spin-orbit contribution to the total energy (yellow ellipsoid) by tailoring the electronic structure. Recent optical pump – x-ray probe experiments established that the shape of this spin-orbit ellipsoid can be changed on the fs timescale ultimately driving the spins to orient in the plane [Boeglin10]. Here we propose to characterize this process with the ultimate time resolution aiming at establishing control of manipulation of spin and electronic structure. **Right)** Illustration of the proposed experiment using the "Ultrafast Stopwatch" approach. To extend the field of view our method applies multiple reference sources to x-ray Fourier transform holography. The key is the strategic arrangement of the reference and object structures such that the individual images tile without overlapping in the autocorrelation. It therefore becomes possible to fold the extended sample region of interest into the autocorrelation without compromising the resolution. A time window of 267fs can be "streaked" in a single-shot using a sample region of about 100µm in size.

Future work:

We aim to study the changes in magneto-crystalline anisotropy of Co/Pd multilayer triggered by fs laser excitation using time-, element- and spatially-resolved X-ray resonant magnetic scattering (TR-XRMS). Recent experiments have shown that fs laser excitation is able to manipulate the magneto-crystalline anisotropy in systems with out-of-plane spin orientation on a 200 fs timescale

[Boeglin10]. The first step is to (resonantly) modify this spin-orbit ellipsoid by excitation with fs laser pulses of variable photon energy (1-0.1 eV) while probing the system response with the shortest soft x-ray pulses available at LCLS. We will characterise and overcome laser pump – FEL probe temporal jitter using the recently developed "stopwatch' holographic imaging approach, see Fig. 3. The ultimate goal is to record the coherent charge and spin oscillations that have been suggested to occur during the driving fs laser pulse. The dephasing of these coherent charge/spin processes should lead to heating of the electronic system and ultrafast demagnetization, respectively.

DOE supported publications:

[Zhu10] D. Zhu, M. Guizar-Sicairos, B. Wu, A. Scherz, Y. Acremann, T. Tyliszczak, P. Fischer, N. Friedenberger, K. Ollefs, M. Farle, J.R. Fienup, J. Stöhr, *High-Resolution X-ray Lensless Imaging by Differential Holographic Encoding*, Phys. Rev. Lett. 105, 043901 (2010).

[Boeglin10] C. Boeglin, E. Beaurepaire, V. Halté, V. Lopez-Flores, C. Stamm, N. Pontius, H. A. Dürr, J.- Y. Bigot, *Distinguishing the ultrafast dynamics of spin and orbital moments in solids*, Nature **465**, 458 (2010).

[Guizar10] M. Guizar-Sicairos, D. Zhu, J.R. Fienup, B. Wu, A. Scherz, and J. Stöhr, *Holographic x-ray image reconstruction through the application of differential and integral operators,* Opt. Lett. 35, 928 (2010).

[Zhu09] D. Zhu, B. Wu, R. Rick, J. Stöhr, A. Scherz, *Phase retrieval in x-ray lensless holography by reference beam tuning*, Opt. Lett. 34, 2604 (2009).

[Bernstein09] D.P. Bernstein, Y. Acremann, A. Scherz, M. Burkhardt, J. Stöhr, M. Beye, W.F. Schlotter, T. Beeck, F. Sorgenfrei, A. Pietzsch, W. Wurth, A. Föhlisch, *Near edge x-ray absorption fione structure spectroscopy with x-ray free-electron lasers*, Appl. Phys. Lett. 95, 134102 (2009).

[Rick09] R. Rick, A. Scherz, W.F. Schlotter, D. Zhu, J. Lüning, J. Stöhr, *Optimal signal-to-noise ratios for soft x-ray lensless imaging*, Opt. Lett. 34, 650 (2009).

[Scherz08] A. Scherz, D. Zhu, R. Rick, W.F. Schlotter, S. Roy, J. Lüning, J. Stöhr, Nanoscale *Imaging with Resonant Coherent X-rays: Extension of Multiple-Wavelength Anomalous Diffraction to Nonperiodic Structures*, Phys. Rev. Lett. 101, 076101 (2008).

Ultrafast X-ray Studies of Dynamics in Complex Materials

Robert W. Schoenlein, Robert A. Kaindl
Materials Science Division, Lawrence Berkeley National Laboratory, Berkeley, CA 94720

RWSchoenlein@lbl.gov, RAKaindl@lbl.gov

Co-PIs: Alessandra Lanzara[1], Zahid Hussain[2]
[1]*Materials Science Division, Lawrence Berkeley National Laboratory, Berkeley, CA 94720*
[2]*Advanced Light Source, Lawrence Berkeley National Laboratory, Berkeley, CA 94720*

ALanzara@lbl.gov, ZHussain@lbl.gov

Program Scope: FY10 is the first year of this research program at LBNL. The central theme of this new program is the application of advanced ultrafast techniques in the VUV/EUV to X-ray range to achieve *direct* measurement sensitivity to changes in atomic structure and valence electronic structure. Studies of atomic and electronic structural dynamics on the ultrafast time scale are indispensable for achieving new insight onto the correlated phenomena underlying complex materials, nanostructures, and novel states of matter.

There are two subtasks associated with this program. One focuses on the application of ultrafast x-ray spectroscopy, diffraction, and dichroism techniques to probe atomic structure, valence charge distributions, bonding, and magnetization dynamics. The second sub-task applies ultrafast VUV/EUV angle-resolved photoemission spectroscopy (ARPES) to probe electronic structural dynamics (transient band structures, electron-phonon coupling, and quasiparticle dynamics), with simultaneous resolution of energy and transverse momentum.

Recent Progress and Future Plans

(1) Ultrafast x-ray spectroscopy of complex materials and phase transitions

In complex materials, measurements in the ultrafast time domain offer a unique capability to separate correlated interactions between charge, spin, and lattice vibrational modes via perturbative (nonequilibrium/nonthermal) excitation on time scales shorter than the fundamental time scales of charge dynamics, atomic structural dynamics, energy relaxation, and energy dissipation processes. Emerging ultrafast x-ray techniques provide important advantages for direct quantitative measurement of material dynamics including: atomic structure, valence charge distributions, nano-scale charge ordering, and orbital/spin contributions to magnetization. Ultrafast x-rays provide new insight to the coupling between correlated electronic structure and atomic structure and how they give rise to the exotic properties of complex materials.

Present research is focused on ultrafast electronic phase transitions in manganites and related transition-metal oxides. This work exploits two beamlines that have been developed at the Advanced Light Source, with the capability for generating ~200 fs x-ray pulses from 200 eV to 10 keV. Experiments at the LCLS x-ray free-electron laser are also being pursued as part of a larger collaboration.

In the colossal magnetoresistive (CMR) manganites $Pr_{0.7}Ca_{0.3}MnO_3$ we have previously shown that an ultrafast insulator to metal phase transition can be triggered by either direct optical excitation, or by coherent vibrational excitation of the Mn-O stretching mode. We are now applying time-resolved x-ray absorption spectroscopy (near-edge structure) to investigate the electronic dynamics associated with the phase transition. Absorption changes at the O K-edge and Mn L-edge directly monitor the evolution of the density of unoccupied states in the transient photoinduced phase. Time-resolved XAS results show that the electronic structure of the photoinduced phase (developing within the 70 psec resolution of present experiments) is remarkably similar to that of the well-known ferromagnetic metallic phase that is accessible in related manganites upon cooling below the Curie temperature. Importantly, since $Pr_{0.7}Ca_{0.3}MnO_3$ does not exhibit a metallic phase-transition with temperature, this is a unique optically-driven transition. Moreover, XAS measurements of $Pr_{0.7}Ca_{0.3}MnO_3$ under applied magnetic field show good agreement between the spectral signatures of the CMR metallic phase, and that generated by ultrafast excitation. Future x-ray experiments are being developed to investigate the evolution of this phase transition on the femtosecond time scale.

A second area of focus applies ultrafast resonant x-ray diffraction techniques to understand the competition between electron localization and itinerancy that underlies many of the exotic properties exhibited by transition metal oxides. In manganites, the competition between itinerant ferromagnetism and localized CE-type charge-, orbital-, and spin-ordered (CO/OO/SO) states is believed to play an important role in the CMR effect. Recent resonant x-ray diffraction experiment show that in $Pr_{0.7}Ca_{0.3}MnO_3$ (which lies at the boundary between CE-type ordering and the FM phase) the spin ordering appears to be enhanced by the ferromagnetic phase, and stabilized only in the canted antiferromagnetic phase. Our results reveal the fragility of the CE-type ordering away from 50% doping and an unexpected cooperative interplay between these two seemingly incompatible states. Time-resolved resonant diffraction studies are now underway at the ALS to investigate the dynamics of charge, orbital, and spin ordering in $Pr_{0.7}Ca_{0.3}MnO_3$ and $Pr_{0.5}Ca_{0.5}MnO_3$. As part of a larger collaboration, we are pursuing similar ultrafast resonant x-ray diffraction studies at LCLS on charge and spin order dynamics in the Mott insulator $La_{2-x}Sr_xNiO_4$ (x=0.25). We have conducted preliminary optical-pump/optical-probe studies and experiments are now underway to investigate direct THz pumping of the Ni-O mode at 15 μm and its influence on the charge-ordered and spin-ordered stripe phase (probing optical properties). These studies are in preparation for ultrafast THz/x-ray studies at LCLS.

(2) Electronic structure dynamics: Ultrafast angle-resolved photoemission spectroscopy

Over the past decade, high-resolution angle-resolved photoemission spectroscopy (ARPES) has emerged as a very powerful experimental tool for quantitative measurements of the time-averaged electronic structure in a wide range of complex materials, most notably high-temperature superconductors. However, the electronic structure in complex materials intrinsically arises from ultrafast *dynamic* correlations ranging from the psec time scale characteristic of electron-phonon interactions to femtosecond or even sub-fs timescales that characterize electron-electron correlation times. Direct measurements of the electronic structure *on the ultrafast time scale* of the fundamental correlations thus has the potential to elucidate the

cause-effect interplay between charge, spin, and orbital excitations and subtle distortions of the atomic lattice, yielding deep insight into complex materials physics.

Recent developments in ultrafast laser technology, harmonic generation, and multi-dimensional photoelectron spectrometers now create an exceptional opportunity to combine high-resolution ARPES probes of electronic structure with ultrafast temporal resolution. We are presently building a novel ultrafast ARPES laboratory in the Materials Sciences Division at LBNL. This facility is based on a new high-repetition rate (50 kHz) femtosecond laser system with generation of EUV pulses for time-resolved ARPES initially using harmonic generation in crystals (at 6 eV) and a future capability for harmonic generation and wave-mixing in gasses for photoemission in the 10-50 eV range. An important feature will be tunable *pump* pulses in the UV to THz range via parametric amplification and nonlinear mixing for tailored sample excitations. A UHV surface science chamber is now being designed, and this will be coupled to an advanced time-of-flight analyzer based on a design developed at the Advanced Light Source.

This new ultrafast ARPES capability will provide the means for novel insight into condensed matter dynamics by resolving non-equilibrium carrier distributions and the ultrafast evolution of the *occupied* electronic eigenstates directly in momentum and energy space. Photo-induced phase transitions between superconducting, metallic, or charge-ordered phases can be investigated to unravel cause-effect relationships between degrees of freedom that comprise the ground state correlations. Ultrafast ARPES experiments will be also employed to resolve the anisotropic nature of quasiparticle and gap dynamics in high-T_C superconductors. Moreover, with this method, dynamics and quasiparticle lifetimes can be probed for states well beyond the thermally accessible regime. In this way, the combination of modern ultrafast and ARPES techniques can provide a powerful tool with high energy, momentum, *and* time resolution to follow the dynamics of complex energy materials and unravel their fundamental interactions.

Publications (2009-2010)

1. M. Rini, R. Tobey, S. Wall, Y. Zhu, Y. Tomioka, Y. Tokura, A. Cavalleri, and R.W. Schoenlein, "Time-resolved x-ray absorption spectroscopy of photoinduced insulator-metal transition in a colossal magnetoresistive manganite," in **Ultrafast Phenomena XVI**, Springer Series in Chemical Physics, **92**, P. Corkum, S. De Silvestri, K.A. Nelson, E. Riedle, R.W. Schoenlein, Eds., Springer-Verlag, (2009).

2. M. Rini, Y. Zhu, S. Wall, R. I. Tobey, H. Ehrke, T. Garl, J. W. Freeland, Y. Tomioka, Y. Tokura, A. Cavalleri, and R. W. Schoenlein, "Transient electronic structure of the photoinduced phase of $Pr_{0.7}Ca_{0.3}MnO_3$ probed with soft x-ray pulses," *Phys. Rev. B*, **80**, 155113 (2009).

Electronic Structure of Superconductors and Related Materials

Zhi-Xun Shen, Tom Devereaux, Donghui Lu (SSRL), Rob Moore, and Yulin Chen
Stanford Institute for Materials and Energy Sciences
SLAC National Accelerator Laboratory and Stanford University
2575 Sand Hill Rd, Menlo Park, CA 94025
zxshen@stanford.edu tpd@stanford.edu

Starting in 2008, we have engaged in the following research activities using angle-resolved photoemission spectroscopy: i) Electronic structure of cuprate superconductors; ii) Electronic structure of Fe-pnictides superconductors; iii) Quantum energy diagram of topological insulators; iv) Other related quantum materials. We have also performed other complementary experiments on these materials. In addition to these activities, we have also engaged in the tool development that is aimed to provide new insights on strongly correlated material. Examples of this include time resolved photoemission and spin resolved photoemission spectroscopy. This activity has strong synergy to another FWP led by Tom Devereaux where soft x-ray scattering and time domain experiment is the focus. A complete list of our results is attached. To provide some focus, we would like to suggest that the following two aspects being considered for presentation.

Suggestion I - Electronic structure of cuprate superconductors – the nature of the pseudogap (with ZX Shen as speaker)

I will report our recent angle-resolved photoemission data from cuprate superconductors. The focus would be the nature and the relationship of the two energy gaps observed – the d-wave superconducting gap below Tc and the anisotropic pseudogap above Tc in the underdoped region of the phase diagram. The question we would like to answer is whether these two gaps are of the same origin. I will provide detailed temperature, doping, energy and momentum dependent data demonstrating that the pseudogap is not a trivial extension of the superconducting gap. Moreover, I will present evidence for particle-hole symmetry breaking in momentum space - suggesting that the pseudogap state is likely related to some form of density wave formation. We will also discuss the possibility of the pseudogap transition to be a true phase transition.
M. Hashimoto et al., Nature Physics 6, 414-418 (2010); R. He et al., Nature Physics, 5, 119 (2009); I. Vishik et al., Nature Physics, 5, 718 (2009); R. He et al., submitted to Science

Suggestion II - Electronic structure of Topological Quantum Matter (with Yulin Chen as speaker)

In this talk, I will report angle-resolved photoemission data from topological quantum matter focusing on the following: i) large gap topological insulator Bi2Te3 with a single diract cone on the surface; ii) massive Dirac fermion on the surface of topological insulator with magnetic dopants; iii) observation of single Dirac cone topological surface state in TlBiTe2 and TlBISe2. Time permits, recent new results will also be presented.
Y.L. Chen et al.; Science 325, 178 (2009); Science 329, in press (2010); arXiv 1006.3843 (2010)

List of publications since 2008

1) W.S. Lee and Z.X. Shen, Superconductivity: Pseudogap Brings About Real Resonance, Nature Physics, 5, 95 (2008)
2) A. Tamai et al, Electronic Structure at the C60/Metal Interface: An angle-resovled photoemission and first principle study, Phys. Rev. B 77, 075134 (2008).
3) W. Meevasana et al, Extracting the Spectral Function of the Cuprates by a Full 2D Analysis, Phys. Rev. B 77, 104506 (2008)
4) A.S. Mishchenko et al, Charge Dynamics of Doped Holes in High-Tc Cuprates – A Clue from Optical Conductivity, Phys. Rev. Lett. 100, 166401 (2008)
5) M. Hashimoto et al, Doping Evolution of the Electronic Structure in the Single-Layer Cuprates Bi2Sr2-xLaxCuO6+d: Comparison with Other Single-Layer Cuprates, Phys. Rev. B 77, 075134 (2008)
6) V. Brouet et al, ARPES Study of the Evolution of Band Structure and Charge Density Wave Properties in Rte3 for R = Y, La, Ce, Sm, Gd, Tb and Dy, Phys. Rev. B 77. 235104 (2008)
7) W.S. Lee et al, The Puzzle of the Missing Energy Shift in the Nodal Electron Self-Energy Across the Superconducting Transition in Optimally-Doped Bi2212, Phys. Rev. B 77, 140504 (2008)
8) T. Cuk et al, A Pressure Tuned Insulator-To-Metal Critical Point in the Copper Oxides, Phys. Rev. Lett. 100, 217003 (2008)
9) A. Tamai et al, Fermi Surface and van Hove Singularity in the Itinerant Metamagnet Sr3Ru2O7, Phys. Rev. Lett. 101, 026407 (2008).
10) D.H. Lu et al, Electronic Structure of LaOFeP – a different type of superconductors. Nature, 455, 81 (2008)
11) F. Schmitt et al, Effect of the Amplitude Mode and the Transient Melting of the Charge Density Wave on the Electronic Structure of $TbTe_3$. Science 321, 1649 (2008)
12) F. Schmitt et al Analysis of the spectral function of Nd1.85C0.15CuO4, obtained by angle-resolved photoemission spectroscopy, Phys. Rev. B, 78, 100505 (2008)
13) K.Tanaka et al Direct Evidence of Two Gaps in Underdoped Bi2212 J. of Phys.: Conference Series 108, 012014 (2008)
14) R.H. He et al Energy Gaps in the Failed High-Tc Superconductor $La_{1.875}Ba_{0.125}CuO_4$ Nature Physics, 5, 119 (2009)
15) Y.L. Chen et al A step closer to visualizing the electron-phonon interplay in real time Proceedings of the National Academy, 106. 963 (2009)
16) A.V. Balatsky et al Bogoliubov Angle, Particle-Hole Mixture and ARPES in Superconductors Phys. Rev. B 79, 020505 (2009).
17) T. Xiang et al Doping Dependent Charge Transfer Gap and Realistic Electronic Model of N-Type Cuprate Superconductors Phys. Rev. B 79, 014524 (2009)
18) W.S. Lee et al A Brief Update of Angle-Resolved Photoemission Spectroscopy on a Correlated Electron System J.Physics – Condensed Matter, 21, 164217 (2009)
19) M. Hashimoto et al Effects of Out of Plane Disorder on the Nodal Quasiparticle and Superconducting Gap in Bi2201 Phys. Rev. B 79, 144517 (2009)
20) T. Yoshida et al Universal versus Material-Dependent Two-Gap Behavior in the High-Tc Cuprates: Angle-Resolved Photoemission Study of $La_{2-x}Sr_xCuO_4$ Phys.

Rev. Lett. 103, 037004 (2009).
21) Y.L. Chen et al Large Gap Topological Insulator Bi2Te3 with a Single Dirac Cone on the Surface Science 325, 178 (2009)
22) Yulin Chen et al Unusual layer dependent charge distribution, collective mode coupling and superconductivity in multilayer cuprate $Ba_2Ca_3Cu_4O_8F_2$ Phys. Rev. Lett. 103, 036403 (2009)
23) W.S. Lee et al Layer Number Dependent Band Renormalization Effect in Tl-base Superconducting Copper Oxides via ARPES Phys. Rev. Lett., 103, 067003 (2009)
24) I.M. Vishik et al A momentum-dependent perspective on quasiparticle interference in Bi2212 Nature Physics, 5, 718 (2009)
25) M.Yi et al Electronic Structure of the BaFe2As2 Family of Iron Pnictides Phys. Rev. B 80, 024515 (2009)
26) D.H. Lu et al ARPES Studies of the Electronic Structure of LaOFe(P,As) Physica C - Superconductivity and Its Applications, 469. 452 (2009)
27) B. Moritz et al Effect of Strong Correlations on the high energy anomaly in hold- and electron-doped high-Tc Superconductors New J. Phys. 11, 093020 (2009)
28) T. Yoshida et al Underlying Fermi Surface of Sr14-xCaxCu24O41 in Two-Dimensional Momentum Space Observed by Angle-resolved Photoemission Spectroscopy Phys. Rev. B 80, 052504 (2009)
29) W.L. Yang et al Evidence for Weak Electronic Correlations in Iron Pnictides Phys. Rev. B 80, 014508 (2009)
30) M.Yi et al Unconventional Electronic Reconstruction in Undoped (Ba,Sr)Fe2As2 across the Spin Density Wave Transition Phys. Rev. B 80, 174510 (2009)
31) Hailin Peng et al Aharonov-Bohm Interference in Topological Insulator Nanoribbons Nature Materials 9, 225 (2010)
32) D.S. Kong et al Topological Insulator Nanowires and Nanoribbons Nano Letters 10, 329 (2010)
33) A. Tamai et al LUMO photoemission lineshape in quasi-one-dimensional C-60 Chains Phys. Rev. B 81, 045423 (2010)
34) Z. Alpichshev et al STM imaging of electronic waves on the surface of Bi2Te3: topologically protected surface states and hexagonal warping effects Phys. Rev. Lett. 104, 016401 (2010)
35) M. Hashimoto et al Anomalous spectral evolution upon the opening of pseudogap in a high-Tc copper oxide Nature Physics 6, 414-418 (2010)
36) R.G. Moore et al Fermi Surface Evolution Across Multiple Charge Density Wave Transitions in ErTe3 Physics Rev. B 81, 073102 (2010)
37) S. Ideta et al Enhanced superconducting gaps in the tri-layer high-Tc cuprate Bi2223 Physical Review Letters, 104, 227001 (2010).
38) W. Meevasana et al Electrons' ignorance of Phonons in the Lightly-Doped Band Insulator SrTiO3 New Journal of Physics 12, 023004 (2010)
39) K. Tanaka et al Evolution of Electronic Structure from Insulator to Superconductor in Bi2Sr2-xLax(Ca,Y)Cu2O8+d Phys. Rev. B 81, 125115 (2010).
40) J.G. Analytis et al, Bulk Fermi Surface Co-existence with Dirac Surface State in Bi2Se3: A Comparison of Photoemission and Shubnikov-de Haas Measurements Phys. Rev. B 81, 205407 (2010).
41) I.M. Vishik et al, Doping Dependence of Low-Energy Kink Observed by Laser

ARPES in Bi-2212 Physics Review Letters, 104, 207002 (2010)
42) T. Cuk et al Signatures of Pressure Induced Signatures of Superconductivity in Insulating Bi2212 Phys. Rev. B 81, 184509 (2010).
43) Y.L. Chen et al Massive Dirac Fermion on the Surface of Topological Insulator with Magnetic Dopants Science, 329, 659 (2010)
44) M. Hashimoto et al, Revealing the hidden node in the octet model of auto-correlation ARPES spectra Phys. Rev. Lett., submitted
45) W. Meevasana et al Creation and control of a two-dimensional electron gas at the bare $SrTiO_3$ Surface, Nature Materials, in review.
46) Y.L. Chen et al, Observation of Single Dirac Cone Topological Surface State in Compounds TlHiTe2 and TlBiSe2 from a New Topological Insulator Family Physical Review Letters, submitted.
47) M. Yi et al Symmetry Breaking Orbital Anisotropy on Detwinned $Ba(Fe_{1-x}Co_x)As_2$ above T_{Neel} Nature, submitted.
48) I. M. Vishik et al Cuprate Fermiology as Revealed by ARPES: a Nodal/Antinodal Dichotomy, to appear in New J. Phys.
49) S. Johnston et al Material and Doping Dependence of the Nodal and Anti-Nodal Dispersion Renormalizations in Single- and Multi-layer Cuprates Advances in Condensed Matter Physics **2010**, 968304 (2010).
50) G. R. Boyd et al, Effect of Disorder on Electronic Raman Scattering in the Superconducting State of Iron Pnictides to appear in *Phys. Rev. B.*
51) I. I. Mazin et al Pinpointing Gap Minima in $Ba(Fe_{0.94}Co_{0.06})_2As_2$ *via* Band Structure Calculations and Electronic Raman Scattering to appear in *Phys. Rev. B. Rapids.*
52) C.-C. Chen et al Orbital Order and Spontaneous Orthorhombicity in Iron Pnictides Phys. Rev. B **82,** 100504(R) (2010).
53) S. Johnston et al A Systematic Study of Electron-Phonon Coupling to Oxygen Modes Across the Cuprates Phys. Rev. B **82**, 064513 (2010).
54) S. Johnston and T. P. Devereaux Density of States Modulations from Oxygen Phonons in *d*-wave Superconductors: Reconciling ARPES and Scanning Tunneling Microscopy Phys. Rev. B **81,** 214512 (2010).
55) C.-C. Chen et al Finite Temperature Spin-Dynamics and Phase Transitions in Spin-Orbital Models Phys. Rev. B **80,** 180418(R) (2009).
56) B. Muschler et al Band- and Momentum-Dependent Electron Dynamics in Superconducting $Ba(Fe_{0.939}Co_{0.061})_2As_2$. Phys. Rev. B **80**, 180510(R) (2009).
57) G. R. Boyd et al, Probing the Pairing Symmetry of the Iron Pnictides with Electronic Raman Scattering Phys. Rev. B **79**, 174521 (2009).
58) S. Johnston, F. Vernay, and T. P. Devereaux The Impact of an Oxygen Dopant in an Ideal Bi-2212 Crystal Europhys. Lett. **86**, 37007 (2009).
59) C. S. Leem et al High Resolution Angle Resolved Photoemission Studies on Quasi-particle Dynamics in Graphite Phys. Rev. B **79**, 125438 (2009).
60) D. Reznik et al, Photoemission Kinks and Phonons in Cuprates, Nature **452**, E6 (2008).
61) F. Vernay et al Cu *K*-edge Resonant Inelastic X-Ray Scattering in Edge-Sharing Cuprate Superconductors Phys. Rev. B **77**, 104519 (2008).
62) B. Moritz et al, Insights on the cuprate high energy anomaly observed in ARPES J. Elec. Spec. Rel. Phen. **181**, 31 (2010).

Presentation Title: Nanoscale X-ray Imaging and Dynamics of Electronic and Magnetic Materials.

Principal Investigator: Oleg Shpyrko
Mailing Address: Department of Physics, University of California San Diego
9500 Gilman Dr., MC 0319, La Jolla, CA 92093-0319
E-mail: oleg@physics.ucsd.edu

A. Lens-less Coherent X-ray Diffractive Imaging of Extended Magnetic Nanostructures

Research Scope: We have successfully performed to our knowledge first ever Coherent X-ray Diffractive Imaging (CDI) of magnetic nanostructures. The approach of CDI is a lens-less alternative to optical element-based techniques, such as magnetic microscopy – whereby the diffraction pattern formed by scattering a coherent x-ray beam from a sample is inverted numerically to form an image of the object. By removing the need for optics, the spatial resolution achievable is no longer limited by the quality of the optical elements, but by the highest spatial frequencies measured in the x-ray diffraction pattern.

Recent Progress: Fig. 1 demonstrates the basic principle of magnetic CDI where by subtracting coherent diffraction patterns collected on- and off- magnetic resonance (in this case at M_5 Gd adsorption edge) one can couple directly to magnetic structure induced by Gd – therefore achieving elemental sensitivity to magnetic moment and eliminating charge scattering contribution. When combined with scanning or "ptychographic" methods any region of arbitrary large lateral dimensions can be imaged with a spatial resolution defined solely by the wavelength and coherent x-ray flux. We have performed the CDI measurements on labyrinthine stripe domains in magnetic multilayers of GdFe, and have successfully demonstrated that both the real-space magnetic structure of the sample and the complex illumination function of the x-ray beam incident on the sample can be recovered in ptychographical approach (see Fig. 2). This is an important landmark since, unlike the CDI of small particles where the beam size and/or beam

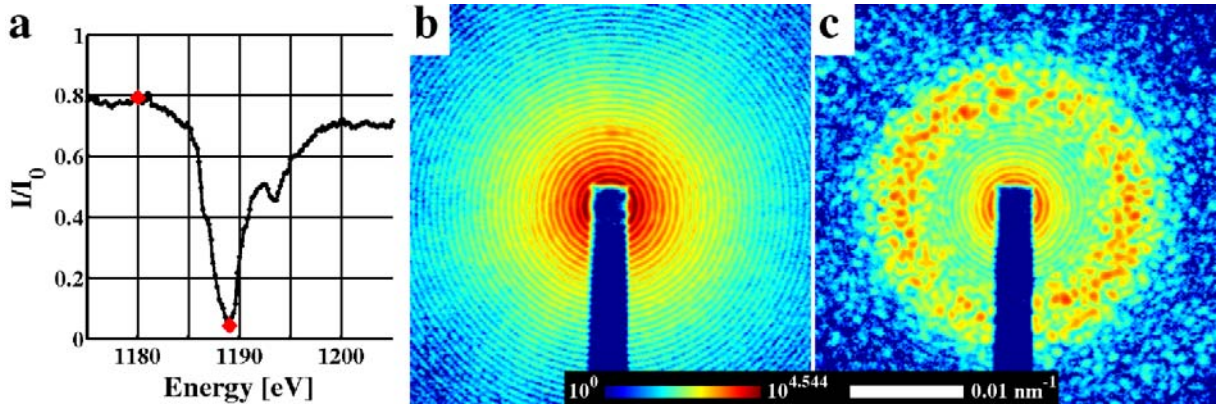

Figure 1: a) X-ray energy absorption scan across the Gd M_5 absorption edge, with red diamonds marking the x-ray energy values for which diffraction patterns (b) and (c) were collected. **(b)** Off-resonance diffraction pattern taken at x-ray photon energy of 1180 eV, has no discernible magnetic scattering and consists only of Fraunhofer diffraction fringes from the circular pinhole used to illuminate the sample. **(c)** On-resonance diffraction pattern taken at 1189 eV showing the first-order scattering ring arising from the ferromagnetic domains in the sample in addition to the Fraunhofer pattern.

coherence length is greater than particle size, in the case of extended objects, the knowledge of illumination function is a necessary condition. Ptychographic approach also provides two important improvements over standard CDI methods – (1) the iterative algorithm converges very rapidly due to additional redundancy in data collection, resulting in 10-20 times faster convergence and (2) the missing data behind the beamstop can be recovered by treating this region as an additional unknown quantity.

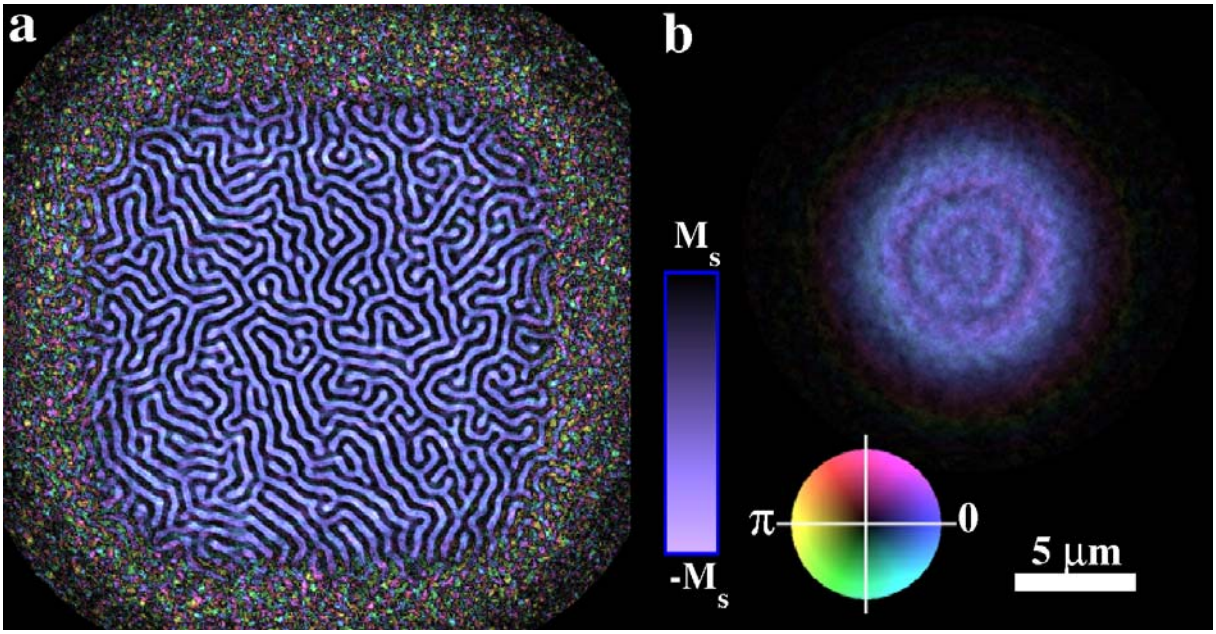

Figure 2: (a) Example of reconstructed magnetic domain structure obtained by 4x4 scanning of overlapping exposures. The extreme dark and light colors represent two anti-parallel fully saturated magnetization values (M_s) normal to the plane of the magnetic film **(b)** Reconstructed complex illumination function (amplitude shown as brightness and phase as hue) of the incident x-ray beam.

The approach taken by us allows detailed mapping of the magnetic domains with spatial resolution on the order of 60 nm, with coherent flux of $3 \cdot 10^6$ photons per second. An important consequence of this approach, however, is that it is scalable to much higher resolution in view of new generation of x-ray sources currently being developed or constructed by DOE. Figure 3 shows magnetic domain evolution in GdFe as a function of magnetic field at various points in the hysteresis loop.

The project demonstrates our ability not only to develop in-house algorithms that work on simulated or man-made objects, but can also be transferred to real-life systems. The measurements were performed at sector 2 of Advanced Photon Source at Argonne in collaboration with Ian McNulty of APS and Eric Fullerton at UCSD.

Future Plans: We plan to carry out measurements of GdFe films in the vicinity of its magnetic compensation temperature, at which magnetic moments of Gd and Fe layers are equal in magnitude but opposite in direction, forming an artificial antiferromagnetic structure.

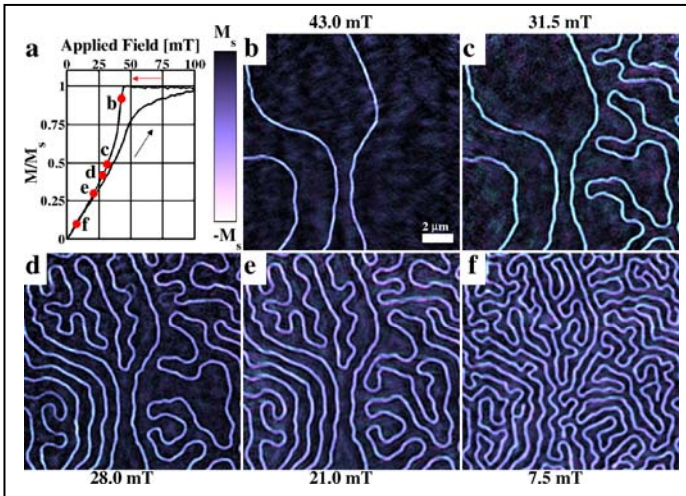

Figure 3: (a) domain evolution as the magnetic field is decreased from saturation towards zero magnetic field. (a) Hysteresis loop of sample magnetization as a function of applied magnetic field; (b-f) magnetic domain reconstructions from series of diffraction patterns taken at various points of magnetic hysteresis curve shown in (a).

At compensation temperature the ground state should not feature stripe domains since stray magnetic fields are zero (moments already fully compensated). However, domain walls could persist due to pinning. This would allow us to investigate the effects of localized pinning in more detail, and the effect pinning has on return point memory in this system. We also plan to pursue imaging studies of other magnetic film systems, such as FeRh, which exhibits an interesting FM-AFM phase transition. Finally, we are exploring the possibilities of applying the CDI techniques to studies of ultrafast spin dynamics at the newly commissioned X-ray Free Electron Laser facility at the Linac Coherent Light Source.

Publications: The manuscript is currently submitted for publication and is under review.

B. Nanodiffraction imaging of Metal-Insulator transition in VO_2

Research Scope: The thermally-driven phase transition in vanadium dioxide at T ~ 340K involves dramatic changes in electronic and structural properties. The structural phase transition is associated with dimerization of vanadium ions and is viewed as Peierls instability. Historically, the electronic insulator-to-metal transition had been thought to occur due to the Peierls instability caused by coupling of electrons to a soft-phonon mode. However, more recent work on the IMT has revealed fingerprints of significant electron-electron interactions. More detailed study of the IMT in this canonical system requires a complimentary nanoscale imaging of both electronic and structural order parameters.

Recent Progress: By using novel capabilities of the hard x-ray Nanoprobe at sector 26 of Advanced Photon Source and Center for Nanoscale Materials at Argonne National Lab, and near-field IR Nanoscopy setup at UC San Diego, we investigated the local structural and electronic properties of VO2. We performed measurements of the local structural changes in VO2 films by using nanoscale X-ray Scanning diffraction measurements that provide 40 nm spatial resolution. We find that the Structural Phase transition, like the insulator-to-metal transition, proceeds in a percolative manner resulting in coexisting structural phases. We also find that the Structural Phase transition exhibits local non-monotonic switching between structural phases, a behavior not seen in the insulator-to-metal transition imaged with near-infrared nanoscopy.

The contrasting behavior between the local structural and electronic changes suggests nanoscale decoupling between the insulator-to-metal transition and Structural Phase transition in the phase transition regime.

These measurements were performed at sector 32-ID at the Advanced Photon Source by our group in collaboration with Prof. Basov's group which specializes in complementary infrared microscopy measurements.

Future plans: We are actively developing the low-temperature capability for x-ray nanodiffraction and near-field infrared microscopy techniques. We would also like to explore the decoupling between structural and electronic phase transitions (observed by us in recent measurements) in more detail. Finally, we have found that IMT can be photo-induced in VO2 devices at room temperature when exposed to x-ray illumination. We are currently investigating the details of the x-ray photoinduced insulator-to-metal phase transitions.

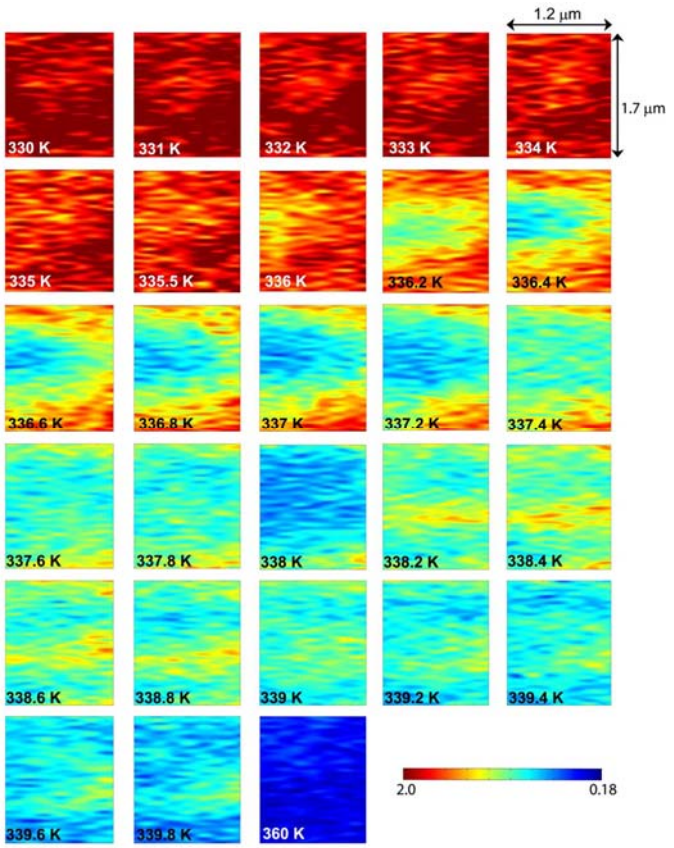

Figure 4: Spatial maps of the same 1.2mm x 1.7 mm area showing the variation in the intensity of the Bragg peak form the M1 phase of VO2 obtained with the detector angle set at 29.58 degrees. These images were obtained while heating VO2 through the SPT. The color scale in arbitrary units is the same for all the images. Higher intensities (dark and bright red) indicate the presence of the M1 structural phase.

Publications: The manuscript is submitted for publication and is currently under review.

Time- and Pressure-Dependent X-ray Diffraction

Eliot D. Specht, Judy W.L. Pang, and Gene E. Ice
Oak Ridge National Laboratory Oak Ridge, TN 37831-6118
spechted@ornl.gov, pangj@ornl.gov, icege@ornl.gov

Research Scope

In this task we use powerful synchrotron methods to provide new information about phase transformations and stability in 3*d* and other alloy systems. These measurements tie directly to applied, basic, and theory programs at ORNL and throughout the DOE system, and exploit unique x-ray and neutron optics and techniques developed within our group. The scope of this research includes time-resolved measurements of phase transformations in advanced steels and Pb-free solders (see Recent Progress) and planned measurements of chemical correlations and magnetic moments that will provide new information to help guide and test theory and neutron diffraction studies of magnetic phases in 3*d* alloys (see Future Plans).

Recent Progress

Phase Transformations in Advanced Steel

Advanced steels owe their outstanding mechanical properties to controlled processing leading to a highly engineered microstructure. The weak link is frequently the welds, where uncontrolled heating and cooling disrupts this microstructure. In collaboration with the ORNL Materials Joining Group, we have studied phase transformations during controlled thermal cycling (simulating a welding operation) to identify mechanisms by which strength and ductility can be retained. *In situ* x-ray diffraction is used to measure phase content as shown in Figure 1.

Recent work has focused on the transformation of Austenite to Bainite, a high-strength microstructure. An earlier study suggested that this transformation must be preceded by phase separation of the Austenite in which carbon is partitioned into a low- and a high-carbon phase. This implies that the alloy must be held at elevated temperature long enough to

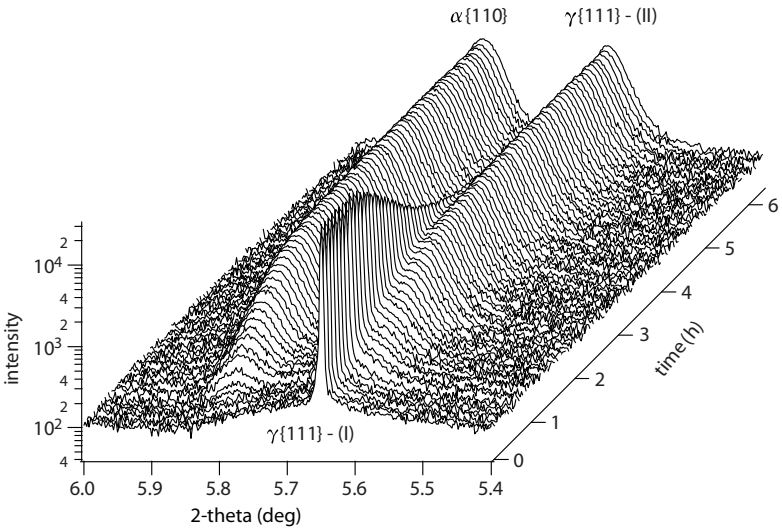

Fig. 1. Austenite (gamma) {111} and ferrite (alpha) {110} peaks during isothermal heat treatment at 300°C. Broadening of the gamma{111} peak does occur during growth of Bainite, demonstrating that carbon diffusion does not occur.

allow carbon to diffuse.

A careful lineshape analysis shows that there is no significant broadening of the Austenite peaks while Bainite is growing, meaning that carbon remains evenly distributed, and the growth of Bainite is diffusionless. Thus, the welded material may be allowed to cool quickly until Bainite begins to form.

Melting and Refreezing of Pb-Free Solders

Pb-based solders are being replaced with more environmentally benign alternatives, primarily Sn-based alloys. Sn suffers from undercooling of up to 100°C, which can lead to nucleation of undesirable hard, brittle intermetallic phases and a low-strength large-grained microstructure.

In collaboration with LLNL, we studied the undercooling of Sn-based alloys under controlled heating and cooling to identify mechanisms for rapid nucleation of solid phases and for the suppression of intermetallic phases. *In situ* x-ray diffraction is used for phase identification. We focused on the effect of substrate and cooling rate.

We first compared the undercooling Sn on graphite substrates, for which the Sn balls up, and on Cu substrates, which are wet by Sn. Average undercooling was 47°C on graphite and 26°C on Cu. The final microstructure for Sn/graphite was a twinned single crystal, while for Sn/Cu a fine-grained eutectic microstructure forms. Reaction with the substrate is critical to obtaining a desirable microstructure.

Nanoparticulate Ag is an alternative to conventional solders. Materials can be bonded at ~200°C as the Ag sinters; after grain growth, Ag has a melting point of 962°C. As shown in Fig. 2, the material sinters in 5 min at 220°C, with the grain size increasing from 2 nm to the resolution limit of 20 nm. When deposited on a Cu substrate, melting occurs at the Ag-Cu eutectic temperature of 780°C.

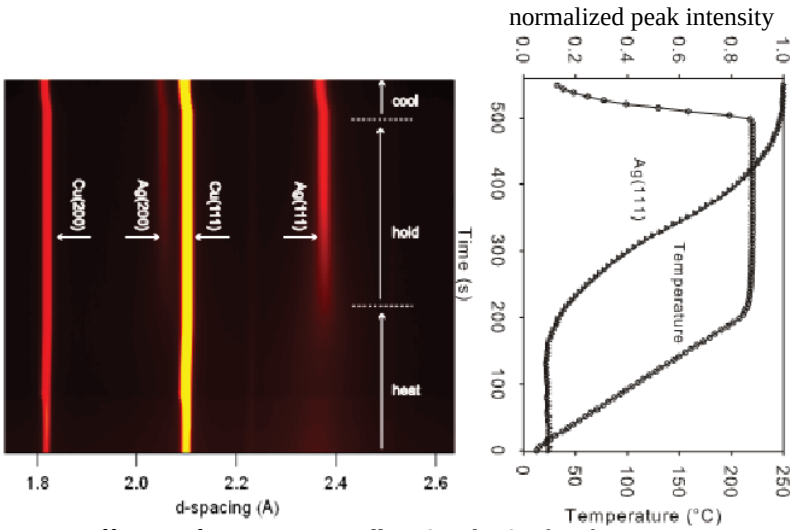

Fig. 2. Diffraction from microcrystalline Ag. the Ag {111} intensity remains fixed until ~ 220°C, where sintering initiates rapid grain growth to the instrumental resolution limit.

Future Plans

Atomic Arrangements and Magnetic Properties of 3d Alloys

Despite their critical importance to information and power transmission technologies, the fundamental mechanisms of magnetic materials based on partially-filled 3*d* orbitals are not well understood. Bulk magnetization can be reduced either by reduced atomic magnetic moments or by

noncollinear atomic magnetic moments. It is not clear how much each of these mechanisms contributes – even in pure elements such as Fe.[1-2] The problem is only complicated by the chemical disorder in useful alloys such as permalloy and Invar. The ORNL Materials Theory Group has developed new theoretical tools that can predict magnetic structure in such disordered alloys. We will provide experimental tests for these models. The subtask led by J.W.L. Pang (see Pang's abstract) will use neutron scattering to measure long-range magnetic structure; here I will describe the applications of x-ray scattering and spectroscopy.

Previous work suggests that much of the magnetic behavior of 3*d* transition metal elements is driven by changes between two states, one with high magnetic moment and high volume, the other with low magnetic moment and low volume.[3] The conjugate fields which couple most directly to these changes are pressure and magnetic field. Ferromagnetic materials are subject to strong internal fields, so they are not easily probed with external magnetic fields: high-pressure experiments are the best venue for comparing theory and experiment.

The input required for *ab initio* calculations of magnetic structure is the atomic structure, i.e. the short-range order of solid-solution alloys. This is readily determined from diffuse x-ray scattering measurements.[4]

The neutron scattering subtask will determine long-range magnetic order. The restrictions imposed by scattering through a high-pressure load cell reduce the number of reflections which can be measured, so the measurement will benefit from an independent check, which can be provided by x-ray magnetic dichroism, which measures the net component of magnetic moment parallel to the direction of an applied field, specific to each element.[5] This must equal the sum of the components on each site measured by neutron scattering.

Neutron scattering will be used to measure long-range magnetic order. In a solid-solution alloy, chemical disorder will lead to a more-or-less disordered magnetic structure. X-ray emission spectroscopy (XES) will be used to measure the magnitude of this disorder and compare it to theoretical predictions. XES is a local, chemically specific probe which measures the shift in the energy of a core-level hole produced by the unpaired electrons.[6] It will be used to calculate the average atomic magnetic moment, and the degree of disorder needed to account for the measured long-range magnetic moments.

Fortunately, a wide range of x-ray structural and spectroscopic measurements have already been made for the widely-studied Fe-Ni permalloy and Invar structures which will be our initial focus.[4-6] We will need to make additional measurements as we expand our program to Fe-Mn, Fe-Cr, and Cu-Mn alloys.

Short-Range Order in High-Entropy Alloys

High-entropy alloys (HEA) combine five or more elements in roughly equimolar proportions. The novelty of these materials is that the entropy of mixing stabilizes dissimilar elements to a simple fcc or bcc structure, combining their high ductility with large solid-solution strengthening. While the long-range order of such a HEA is simple, its properties will be sensitive to short-range order as well. It is not clear to what extent HEA resemble a solid solution or an

intermetallic at the nanoscale; the difference is critical in understanding and controlling mechanical properties.[7]

While anomalous x-ray scattering is a well-established tool for determining the short-range order and displacements from atomic sites in binary and ternary alloys, unraveling the contributions of five or more elements to a diffraction patterns is too difficult a problem: experimental parameters such as atomic scattering factors cannot determined precisely enough. Rather, we will use anomalous scattering to obtain partial pair correlation coefficients.[8] We will determine what range of short-range order and atomic displacements are consistent with these measurements. In collaboration with the ORNL Alloy Behavior and Design Group, we will determine to what extent the local behavior of HEA is similar to a solid solution alloy or an intermetallic.

References

1. D. M. Roy and D. G. Pettifor, J Phys F Met Phys **7** L183 (1977).
2. M. Uhl and J. Kubler, Physica B **237** 496 (1997).
3. P. Entel, E. Hoffmann, P. Mohn, K. Schwarz and V. L. Moruzzi, Phys. Rev. B **47** 8706 (1993).
4. G. E. Ice, C. J. Sparks, A. Habenschuss and L. B. Shaffer, Phys. Rev. Lett. **68** 863 (1992).
5. L. Nataf, F. Decremps, J. C. Chervin, O. Mathon, S. Pascarelli, J. Kamarad, F. Baudelet, A. Congeduti and J. P. Itie, Phys. Rev. B **80** 134404 (2009).
6. J. P. Rueff, A. Shukla, A. Kaprolat, M. Krisch, M. Lorenzen, F. Sette and R. Verbeni, Phys. Rev. B **63** 132409 (2001).
7. Y. P. Wang, B. S. Li and H. Z. Fu, Adv Eng Mater **11** 641 (2009).
8. A. K. Soper, Phys. Rev. B **72** 104204 (2005).

Publications

1. Mayr, P., T. A. Palmer, J. W. Elmer and E. D. Specht (2008). "Direct observation of phase transformations in the simulated heat-affected zone of a 9Cr martensitic steel." *International Journal of Materials Research* **99**(4): 381-386.
2. Stone, H. J., M. J. Peet, H. K. D. H. Bhadeshia, P. J. Withers, S. S. Babu and E. D. Specht (2008). "Synchrotron x-ray studies of Austenite and Bainitic ferrite." *Proceedings of the Royal Society of London, Series A: Mathematical and Physical Sciences* **464**: 1009-1027.
3. Elmer, J. W., E. D. Specht and M. Kumar (2010). "Microstructure and in situ observation of undercooling for nucleation of β-Sn relevant to lead-free solder alloys." *Journal of Electronic Materials* **39**: 273-282.
4. Elmer, J.W. and E.D. Specht. “Direct Observations of Silver Nanoink Sintering and Eutectic Remelt Reaction with Copper.” *Scripta Materialia*, accepted for publication.

Title: **Using X-rays to Probe Quantum Criticality***
Presenter: **George Srajer**
Mailing Address: **Advanced Photon Source, Argonne National Laboratory, Argonne, IL 60439**
Email: **srajerg@aps.anl.gov**
Collaborators: **R. Jaramillo, Y. Feng, J. C. Lang, Z. Islam, P. B. Littlewood, D. B. McWhan and T. F. Rosenbaum**

Since electrons carry both charge and spin, how magnetic order develops in metals where charge carriers remain itinerant continues to be a central problem in both condensed matter and device physics. As technology progresses and device dimensions shrink, quantum effects become more pronounced and a variety of potential ground states can emerge with coupled charge, spin, and orbital order. These effects are most acute near quantum phase transitions, where magnetism first emerges at the absolute zero of temperature. In particular, antiferromagnetic coupling between interacting mobile electrons is believed to underlie some of the most profound puzzles in modern metal physics, most notably exotic superconductivity, heavy fermions, and other non-Fermi-liquid phenomena.

The application of high pressure has been used previously as an experimental tool for investigating the origins of magnetism in condensed matter systems. Recently, such pressure studies have been also applied to study quantum phase transitions (i.e. phase transitions that are driven by quantum rather than thermal fluctuations). However, the clear identification of pressure-driven quantum critical behavior in a stoichiometric ("clean") magnet had remained elusive. In our work that appeared in the journal *Nature*[1], we directly measured quantum singularity by combining cryogenic diamond anvil cell and single crystal synchrotron x-ray diffraction measurements.

Chromium is a simple metallic crystal that exhibits a form of antiferromagnetism known as an itinerant spin density wave. This magnetic ground state, which is theoretically analogous to classical Bardeen-Cooper-Schrieffer (BCS) superconductivity varies exponentially with pressure and it is expected to be stable for very high pressures. This exponential behavior with pressure was firs demonstrated by Feng et al.[2] and Jaramillo et al.[3] for pressures up to 7 GPa. The work published in Nature describes results above 7 GPa (and up to 9.5 GPa), where the BCS-like mean field ground state is destabilized and suppressed towards a continuous quantum phase transition. The saturated magnetic moment at the highest measured pressure is a tiny 0.05 μ_B which as an order of magnitude weaker than the value at ambient pressure and is 60% weaker than the value at the weakly first-order Néel transition at ambient pressure ($T_{N,P=0}$ = 311K). The Néel transition therefore passes over from first-order in the thermal regime to second-order phase transition in the quantum regime. The discovery of a low-temperature magnetic instability in pure chromium at high pressure and low temperature raises the question of how a system can escape quantum mechanically from a ground state, which classically allows no phase transition. This question is addressed by high-resolution

measurements of the diffraction lineshapes and spin density wavevector. Which point to the role of transverse quantum fluctuations of the order parameter in the critical regime.

Future plans involve applying pressures above 9.5 GPa to further refine the departure from classical to quantum phase transition.

These measurements were made possible by the technical development of high-pressure diamond anvil cells at the University of Chicago and by the development of the high-resolution diffraction synchrotron scattering facility at the Advanced Photon Source.

References:

1. R. Jaramillo, Y. Feng, J. C. Lang, Z. Islam, G. Srajer, P. B. Littlewood, D. B. McWhan and T. F. Rosenbaum**,** Nature **459,** 405 (2009).
2. Y. Feng, R. Jaramillo, G. Srajer, J. C. Lang, Z. Islam, M. S. Somayazulu, O. G. Shpyrko, J. J. Pluth, H.-k. Mao, E. D. Isaacs, G. Aeppli and T. F. Rosenbaum. Phys. Rev. Lett. **99**, 137201 (2007).
3. R. Jaramillo, Y. Feng, J. C. Lang, Z. Islam, G. Srajer, H. M. Ronnow, P. B. Littlewood and T. F. Rosenbaum. Phys. Rev. **B 77**, 184418 (2008).

*Use of APS is supported by the U.S. Department of Energy Office of Science, under Contract No. DE-AC02-06CH11357**.**

Title: **X-ray Studies of Growth and Phase Transitions in Ultrathin Films**

PIs: G. Brian Stephenson, Paul. H. Fuoss, Dillon D. Fong
Materials Science Division, Argonne National Laboratory
9700 S. Cass Ave., Argonne, IL 60439
630-252-3214, stephenson@anl.gov

Research Scope

In situ x-ray studies of growth and evolution of thin films. X-ray techniques are uniquely suitable for study of atomic-scale processes in the non-vacuum, reactive environments often used for synthesis of multicomponent systems such as complex oxides. *In situ* observation of crystal and surface structure during growth allows understanding and optimization of materials synthesis. In addition, the ability to produce ultrathin films with well-controlled strain and interface structure provides model systems for study of size effects on phase transitions.

Ferroelectric phase transition in ultrathin films. These systems exhibit strong coupling between polarization, strain and electrostatic boundary conditions. The structure of the complete film responds to environmental changes at its boundaries. X-ray scattering is well suited to directly observe the atomic structure underlying polarization inside the active ferroelectric layer.

Recent Progress

(In collaboration with J.A. Eastman and S.K. Streiffer of ANL and C. Thompson of Northern Illinois Univ.)

X-ray scattering determination of polarization switching

The switching of polarization orientation in ultrathin ferroelectric films is both fascinating scientifically and important to current advanced electronic technologies and potential applications such as solar cells and catalysts. It has proven difficult to characterize polarization in ultrathin films using conventional electrical switching measurements because of unknown and variable voltage offsets at interfaces. We have shown that *in situ* synchrotron x-ray scattering measurements can be used to determine the polarization orientation and domain structure in ultrathin ferroelectric films [1]. While x-ray scattering is not sensitive to the interfacial charge from polarization, it is very sensitive to the atomic positions in the crystal structure of the ferroelectric that produce its polarization. By fitting the crystal truncation rod (CTR) scattering to an atomic-scale structural model, film structural parameters including its polarization and domain fractions can be obtained. We have used this technique to show that the polarization of an ultrathin film of $PbTiO_3$ can be switching by changing the oxygen partial pressure

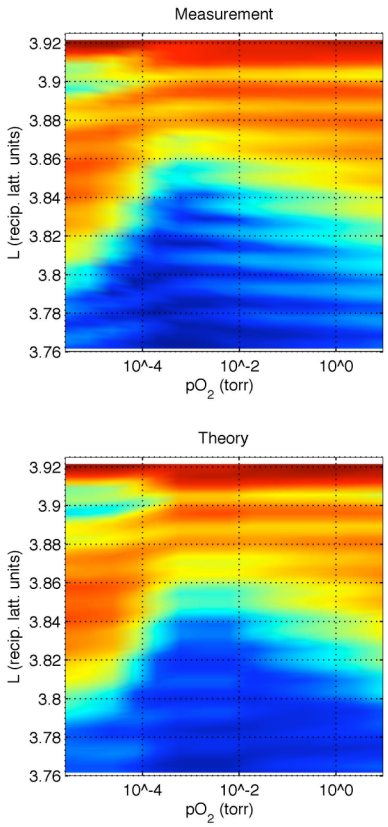

Fig. 1. (Top) Measured and (bottom) calculated scattering along the CTR through the 304 peaks during switching of a 5 nm $PbTiO_3$ film on a 25 nm $SrRuO_3$ electrode by changing the oxygen partial pressure at its surface. As the film polarization changes, not only does the $PbTiO_3$ lattice parameter respond but the fringes from the $SrRuO_3$ layer also shift, providing a direct interferometric measure of the atomic displacements underlying polarization switching.

in equilibrium with its surface [1].

Polarization switching without domain formation at the intrinsic coercive field in ultrathin ferroelectric $PbTiO_3$

In studies of the prototypical perovskite-structure ferroelectric, $PbTiO_3$, we have for the first time observed polarization reversal occurring as a continuous transition at the intrinsic coercive field, reaching the ultimate limit of polarization stability [2]. Until now, the observed behavior of the ferroelectric phase transition has been an anomaly. The ferroelectric switching process has always been found to occur by nucleation and growth of inverted domains at defects, typically giving coercive fields well below the intrinsic coercive field. In this work we investigated ultrathin, single crystal films under a uniform electric field produced chemically, and found that in sufficiently thin films, nucleation is suppressed and switching occurs by a continuous mechanism at the thermodynamic instability. The *in situ* synchrotron x-ray methods used allow direct observation of the domain structure and the piezoelectric strain for environmental conditions and film thicknesses well beyond what can be studied by other techniques. The experiments are in agreement with new theoretical models that take into account the ionic compensation at the surface of the film. In addition to achieving higher values of coercive field and compressive strain than previously thought to be possible, the results open for study a new regime of ferroelectric switching behavior with fundamental parallels to other types of phase transitions where both nucleated and continuous mechanisms occur.

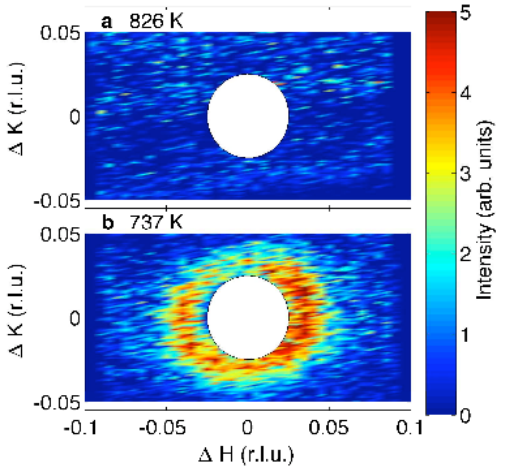

Fig. 2. Diffuse scattering around the 304 peak of a $PbTiO_3$ film at the midpoint of switching, showing switching (a) without and (b) with domain formation.

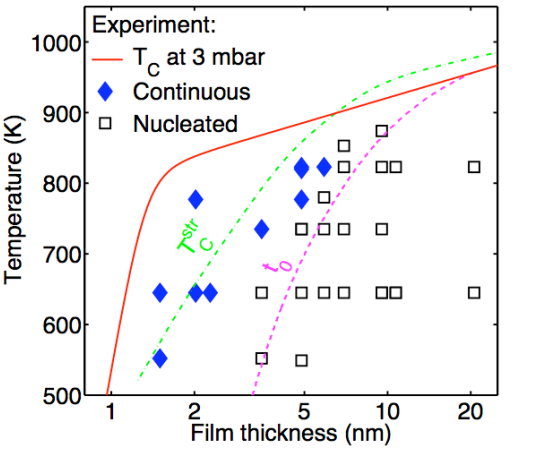

Fig. 3. Temperature-thickness phase diagram showing regions of continuous and nucleated switching, as well as equilibrium and kinetic theory for the cross-over between the two mechanisms.

Because of their electrically controllable polarization and extreme dielectric properties, ferroelectric thin films are key materials not only for current applications such as non-volatile memories, frequency-agile dielectrics, and sensors, but also for potential future breakthroughs in low-power electronics, tunable catalysts, and solar energy. This work provides new insight into the ultimate limit of stability for switchable polar states, showing that the nature of ionic compensation at interfaces can suppress inverted domain nucleation and lead to highly polarized, stable single-domain states even in small devices. The boundary we observe between nucleated and continuous behavior is in a thickness range (~5 nm) that is relevant to both current fundamental research and potential applications.

Imaging and alignment of nanoscale 180° stripe domains in ferroelectric thin films.

We have obtained the first images of equilibrium 180° ferroelectric stripe domains $PbTiO_3$ epitaxial thin films using atomic force microscopy [3]. These room-temperature images show that the stripe domains in the film can be aligned crystallographically or with unit-cell step edges on the film surface. X-ray scattering studies as a function of temperature, film thickness, and surface miscut show the regions where each of these interactions dominates the behavior of the stripes. Understanding the competing interactions that produce such nanoscale structures in complex oxides is key to developing high performance materials for energy applications.

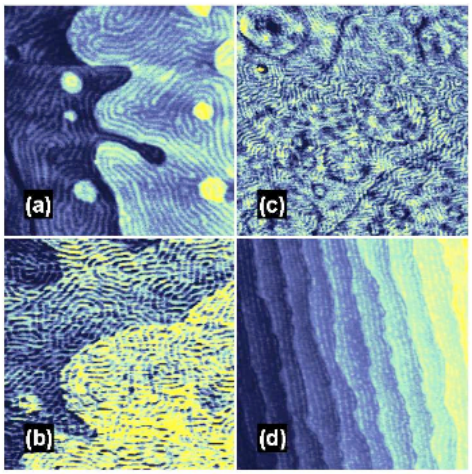

Fig. 4. Atomic force microscopy images of 180° ferroelectric stripe domains (fine fingerprint-like structures) and single-unit-cell-height surface steps and islands (coarser high contrast edges) in $PbTiO_3$ epitaxial films.

Future Plans

In situ x-ray studies of growth and evolution of thin films. Direct observation of step, island, and adatom dynamics during growth of complex oxide thin films would allow unprecedented understanding of atomic-scale mechanisms and control of materials synthesis. The availability and development of techniques using coherent x-rays show great promise in this regard [4]. We plan to develop and apply x-ray photon correlation spectroscopy and coherent diffraction imaging to crystal surfaces and interfaces *in situ* during growth and processing in reactive environments, e.g. during chemical vapor deposition and magnetron sputtering. The understanding of fundamental atomic scale processes will allow design of synthesis routes for new materials with desirable bulk and interfacial structures.

Ferroelectric phase transition in ultrathin films. Our results on chemical switching, continuous switching, and equilibrium stripe domains indicate that ultrathin ferroelectrics with controlled electrical boundary conditions offer a rich area for developing materials systems with unique structures and properties, and that these are best explored using *in situ* x-ray scattering. In particular, it appears that the equilibrium polarization phase diagrams of ultrathin ferroelectrics with realistic electrostatic boundary conditions contain unexplored phase boundaries with associated divergent properties. For example, for films with ionic surface compensation controlled by external chemical potential, the topology of the phase

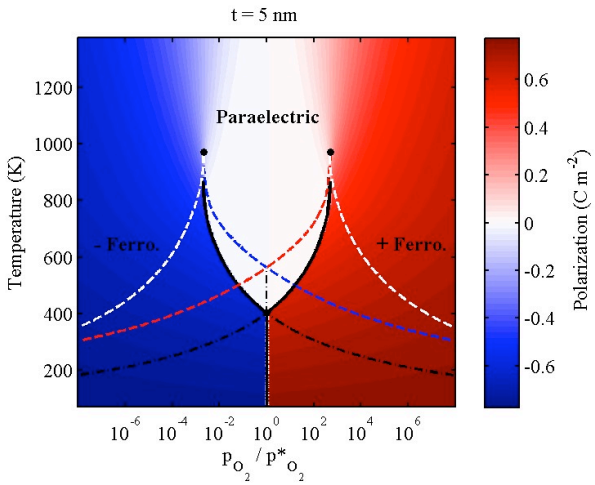

Fig. 5. Predicted phase diagram for a $PbTiO_3$ film with ionic surface compensation from a vapor, showing a stable non-polar phase between the polar phases, and new instability curves.

diagram is predicted [5] to differ from the standard one for electronic compensation (see Fig. 5). Regions of "negative capacitance" due to incomplete polarization compensation at interfaces are predicted [6] that could lead to breakthroughs in low power electronics [7]. Synthesis of structures in which equilibrium stripe domains can respond to applied field is predicted to produce high dielectric susceptibility [8]. Correlation spectroscopy with coherent x-rays will provide a powerful probe of the equilibrium and driven stripe domain dynamics.

References

[1] R.-V. Wang et al., Phys. Rev. Lett. **102**, 047601 (2009)
[2] M. J. Highland et al., to appear in Phys. Rev. Lett. (2010)
[3] C. Thompson et al., Appl. Phys. Lett. **93**, 182901 (2008)
[4] M. Pierce et al., Phys. Rev. Lett. **103**, 165501 (2009)
[5] G. B. Stephenson and M. J. Highland, unpublished (2010)
[6] S. Salahuddin and S. Datta, Nano Letters **8**, 405 (2008)
[7] L. Chang et al., Proc. of IEEE **98**, 215 (2010)
[8] A. M. Bratvoksky and A. P. Levanyuk, J. Computat. Theor. Nanoscience **6**, 465 (2009)

Publications (2008-2010)

"Continuous Switching at the Intrinsic Coercive Field in Ultrathin $PbTiO_3$," M. J. Highland, T. T. Fister, M.-I. Richard, D. D. Fong, P. H. Fuoss, Carol Thompson, J. A. Eastman, S. K. Streiffer, and G. B. Stephenson, to appear in *Physical Review Letters* (2010).

"In-Situ Synchrotron X-Ray Studies of Strain and Composition Evolution during Metal-Organic Chemical Vapor Deposition of InGaN," M.-I. Richard, M. J. Highland, T. T. Fister, A. Munkholm, J. Mei, S. K. Streiffer, Carol Thompson, P. H. Fuoss, and G. B. Stephenson, *Applied Physics Letters* **96,** 051911 (2010).

"Ferroelectricity in ultrathin strained $BaTiO_3$ films: probing the size effect by ultraviolet Raman spectroscopy," D. A. Tenne, P. Turner, J. D. Schmidt, M. Biegalski, Y. L. Li, L. Q. Chen, A. Soukiassian, S. Trolier-McKinstry, D. G. Schlom, X. X. Xi, D. D. Fong, P. Fuoss, J. Eastman, G. B. Stephenson, C. Thompson, and S. K. Streiffer, *Physical Review Letters* **103**, 177601 (2009).

"Stoichiometry optimization of homoepitaxial oxide thin films using x-ray diffraction," J. M. LeBeau, R. Engel-Herbert, B. Jalan, J. Cagnon, P. Moetakef, S. Stemmer, and G. B. Stephenson, *Applied Physics Letters* **95**, 142905 (2009).

"Reversible Chemical Switching of a Ferroelectric Film," R.-V. Wang, D. D. Fong, F. Jiang, M. J. Highland, P. H. Fuoss, C. Thompson, A. M. Kolpak, J. A. Eastman, S. K. Streiffer, A. M. Rappe, and G. B. Stephenson, *Physical Review Letters* **102**, 047601 (2009).

"Imaging and alignment of nanoscale 180° stripe domains in ferroelectric thin films," C. Thompson, D. D. Fong, R.-V. Wang, F. Jiang, S. K. Streiffer, K. Latifi, J. A. Eastman, P. H. Fuoss, and G. B. Stephenson, *Applied Physics Letters* **93**, 182901 (2008).

"Spontaneous oscillations and waves during chemical vapor deposition of InN," F. Jiang, A. Munkholm, R.-V. Wang, S. K. Streiffer, C. Thompson, P. H. Fuoss, K. Latifi, K. R. Elder, and G. B. Stephenson, *Physical Review Letters* **101**, 086102 (2008).

Magnetic and Superconducting Materials at High Pressures

Viktor V. Struzhkin, R. J. Hemley, H.-K. Mao

Geophysical laboratory, Carnegie Institution of Washington,
5251 Broad Branch Rd., N. W., Washington DC 20015
Email: vstruzhkin@gl.ciw.edu

• Research Scope

During the lifetime of this project we took the advantage of extraordinary opportunities brought about by recent breakthroughs in the creation and characterization of magnetic and superconducting materials under pressure. The project is focused on several high priority topics, e. g. insulator-metal transitions in correlated materials and superconductivity of their metallic phases under pressure, insulator-metal transition and superconductivity in compressed hydrogen compounds, superconductivity in alkali metals. We characterize magnetic and superconducting properties of transition metals and compounds (including high-T_C superconductors), that are potentially important for fundamental science or for application as high-temperature/high-critical parameter superconductors. Important part of the proposal is further improvement in the resistive and magnetic techniques based on focused ion beam (FIB) technologies and photolithography tools. We perform our measurements approaching the static limit of the diamond anvil cell techniques at high and very low temperatures, thus greatly expanding the horizon in the search for novel physical phenomena at ultrahigh pressures.

• Recent Progress

1. A pressure tuned quantum critical point in the triple-layer Bi-copper-oxides

The appeal of a universal critical point inside of a superconducting dome has stimulated extensive effort in searching for such a critical point, and a proliferation of theoretical ideas for a possible mechanism. Very recently, we have discovered re-entrant increase of T_c under pressure in Bi-2223 (triple layer) high-T_c compound. The inner plane in this material appears to be insulating even in optimally doped material. By applying pressure, we were able to tune the inner plane into metallic state (Lifshitz-type transition previously discussed by us for Bi2212 material – Cuk et. al., 2008), which provided conditions for further dramatic enhancement of critical superconducting temperature in the material.

Our recent results clearly demonstrate that the understanding of the connection between magnetic properties, electronic and crystal structures can lead to an improvement of the critical temperature of high-T_c superconducting composites such as Bi-2223.

2. Insulator-metal transitions in 3d-materials.

We have completed a series of experiments and theoretical analysis of insulator metal transition (Mott transition) in strongly correlated materials, and have found direct influence of the spin crossover effects on the Mott-type transition in several 3d materials.

a) $FeBO_3$

We have collected first high-pressure Fe pre-edge Resonant Inelastic X-ray Scattering (RIXS) spectra under pressure. Our measurements confirm the closure of Mott gap and provide further details on the interplay between multiorbital effects and Mott physics in $FeBO_3$. This study opens a new way to explore electronic energy structure of correlated materials at high pressure conditions.

b) NiO

We have observed an insulator-metal transition in nickel mono-oxide NiO at very high pressures ~240 GPa. We observed a sharp drop of resistance at about 240 GPa by about three orders of magnitude indicating transition into metallic state. This is the first experimental observation of insulator-metal

transition in NiO anticipated by Mott. Optical gap decreased approximately linearly in the region 100-240 GPa. The new metallic phase of NiO visually arises as black areas in a brown body of semiconducting phase. A sharp drop of resistance implies possible first-order type structural transition in NiO during metallization. The ongoing structural studies across the insulator-metal transition will be completed soon.

3. Hydrogen-rich solids: silane.

Structural stability of silane at high densities: Understanding the structural properties of this hydrogen-rich alloy is the first step towards understanding the observed electronic properties. Experimentally, structural determination of the hydrogen positions in materials at high-pressures is difficult, due to the very low hydrogen scattering cross section in x-ray diffraction. The structural stability at high compression remains unknown; we explored several new candidate structures and we also predicted intriguing superconducting properties for some high-pressure phases. We extended theoretical work directed towards the determination of the optimal crystal structure based on both the electronic structure and lattice dynamics calculation. Six new thermodynamically stable phases were identified and eight closely related structures were examined to address the stability issue. Three layered structures were found to favor metallization. The layered *C2/c* phase was predicted to have a superconducting transition as high as 80 K at 250 GPa. These results and findings provide important information for the future search of metallic hydrides.

4. Simple d-metals.

a) Os. Raman scattering by electrons and phonons has been studied in single crystals of 5d transition metal osmium under pressures up to 60 GPa in the temperature range of 10-300 K. An anomalous increase of the electronic light scattering cross section was found in the pressure range of 20-30 GPa with the use of green and blue excitation wavelengths. At these conditions, we observe an appearance of well defined electronic peaks at ~ 580 cm^{-1} for the wave vector direction q along [0001] and at ~ 350 cm^{-1} for q along [1010]. The comparison of q-dependencies of measured spectra and spectra calculated from the first principles suggests a strong volume and temperature-dependent renormalization of the energies and damping of the electronic states near the Fermi level.

b) Mn. We have completed the x-ray emission and x-ray diffraction studies of β-Mn. β-Mn is a metal with interesting magnetic properties involving non-collinear magnetic order and magnetic frustration. The experiments show gradual depletion of the magnetic moments under pressure, consistent with theoretical predictions.

5. Magnetic Susceptibility and Transport Techniques for Ultrahigh Pressures

We developed ultra-sensitive induction techniques for magnetic measurements in the diamond cell. Using these techniques, we completed the first magnetic measurements of superconductivity into the megabar pressure range and proceeded further to 230 GPa.

We have developed recently a new technique to attach electrical leads to the sample in the diamond anvil cell in quasihydrostatic pressure media. The platinum electrodes are deposited with the help of the Focused Ion Beam (FIB) , and he sample is attached to the 4 electrodes using FIB-deposited platinum, and the cell is loaded with gas in the insulating BN gasket with four matching electrodes extending outside the high pressure. Since FIB contacts have quite high resistance (of the order of few hundreds of Ohms) we have developed an alternative photolithography-based technique to prepare low-resistance electrodes for metal studies. The described techniques allow preparation of a "microchip"-like assembly inside of the high-pressure volume of anvil cell. These techniques are used with a new generation of non-magnetic miniature high pressure cells suitable for experiments in tiny spaces (8 and 12 mm in diameter) which fit standard magnet bore used in commercial systems (e. g. PPMS system from Quantum Design).

6. Advancement of Synchrotron Techniques for Characterization of Correlated Materials.

In addition to well developed synchrotron Mössbauer and XES high pressure techniques, we are developing also RIXS (Resonant Inelastic X-ray Scattering) techniques at the APS, ANL, in collaboration with sector 30 XOR at the Advanced Photon Source in Argonne. First high-pressure data have been obtained on $GuGeO_3$ (Cu RIXS) to 8 GPa and on $FeBO_3$ (Fe RIXS) to 70 GPa.

- **Future Plans**

The above results demonstrate the feasibility of a suite of magnetic/transport measurement techniques. As a result of recent advances, experiments utilizing an unprecedented number of probes are now straightforward to perform over a wide range of pressures. This is especially important for testing theory; for example, a fundamental understanding of the mechanisms of superconductivity requires knowledge of crystal structure, electronic structure, and vibrational properties, including the interaction of the conduction electrons with lattice vibrations. Thus, our studies will be centered around magnetic and transport measurements and complemented by a wide variety of high-pressure structural and spectroscopic methods involving laser and synchrotron radiation. The experimental challenges are listed below.

The project will encompass the following objectives, adjusted to meet new challenging goals:

(i) Exploring new potential elemental superconductors (Hydrogen) and already known superconductors (simple metals) at the limit of static high pressure techniques.

(ii) Investigating special classes of superconducting compounds (high-Tc superconductors, hydrogen compounds) that may provide new fundamental knowledge and may prove important for application as high-temperature/high-critical parameter superconductors.

(iii) Investigating the pressure dependence of superconductivity and magnetic/phase transformations in 3d transition metal compounds, including transitions from ferromagnetic to nonmagnetic phases in a broad pressure-temperature range; using the developed RIXS high-pressure technique to explore pressure-tuned electronic excitations in strongly correlated 3d-materials.

(iv) Advancing transport and magnetic techniques for measurements on small samples at very high pressures in a wide temperature range, with the application of focused ion beam technology and photolithography tailored to the design of microcircuits down to a nanoscale size, thus expanding the horizon in the search for novel physical phenomena at ultrahigh pressures.

We will use the aforementioned techniques to measure the onset of superconducting Tc as a function of pressure at the static pressure limit of the diamond anvil cell. The pressure-tuning of high-T_C superconductors will be used to uncover novel phenomena and critical points in the varying pressure-temperature-magnetic field conditions. We will also continue development of magnetic susceptibility technique to very high pressures and high temperatures, combining it with pulsed temperature regimes. We will implement miniature diamond anvil cell suitable for superconductivity studies down to 100 mK.

Complimentary X-ray fluorescence measurements of valence and core level excitations will be performed to probe the local spin state of 3d-metal ions. The RIXS technique will be used to explore multiorbital effects in Mott insulators, and the RIXS spectroscopy at the K-edges of Cu, Ni, Fe, Mn, and Co will be implemented at high pressure. Raman scattering and synchrotron infrared techniques that we have developed will be used to study optical conductivity, magnon and phonon excitations, and phase transitions. A complimentary suite of x-ray diffraction techniques will be used for structural studies.

- **References to DOI sponsored research**

Chen, X.-J., V. V. V. Struzhkin, Y. Yu, A. F. Goncharov, C.-T. Lin, H.-k. Mao, R. J. Hemley, "Novel enhancement of superconductivity by pressure-driven competition in electronic order", *Nature*. **466** , 950–953 (2010).

Gavriliuk, AG, AA Mironovich, VV Struzhkin, Miniature diamond anvil cell for broad range of high pressure measurements, Rev. Sci. Instrum. **80,** 043906 (2009).

Lyubutin, I. S., S. G. Ovchinnikov, A. G. Gavriliuk, and V. V. Struzhkin, Spin-crossover-induced Mott transition and the other scenarios of metallization in $3d^n$ metal compounds, *Phys. Rev. B **79**,* 085125, 2009.

Struzhkin, V. V., H.-K. Mao, R. J. Hemley, High-Pressure Synchrotron X-Ray Spectroscopy with Diamond Anvil Cell, a book chapter in "Perspectives in Materials Characterization", p.151-178, Universitties Press (India), Baldev Raj, ed., 2009.

Cuk, T., V. V. Struzhkin, T. P. Devereaux, A. F. Goncharov, C. A. Kendziora, H. Eisaki, H.-k. Mao and Z.-X. Shen, Determining a critical pressure of an electronic transition in cuprates, Phys. Rev. Lett. **100**: 217003 (2008).

Chen, X. J., V. V. Struzhkin, Y. Song,¤ A. F. Goncharov, M. Ahart, Z. X. Liu, H. K. Mao, and R. J. Hemley, Pressure-Induced Metallization of Solid Silane, PNAS **105**: 20-23 (2008).

Chen, X.-J., J.-L. Wang, H.-K. Mao, R. J. Hemley, and H.-Q. Lin. " Superconducting Behavior in Compressed Solid SiH_4 with a Layered Structure." Phys. Rev. Lett. **101**: 077002(2008).

Struzhkin, V. V., A. F. Goncharov, R. Caracas, H. K. Mao and R. J. Hemley, Synchrotron infrared spectroscopy of the pressure induced insulator-metal transitions in glassy As_2S_3 and As_2Se_3, Phys. Rev. B **77**, 165133 (2008).

Gavriliuk, A. G., V. V. Struzhkin, I. S. Lyubutin, S. G. Ovchinnikov, M. Y. Hu, and P. Chow, Phys. Rev. B **77**, 155112 (2008).

Ponosov, Yu.S., V.V. Struzhkin, S.V. Streltsov,and A.F. Goncharov, Q−dependent electronic excitations in osmium: pressure- and temperature−induced effects,, Phys Rev. B **78**, 245106 (2008)

Ponosov, Y S, V V Struzhkin, S V Streltsov and A F Goncharov, Pressure-induced effect on electronic excitations in osmium ,J. Phys.: Conf. Ser**. 121**, 042001 (2008).

Partially sponsored:

Cuk, T., D. A. Zocco, H. Eisaki, V. Struzhkin, F. M. Grosche, M. B. Maple, and Z.-X. Shen, "Signatures of pressure-induced superconductivity in insulating $Bi_{1.98}Sr_{2.06}Y_{0.68}CaCu_2O_{8+\delta}$", Phys. Rev. B **81,** 184509 (2010).

Q. S. Zeng, V. V. Struzhkin, Y. Z Fang, C. X. Gao, H. B. Luo, X. D. Wang, C. Lathe, Wendy L. Mao, F. M. Wu, H.-K. Mao, and J. Z. Jiang, Properties of polyamorphous $Ce_{75}Al_{25}$ metallic glasses, Phys. Rev. B **82**, 054111 (2010).

Zhang, Chao, Xiao-Jia Chen, Yan-Ling Li, Viktor V. Struzhkin, Russell J. Hemley, Ho-Kwang Mao, Rui-Qin Zhang and Hai-Qing Lin, "Superconductivity in Hydrogen-rich Material: GeH_4", J. of Supercond. And Novel Magnetism, **23**, 1557-1939, 2010.

Tang, Y., A. F. Goncharov, V. V. Struzhkin, R. J. Hemley, and M. Ouyang, Spin of semiconductor quantum dots under hydrostatic pressure, *Nano Lett. **10,*** 358-362, 2010.

Chellappa, R. S., T. Autrey, M. Somayazulu, V. V. Struzhkin, and R. J. Hemley, High-pressure hydrogen interactions with polyaminoborane and polyiminoborane, *Chem. Phys. Chem. 11,* 93-96, 2010.

Lazicki, A., A. F. Goncharov, V. V. Struzhkin, R. E. Cohen, Z. Liu, E. Gregoryanz, C. Guillaume, H. K. Mao, and R. J. Hemley, Anomalous optical and electronic properties of dense sodium, *PNAS **106,*** 6525-6528, 2009.

Chellappa, R. S., M. Somayazulu, V. V. Struzhkin, T. Autrey, and R. J. Hemley, Pressure-induced complexation of NH_3BH_3-H_2, *J. Chem. Phys. **131***, 224515, 2009.

Goncharov, A. F. , B. D. Haugen, V. V. Struzhkin, P. Beck, and S. D. Jacobsen, Radiative conductivity and oxidation state of iron in the Earth's lower mantle, *Nature*, **456**, 231-234 (2008).

Lin, J-F., G. Vankó, S. D. Jacobsen, V. Iota, V. V.Struzhkin, V. B. Prakapenka, A. Kuznetsov,, C.-S. Yoo, Electronic Spin Crossover of Iron in Ferropericlase in Earth's Lower Mantle, *Nature Geoscience* **1,** 688-691 (2008).

Quantifying Damage Accumulation During Ductile Plastic Deformation Using Synchrotron Radiation

PI's: Robert M. Suter[1] and Anthony D. Rollett,[2]
[1] Department of Physics, Carnegie Mellon University, Pittsburgh, PA 15213
suter@andrew.cmu.edu
[2] Department of Materials Science and Engineering, Carnegie Mellon University, Pittsburgh, PA 15213
rollett@andrew.cmu.edu

Polycrystals play key roles in infrastructure systems that serve in hospitable and extreme environments in energy, transportation and many other sectors of the economy (bridges, car frames, nuclear reactor cores, propulsion and power turbines, and fuel cells, to name a few). Application critical macroscopic properties emerge from nanoscopic and mesoscopic features such as crystalline grain sizes and relative orientations, grain boundary types, defect content, and stress states. Due to a lack of appropriate experimental probes, there have been virtually no measurements that follow these structures in a volume of material as it responds to the thermo-mechanical treatments encountered in processing and applications. However, it has recently become possible using synchrotron based High Energy X-ray Diffraction Microscopy (HEDM), to non-destructively measure the positions, shapes, and crystallographic orientations and orientation gradients of grains deep inside of generic polycrystalline bulk materials. [1, 2, 3, 4, 5, 6, 7] This technique promises to allow studies of materials responses to a wide variety of in-situ or ex-situ treatments including thermal, mechanical, radiation and combinations thereof. By tracking the response of statistically significant volumes of material, these studies will be used to constrain and validate computational models: the measured three dimensional, digitally represented structure can be used as a starting point for the computation and evolution can be compared directly to experiment. Validated and trusted computational models are a critical requirement for "integrated computational materials engineering." [8]

We are applying HEDM to the problem of tracking damage accumulation in metal wires as they are subjected to tensile strain. Combining HEDM with x-ray absorption tomography allows for early detection of voids as they nucleate, coalesce and ultimately lead to failure. Combining near-field HEDM mapping with far-field measurement of elastic lattice strain will allow correlation of stress "hot spots" with microstructural environments. Development of the capabilities needed for the current studies will significantly broaden the applicability of the HEDM technique and should lead to greatly increased usage. Here, we describe first measurements of strain response using a small diameter copper wire.

Measurement Method. Measurements are carried out at Advanced Photon Source (APS) beamline 1-ID, a dedicated high energy scattering facility. A combination of a double bent Laue monochromator and refractive optics yield a line focused x-ray beam (typically 64 keV) with dimensions at the sample position of approximately 2μm vertically by 1.3 mm horizontally. A high precision air bearing rotation stage rotates the sample in the beam. Three orthogonal translations allow sample positioning relative to the rotation axis and a translation under the rotation stage is used to center the axis in the beam. Semi-automated alignment macros provide for efficient set-up of the apparatus and samples.

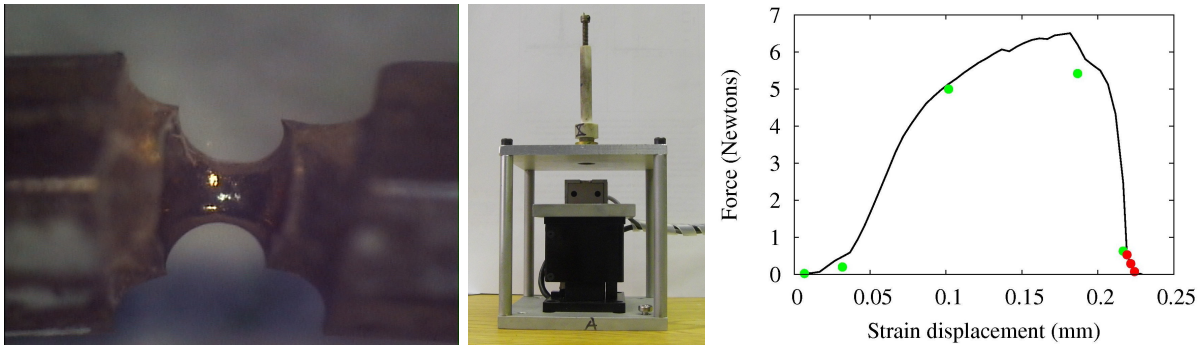

Figure 1: (a) Optical image of a doubly necked copper wire, (b) custom built (first generation) wire pulling apparatus, and (c) the force-extension curve for the copper strain measurement. See text for discussion.

Diffraction patterns are measured with a high spatial resolution detector system that uses a lens coupled 2k × 2k CCD to image scintillation light generated when x-rays strike a free standing, 25μm thick LAG scintillation crystal. With an effective pixel size of $1.5 \times 1.5\mu m^2$ the system has a $3 \times 3mm^2$ field of view. The LAG scintillator has greatly improved the quantum yield compared to previous and has allowed a reduction in data collection time by roughly a factor of five. This in turn allowed the collection of a much larger data volumes in multiple strain states for the Cu sample discussed below. Diffraction patterns are measured at either two or three rotation axis-to-detector distances, L, in the range of five to ten millimeters.

In addition to HEDM orientation mapping, we use absorption tomography to measure the wire profile and to search for void formation. In the present measurements, we removed the refractive focusing lens and measured the intensity pattern over a 300μm high cross-section of the wire. The same high resolution imaging detector discussed above is used here. A layer-by-layer tomographic measurement which completely removes registration issues has been demonstrated. [9]

Measurement of strain response of a copper wire. Fig. 1 shows the copper wire, the wire pulling apparatus and the force-extension curve observed in the in-situ measurement. The wire has been electropolished from its nominal 1 mm diameter (see at left and right sides). The necking procedure focuses strain in a restricted length of the wire (allowing foreknowledge of where to do the measurements) and reduced the needed force to the range of the apparatus shown in Fig. 1b. The smallest diameter is roughly 200μm and the necked region is about 300μm in length. Fig. 1b shows the pulling apparatus which uses a ceramic cylinder (Macor) as the load bearing element (top). The wire is fixed at the top, passes through the hollow cylinder and is fixed to the load cell below the aluminum frame. A translation stage (bottom) pulls the wire. This design allows the x-ray detector to approach within 5 mm of the wire which is positioned on the axis of the air-bearing rotation stage. Fig. 1c shows the force-extension curve for the necked Cu wire. The curve is rounded due to the strain gradients caused by the variable diameter along the length of the wire. Green points indicate states in which both microstructure mapping and tomographic data were collected;

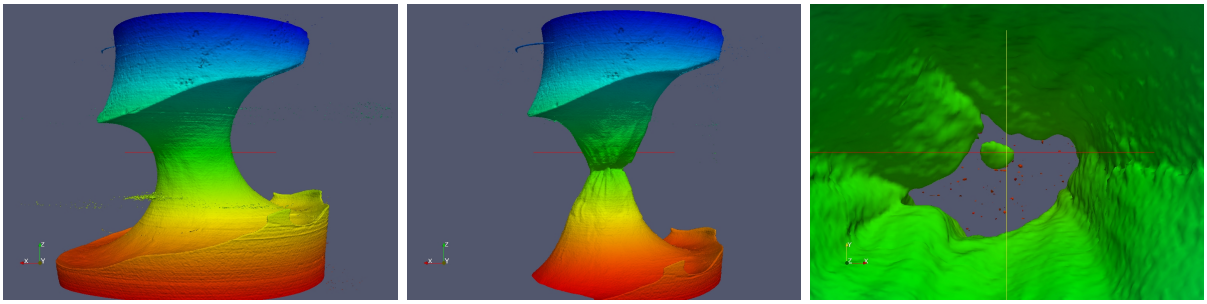

Figure 2: Tomographic images of the copper wire as it is strained to failure. Colors are by z-coordinate and are scaled for each image independently. (a) Contour showing the initial shape of the necked wire. The large diameter is 0.5 mm (the first neck step seen in Fig. 1a) while the necked region is roughly 0.2 mm. (b) In the stain 4 state, the neck is reduced to $\approx 0.1mm$ diameter and the cross-section has become non-uniform. In the top view of (c) at strain 4, one can see a large void that has formed near the narrowest region of the neck. The shape of the void is non-trivial.

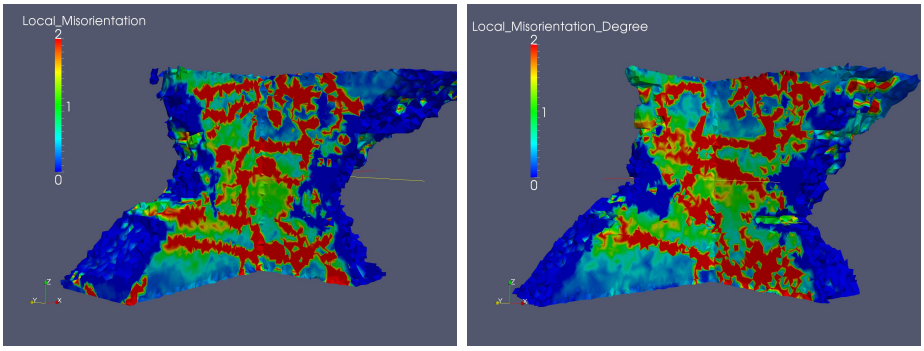

Figure 3: Local misorientations mapped inside the copper wire at zero strain and at 0.1 mm strain displacement. Note that the color scale saturates at two degrees.

the red points, just prior to failure, correspond to tomography-only points. Measurement points are plotted at fully relaxed force values.

Fig. 2 shows tomographic reconstructions of the wire in two strain states (0.01 and 0.18 mm extension of Fig. 1c). Fig. 2c shows a view looking down from the stop in the 0.18 mm extension state and shows a void formed at the narrowest part of the collapsing wire. Fig. 3 shows examples of 3D orientation maps and local misorientation maps in two strain states.

Fig. 3 illustrates the degree of reproducibility in reconstructions and the measurement's sensitivity to even the beginning of response to strain. The images are cut-aways of the cylindrical wire cross-section. The color scale indicates, on a voxel-by-voxel basis, the maximum nearest-neighbor misorientation angle, a measure of local disorder. Well ordered material is blue. Red indicates misorientations greater than two degrees which predominately show on grain boundaries. One can see that some boundaries have moved but the boundary network has not changed dramatically. Careful examination also indicates an increase in the occur-

rence of ≥ 1 degree misorientations in the strained state. Further analysis of this and higher strain states will be presented at the meeting.

These studies will be supplemented by additional tests on larger wires (with a modified apparatus) containing more grains in the active region and by similar work on zirconium wires. We continue to improve data acquisition speed and reconstruction algorithms. In the latter case, we are incorporating a multi-pass scheme that ultimately will lead to more detailed intensity matching and lattice strain parameter adjustment.

References

[1] S.F. Li, J. Lind, C.M. Hefferan, U. Lienert, A.D. Rollett, R.M. Suter, "Grain boundary character distributions measured with high energy x-ray diffraction microscopy", in preparation. (document)

[2] U. Lienert, M.C. Brandes, J.V. Bernier, M.J. Mills, M.P. Miller, S.F. Li, C.M. Hefferan, J. Lind, R.M. Suter, "3DXRD at the Advanced Photon Source: Orientation Mapping and Deformation Studies," Risoe 2010 Symposium proceedings, accepted. (document)

[3] S.R. Wilson, C. Hefferen, F. Li, R. Suter and A.D. Rollett, "Microstructural Characterization and Evolution in 3D," Risoe 2010 Symposium proceedings, accepted. (document)

[4] U. Lienert, M. Miller, S.F. Li, J. Lind, C.M. Hefferan, R.M. Suter, "High Energy Diffraction Microscopy at the Advanced Photon Source," submitted to the Journal of Materials (invited). (document)

[5] C. M. Hefferan, S. F. Li, J. Lind, U. Lienert, A. D. Rollett, R. M. Suter, "In-situ Observation of Recovery and Grain Growth in High Purity Aluminum," Proceedings of the 2010 International Conference on Recrystallization and Grain Growth, Sheffield, England, July 2010. (document)

[6] C.M. Hefferan, S.F. Li, J. Lind, U. Lienert, A.D. Rollett, P. Wynblatt, R.M. Suter, "Statistics of High Purity Nickel Microstructure From High Energy X-ray Diffraction Microscopy," Computers, Materials and Continua, **14**, 209-219 (2009). (document)

[7] C.M. Hefferan, S.F. Li, J. Lind, R.M. Suter, "Tests of microstructure reconstruction by forward modeling of high energy X-ray diffraction microscopy data," Powder Diffraction, **25**, 132-137 (2010). (document)

[8] National Research Council report, "Integrated Computational Materials Engineering: A Transformational Discipline for Improved Competitiveness and National Security," available at http://www.nap.edu/catalog/12199.html (2008). (document)

[9] P. Kenesi, A. Khounsary, U. Lienert, S. F. Li, J. Lind, C. M. Hefferan, R. M. Suter, "A single crystal attenuator for combined high energy microstructure mapping and tomography measurements," in preparation. (document)

Sub-micron Resolution 3D X-Ray Microscopy Studies of Materials Microstructure and Deformation

J.Z. Tischler, B.C. Larson, J.D. Budai, and G.E. Ice
Materials Science & Technology Division, Oak Ridge National Laboratory
Oak Ridge, TN 37831
tischlerjz@ornl.gov

RESEARCH SCOPE

The research goal of this program is directed toward a fundamental understanding of the underlying atomic and mesoscale origins of the properties of materials using x-ray scattering and microscopy investigations combined with collaborative, first-principles theory and modeling analyses. The physical properties of real materials are controlled by more than their local atomic structure. Much of the behavior comes from microstructure and defect interactions that occur on mesoscopic length scales of tens of nanometers to hundreds of microns. 3D x-ray structural microscopy (3DXM) provides the ability to nondestructively measure the local crystal structure, orientation, and local lattice curvature and elastic strain tensors with submicron spatial resolution. Investigations in this program include three-dimensional submicron-resolution (~300 nm) x-ray microscopy studies of the microstructure and evolution of materials on mesoscopic length scales (tenths-to-hundreds of microns).

The 3D spatial resolution microstructure measurements capability made it possible in this program to measure the strain in the interior of individual dislocation cells associated with dislocation patterning in heavily deformed copper. To further probe the underlying processes of deformation, the strain state of the much thinner (~100 nm) dislocation cell walls in deformed Cu have now been measured. The confined deformation distribution below spherical micro-indents has been probed, and the processes associated with initial crystal breakup during deformation are under investigation in conjunction with first principles based discrete dislocation theory simulations. The submicron spatial resolution of 3DXM has been used to investigate the local structure and microstructure of materials ranging from phase-separated manganite alloys to nano-ribbons to strongly correlated oxide nano-flakes, and it has been used to correlate the impact of grain boundaries and microstructure on the local efficiency of multicrystalline silicon solar cells.

RECENT PROGRESS

Elastic Strain of Individual Dislocation Cell Walls in Deformed Cu: Deformed Cu develops an inhomogeneous dislocation cell structure in which dislocation-rich walls surround lightly dislocated crystalline cell interiors. Previous 3DXM measurements in this program on 30% deformed Cu single crystals yielded the first direct demonstration of back stress strain in the cell interiors as postulated by the ”composite” model of Mughrabi. We have made the first direct measurement of the strain in the surrounding cell walls by combining angle-resolved and spatially-resolved 3DXM. As illustrated in the middle panel of Fig. 1a, by masking out the sharp spot scattering from the low dislocation density cell interiors and analyzing only the diffusely scattered intensity between and around the spots, it is possible to determine the Bragg angle (and hence the strain state) of the highly dislocated cell walls. By analyzing the scattering from *only* the upper and lower peaks in the center diffraction panel in Fig. 1a, the Q-distribution from the two cell interiors are determined as the dashed lines in Fig. 1b. By excluding the scattered intensity from the two spots, and analyzing only the diffusely scattered intensity at 4 μm, gives a wave vector Q-distribution of the intervening cell wall that is shown by the solid red curve in part b. The mean stress in the cell wall is essentially zero (–1 ± 7) MPa, while the mean stresses of the adjacent cell interiors are a much larger 60 and 21(± 7) MPa. The “composite” model predicted this type of result, arguing that the cell walls are smaller in volume but because they are highly dislocated are more difficult to deform than the more perfect cell interiors. The fact that the widths of the Q-distributions (i.e. strain fluctuations) for both the cell interiors and

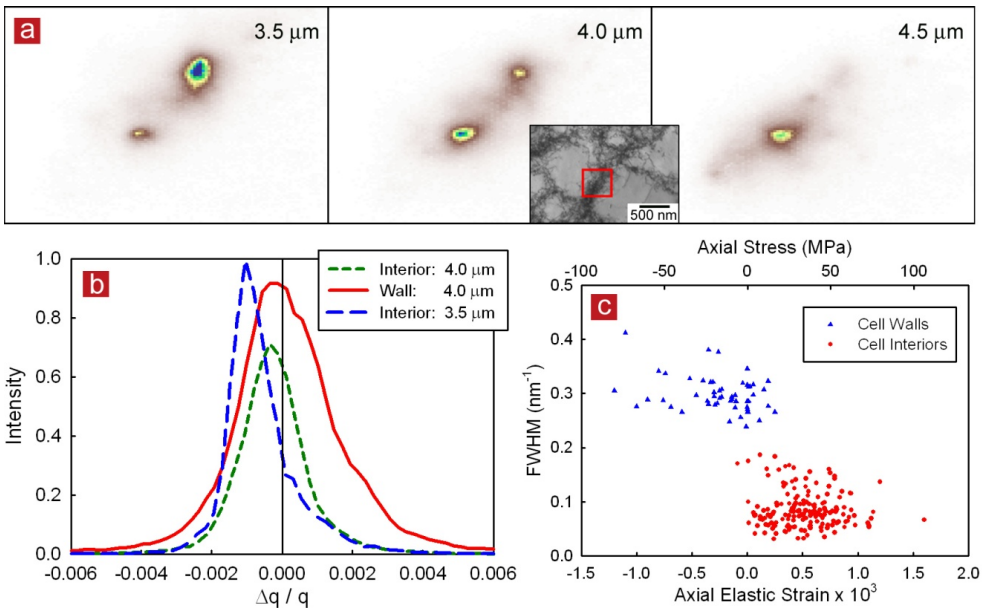

Figure 1. (a) Polychromatic diffracted intensity from two adjacent dislocation cell interiors at measured depths of 3.5 and 4.5 µm. The diffuse scattered intensity between the two peaks at a depth of 4 µm comes from the highly dislocated cell wall that separates the cells. The red box on the TEM micrograph is a representative example of the volume measured by this series of three diffraction patterns. (b) Q-distributions of the 006 reflection from the two cell interiors and the surrounding diffuse scattering from the 4 µm depth in part a. (c) FWHM from many volume elements showing variation of width with elastic strain along the 006 direction; there are two distinct populations.

the cell walls in Fig. 1b are much larger than the (0.02 nm^{-1}) measurement resolution indicates that cell interiors are not dislocation free as implied by the TEM measurements, but only much less defected than the cell walls; the plot in Fig. 1c of the widths *vs*. the strains for a large number of measurements also shows this to be true in general. The magnitudes of the strains in Fig. 1c, the strain distributions, and the positive *vs*. negative separation of the strain magnitudes in the cell interiors and walls into two populations, provide previously missing constraints for testing theoretical deformation models.

Orientation Dependence of Deformation Under Spherical Indents in Cu: The highly confined nature of deformation below surface indents provides an opportunity for detailed investigation of deformation on mesocopic length scales. Fig. 2 shows an absolute comparison of measured and calculated surfaces of (± 0.4°) rotational deformation under 100 µm radius spherical indents with 100 mN force in ‹111› and ‹001› oriented Cu single crystals. Remarkably, the measured deformation penetrates more than 50% deeper into the ‹111› oriented Cu than for the ‹100› case. The crystal plasticity deformation simulations (by Y. Gao; UT-K/ORNL) predict both the magnitudes of the (blue) outward rotations and the strong asymmetry with surface orientation; however they predict substantially larger inward rotations (red) than those observed for both orientations. There is also an oscillating substructure in the rotations as a function of depth corresponding to dislocation patterning. Initial finite element modeling simulations have shown that the introduction of strain-gradient-based plasticity into the deformation model does not explain the differences between experiment and theory. These results underscore the importance of quantitative experiment-theory comparisons with confined indentation volumes.

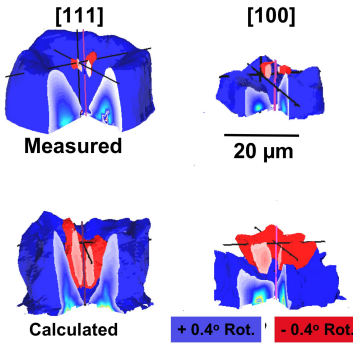

Fig 2. Comparison of measured and calculated deformation-induced lattice rotations for spherical indents in ‹100› and ‹111› oriented Cu. The blue and red surfaces represent surfaces ±0.4° rotations relative to the surface normal.

Multicrystalline silicon solar cells: 3D x-ray microscopy was used to investigate the effect of grain boundaries on solar cell efficiency in multicrystalline silicon, one of the primary starting materials for commercial solar cells. Although solar cells made from single crystal silicon are more perfect than those from multicrystalline silicon, the multicrystalline silicon is much cheaper and easier to produce. However, the efficiency of multicrystalline silicon is reduced by electron-hole recombination at grain boundaries and other defects. We have made spatially-resolved measurements of the crystal orientation in multicrystalline solar cells and correlated them with area scanned light beam induced current (LBIC) measurements to investigate how the silicon grain boundaries affect the local solar cell quantum efficiency.

X-ray and LBIC measurements were obtained from multicrystalline Si produced by two different techniques, commonly referred to as the heat exchanger method (HEM) and the ribbon technology. The x-ray orientation map in Figure 2 (b) shows the grain structure from ribbon grown multicrystalline silicon measured with 8 µm step size (500 nm beam). The different colors represent the crystal orientations and are assigned from the pole figure in (a). The x-ray results reveal an overall (110) texture with ~20° misoriented regions containing thin parallel twins. The HEM silicon (results not shown) had a nearly perfect (110) fiber texture (within 0.2°) and grains with large in-plane rotations separated by more irregular boundaries. Figure 2 (c) and (d) show LBIC measurements for the ribbon sample at two different wavelengths (different penetrations) with 5 µm resolution. Comparing the maps of quantum efficiency with orientations for both types of silicon shows that a drop in conversion efficiency coincides with a structural boundary, showing that the grain boundaries are indeed important recombination sites. However, the correlation was not complete and some benign grain boundaries did not lead to a reduction in quantum efficiency. Additional analysis to identify and understand structural or chemical grain boundary differences controlling efficiency is ongoing.

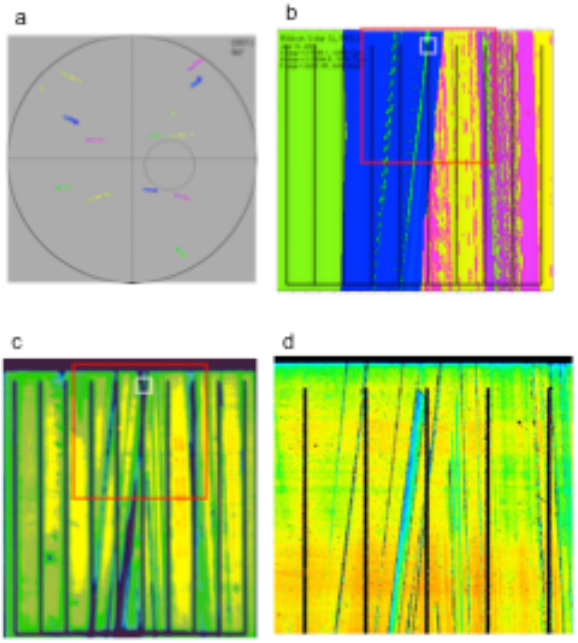

Figure 2. (a) (001) Stereographic projection of the orientation map in part b. (b) spatially resolved orientations with colors from the 001 pole figure in part a for the ribbon multicrystalline silicon sample. The vertical black lines are from the electrical contacts that are 2mm apart. (c) LBIC measurements at 980 nm and (d) 633 nm. The red box in part c indicates the region shown in d. The color scale for the 980 nm LBIC measurements goes from black to orange (high), while the scale for the 633 measurements goes from black to red (high).

FUTURE PLANS

3D X-Ray Microscopy: The 3D x-ray microscopy technique used in this program is the only nondestructive method capable of measuring the strain and orientation of every point within a volume at submicron resolution. This is a needed capability for determining the geometrically necessary dislocation (GND) density within deformed volumes. Fundamental investigations of deformation and strain localization will be directed toward detailed comparisons of experimental measurements with computer simulations. This work will build on present 3D x-ray microscopy capabilities to pursue a predictive understanding of deformation on mesoscopic length scales.

The inhomogeneous nature of deformation on mesoscopic length scales resulting from the complex and collective interactions of dislocations requires measurements with high spatial resolution covering substantial sample volumes to ensure that the effects of long range dislocation interactions are included. Thus we plan

to use smaller beam sizes to allow us to completely isolate individual dislocation cells and walls so as to clearly see the nature of the interaction between cells and the surrounding walls. We also plan to make simultaneous measurements of the strain in widely separated directions to permit determining all components of the dislocation tensor; the current measurements have all been along only one direction. Studies of lightly (~1%) deformed crystals will be used to characterize the initial stages of crystal breakup and can be directly compared to the results of discrete dislocation simulations. We also plan to extend our investigation of deformation to Ni, Al, and iron-based alloys adding *in-situ* indentation studies and the examination of indents in the neighborhood of grain boundaries to understand the role of boundaries in deformation.

We will exploit recent hardware and analysis software improvements to collect and evaluate larger volumes with finer resolution. Measuring large 3D volumes is both time consuming and data intensive, but extremely important for making progress in all parts of this program, including: dislocation cells in copper, deformation under nano-indents, phase coexistence in manganites (*e.g*. LaPrCaMnO), mesoscopic phase separation in multiferroics (*e.g*. (Y,Eu)MnO), 3D grain growth, and the role of the domain structure during metal-insulator transitions (*e.g*. VO_2). To date only very limited volumes have been measured, so we will exploit recent improvements to acquire the larger data sets needed to understand these systems.

Journal Publications

1. A. Tselev, E. Strelcov, I.A. Luk'yanchuk, J.D. Budai, J.Z. Tischler, I.N. Ivanov, K. Jones, R. Proksch, S.V. Kalinin, and A. Kolmakov, "Interplay between Ferroelastic and Metal-Insulator Phase Transitions in Strained Quasi-2D VO2 Nanoplatelets," *Nano Letters* **10**, 2003-2011 (2010).
2. R.I. Barabash, J. Tischler, G.E. Ice, O.M. Barabash. "Small Scale Mechanical Behavior and Interface strength in Ni-Mo Composites from 3D X-Ray Microdiffraction", in: 31st Risø International Symposium on Materials Science: Challenges in Materials Science and possibilities in 3D and 4D techniques, Denmark, 1-9, (2010).
3. T. Hoffmann, J. Kalisch, A. Bertram, S. Shim, J.Z. Tischler, H. Bei, and B.C. Larson, "Experimental Identification and Validation of Models in Micro and Macro Plasticity", *Technische Mechanik*, **30**, 136–145 (2010).
4. T. Hoffmann, A. Bertram, S. Shim, J.Z. Tischler, and B.C. Larson, "Experimental Identification and Validation of a Crystal Plasticity Model for a Low Carbon Steel on Different Length Scales", *International Journal of Material Forming*, 3, **65-68**, (2010)
5. G.E. Ice, J.W.L. Pang, B.C. Larson, J.D. Budai, J.Z. Tischler, J.-Y. Choi, W. Liu, C. Liu, L. Assoufid, D. Shu, and A. Khounsary, "At the Limit of Polychromatic Microdiffraction," *Mater. Sci. Eng. A* **524**, 3-9 (2009).
6. T.Z. Ward, J.D. Budai, Z. Gai, J.Z. Tischler, Lifeng Yin, and J. Shen, "Elastically-Driven Anisotropic Percolation in Electronic Phase-Separated Manganites," *Nature Physics* **5**, 885-888 (2009).
7. L.E. Levine, B.C. Larson, J.Z. Tischler, P. Geantil, M.E. Kassner, W. Liu, and M.R. Stoudt, "Impact of dislocation cell elastic strain variations on line profiles from deformed copper", *Zeit. für Kristallogr.* Suppl. **27**, 55 (2008).
8. H. Bei, R.I. Barabash, G.E. Ice, W. Liu, J.Z. Tischler, and E.P. George, "Spatially resolved strain measurements in Mo-alloy micropillars by differential aperture x-ray microscopy", *Appl. Phys. Lett*. **93,** 071904 (2008).
9. J.D. Budai, W.-J. Liu, J.Z. Tischler, Z.W. Pan, D.P. Norton, B.C. Larson, W. Yang, and G.E. Ice, "Polychromatic X-ray Micro and Nanodiffraction for Spatially-Resolved Structural Studies", *Thin Solid Films* **516,** 8013 (2008).
10. B.C. Larson, J.Z. Tischler, A. El-Azab, and W.J. Liu, "Dislocation density tensor characterization of deformation using 3D X-ray microscopy", *J. Eng. Mater. Technol.* **130** (2), 021024 (2008).

Structure-function studies in organic photovoltaic materials for sustainable energy generation

Michael F Toney
Stanford Synchrotron Radiation, Lightsource, SLAC National Accelerator Laboratory,
2575 Sand Hill Road, Menlo Park, Ca 94025
mftoney@slac.stanford.edu

"Plastic" solar cells based on interpenetrating blends of a semiconducting polymer and a fullerene are becoming a viable technology for sustainable energy generation due to the promise of low-cost manufacturing. A rapid increase in efficiency over the last decade has been accomplished through a result of a deeper understanding of the influence of microstructure on performance. This has lead to improved materials design and better control over the microstructure and morphology. Both the nanoscale morphology of the two-phase film and the molecular packing within the polymer and fullerene are tremendously important to device performance. We have used X-ray scattering to probe both the nm length scale microstructure and the molecular packing in organic solar cells. Grazing incidence X-ray scattering (GIXS) was used to investigate the local molecular packing [1-5] and small angle X-ray scattering is being developed to probe the polymer-fullerene phase separation.

This contribution will focus on blends of the fullerene, phenyl-c71-butyric acid methyl ester (PCBM), and the high performance semiconducting polymer poly(2,5-bis(3-alkylthiophen-2-yl)thieno[3,2-b]thiophenes (PBTTT). Our previous diffraction results [6,7] showed that, unexpectedly, the PBTTT and PCBM intermix or intercalate on a molecular level and form bimolecular co-crystals (see Figure 1). This explains many previous results on the optimal mixing ratios of various polymer fullerene blends. However, a detailed picture of the co-crystal structure was not obtained. This is important because the self-ordering of the co-crystal affects the physical processes involved in light absorption and charge separation and transport; it is also of interest from a fundamental point of view of materials mixing.

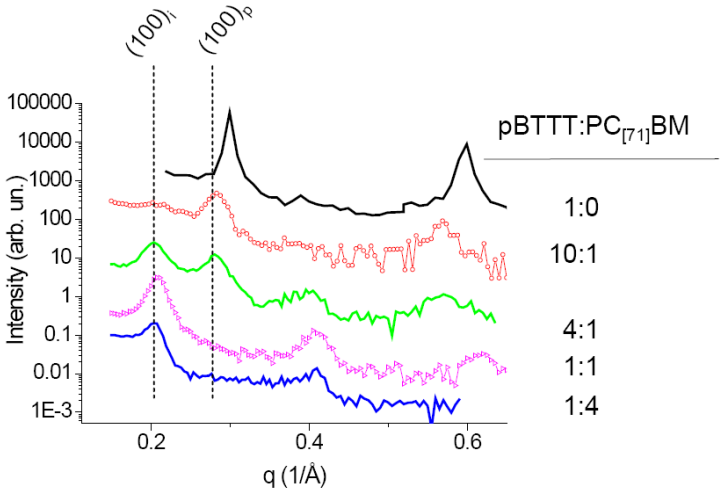

Figure 1. Specular X-ray diffraction of annealed pBTTT:PCBM films with varying weight ratios demonstrating the intercalation. Pristine film (black); 10:1 blend (red); 4:1 blend (green) shows a coexistence of the pBTTT lattice and the intercalated lattice; 1:1 blend (purple) and 1:4 (blue). Here i is intercalated and p is pristine.

To determine the structure of the polymer-fullerene co-crystal, we used a combination of x-ray diffraction and molecular mechanics (MM) simulations. We start by using the empirical diffraction data to obtain the polymer-fullerene ratio and to develop two potential unit cells. We then refine these unit cells with MM modeling using the Universal force field model to find low energy configurations for the system. We finally compare the diffraction pattern from the model with that of the experiment. Such a multi-pronged approach is necessary for our thin films of poorly ordered soft materials that have diffraction patterns without many well defined peaks. Using this approach, we obtain an energetically optimized triclinic unit cell. This is shown in Figure 2 This structure is characterized by edge-on stacked conjugated backbones (red color), fullerene molecules that are intercalated between the side chains of the polymer, and bent side chains. The structure suggests that well-separated channels, where the PCBM molecules intercalate, exist along the *b* axis. The fullerenes are in immediate vicinity to every part of the polymer backbone and the conjugated rings orient towards fullerenes. The arrangement of the polymer chains and the PCBM in the polymer framework has a critical impact on charge transport as this enables rapid exciton dissociation.

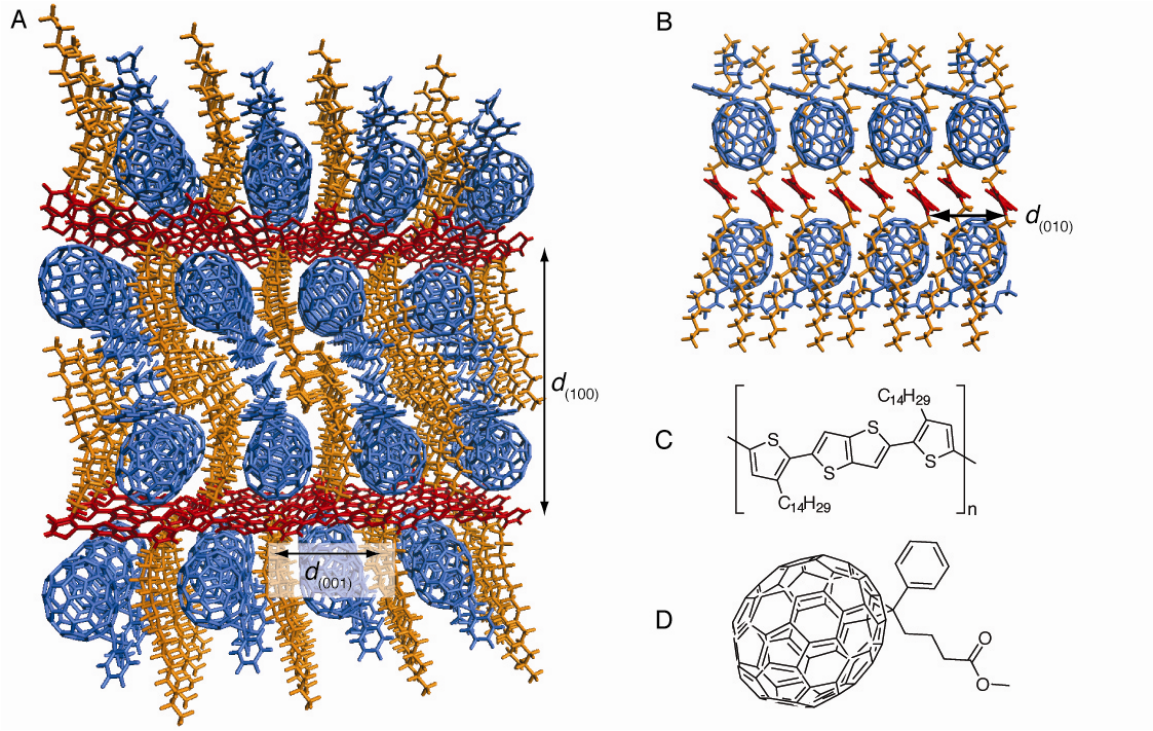

Figure 2. Ordering of PCBM and PBTTT in the co-crystal in views (A) along PCBM channels and (B) along the backbones. Chemical structures of (C) the polymer PBTTT and (D) the C_{70} fullerene derivative PCBM.

The comparison between modeled and experimental diffraction patterns are shown in Figure 3B and C, respectively. The calculated XRD structure agrees well with the experiment in terms of the peak positions, but the intensity distribution is somewhat

different; the simulated image (Figure 3C) has more peaks with generally smaller widths than the experimental image (Figure 3B), and the simulation overestimates the intensity of the peaks at higher *q*. Molecular mechanics methods determine energy minima at 0 K; while this is in general a good first approximation for the packing of the molecules at room temperature, it cannot predict thermal fluctuations and structural disorder. We find the energy landscape is very shallow with numerous molecular conformations and arrangements in local minima that have comparable energies. These geometric fluctuations or disorder (within a small energy range) explain the broader peaks that we see in the experiment (Figure 3B) compared to the model in (Figure 3C). The co-crystal has many defects not captured in the model.

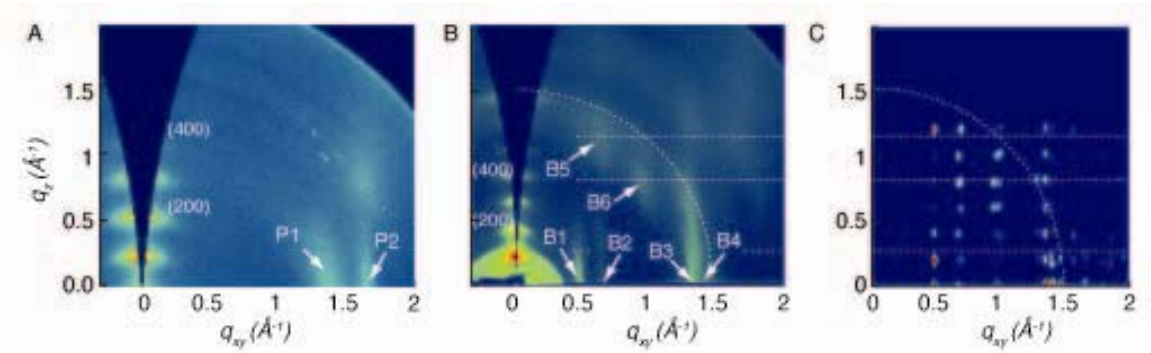

Figure 3. Experimental grazing incidence x-ray scattering patterns for thin films of (A) the pure PBTTT-C_{14} polymer and (B) the blend of PBTTT-C_{14}:$PC_{71}BM$. The main peaks (B1-B4) in the experimental image are reproduced by (C) the simulated diffraction image of the blend. The dashed lines are a guides to compare peak positions in images B and C.

The resulting structure demonstrates molecular intermixing of polymers and fullerenes without any synthetic or processing efforts, but rather by self-organization. The established structure can serve as a model system for fundamental studies on ordering in co-crystals, as well as on electronic properties. It may also help to improve the physical basis of ab initio modeling of polymers and polymer-fullerene blends. Mixing of two synthetically tailored components is of particular interest in a wide range of functional materials with properties defined largely by the interaction between two constituents.

In the future, these bimolecular crystals, whose structure can accurately characterized and modeled at the molecular level, will serve as models of a perfectly defined donor-acceptor interface and will permit studies of photophysical properties.. It is also important to develop methods to characterize the disorder inherent in these soft materials. We are beginning this by adopting the modeling to handle finite temperatures and by developing Warren-Averbach approaches to extracting disorder in the polymer blends.

Acknowledgments

This work was done in collaboration with Nicky Miller, Roman Gysel, Michael McGehee (Stanford), Chad Risko, Eunkyung Cho, Jean-Luc Brédas (Georgia Tech), and Chad Miller (SSRL). Financial support for this project was provided by Department of Energy (DOE). Portions of this research were carried out at the Stanford Synchrotron Radiation Laboratory, a national user facility operated by Stanford University on behalf of the US Department of Energy, Office of Basic Energy Sciences.

References

1. "Molecular Characterization of Organic Electronic Films", D.M. DeLongchamp, R.J. Kline, D.A. Fischer, L.J. Richter, M.F. Toney, Adv. Mat., in press (2010).
2. "Quantification of thin film crystallographic orientation using X-ray diffraction with an area detector", J.L. Baker, L.H. Jimison, S.M.M. Mannsfeld, S. Volkman, S. Yin, V. Subramanian, A. Salleo, A.P. Alivisatos, M.F. Toney, Langmuir 26, 9146–9151, (2010).
3. "Unconventional Face-on Texture and Exceptional In-plane Order of a High Mobility n-type Polymer", J. Rivnay, M.F. Toney, Y. Zheng, I.V. Kauvar, Z. Chen, V. Wagner, A. Facchetti, A. Salleo, Adv. Materials, in press, (2010).
4. "Large Modulation of Carrier Transport by Grain-Boundary Molecular Packing and Microstructure in Organic Thin Films", J. Rivnay, L.H. Jimison, J.E. Northrup, M.F. Toney, R. Noriega, T.J. Marks, A. Facchetti, A. Salleo, Nature Materials 8, 952 (2009).
5. "Solid-State Supramolecular Organization of Polythiophene Chains Containing Thienothiophene Units", P. Brocorens, A. Van Vooren, M. Chabinyc, M.F. Toney, M. Shkunov, M. Heeney, I. McCulloch, J. Cornil, R. Lazzaroni, Adv. Mater. 21, 1193-1198 (2009).
6. "Tuning the properties of polymer bulk heterojunction solar cells by adjusting fullerene size to control intercalation", N.C. Cates, R. Gysel, Z. Beiley, C.E. Miller, M.F. Toney, M. Heeney, I. McCulloch, M.D. McGehee, NanoLetters 9, 4153-4157 (2009).
7. "Bimolecular crystals of fullerenes in conjugated polymers and the implications of molecular mixing for solar cells", A.C. Mayer, M.F. Toney, S.R. Scully, J. Rivnay, C.J. Brabec, M. Scharber, M. Koppe, M. Heeney, I. McCulloch, M.D. McGehee, Adv. Func. Mater. 19, 1173-1179 (2009).

Superconductivity induced in FeTe films by oxygen incorporation

PI - Barrett O. Wells
Department of Physics
University of Connecticut
Storrs, CT 06269-3046

email: wells@phys.uconn.edu

Co-PI – Joseph I. Budnick
Department of Physics
University of Connecticut
Storrs, CT 06269-3046

budnick@phys.uconn.edu

Research Scope

Our DOE funded program currently has two main projects: a study of large scale phase separation in super-oxygenated $La_{2-x}Sr_xCuO_{4+y}$ and an investigation of films of Fe-chalcogenide superconductors with an emphasis on properties uniquely associated with film structures. Our group synthesizes interesting materials and we have substantial experience exploring issues connected to intercalation of oxygen into samples. We explore our materials using a variety of techniques as appropriate to the physics problem at hand, mostly pursued at DOE laboratories. Techniques that have been very important for our work include ARPES, neutron scattering, X-ray absorption, and muon Spin Rotation. We are currently moving to de-emphasize the phase separation in cuprate superconductors project in order to better exploit our discoveries in films of Fe-based superconductors. This presentation will thus focus on the discovery of a new superconductor, $FeTeO_x$ films.

Recent Progress – Superconductivity in $FeTeO_x$ Films.

Bulk FeTe is antiferromagnetic and non-superconducting and considered a parent compound for the Fe-chalcogenide family of superconductors. Chemical pressure via isoelectronic substitution of Se or S onto Te sites produces a superconductor **[1-3]**. However, no form of charge doping or physical pressure on bulk FeTe has been shown to produce a superconductor.

We have grown magnetic, nonsuperconducting FeTe films epitaxially on MgO and STO substrates using pulsed laser deposition (PLD). Further, we recently found **[4]** that superconductivity can be induced post growth by either a short, low temperature (100°C) annealing in oxygen or a longer term exposure to oxygen in the ambient atmosphere at room temperature. A superconducting transition with a onset temperature of 12K has been observed. In addition, all of the resistivity vs temperature curves show a broad peak around 65K for both superconducting and non-superconducting samples. In the bulk, this peak in the resistivity is associated with a concurrent antiferromagnetic (AFM) and structural transition **[5-7]**. As shown below, our films also appear to have this structural transition, but so far the magnetic state is unknown.

A series of annealing experiments show that the oxygen incorporation process is reversible: the superconducting state can be removed by driving oxygen out through a vacuum anneal and then restored again through another oxygen anneal. The resistivity profiles of these films and the reversible nature of the oxygen absorption is shown in Fig 1a. Fig 1b shows both the shielding (zero field cooled) and Meissner (field cooled) magnetic transition for a superconducting FeTeOx film. These are large signals with particular notice that the Meissner signal is almost as large as the shielding, rarely the case in cuprate superconductors such as $La_{2-x}Sr_xCuO_4$. The ease of cycling the oxygen content suggests one might be able to perform well controlled experiments on the changes that lead to superconductivity without changing the sample studied.

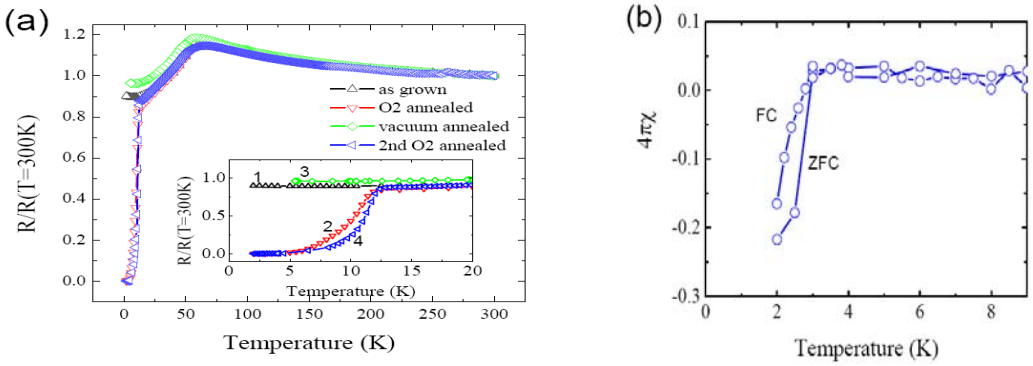

Fig 1. a) Resistivity of an FeTe film after different annealing steps demonstrating the reversibility of the superconducting state with oxygen uptake/expulsion. b) the shielding and Meissner signal from a superconducting film of $FeTeO_x$.

The process of incorporating oxygen appears to induce only a small change in the structure. Fig. 2 shows a broad, XRD scan of one film in its as-grown non-superconducting state and then in the O_2 annealed superconducting state. There is little change. Higher resolution studies at beamline X22C at the NSLS at Brookhaven revealed that there was a small contraction in-plane and a small expansion along the c-axis. Our own DFT calculations indicate that a likely low energy site for excess oxygen is just below the Fe plane, at a symmetry equivalent site to that occupied by the Te atoms. With O in this site, the DFT confirms that $FeTeO_x$ will remain in the tetragonal phase with only a small change in lattice constant.

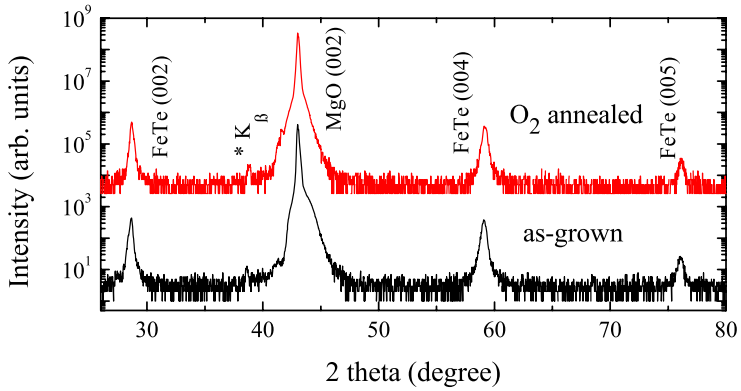

FIG. 2. X-ray diffraction profiles in the (00L) direction of the as-grown and oxygen annealed FeTe films taken at room temperature.

We have recently studied the c lattice constant of a superconducting $FeTeO_x$ films as a function of temperature using elastic neutron scattering, with the results shown in Fig. 3. Two transitions were observed, one at 65 K and the other at 12 K. The transition at 65 K appears to be associated with the maximum in the resistivity and presumably the same structural phase transition seen in the bulk. The lower temperature transition is not seen in bulk FeTe but occurs at the supercocnducting T_C. As far as we are aware, there are no other reports of a structural transition occurring simultaneously with superconductivity in Fe-based superconductors and we feel this low temperature structure may hold the key to superconductivity in this compound.

We have performed X-ray absorption spectroscopy and X-ray photoemission measurements to understand the changing valence states induced by oxygen incorporation. We have found a surprisingly large change in the Fe valence state, from metallic like Fe0 in the as-grown film to predominantly Fe3+ in the superconducting films. Fig. 4 shows a series of XAS measurements taken at different stages of oxidation showing a progression from Fe^0/Fe^{2+} in the fresher films to a spectrum reminiscent of Fe3+ in the superconductor. Our results on the Fe valence states are different from the literature on other Fe pnictides where the Fe *L*edge spectra were reported to be metallic-like in both parent and superconducting compounds **[8]**. Our data might be consistent with claims that the FeTe is more strongly correlated than the pnictides **[9, 10]** and with the observation of a larger moment in the chalcogenides **[11, 12]**.

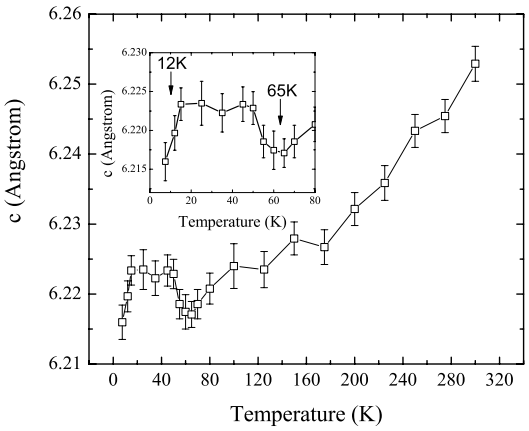

FIG. 3. The c lattice constant as a function of temperature using elastic neutron scattering. There are two transitions with critical temperatures around 55K and 12K.

In summary, by introducing excess oxygen at low temperature, superconductivity was induced in the FeTe films. When the films are superconducting, XRD indicates only a small structural change and XAS indicates that the majority of the Fe has a nominal valence of 3+. A structural transition associated with the superconducting transition has been observed. This method for creating a superconductor is quite different from the better known procedure of substituting isovalent Se or S for Te. Thus superconductivity occurs in very different places in the phase space of strain and Fe valence and the correct combination of both appears to be necessary for superconductivity.

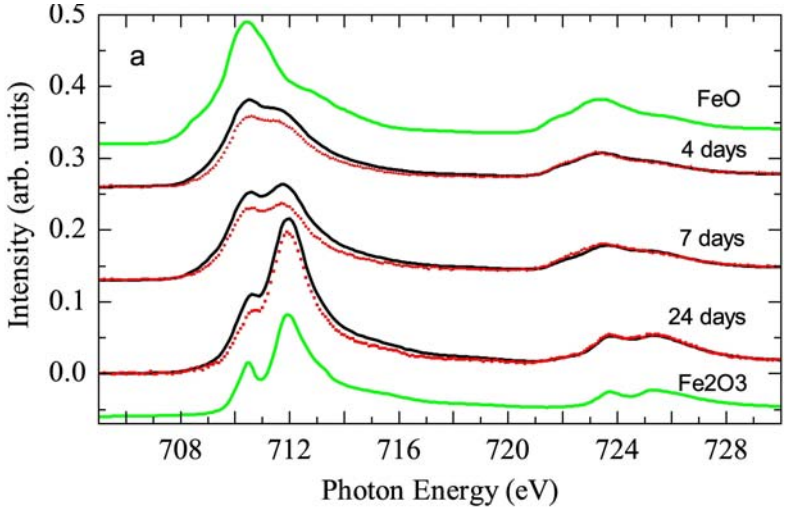

Fig 4. X-ray absorption spectroscopy of FeTe films. The Fe *L* edges TEY (black or upper solid curve) and TFY (red or lower dashed curves) show that the nominal valence state of Fe increases with longer exposure to air, from 2+ to 3+, by comparing with the FeO and Fe_2O_3 curves.

Future Plans

The existence and physical characteristics of $FeTeO_x$ superconductor raise some broad questions for the Fe-chalcogenide doping-strain-temperature phase diagram and for our understanding of just how a superconductor is created from a parent compound. Coupled to this, it is very surprising that we can create a superconductor without large changes in the normal state conductivity, which might suggest either some sort of phase separation or a low temperature structural transition that allows the superconducting phase to form. To examine these questions we intend to pursue more detailed microscopic measurements such as neutron diffraction to look for the antiferromagnetic state and ARPES to examine more detailed changes in electronic structure. Our preliminary neutron work showed that Bragg scattering off of our films is plausible, but we do need to improve the in-plane mosaic of the films. Our initial ARPES work has shown that we can get angular-resolved data from a cleaved film.

Another interesting problem is why this process appears to robustly produce a superconductor in films but so far has not worked in bulk samples. Our preliminary results indicate that diffusion in the bulk is not sufficient to get oxygen properly incorporated into the structure. A depth sensitive measurement of the oxygen profile and Fe/Te oxidation states will be necessary.

Finally, we are looking for better techniques for studying the magnetic state of the films, the low temperature structural transition, and any sign of oxygen ordering in the films. We hope that X-ray scattering experiments may be helpful.

Publications since 2008

1. Hashini E. Mohottala, B. O. Wells, J. I. Budnick, W. A. Hines, Ch. Niedermayer, and F. C. Chou, "Flux pinning and phase separation in oxygen rich $La_{2-x}Sr_xCuO_{4+y}$ system" *Phys. Rev. B* **78**, 064504 (2008).

2. S.B. Emery and B.O. Wells, Properties of Phase-Separated, Super-Oxygenated $La_{2-x}Sr_xCuO_{4+y}$" *J Supercond Nov Magn*, **22**, 33 (2009)

3. Y. Nie, E. Brahimi, J. I. Budnick, W. A. Hines, M. Jain, and B. O. Wells, "Suppression of superconductivity in FeSe films under tensile strain" *Appl. Phys. Lett.* **94**, 242505 (2009).

4. L. Udby, N.H. Andersen, F.C. Chou, N.B. Christensen, S.B. Emery, K. Lefmann, J.W. Lynn, H.E. Mohottala, Ch. Niedermayer, B.O. Wells, "Magnetic ordering in electronically phase separated Sr/O co-doped $La_{2-x}Sr_xCuO_{4+y}$" *Phys. Rev. B* **80**, 014505 (2009).

5. Y. F. Nie, D. Telesca, J. I. Budnick, B. Sinkovic, and B. O. Wells, "Superconductivity induced in iron telluride films by low-temperature oxygen incorporation" *Phys Rev B* **82**, 020508 -R (2010)

6. L. Udby, P.K. Willendrup, E. Knudsen, Ch. Niedermayer, U. Filges, N.B. Christensen, E. Farhi, B.O. Wells and K. Lefmann, "Analysing neutron scattering data using McStas virtual experiments" *Nucl. Instr. and Meth. A* (2010), doi:10.1016/j.nima.2010.06.235

References:

[1] Y. Mizuguchi, *et al.*, Appl. Phys. Lett. **94**, 012503 (2009)

[2] F.-C. Hsu, *et al.*, Proc. Natl. Acad. Sci. U.S.A. **105**, 14262 (2008).

[3] M. H. Fang, *et al.*, Phys. Rev. B **78**, 224503 (2008)

[4] Y. Nie, D. Telesca, J.I. Budnick, B. Sinkovic, B.O. Wells, Phys. Rev. B **82**, 020508(R) (2010)

[5] M. J. Wang, *et al.*, Phys. Rev. Lett. **103**, 117002 (2009)

[6] R. Hu, *et al.*, Phys. Rev. B **80**, 214514 (2009)

[7] G. F. Chen, *et al.*, Phys. Rev. B **79**, 140509(R) (2009)

[8] W. L. Yang, *et al.*, Phys. Rev. B **80**, 014508 (2009)

[9] A. M. Turner, *et al.*, Phys. Rev. B **80**, 224504 (2009).

[10] A. Tamai, *et al.*, arXiv (2009), 912.3152v2

[11] S. Li, *et al.*, Phys. Rev. B **79**, 054503 (2009).

[12] C. de la Cruz, *et al.*, Nature **453**, 899 (2008)

Dynamics and Reactivity of Metallic Interfaces Important to Heterogeneous Catalysis and Electrocatalysis

PI: H. You
Materials Science Division
Argonne National Laboratory
9700 S. Cass Ave., Argonne, IL 60439
(630) 252-3429; (630) 252-7777(Fax), hyou@anl.gov

Research Scope

Surface structure and dynamics are key to catalytic processes and other chemical interactions, but it is often difficult to study them at the atomic scale in operating environments. We study dynamics and reactivity of model catalysts, single crystal surfaces, and nanostructured surfaces interacting with simple molecules such as H_2O, CO, and O_2, under pressure, temperature, and other materials processing conditions that have not been explored before using atomic-scale probes. X-ray techniques are unique avenues in studying such interfaces and we develop further new x-ray techniques in order to achieve a greater insight into the dynamics of surface phase transitions and how solid surfaces interact with liquids and gases, especially under extreme environments. The scope of the project encompasses i) fundamental understanding of molecular reactions occurring on buried interfaces relevant to heterogeneous catalysis and electrocatalysis using *in situ* synchrotron x-ray techniques, ii) development of forefront synchrotron x-ray techniques enabling measurements of the previously unavailable molecular-level *dynamic* information at surface and interfaces, and iii) extend the synchrotron x-ray techniques to study interfaces buried under materials processing environments, such as extreme pressures and temperatures.

Recent Progress

Dynamics and reactivity of interfaces buried under reactive environments such as gases and liquids, often at high pressure and high temperature, are important to energy conversion and storage technologies, yet under-explored due to the lack of the molecular-level experimental probes. Synchrotron x-rays are uniquely suited for such investigations. Unlike the study of static properties of such interfaces, study of dynamics and reactivity requires the development of new x-ray techniques to capture and measure phase transitions and reactions in motion. In the last three years, we have studied oxygen reduction and carbon monoxide oxidation reactions and developed a new x-ray technique for studying surface dynamics.

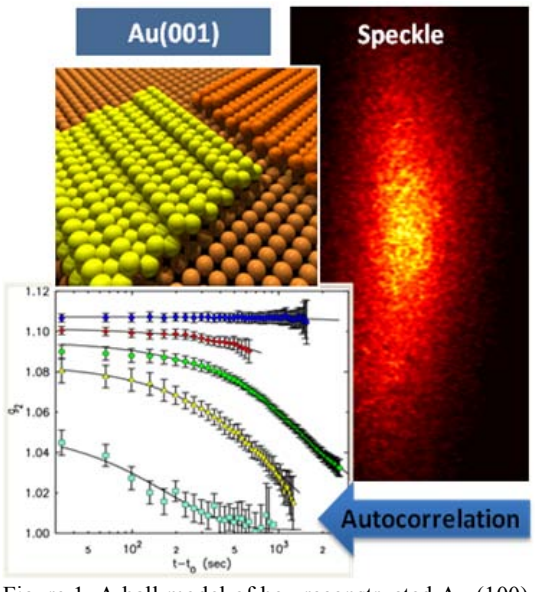

Figure 1. A ball model of hex-reconstructed Au (100), a speckle pattern, and the autocorrelation functions.

Coherent x-ray scattering from a surface: We have demonstrated that an x-ray speckle pattern can be measured from a single atomic monolayer.[1] Because each speckle pattern is uniquely related to the atomic arrangement, changes in these patterns show the motions of surface atoms with monolayer sensitivity. Using the surface-monolayer speckle pattern, we developed the surface x-ray photon correlation spectroscopy (SXPCS) technique and used it to observe dynamics of the surface atoms of gold with unprecedented clarity in real time.

The square lattice of the Au (100) surface reconstructs spontaneously to a hexagonal lattice. Using SXPCS, we showed that the top monolayer of surface atoms is highly mobile, and that their equilibrium dynamics displays unexpectedly rich behavior even when their ensemble average structure appears static.

Our study of Au (100) revealed a previously unidentified 'dynamic transition' in the atomic motions of the reconstructed gold surface. Below the dynamic transition, the motions are slow and dominated by rearrangement of the hexagonal domains, where the rearrangements are thermally activated and follow a simple Arrhenius form. Above the dynamic transition, however, the motions become much faster and consist of hexagonal/square interconversions. This change in dynamics is explained by a Landau-type free energy difference between the hexagonal and square lattices that decreases as temperature approaches the phase transition temperature.

Structure and catalytic activity of model nanoparticle and nanofacet arrays: We produced 2d arrays composed of millions of morphologically identical platinum catalyst nanoparticles epitaxially grown on (111), (100) and (110) strontium titanate substrates using electron beam lithography. Our rigorous approach to design, produce and characterize the catalyst nanoparticles allowed us to relate microscopic morphologies with macroscopic catalytic reactivities. The particle shapes were predicted using a Wulff construction based on density functional theory calculations of surface energies. Then, in accordance with theoretical predictions, we are able to tweak morphologies of the already produced nanocrystals by changing annealing conditions.[2] In the case of platinum single crystals, the (100) surface has a higher affinity towards oxide species than the (111) surface,[3] which results in a lower activity of the (100) than the (111) surface. Therefore, the unexpectedly high oxygen reduction activities proportional to the supposedly inactive (100) facets were surprising. In addition, Tafel slopes of the reaction were consistent with the reactivity of (111) facets, confirming that the reaction still takes place on the (111) surface as expected.

It is therefore remarkable that the ORR activities are proportional to the (100) facet area, as shown in Figure 2 (right). Based on this observation and similar properties seen in the case of one-dimensional arrays of alternating (100) and (111) nanofacets formed on single crystal surfaces, we suggested the following scenario:[4] The (100) facets adsorb oxygen well, but cannot reduce it efficiently, while the (111) facets can reduce oxygen, but cannot easily adsorb it. The nanoscale proximity allows oxygen that is adsorbed on (100) to diffuse to the (111) facets, where it can be more efficiently reduced. The schematics shown in Figure 2 suggest that the (100) facets simply act as "collectors of oxygen", and the linear dependence of kinetic current densities on the (100) facet area can be expected as long as the (111) facets can efficiently process the reaction.

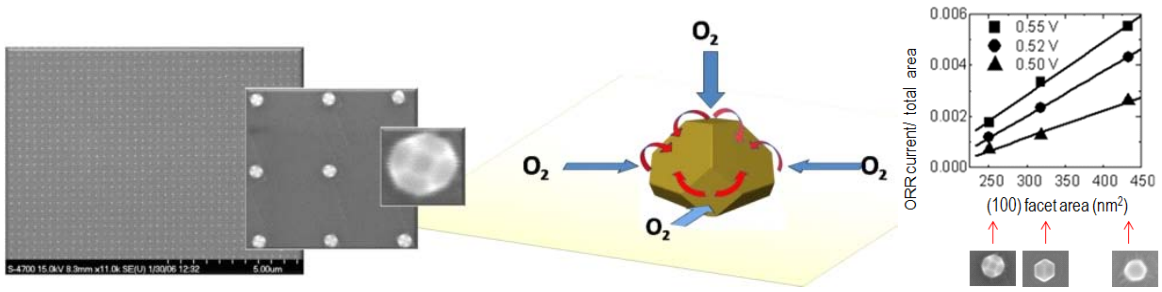

Figure 2. Increased catalytic activity of the arrays points to a cooperative interplay between facets with different affinities to oxygen. We suggest that the surface area of (100) facets is one of the key factors governing catalyst performance in electrochemical reduction of oxygen molecules.

While the detailed structures of nanoparticle surfaces are difficult to study, certain aspects can be inferred from model nanofacets. We made previously such (111) and (100) nanofacets formed on a single crystal surface and studied the oxygen reduction and CO oxidation reactions.[5] Recently we continued with studies of the surface structure of such facets and of the influence of reactions on the surface structure. The main challenges in this case are that the CTR signals from the facets are not very strong and generally sit on high backgrounds. However, we found that several cycles of CO oxidation reactions effectively anneal the nanofacets to near perfection, restoring the ideally terminated (111) and (100) facets. The CTR examples are shown in Figure 3.

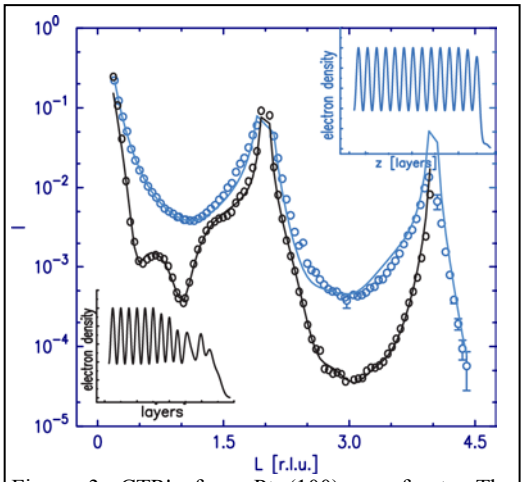

Figure 3. CTR's from Pt (100) nanofacets. The black circles and lines are data and fit, respectively as prepared in oxygen annealing. The blue circles and fit are the results after several CO oxidation cycles. The density profiles suggest the surface oxide formation and removal by CO cycles.

Future Plans

Immediate and exciting applications of the SXPCS technique include study of the dynamics of electrochemical interfaces as surface structure changes during phase transitions, electrodeposition, oxidation/reduction reactions, corrosion, and passivation. Dynamic behaviors of many important reactions of electrochemistry have not been elucidated, despite their importance, primarily due to the lack of such experimental probes. Coherent x-ray scattering, therefore, opens a whole new dimension in studying electrochemical interfacial sciences. We have just begun dynamic measurements on some of our model electrochemical systems.

The ultimate goal of surface coherent x-ray scattering is to achieve an x-ray imaging tool that can be used to 'see' buried surfaces or interfaces. Since x-rays can penetrate most extreme environments, this new x-ray imaging tool can be used to observe interfaces in real time during chemical reactions and phase transitions. In past years, we have demonstrated the surface sensitivity of coherent x-ray scattering. We have shown that coherent x-ray scattering can be done from a single or sub-monolayer of atoms and provide dynamic information on the surface or interface using SXPCS analysis. In doing so, we have often found that the speckle patterns often exhibit tantalizing details and symmetries of the surfaces. In certain cases, the pattern is almost simple enough for a direct inversion to a real space image based on what we already know about the surface. These cases will provide excellent examples for us to develop an inversion technique using established oversampling methods.[6] Initially we will use well-prepared and well-controlled Pt (100) as the initial test case for concept development. In the following we briefly describe our preliminary measurements and calculations to demonstrate the feasibility of this approach.

The Pt (100) surface has the same hex reconstruction as Au (100). The transition temperature is much higher but there is a temperature range where the platinum surface becomes highly ordered with large terraces. Since the average terrace size is large we are able to set the illuminated area to include only a few terraces and steps. The simulated speckle pattern from such a surface is shown in the inset of Figure 4. The pattern is relatively simple since there are only a few steps illuminated. In our preliminary measurement, we indeed find a simple

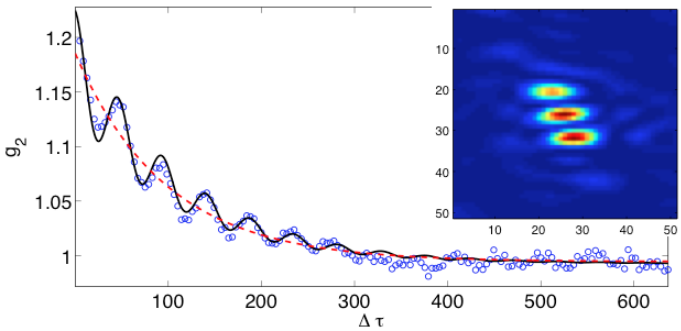

Figure 4. Autocorrelation from Pt (100) surface at an elevated temperature. Inset: Calculated coherent scattering pattern from the surface.

speckle pattern similar to the simulated one. In addition, the intensity at a given pixel is highly fluctuating as we expect from a surface in a dynamic equilibrium. However, a closer examination of the fluctuation unveils a behavior of the autocorrelation function previously unobserved in the gold surface speckle patterns. Instead of a simple exponential decay, the measured autocorrelation function includes an oscillatory term riding on an exponential decay and the oscillation persists over tens of minutes. A simple exponential decay is expected if the surface is sufficiently complex with many fluctuating domains within the illuminated area. We believe that the oscillatory autocorrelation is a result of step flow that is fairly constant over the time scale of the measurement.[7]

We will use the established concept of oversampling to invert the speckle pattern to a real space image. We will apply the technique to our cases of stepped platinum surfaces. Once the algorithm of the inversion is established, we can essentially 'see' in real time the motion of the steps. Then we will move on to more complex and corrugated domain structures and attempt to invert these speckle patterns to a real space structure.

[1] M. S. Pierce, et al., Phys. Rev. Lett., 103, 165501 (2009)
[2] H. Iddir, J. Phys. Chem. C, 111, 14782 (2007)
[3] A. Panchenko, et al., J. Electrochem. Soc. 151, A2016 (2004)
[4] V. Komanicky, J. OF Am. Chem. Soc., 131, 5732 (2009)
[5] V. Komanicky, A. Menzel, K.-C. Chang, H. You, J. Phys. Chem. B109(49), 23543-49 (2005)
[6] I.K. Robinson and R. Harder, Nature Mat. 8 291 (2009); M. Dierolf, et al., Europhys. News, 39, 22 (2008)
[7] M.S. Pierce and H. You, unpublished.

Publications FY2008-FY2010

1. V. Komanicky, H. Iddir, K. Chang, A. Menzel, G. Karapetrov, D. Hennessy, P. Zapol, H. You, *Shape-Dependent Activity of Platinum Array Catalyst,* J. Am. Chem. Soc., 131, 5732 (2009)
2. C. Lucas, P. Thompson, M. Cormack, A. Brownrigg, B. Fowler, D. Strmcnik, V. Stamenkovic, J. Greeley, A. Menzel, H. You, N. Markovic, *Temperature-Induced Ordering of Metal/Adsorbate Structures at Electrochemical Interfaces ,* J. Am. Chem. Soc., 131, 7654 (2009)
3. K. Chang, B. Ingram, B. Kavaipatti, B. Yildiz, D. Hennessy, P. Salvador, N. Leyarovska, H. You, *In situ Synchrotron X-ray Studies of Dense Thin-Film Strontium-Doped Lanthanum Manganite Solid Oxide Fuel Cell Cathodes ,* Solid-State Ionics-2008, 1126, 27 (2009)
4. M. S. Pierce, K. Chang, D. Hennessy, V. Komanicky, M. Sprung, A. Sandy, H. You, *Surface X-Ray Speckles: Coherent Surface Diffraction from Au(001),* Phys. Rev. Lett., 103, 165501 (2009)
5. C. Wang, D. van der Vilet, K. Chang, H. You, D. Strmcnik, J. Schlueter, N. Markovic, V. Stamenkovic, *Monodisperse Pt3Co Nanoparticles as a Catalyst for the Oxygen Reduction Reaction: Size-Dependent Activity ,* J. Phys. Chem. C, 113, 19365 (2009)
6. M. Pierce, K. Chang, D. Hennessy, V. Komanicky, A. Menzel, H. You, *CO-induced lifting of Au(001) surface reconstruction,* J. Phys. Chem. C, 112, 2231 (2008)
7. D. Hennessy, M. Pierce, K. Chang, S. Takakusagi, H. You, K. Uosaki, *Hydrophilicity transition of the clean rutile TiO2 (110) surface,* Electrochimica Acta, 53, 6173 (2008)
8. D. Strmcnik, D. Tripkovic, D. van der Vliet, K. Chang, V. Komanicky, H. You, G. Karapetrov, J. Greeley, V. Stamenkovic, N. Markovic, *Unique Activity of Platinum Adislands in the CO Electrooxidation Reaction ,* J. Am. Chem. Soc., 130, 15332 (2008)
9. H. Iddir, V. Komanicky, S. Ogut, H. You, P. Zapol, *Shape of platinum nanoparticles supported on SrTiO3: Experiment and theory ,* J. Phys. Chem. C, 111, 14782 (2007)
10. J. Inukai, D. Cao, A. Wieckowski, K. Chang, A. Menzel, V. Komanicky, H. You, *In situ synchrotron X-ray Spectroscopy of ruthenium nanoparticles modified with selenium for an oxygen reduction reaction ,* J. Phys. Chem. C, 111, 16889 (2007)

Book chapter:

1. Z. Nagy and H. You, *Applications of synchrotron x-ray scattering for the investigation of the electrochemical interphase*, in "Modern Aspect of Electrochemistry", Vol. 45, ed. R.E. White, 247-335 (2009).

Author Index

Participant List

Name	Organization	E-mail Address
Abbamonte, Peter	University of Illinois, Urbana-Champaign	abbamonte@mrl.uiuc.edu
Barabash, Rozaliya	Oak Ridge National Laboratory	barabashr@ornl.gov
Bedzyk, Michael	Northwestern University	bedzyk@northwestern.edu
Billinge, Simon	Columbia University/BNL	sb2896@columbia.edu
Bostwick, Aaron	Lawrence Berkeley National Laboratory	abostwick@lbl.gov
Bucksbaum, Philip	PULSE Institute/SLAC	phb@slac.stanford.edu
Budai, John	Oak Ridge National Laboratory	budaijd@ornl.gov
Burns, Clement	Western Michigan University	clement.burns@wmich.edu
Campuzano, Juan-Carlos	Argonne National Laboratory	campuzano@anl.gov
Chen, Jiuhua	Florida International University	chenj@fiu.edu
Chen, Yulin	SLAC National Accelerator Laboratory	chenyl@stanford.edu
Chiang, Tai	University of Illinois, Urbana-Champaign	tcchiang@illinois.edu
Clarke, Roy	University of Michigan	royc@umich.edu
Cornelius, Andrew	University of Nevada, Las Vegas	cornel@physics.unlv.edu
Crockett, Teresa	DOE Basic Energy Sciences	teresa.crockett@science.doe.gov
Dessau, Dan	University of Colorado	Dessau@Colorado.edu
Devereaux, Thomas	SLAC National Accelerator Laboratory	tpd@stanford.edu
Dobbins, Tabbetha	Louisiana Tech University	tdobbins@latech.edu
Durakiewicz, Tomasz	Los Alamos National Laboratory	tomasz@lanl.gov
Dürr, Hermann	SLAC National Accelerator Laboratory	hdurr@slac.stanford.edu
Eastman, Jeffrey	Argonne National Laboratory	jeastman@anl.gov
Evans, Paul	University of Wisconsin-Madison	evans@engr.wisc.edu
Fadley, Charles	Lawrence Berkeley National Laboratory	fadley@lbl.gov
Fong, Dillon	Argonne National Laboratory	fong@anl.gov

Fuoss, Paul	Argonne National Laboratory	fuoss@anl.gov
Goldman, Alan	Ames Laboratory/Iowa State University	goldman@ameslab.gov
Hasan, M. Zahid	Princeton University	mzhasan@princeton.edu
Headrick, Randall	University of Vermont	rheadrick@uvm.edu
Hill, John	Brookhaven National Laboratory	hill@bnl.gov
Horton, Joe	DOE Basic Energy Sciences/ORNL	joe.horton@science.doe.gov
Horton, Linda	DOE Basic Energy Sciences	linda.horton@science.doe.gov
Hufnagel, Todd	Johns Hopkins University	hufnagel@jhu.edu
Ice, Gene	Oak Ridge National Laboratory	IceGE@ornl.gov
Jacobsen, Chris	Argonne National Laboratory	c-jacobsen@northwestern.edu
Kaindl, Robert	Lawrence Berkeley National Laboratory	RAKaindl@lbl.gov
Kaminski, Adam	Ames Laboratory/Iowa State University	kaminski@ameslab.gov
Kao, Chi-Chang	SLAC SSRL	ckao@slac.stanford.edu
Kevan, Stephen	University of Oregon	kevan@uoregon.edu
Kortright, Jeffrey	Lawrence Berkeley National Laboratory	jbkortright@lbl.gov
Kreyssig, Andreas	Ames Laboratory/Iowa State University	kreyssig@ameslab.gov
Larson, Bennett	Oak Ridge National Laboratory	larsonbc@ornl.gov
Lindenberg, Aaron	Stanford University/SLAC	aaronl@stanford.edu
Ludwig, Karl	Boston University	ludwig@bu.edu
Lyman, Paul	University of Wisconsin-Milwaukee	plyman@uwm.edu
Mao, Hokwang	Carnegie Mellon University	mao@gl.ciw.edu
Mao, Wendy	Stanford University	wmao@stanford.edu
Mochrie, Simon	Yale University	simon.mochrie@yale.edu
Murnane, Margaret	University of Colorado at Boulder/JILA	margaret.murnane@colorado.edu
Nilsson, Anders	SLAC National Accelerator Laboratory	nilsson@slac.stanford.edu
Ocko, Benjamin	Brookhaven National Laboratory	ocko@bnl.gov

Pang, Judy	Oak Ridge National Laboratory	pangj@ornl.gov
Parise, John	Stony Brook University/BNL	john.parise@sunysb.edu
Reichert, Harald	European Synchrotron Radiation Facility (ESRF)	reichert@esrf.fr
Reis, David	PULSE Institute/SLAC	dreis@slac.stanford.edu
Scherz, Andreas	SLAC/Stanford University	scherz@slac.stanford.edu
Schoenlein, Robert	Lawrence Berkeley National Laboratory	rwschoenlein@lbl.gov
Shen, Zhi-Xun	Stanford University	zxshen@stanford.edu
Shpyrko, Oleg	University of California, San Diego	oleg@physics.ucsd.edu
Silva, Thomas	National Institute of Standards and Technology (NIST)	silva@boulder.nist.gov
Specht, Eliot	Oak Ridge National Laboratory	spechted@ornl.gov
Srajer, George	Argonne National Laboratory	srajerg@aps.anl.gov
Stephenson, G. Brian	Argonne National Laboratory	aps-director@aps.anl.gov
Stöhr, Joachim	SLAC/LCLS	irene@slac.stanford.edu
Struzhkin, Viktor	Carnegie University of Washington	vstruzhkin@gl.ciw.edu
Suter, Robert	Carnegie Mellon University	suter@andrew.cmu.edu
Talley, Lee-Ann	Oak Ridge Institute for Science and Education	Lee-Ann.Talley@orise.orau.gov
Thiyagarajan, Thiyaga	DOE Basic Energy Sciences	P.Thiyagarajan@science.doe.gov
Thompson, Joe	Los Alamos National Laboratory	jdt@lanl.gov
Tischler, Jonathan	Oak Ridge National Laboratory	TischlerJZ@ornl.gov
Toney, Mike	SLAC SSRL	mftoney@slac.stanford.edu
Wells, Barrett	University of Connecticut	wells@phys.uconn.edu
Wilkins, Stuart	Brookhaven National Laboratory	swilkins@bnl.gov
Wilson, Lane	DOE Basic Energy Sciences	Lane.Wilson@science.doe.gov
You, Hoydoo	Argonne National Laboratory	hyou@anl.gov